Green Leaf Lipid Extract as a Yield Stress Modifying Emulsifier in Reduced-Fat Chocolate

Ruth J Price

Thesis submitted to the University of Nottingham

for the degree of Doctor of Philosophy

University of Nottingham
School of Biosciences
Sutton Bonington Campus
Leicestershire LE12 5RD

May 2021

Acknowledgements

Table of Contents

List of abbreviations

Abbreviation	Meaning
General	
°C	Degrees centigrade
Å	Angstrom
Da	Dalton
FAO	Food and Agriculture Organisation
g	Gram
G.90	Grindsted 90 (PGPR)
IOCCC	International Office of Cocoa, Chocolate and Sugar Confectionery
L	Litres
m	Metre
min	Minute
P.4150	Palsgaard 4150 (PGPR)
PGPR	Polyglycerol polyricinoleate (E476)
ppm	Parts per million
rpm	Revolutions per minute
s	Seconds
vol	By volume
WHO	World Health Organisation
wt	By weight
Chemistry	
ATP	Adenosine triphosphate
CO_2	Carbon dioxide
ESI-MS	Electrospray-Ionization Mass Spectrometry
I_2	Iodine molecule
NADPH	Nicotinamide adenine dinucleotide phosphate
OH	Hydroxyl group
S. Deoxy	Sodium deoxycholate
Sodium deoxy	Sodium deoxycholate
TAG	Triacylglycerols

Rheology

A	Area
CSR	Controlled by shear rate
CSS	Controlled by shear stress
F	Force
G'	Elastic or storage modulus
G"	Viscous or loss modulus
$\dot{\gamma}$	Shear strain rate
γ^*	Windhab shear stress at a 63.2% defined point
h	Distance
η_∞	High shear viscosity
η_B	Bingham plastic viscosity
H-B	Herschel Bulkley
η_C	Casson plastic viscosity
η_{HB} or c	Flow coefficient
LVR	Linear viscoelastic region
M	Torque
n	Rotational speed
p	Herschel-Bulkley index
QC	Quality control
τ	Shear stress
τ_0	Initial yield stress
τ_1	Shear stress that leads to a maximum shear-induced structuring
τ_B	Bingham yield value
τ_C	Casson yield value
τ_{HB}	Yield point according to Herschel-Bulkley
v	Velocity
η	Viscosity
φ	Deflection angle

Lipids

acyl-MGDG	Acylated monogalactosyl diacylglycerol
C18	A fatty acid with 18 carbon atoms (the number can vary)
C18:3	A fatty acid with 18 carbon atoms and three double bonds (α-linolenate)
C-6 position	The sixth carbon on a galactose when drawn as a Fischer projection
DGDG	Digalactosyl diacylglycerol

MGDG	Monogalactosyl diacylglycerol
nFA	Number of fatty acids
OH	Hydroxyl moiety
sn-1	Designation of the carbon on glycerol molecule that is at the top, when drawn vertically
sn-2	Designation of the carbon on glycerol molecule that is at the middle, when drawn vertically
sn-3	Designation of the carbon on glycerol molecule that is at the bottom, when drawn vertically
SQDG	Sulfoquinovosyl diacylglycerol

Analytical terminology

^{13}C	Carbon-13, a stable isotope, used in NMR
^{1}H	Proton NMR
^{31}P	Phosphorus-31, a stable isotope, used in NMR
CMC	Critical Micelle Concentration
DRI	Differential refractive index
ESI-MS	Electrospray Ionisation-Mass Spectrometry
FAME	Fatty Acid methyl esters
GC	Gas Chromatography
GC-MS	Gas chromatography-Mass Spectrometry
GC-MS/FID	Gas chromatography-Mass Spectrometry/Flame Ionisation Detector
GPC	Gel Permeation Chromatography
HPLC	High-performance liquid chromatography (LC)
HPTLC	High-performance thin-layer chromatography
HV	Hydroxyl value
IV	Iodine value
KOH	Potassium Hydroxide
LC-MS/MS	Liquid chromatography (LC) tandem mass spectrometry (MS)
LS	Light scatter
m/z	Mass-to-charge ratio
MW	Molecular weight
n_i	Number of olefinic double bonds
NMR	Nuclear Magnetic Resonance
PG	Polyglycerol (often followed by a number denoting the number of molecules)
PMMA	Poly(methyl methacrylate)

PR	Polyricinoleate (often followed by a number denoting the number of molecules)
PTFE	Polytetrafluoroethylene
R^2	Coefficient of determination
RT	Retention time
SEC	Size Exclusion Chromatography
SN	Saponification number
TLC	Thin-layer chromatography
TMSH	Trimethyl sulfonium hydroxide
VS	Viscometry

Recombinant protein technology

AGAP-1	Acylated Galactolipid Associated Phospholipase 1 (AGAP-1)
BSA	Bovine serum albumin
BUME	Butanol-Methanol extraction method
IPTG	Isopropyl β-D-1-thiogalactopyranoside
LB	Lysogeny broth
OD_{600}	Optical density of a sample measured at a wavelength of 600 nm
SDS-PAGE	Sodium dodecyl sulphate–polyacrylamide gel electrophoresis

Abstract

Chocolate is a composite material of sugar and cocoa particles, sometimes also containing milk powder, in a crystallised fat phase of mostly cocoa butter. As a melt above 40°C, chocolate represents a highly-filled suspension, often formulated close to the maximum packing fraction, especially in the case of lower-fat recipes. Emulsifiers are added to control the rheological properties of chocolate through adsorption at the hydrophilic sugar surfaces, thus inhibiting aggregate formation in the hydrophobic continuous phase. The most commonly applied emulsifier is lecithin (E322). It reduces the viscosity of chocolate and can lower its yield stress. However, polyglycerol polyricinoleate (PGPR, E476) has a much more substantial yield stress lowering effect, unique amongst food-grade emulsifiers. Unfortunately, PGPR is label adverse, perhaps due to its unfamiliar and chemical-sounding name; PGPR has an E-number, and even though lecithin also does, its name is often used in the ingredients list instead, as consumers are more familiar with or even approve of "lecithin"; or perhaps consumers reject it due to the fact that it is "processed" from castor oil. Therefore, the overall aim of this PhD research was to determine a natural alternative that provides a similar yield stress lowering effect. To achieve this goal, the research set out to analyse five commercially available PGPR samples with observationally reported differences in yield stress lowering efficacy, generating analytical data to validate the empirically reported difference in functionality and analysing molecular make-up in order to understand the molecular characteristics that are present in more efficient PGPRs. This new knowledge was then exploited to select a natural molecule possessing the identified molecular properties and yield stress lowering properties comparable with PGPR.

Initially, a chocolate model consisting of a 65% (wt) sugar-in-oil suspension, where the oil was pre-treated to remove naturally present surface-active molecules, and a rheology protocol to obtain yield stress data for these suspensions, with and without

added emulsifier, was developed. The rheology protocol developed comprised the concentric cylinder geometry to perform a shear stress sweep from high to low stress values and data analysis to compute the Herschel-Bulkley (H-B) yield stress value to allow sample comparison. Applying the commercial PGPR samples at 0.3% (wt) (total sample weight) in the chocolate model revealed that the PGPRs could be separated into those more or less efficient at reducing yield stress, although all PGPRs reduced the yield stress significantly compared to the baseline samples with no added PGPR. The impact of PGPRs on the interfacial tension between treated oil and water was then investigated as a way of interrogating their surface-active character. It was found that the H-B yield stress values were directly proportional to critical micelle concentration data, determined from equilibrium interfacial tension values between water and the chocolate model oil phase with PGPR added at a range of concentrations. The data inferred that the PGPRs that were more efficient at lowering the yield stress probably had a larger hydrophilic head group and straight hydrophobic tails, thus enabling reverse micelle formation at a lower concentration of PGPR.

Further analysis via electrospray ionisation-mass spectrometry and size exclusion chromatography revealed that the five PGPR samples were virtually indistinguishable from each other regarding their range of molecular weights. As a verification of this finding, analysis using ^{13}C nuclear magnetic resonance on two samples, the least and most efficient yield stress reducing PGPR samples, showed that the polyricinoleate chain lengths appeared identical. Finally, transmethylation of the samples followed by gas chromatography-mass spectroscopy revealed that a significantly greater amount of ricinoleic acid molecules were present at the terminus of the polyricinoleate chains of the least efficient PGPR sample. Therefore, it was hypothesised that hydroxyl groups at the end fatty acid are attracted to the hydrophilic sugar causing the hydrophobic chain to fold back on itself. The long length of the polyricinoleate chain extending into the continuous phase has been shown in previous research to be

essential in the yield stress reducing abilities of PGPR; therefore, any restriction on this chain is detrimental to its functionality.

Since most natural polar lipids lack ricinolic acid, the molecular criterion selected to identify a possible alternative to PGPR was the large headgroup configuration of a glycerol-based molecule that separates the acyl chains; acylated monogalactosyl diacylglycerol (acyl-MGDG). Purified acyl-MGDG is commercially not available, so it was obtained in two ways. The enzyme identified as responsible for forming acyl-MGDG, named AGAP-1, was acquired and multiplied using recombinant protein expression technology. This enzyme was used to convert commercially available MGDG and DGDG into acyl-MGDG, validated by high-performance thin-layer chromatography (HPTLC). Only a very small quantity could be obtained, not allowing conclusive statements to be made concerning yield stress lowering efficacy. Alternatively, cocoa leaves were collected from cocoa farms in the Côte D'Ivoire, and the Eden Project biodomes, UK, and mechanically stressed to trigger the formation of acyl-MGDG. HPTLC revealed that both the stressed and the control cocoa leaf lipids contained acyl-MGDG and other acylated galactolipids. The presence of acyl-MGDG without mechanical or biotic stress has not been shown before; however, the leaves showed other signs of lipid breakdown with lower amounts of galactolipids, chlorophyll and carotenoids than expected for a leaf. It may be that the creation of acyl-MGDG is naturally occurring in all senescing leaves, whether or not they have had biotic or abiotic stress applied. The leaf lipids applied to the chocolate model at 0.15% (wt) showed a yield stress lowering ability that was statistically similar to 0.3% (wt) PGPR. This finding is promising for food-grade emulsifier development and one which deserves further development.

Additional achievements

The research in this PhD has led to:

Paper in draft:

"Comparative study of polyglycerol polyricinoleate linking yield stress reducing efficacy to structural attributes" Price, RJ; Gray, D; Watson, N; Vieira, J; Wolf, B.

Oral Presentations:

Investigating PGPR to understand its effect on the flow properties of chocolate. British Society of Rheology Midwinter Meeting, Birmingham, UK, Dec 2019.

Synthetic additive in chocolate: can we find a natural replacement? School of Biosciences and School of Veterinary Medicine Postgraduate Symposium University of Nottingham, Jun 2019.

The Role of Surfactants in Chocolate Processing and Quality. School of Biosciences and School of Veterinary Medicine Postgraduate Symposium University of Nottingham, May 2017.

Poster presentations:

Price, R., Vieira, J. and Wolf, B. Replacing Polyglycerol Polyricinoleate (PGPR) in chocolate: research methods and preliminary results. School of Biosciences and School of Veterinary Medicine Postgraduate Symposium University of Nottingham, May 2018

Price, R., Wolf, B. and Vieira, J. Challenges to measuring the rheology of chocolate and chocolate models. British Society of Rheology Midwinter Meeting, Bristol, 2017.

Community engagement:

Science of Chocolate. Talk with practical activities for Y3 children at local school. Jan 2017 and 2019

1. Introduction

1.1. Context

This PhD project aims to address a challenge that the Food Industry faces more and more: to find natural ingredients to replace currently used additives to create a "clean label" product. Although the definition of a clean label product is yet to be defined and agreed upon by all stakeholders, Ingredion is credited with suggesting a three-point definition (Osborn, 2015):

- *Free from additives*: remove or replace food additives
- *Simple ingredient listing*: choose recognisable ingredients that do not sound chemical or artificial
- *Minimally processed*: process foods using traditional techniques that are understood by consumers and not perceived as being artificial.

The particular substance examined in detail in this PhD project is polyglycerol polyricinoleate (PGPR, E476), used in chocolate and confectionary, baked goods and margarine. Here, the functionality of PGPR in chocolate was the main focus.

Chocolate is a delicious treat enjoyed by many people around the world today. It is a composite material of particles of sugar, cocoa mass and sometimes milk powder dispersed in a crystallised fat phase, mainly of cocoa butter. Upon the melting of the fat phase, the solid composite transforms into a highly-filled suspension; this was the state of the chocolate of interest in this PhD research. Without proper processing and the addition of emulsifiers, the mouthfeel of chocolate can be gritty or pasty due to inappropriate rheology. The emulsifiers often used in chocolate are lecithin (E322), most commonly derived from the processing of soya bean oil, and PGPR. These two emulsifiers have different effects on the rheology of chocolate and together give manufacturers good control of the flow of the molten confection.

PGPR was initially patented in 1935 (Harris, 1935); however, it was first used in chocolate recipes in the UK only in 1952 following rat feeding trials and subsequent more stringent acute toxicity animal trials in the late 1950s. Further safety trials have continued with reviews by the Joint FAO/WHO Expert Committee on Food Additives and other national regulatory bodies (Wilson et al., 1998). Despite being generally recognised as safe for consumption and formed from natural ingredients, the processing required to create the PGPR molecules, see section 1.4.5, or perhaps merely its name, makes it objectionable to some consumers.

The desirable attribute that PGPR confers to chocolate is a reduced yield stress even when added at very low concentrations: 0.2-0.3% in most cases. This alteration to the yield stress impacts the manufacturing of chocolate as it flows through the pipes, is poured into moulds and is used for enrobing fillings, biscuits and ice cream. A graphic representation of the difference a reduction of yield stress makes to chocolate processing is shown in Figure 1.1. PGPR also has a beneficial effect in chocolate manufacture by sequestering any remaining moisture in the mixture (Rector, 2000) that would otherwise cause sugar crystals to aggregate and increase the viscosity of the chocolate (Afoakwa et al., 2007). This attribute is particularly important when molten chocolate is used for enrobing ice cream or when chocolate is made in humid conditions (Rector, 2000).

The effect of chocolate with inappropriate rheology also impacts the consumer. Chocolates with a high viscosity have a pasty mouthfeel, persisting in the mouth (Beckett, 2019). Sugar aggregates caused by excess moisture cause the chocolate to have a gritty mouthfeel (Krüger, 2009). With an increased yield value, the chocolate requires the consumer to provide more effort to melt, manipulate and swallow the sample (Ziegler and Hogg, 2009). This effect may or may not be desirable depending on the individual; however, this may be a problem for people with dysphagia.

Figure 1.1: The effect of the yield value when pouring chocolate. Left-hand side – yield value: 15.0 Pa, plastic viscosity: 3.5 Pa.s. Right-hand side – yield value: 5.0 Pa, plastic viscosity: 3.5 Pa.s (Palsgaard, Denmark).

There is no alternative food-grade emulsifier to PGPR that provides the same yield stress lowering performance, whether 'synthetic' or 'natural'. Research into a natural alternative has generally focussed on lipids extracted from oat seeds (Lindecrantz et al., 2015, Lloyd, 2020), and more recently, lipids from the chloroplasts of green leaves (Mohamad et al., 2020). These have both shown surface-active properties in the molecules of interest, with the ability to reduce the viscosity of chocolate or a chocolate model; however, they do not reduce the yield stress comparably to PGPR.

1.2. Objectives

The overall aim of this PhD research was to further the understanding of the unique yield stress lowering properties of PGPR in a chocolate model by considering molecular properties alongside physical material properties and exploiting these new insights to devise an alternative yield stress lowering emulsifier to PGPR from natural sources.

To this end, the specific project objectives were:

1.   Devise a methodology to determine the impact of PGPR on the yield stress of chocolate, using a chocolate model;

2.   Quantify yield stress effects of five commercially available PGPRs;

3.   Determine molecular characteristics of the PGPRs and highlight differences between them;

4.   Determine which PGPR characteristics are responsible for yield stress modification within chocolate;

5.   Exploit the new knowledge to propose novel natural lipid alternatives to PGPR;

6.   Assess selected alternatives for impact on yield stress compared with PGPR.

The hypotheses, linked to the objectives, tested in this research were:

1.   The observed differences between PGPRs in manufacturing can be determined as fact using rheological measurements and a chocolate model.

2.   There are differences in the molecular characteristics in the PGPRs, which can be ascertained using analytical techniques.

3.   The differences in the functionality relate to molecular differences in the PGPRs.

4.   There are natural molecules that reflect these molecular characteristics.

5.   These molecules can be extracted from leaves or other material, and they will have a yield stress reducing power akin to PGPR.

1.3. Structure of the thesis

At the start of this introductory chapter, the research context has been outlined. A summary of the purpose of this project and a list of objectives and hypotheses tested was given. There now follows an overview of relevant publications important to the current work in two sections – PGPR and leaf lipids.

The thesis then proceeds to the experimental work, starting with a brief chapter detailing the materials and methods used that apply to multiple chapters. If a method is specific to a single chapter, the method will only appear in that chapter. Chapter 3 describes the method development process for the chocolate model and rheological protocol, includes the justification that these procedures are robust and reliable, and details any limitations that must be considered. Chapter 4 outlines the results of the functionality assessment experiments of the PGPR samples performed using rheology. Interfacial tension measurements are used to begin to understand the differences between the PGPRs using the knowledge of emulsifiers at the oil-water interface and their behaviour in reverse micelles. Chapter 5 charts the methods used to characterise the molecular structure of the different PGPRs, discusses the findings from these results and identifies what this means for the discovery of a natural alternative. These experiments are more in-depth than in current literature and include an analysis of the fatty acid composition at the end of the PGPR acyl chains. This chapter also investigates how the regulations imposed on the PGPR manufacturers impact the possible size and character of the samples. This analysis may be of benefit to the manufacturers themselves as they attempt to improve their products. A natural alternative is proposed in chapter 6, and this, with chapter 7, summarise the methods used to generate the natural replacement. This molecule has never before been assessed for its surfactant effect in literature. Chapter 6 outlines the process and results of creating the proposed replacement using an enzymatic assay and applying this to the chocolate model. Chapter 7 delineates the outcome of attempting to compel

leaves to make the proposed replacement molecule by enforced stress conditions. In this chapter, an analysis of the lipid content of cocoa leaves, at around eight hours post-harvest, is reported for the first time to provide further information to a commercial enterprise wishing to use cocoa leaf lipid in a food product.

1.4. Literature review: Control of chocolate rheology with PGPR

1.4.1. Chocolate

Chocolate is a prized confection consumed worldwide, with Europe currently holding the largest share of the global chocolate market, valued at almost 54,000 million USD in 2020 (MordorIntelligence.com). Several large companies dominate the market, including Nestlé, Mars, Mondelez and Barry Callebaut; however, there has been increased interest from consumers in small artisanal chocolatiers. Vegan chocolate products and a desire for organic and fairly-traded ingredients have recently been big drivers in the chocolate market (MordorIntelligence.com).

Chocolate started as early as 1900 BC as a drink consumed by the Mokaya people in Mexico. It was astringent, fatty and rather offensive compared to the product enjoyed today. The eating chocolate was first presented to the public by Joseph Fry in 1847, but the invention of the conche by Rodolphe Lindt in 1879 created a smooth, better tasting chocolate (Beckett, 2019).

Chocolate starts as cocoa beans within a pod on the *Theobroma cacao* tree. The pods go through a fermentation process, after which the beans are dried and transported to the processing factory. Here, they are cleaned and roasted, and the shell is removed. The nibs contain around 55% cocoa butter, so a portion of the nibs are pressed to remove cocoa butter, leaving a cocoa press cake that may now contain between 8% and 24% fat. This press cake is ground to create cocoa powder for different products. The unpressed ground nibs are ground and mixed with sugar and dried milk particles (if used). The friction caused by the grinding process warms the mixture, and the cocoa butter within the nubs melts, causing the initial dry mixture to become liquid. It is then further milled to a particle size less than 30 μm (Beckett, 2019). This milling process substantially increases the surface area of the solid particles so that the liquid chocolate that entered the mill has changed to a dry, pasty

consistency. This mixture is transferred to a conche, where it is agitated and sheared for a number of hours, as specified in the recipe. An illustration of a conche is shown in Figure 1.2. The ground chocolate mass that enters the conche contains most of the fat of the finished chocolate; however, the fat must be melted, released from aggregates and smeared over all the surfaces of the solid particles (Beckett et al., 2017). Emulsifiers are added towards the end of the conching process with any additional cocoa butter as specified in the recipe.

The structure of the finished product can be thought of as a concentrated suspension of fine solid particles of cocoa, sugar and milk powder (if used), in a continuous fat phase predominantly composed of cocoa butter, small amounts of other fats (if used) and emulsifiers.
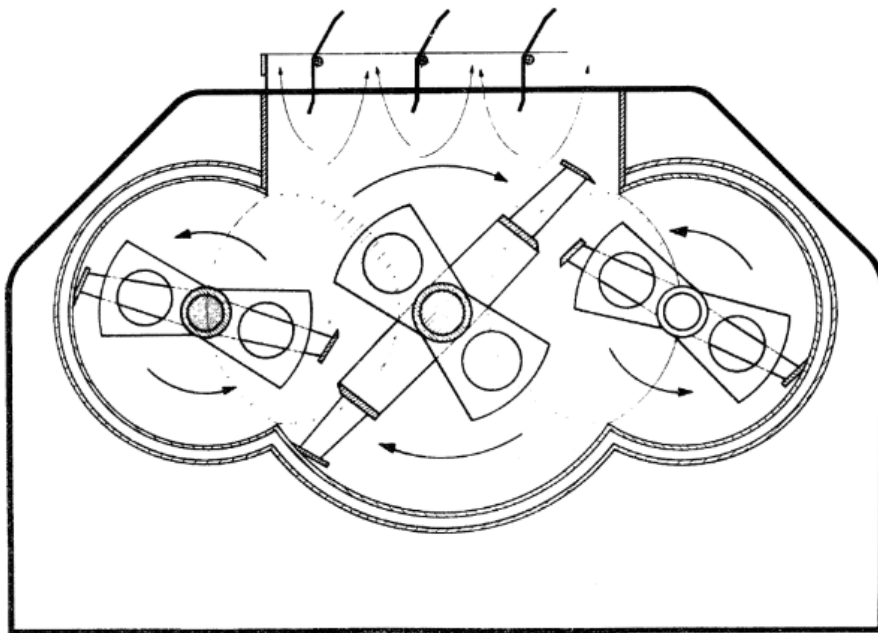
Figure 1.2: Diagram of the Frisse conche. [Republished with permission of John Wiley & Sons Ltd, from Ch 9. Conching, Beckett, S.T. from Industrial Chocolate Manufacture and Use: Fourth Edition Ed Beckett, S.T. 2009; permission conveyed through Copyright Clearance Center, Inc.]

1.4.2. Chocolate rheology

The rheological properties of chocolate are affected by its final mixing stage in the conche and the addition of emulsifiers, see Figure 1.2; the time, shear, and temperature applied to the chocolate depend on the recipe. The conching period develops flavour, particularly the removal of acidic off-flavours, and is also used to optimise the flow properties of the chocolate for the purpose to which the chocolate will be used. The yield stress is related to the energy required to start the molten chocolate flowing, for example, when pouring. It is crucial during coating a biscuit or enrobing centres. A high yield stress may be required to make chocolate chips to put in cookies; however, it can cause problems during enrobing. A low yield stress will give a thin coating on a biscuit and is useful for low-density centres in chocolate panning (e.g. Maltesers); however, it can slip on the higher density centres resulting in bare patches (Aebi, 2009). The plastic viscosity is related to the energy required to keep the chocolate moving once the flow has commenced. Plastic deformation refers to a loss of mechanical energy, and the deformation imposed remains on the material after the stress is removed. A high viscosity will give enrobed chocolates a thicker coating (increased cost to manufacturers), and a low viscosity will provide a thin coat (which may risk incomplete coverage). The flavour is also impacted by the viscosity of the chocolate in the mouth. The amount of time it takes for the particles to reach the taste receptors on the tongue, longer with a more viscous product, will determine flavour perception (Beckett, 2019).

The rheology of chocolate is also important in the manufacturing plant. When specifying a chocolate delivery system, the yield stress, viscosity and temperature should be considered. The higher the viscosity, the higher the internal friction imposed and the higher the force, or shear, required to pump the chocolate. Attempting to apply a chocolate batch to the system with a viscosity or yield stress value for which it is not designed can cause considerable problems (Walker, 2009).

1.4.3. Emulsifier action

Emulsifiers are vital compounds available to the chocolate manufacturer to achieve the correct rheology for the purpose for which they wish to use their chocolate. The key molecular characteristic of an emulsifying agent is that it is amphiphilic, which means that it includes a hydrophobic portion, often a long-chain fatty acid, and a hydrophilic portion that can be charged or uncharged. The molecule adsorbs at the interface between the hydrophobic oil phase or air, in the case of foams, and the hydrophilic liquid or solid. This action allows a stable dispersion of foams (gas bubbles suspended in liquid), emulsions (liquid drops suspended in liquid) or suspensions (solid particles suspended in liquid) to occur where it would not otherwise be possible (Stauffer, 2005). Emulsion stability is a term used to describe the ability of the emulsion to resist changes to its physical characteristics over time. Emulsions are prone to instabilities, such as are shown in figure Figure 1.3. Creaming and sedimentation are forms of gravitational sedimentation, and the direction of movement of the droplet depends on its density compared to the surrounding liquid. Flocculation and coalescence are both types of droplet aggregation: the difference being that droplets in the flocs maintain their individual integrity, whereas drops merge in coalescence. Ostwald ripening occurs where mass transport of the dispersed phase (within the drop) occurs through the intervening continuous phase resulting in large droplets growing larger at the expense of the smaller ones. Most food emulsions are formed from oil and water, which have a negligible mass transport rate because the mutual solubilities of triacylglycerol and water are so low. However, it can occur with some more water-soluble lipids or where alcohol is added to the aqueous phase (McClements, 2015).

A phenomenon known as depletion interaction is often responsible for some of the emulsion instabilities mentioned. The presence of small colloidal particles, e.g. surfactant micelles, polymer molecules, within the continuous phase causes an

attractive interaction between the drops that promotes emulsion instability. The colloidal particles are excluded from a narrow region around each particle. The concentration of colloidal particles is essentially zero in this depletion zone, while it is finite in the rest of the continuous phase. This results in an osmotic potential difference that causes the solvent to move from the depletion zone to the surrounding phase to dilute the colloidal particles and reduce the concentration gradient. The particles, therefore, move closer together, and the instabilities occur (McClements, 2015).
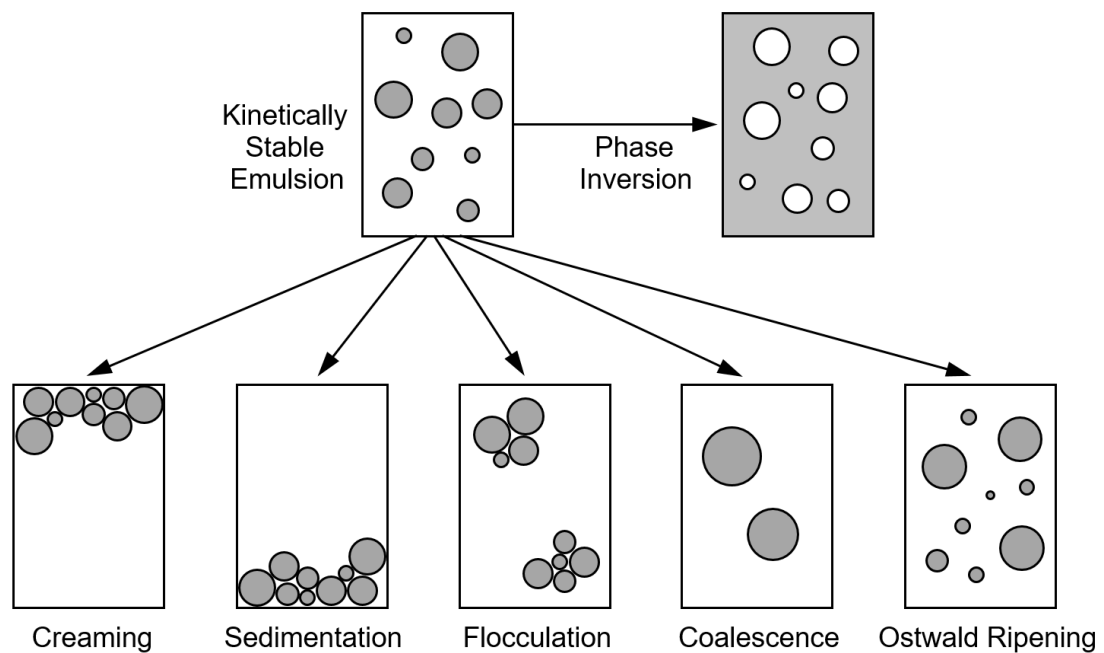
Figure 1.3: Food emulsions may become unstable through a variety of physical mechanisms, including creaming, sedimentation, flocculation, Ostwald ripening, coalescence and phase inversion, based on a figure by McClements (2015)

The system considered in this PhD is chocolate. As already stated, chocolate is a concentrated suspension of solid particles, including sugar, in a fat phase formed primarily of cocoa butter. Sugar, being hydrophilic, does not disperse well in its hydrophobic surroundings and tends to form aggregates. The purpose of emulsifiers in chocolate is to aid this dispersion: the hydrophilic head groups adsorb to the sugar, and the hydrophobic tail groups extend into the oil/fat. They increase the wettability of the dispersed particles, predominantly the sugar, by increasing the kinetic stability

between the particles surface and the continuous phase, which aids their distribution (Johansson and Bergenståhl, 1992a). The presence of the emulsifier displaces fat immobilised at the sugar surface, which increases the fat in the mobile phase (Christiansen, 2015). Perhaps more importantly, the emulsifier changes the hydrophilicity of the surface of the sugar particles, and it now acts as if it is hydrophobic. This change prevents aggregation by steric repulsion, preventing large particles in the chocolate that would feel gritty in the mouth. Any cocoa butter that would otherwise be trapped within the aggregate will join the fat available in the mobile phase. PGPR is one of these emulsifiers, but other types of emulsifiers are also found in commercial chocolate. These include lecithin (E 322) and ammonium phosphatides (E 442), although the most frequently applied is lecithin alone or in combination with PGPR.

Figure 1.4 shows a representation of PGPR and phosphatidyl choline, a phospholipid found in lecithin, as a visual comparison of the structures.
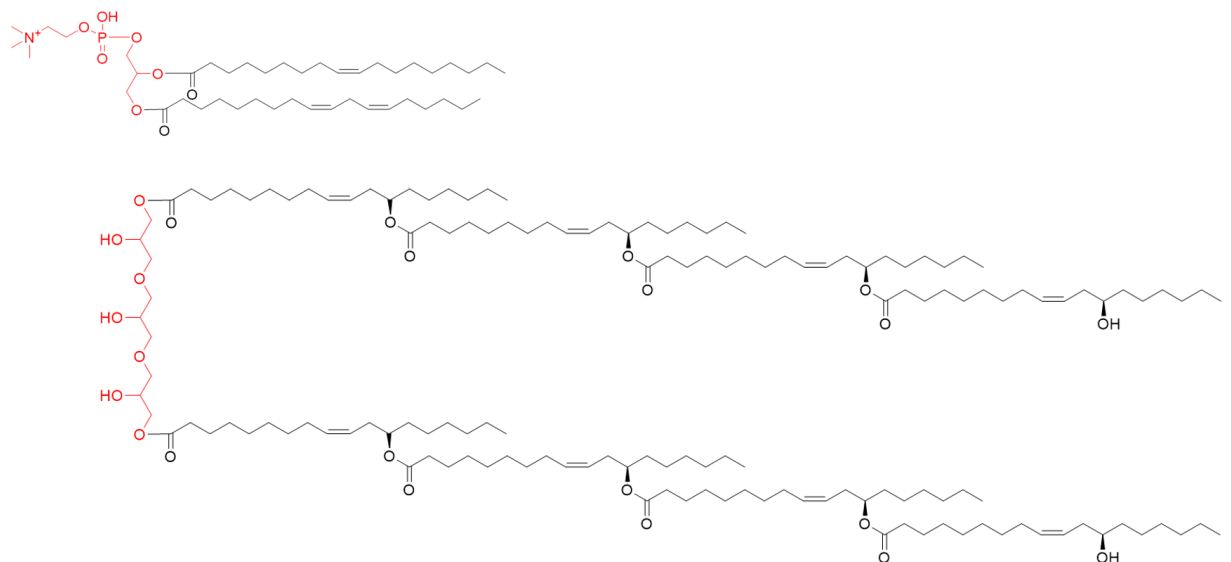
Figure 1.4: Structural representation of phosphatidyl choline (a phospholipid found in lecithin), top, and PGPR, bottom. The hydrophilic portions are highlighted in red, whilst the hydrophobic portion is in black.

1.4.4. PGPR and lecithin

The complementary action of lecithin and PGPR on the rheological properties of chocolate is well-established (Rector, 2000, Schantz and Rohm, 2005, Bamford et al., 1970). Lecithin, a collective term for phospholipid-rich extracts from plants such as soybean, is primarily added to lower the high-shear viscosity of chocolate and can save on the most expensive chocolate ingredient: cocoa butter. Minifie (1980) showed that including 0.5% of lecithin in a chocolate formulation had the same viscosity lowering effect as an additional 5% fat. They also established that the effect of the emulsifier was primarily on the sugar particles. However, the application of lecithin at levels exceeding 0.3-0.5% (depending on the formulation) leads to reverse micelle formation or multi-layer adsorption on the sugar particles, which causes an undesirable increase in the yield stress of the chocolate (Fincke, 1965, Vernier, 1997).

In contrast, PGPR has a considerable yield stress lowering effect, unique amongst food-grade emulsifiers (Christiansen, 2015), and a smaller impact on the viscosity than lecithin (Harris, 1968). Adding just 0.1% (total weight) of PGPR to a chocolate formulation has been shown to affect a yield stress reduction equivalent to the addition of 3% of extra cocoa butter (Rector, 2000). If PGPR is added at 1% (total weight), the yield value will become zero (Bamford et al., 1970).

1.4.4.1. PGPR and lecithin at the sugar/oil interface

Lecithin is an amphiphilic molecule that tightly adsorbs to the surface of the sugar (Minifie, 1980). Its hydrophilic head adsorbs to the sugar while its hydrophobic tail extends into the cocoa butter, making the sugar crystal appear to be hydrophobic (Dedinaite and Campbell, 2000). It appears that lecithin releases more immobilised fat than PGPR and that this action is more effective for reducing the viscosity of the chocolate (Heinz and Franke, 2010).

PGPR is also an amphiphilic molecule, but its action at the sugar-oil interface is less well described. It has been suggested that PGPR provides a better steric barrier than lecithin in the suspensions due to the longer acyl chains (Vernier, 1997). Using a surface force apparatus, it has been demonstrated that the steric barrier of PGPR consists of an outer region of about 75 Å from the surface, which is dilute concerning polymer segments, and a dense inner area (about 22 Å – approximately one fatty acid length) close to the surface of the sugar particles (Dedinaite and Campbell, 2000). Middendorf et al. (2015) used atomic force microscopy and scanning electron microscopy to investigate the surface of sugar crystals that had been subjected to immersion in cocoa butter containing either PGPR and lecithin, followed by grinding in a ball mill. They showed that the amount of PGPR on the surface of the sugar was only 0.18 mg/m^2 compared to 2.69 mg/m^2 for lecithin, but that the interfacial layer created by PGPR consisted of at least 83% of cocoa butter. They concluded that instead of releasing immobilised fat, the PGPR interacts with cocoa butter on the surface of the sugar crystals to form "pillow-like deposits" and argued that these structures act as a buffer between the particles separating them by steric hindrance. This means that the outer layer of the steric barrier formed by PGPR on the surface of sugar consists of mostly entrapped cocoa butter triacyl-glycerols (TAGs). Another study has shown that the adsorption of lecithin or PGPR at the sugar surface decreases the acidic character of the sugar by a similar amount. Decreasing the acidic character makes the surface more lipophilic, causing an increase in the fluidity of fat-based sugar suspensions like chocolate. However, they also found that PGPR increases the basic character of the sugar surface more than lecithin. They hypothesise that the oxygen atoms in the polyricinoleate are important in this action but do not go so far as to suggest this is the reason for the yield stress lowering action provided by PGPR (Rousset et al., 2002).

1.4.4.2. PGPR and lecithin at high concentrations in the continuous phase

At high concentrations, e.g. above 0.5% (wt) in chocolate, lecithin causes an increase in the yield stress of the chocolate because of reverse micelle formation and multi-layer adsorption (Bamford et al., 1970, Vernier, 1997). However, this is not the case with PGPR, where increasing the concentration above 0.5% (wt) in chocolate eliminates the yield stress. There are different views within the literature about whether PGPR forms reverse micelles at higher concentrations or whether it merely dissolves in the oil and adds to the total volume (Vernier, 1997).

1.4.5. Synthesis of polyglycerol polyricinoleate

PGPR is synthesised by first hydrolysing the fatty acids from the triacylglycerols in castor oil (80-90% are purported to be ricinoleic acid). These fatty acids are then condensed into polyricinoleate chains, formed with estolide bonds connecting the acid part of one fatty acid to the hydroxyl group on a ricinoleic acid. The polyglycerol chains are created by condensing glycerol and forming ether bonds, and free glycerols are removed via distillation at the end of the reaction. Finally, the polyglycerols are added to the polyricinoleates, a condensation reaction occurs, and esterification links the two groups of chains together (Wilson et al., 1998). Other types of fatty acids present in the castor oil will act as caps for the chains halting the extension process (Isbell, 2011, Zerkowski, 2008). This hypothetically means that a PGPR made from a fatty acid feedstock with more "non-ricinolate" fatty acids will result in shorter polyricinoleate chains. The length of the polyricinoleate and polyglycerol chains in the PGPR can also be changed by adjusting the temperature or pressure conditions of the condensation steps of the fatty acid and glycerol feed stocks, respectively. Thus, the commercial process forms a mixture of different-sized molecules based on different quantities of glycerol units and ricinoleic acid/fatty acid units. Manufacturers seem to make PGPR by following a production method that yields a batch with the desired

properties rather than designing the molecules in detail. Figure 1.5 shows a diagrammatic illustration of a molecule within a PGPR sample.
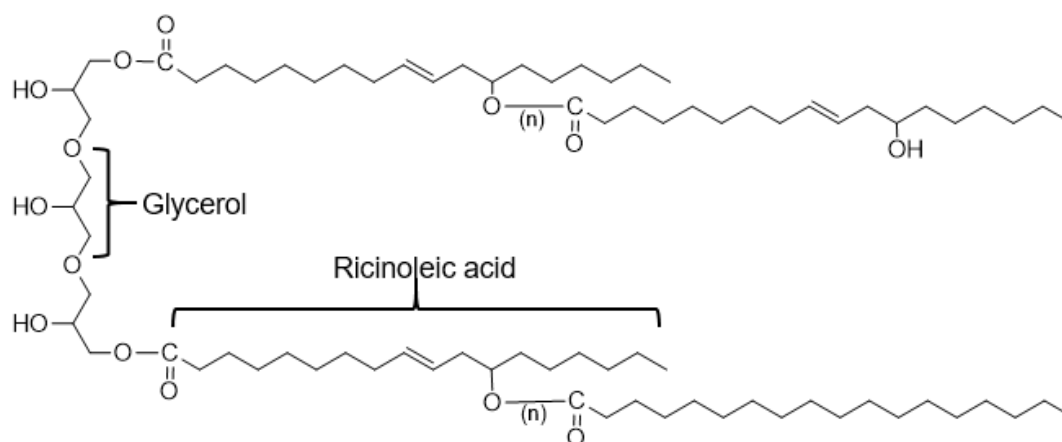
Figure 1.5: The molecular structure of Polyglycerol Polyricinoleate. "n" indicates that a number of ricinoleic acids can be included in this chain. In Wilson et al. (1998), the most abundant length of the polyricinoleate chain is 5, meaning that n=3. The structure also illustrates that the terminal fatty acid on the polyricinoleate chain can be a ricinoleic acid or another fatty acid; here, stearic acid is shown.

In a review of PGPR, Bastida-Rodriguez (2013) states that the average number of glycerol molecules in the polyglycerol chain is three and the average number of fatty acids in each of the polyricinoleate chains is between five and eight. A PGPR molecule with three glycerol molecules and ten ricinoleic acid molecules (i.e. two chains of a five-chain polyricinoleate) would have a molar weight of 3045 g/mol. Personal communication with the manufacturer of one of the PGPR samples used in this research, Kerry, indicated that the average molecular mass of Admul WOL 1408 is 2000 g/mol. Electrospray Ionization-Mass Spectrometry (ESI-MS) was used to measure two PGPR samples (different samples from the five used in this PhD), and molecular weight values averaging at around 1170 g/mol were obtained, ranging between 400 and 2000 g/mol (Orfanakis et al., 2012). These differences show that there is still a gap of knowledge concerning the precise molecular characteristics of PGPR.

PGPR is a highly regulated substance as it is used in food. The Committee for the European Community (2008) and the Joint FAO/WHO Expert Committee on Food Additives (1992) both specify that its acid value should be no more than 6 mg KOH/g, and hydroxyl value should be between 80-100 mg KOH/g. The acid measured here would most likely come from any free fatty acids remaining in the sample. During the final stage of PGPR manufacture, the acid value is tested regularly. The batch is said to be finished when the acid value is at a 'suitable' value for the recipe (Wilson et al., 1998), but this value will be below 6 mg KOH/g. The hydroxyl value is a measure of the number of hydroxyl (-OH) groups on the molecule. These groups are present on the polyglycerol chain and, if the end fatty acid of the polyricinoleate chain is ricinoleate, this will also contain a hydroxyl group, as shown in Figure 1.5. The regulators also require the manufacturer to control the polyglycerol chain length; the mixture of molecules within the sample should be composed of at least 75 % of di-,tri- and tetraglycerols and not more than 10 % polyglycerols equal to or higher than heptaglycerol. The Food Chemicals Codex (FCC, 2016) adds that the iodine level should be 72-103 g I/100g, and the saponification value should be 170-210 mg KOH/g. The iodine value is a measure of the unsaturation, or the number of olefinic double bonds, present. Ricinoleate has one double bond; see Figure 1.5. One molecule of iodine (I_2) reacts with one double bond. The iodine value relates the number of double bonds to the molecular weight of the molecule. The saponification value reflects the number of fatty acids in a molecule compared with the size of the entire molecule.

1.4.6. Research into alternatives to PGPR

In 1997, Vernier (1997) researched PGPR alternatives and found that other synthetic emulsifiers that reduced the yield stress were those that had long tail groups. This research concluded that polyglycerol esters of fatty acids with a low hydrophile-

lipophile balance (a number assigned to an emulsifier to reflect the balance of the size and strength of the hydrophilic and the hydrophobic groups of the emulsifier – a low value reflects a large hydrophobic portion with a small hydrophilic portion) afforded the best yield stress reduction and that a strong interaction of the head group with the sugar surface was crucial for this rheological modification. When it came to natural alternatives, he found that an extract from oats (*Avena sativa*) provided some reduction in yield stress, along with a reduction of viscosity similar to lecithin. This yield stress reducing quality was thought to be due to the high amount of polar lipids found in oat extract, plus minor amounts of several hydroxy and epoxy FAs in the lipids and a galactolipid where one of the fatty acids was esterified to 15-hydroxy 18:2 Δ9,12 (avenoleic acid) (Ben Halima et al., 2015). This molecule is shown in Figure 1.6. However, high concentrations of oat extract were required to achieve this change: the addition of 4.6 % oat extract reduced the yield stress to 0.8 Pa.s, whereas 0.5% PGPR reduced it to 0.1 Pa.s. In addition, although this action occurred with a sugar-in-oil chocolate model, when the oat extract was trialled in a chocolate sample, a similar yield stress reduction was not found. The oat extract contained a large concentration of triacylglycerols that were postulated to contribute to the viscosity lowering ability of the oat extract; however, the additional oil component in the continuous phase did not affect the yield stress. Vernier also extracted lipids from other plant materials, including wheat bran, rice flour, maize, chick peas, lentils and barley, but no lipid extract gave a better result than oat extract (Vernier, 1997).
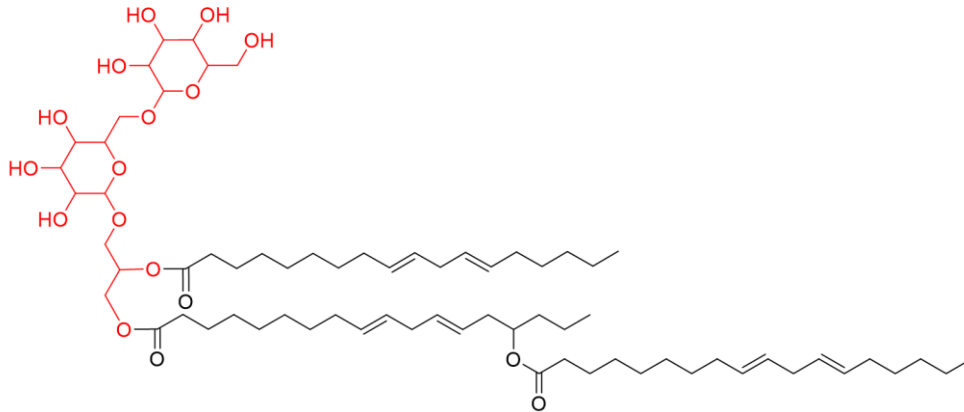
Figure 1.6: Digalactosyl diacylglycerol estolide with 15(R)-hydroxy linoleic acid (avenoleic acid) found in the extract of oat (A. sativa).

The research into oat oil (extract) as a replacement for PGPR was continued by the Swedish Oat Fibre organisation with some success (Prothon, 2017, Lindecrantz et al., 2015). Oat oil does show a good oil-in-water emulsification effect (Kaimainen et al., 2012), and the manufacturer has claimed it has a healthy lipid profile for human nutrition, given the predominance of α-linolenic acid, an omega-3 polyunsaturated fatty acid (Ben Halima et al., 2015, Singh et al., 2013). It can be extracted under mild conditions: ethanol or isopropanol and methanol at room temperature (Evans et al., 1991), but oat oil has not been shown to match the yield stress reducing power of PGPR. Lloyd (2020) compared the rheology modifying action of PGPR, oat extract, and soya lecithin on chocolate to be used in Easter Eggs at Nestlé Confectionery UK & Ireland. The author found that oat extract and soya lecithin had a more similar effect on chocolate viscosity than PGPR; however, the oat extract did not cause the increase in yield stress at higher concentrations (over 0.7%) that lecithin is known to instigate (Lloyd, 2020). Vernier (1997) also saw this effect, which may indicate that oat extract does not form multi-layers at the surface of the sugar at high concentrations.

Inspired by the fact that oat oil contains high levels of galactolipids (Sahasrabudhe, 1979), Mohamad et al. (2020) decided to assess the lipids found in spinach leaves

and their chloroplasts, where the galactolipids are concentrated, as a rheology modifier, perhaps to rival PGPR. They measured the yield stress reduction produced by the spinach lipids from both extracts, lecithin and PGPR, at 0.1, 0.3, 0.5, and 0.7 % (wt) in a sugar-in-sunflower oil chocolate model formulated with a sugar fraction of 40, 45 and 50 wt%. They found that the reduction caused by the spinach lipids was not significantly different from PGPR ($p < 0.05$) in all cases apart from a few at the 40 % (wt) sugar in oil formulation (0.3 and 0.7 % concentration of emulsifier). The author did not discuss these specific differences but noted that PGPR did not decrease the yield stress as much as expected compared to lecithin, which might have been due to the relatively low phase volumes employed in these experiments. As the differences between PGPR are spinach lipids are in the lowest phase volume samples, this may have produced the differences seen here. However, when spinach lipids were added to chocolate, it functioned more like lecithin but with a slightly greater impact on the yield stress reduction (Mohamad, 2017).

An alternative method of dealing with the consumer rejection of PGPR may be to retain it in chocolate manufacture but replace the use of solvents, high temperatures and pressures during its production with a 'green' method. Resins have been used to immobilise lipase enzymes that generate PGPR molecules in a one-step process from the glycerol and ricinoleic acid substrates. The PGPR formed has been shown to meet the requirements of the food industry regulators (Ortega-Requena et al., 2014, Bódalo et al., 2009, Gómez et al., 2011, Ortega-Requena et al., 2014). The latest development involved optimising the resins used to immobilise the enzymes to aid the separation of the PGPR from the resin at the end of production (Ortega-Requena et al., 2019). This research is ongoing, and scaling up is planned; currently, only around 32.5 g of PGPR is created after 159 hours in a vacuum reactor. Research into whether this new manufacturing method will improve customer perception of the product also needs to be conducted.

1.4.7. Rheological methods to measure yield stress

1.4.7.1. Introduction to Rheology

Rheology is the study of the flow and deformation of materials. Some materials flow easily, like water, and show low resistance to deformation and are known as ideally viscous. Other materials deform only under a strongly applied force and return to their original shape after deformation, like a tall metal structure under strong winds; these are known as ideally elastic. Materials that fall between these two extremes are said to show viscoelastic behaviour.

1.4.7.2. Terms used in rheology

The two-plates model shown in Figure 1.7 can be used to define the parameters needed for a description of flow behaviour. The lower plate is stationary with a velocity of 0, while the upper plate, with area A, is set in motion with a force F and moves parallel to the lower plate with a velocity v. Between the plates is a distance h, and the sample is sheared within this gap.
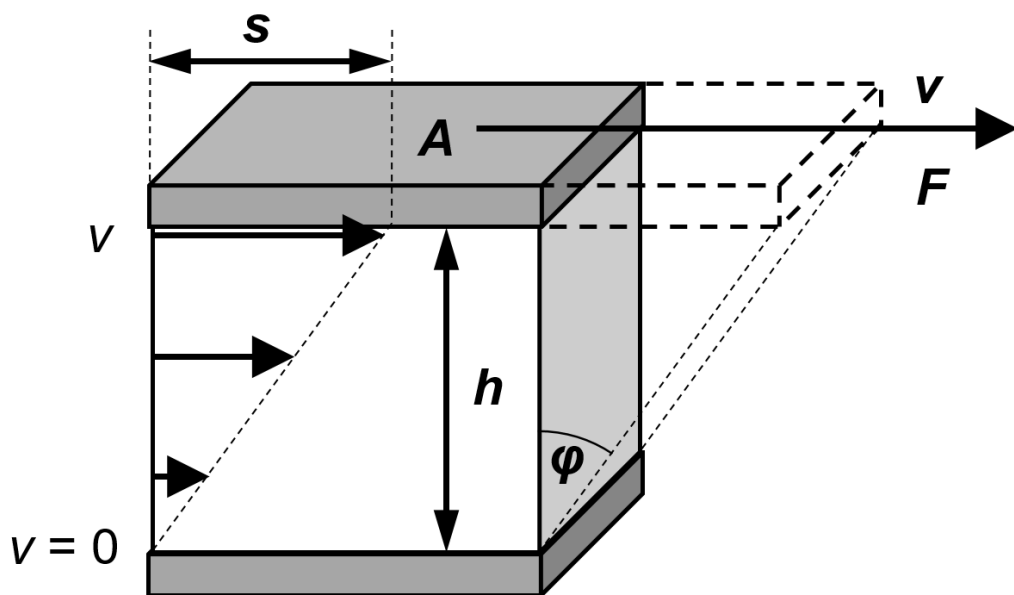
Figure 1.7: The two-plates model for shear tests, based on Mezger, 2014.

Two assumptions are made in the two-plates model: that there are laminar flow conditions and that the sample shows adhesion to the walls. Laminar flow is pictorially described in Figure 1.8. For laminar flow, the velocity difference between all neighbouring layers is the same value: dv = const. All layers are assumed to have the same thickness: dh = const. Therefore, there is a constant shear rate everywhere between the plates using the Two-Plates-model.
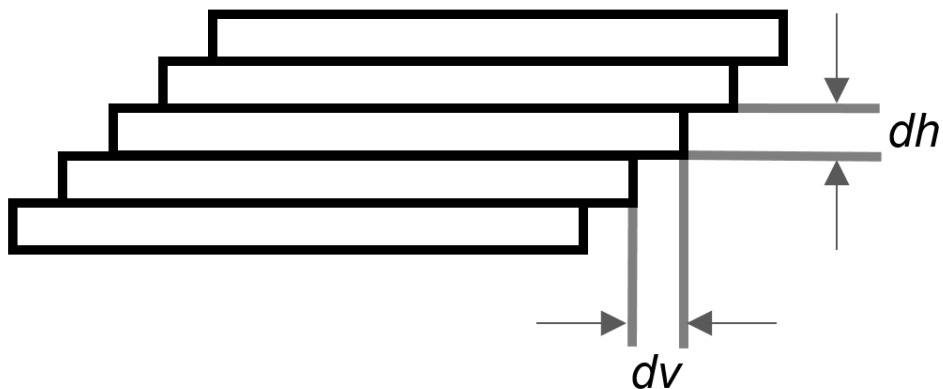
Figure 1.8: Laminar flow in the form of planar fluid layers, based on Mezger, 2014. dv is an infinitely small velocity difference, and dh is an infinitely small thickness of a single flowing layer of the sample between the plates.

If the sample does not show adhesion to the walls, the system is said to show slip: this is discussed later in section 1.4.7.9. There is a critical upper limit between laminar and turbulent flow conditions in the gap. Exceeding this limit by imposing a high shear rate or stress can cause secondary flow effects or turbulent flow behaviour because of centrifugal or inertial forces in the material. These secondary effects may display in the data as an increase in shear stress and viscosity at the higher end of the measurement, and the sample may erroneously appear to display shear thickening behaviour (Mezger, 2011b).

Shear stress

Shear stress is defined in equation 1.1 and has the unit Pa.

$$\tau = {F}/{A}$$ (Eq. 1.1)

where τ is the shear stress, F is the shear force [N], and A is the shear area [m²].

Shear strain rate

Shear strain rate is the slope of the velocity profile and is defined for the two plates theory in equation 1.2. It has the unit s⁻¹.

$$\dot{\gamma} = {v}/{h}$$ (Eq. 1.2)

where $\dot{\gamma}$ is the shear rate, v is the velocity [m.s⁻¹], and h [m] is the gap between the plates.

Viscosity

Viscosity is defined in equation 1.3 and has the unit Pa.s.

$$\eta = {\tau}/{\dot{\gamma}}$$ (Eq. 1.3)

where η is the viscosity, τ is the shear stress, and $\dot{\gamma}$ is the shear rate.

Shear strain or shear deformation

Shear strain or deformation is defined in equation 1.4 and is a dimensionless number, normally given as a percentage because deformation values are often small.

$$\gamma = {s}/{h}$$ (Eq. 1.4)

where γ is the shear strain, s is the deflection path [m] and h is the shear gap [m].

Shear modulus

Shear modulus (G) is defined in equation 1.4 and has the unit Pa.

$$G = {^{\tau}/_{\gamma}}$$ (Eq. 1.5)

This is the law of elasticity or Hooke's law: for solid matters, force is proportional to deformation. The higher the G value, the stiffer the material (Mezger, 2015)

1.4.7.3. Shear rheometer

There are two ways to perform rotational rheological tests with a shear rheometer – controlled by shear stress or controlled by shear rate. When performing a measurement that is controlled by the shear stress, the rheometer pre-sets a certain current that correlates to a defined torque M [Nm], which acts through the measuring system on the sample. The sensor within the rheometer measures the resulting deflection angle φ [rad]. The corresponding time interval is also recorded and, with the corresponding angle, the rotational speed n [min^{-1}] can be calculated. The raw data is dependent on the friction of the rheometer bearing and the inertia of the motor, measuring system and sample, which must be corrected by the electric controller (Mezger, 2011c). The raw data is also correlated to the geometry of the measuring system, and so the supplier provides two conversion factors for each measuring system that are used by the rheometer software. One enables the conversion of torque into shear stress τ [Pa], and the other enables the conversion of rotational speed into shear rate $\dot{\gamma}$ [s^{-1}] (Mezger, 2015). All other parameters, such as viscosity, are not measured but calculated.

Similarly, there are two ways to perform oscillatory rheological tests with a shear rheometer – controlled by shear strain or controlled by shear stress. When the experiment is controlled by shear strain, the deflection angle φ is pre-set, and the torque M and phase shift δ are measured. The rheometer calculates the strain γ and

reports the shear stress τ. When an oscillatory measurement is controlled by shear stress, the torque M is pre-set, and the deflection angle ϕ and phase shift δ are measured. The rheometer calculates the shear stress τ and reports the strain γ.

1.4.7.4. *Complex shear modulus, elastic (storage) modulus and viscous (loss)*
modulus

Complex shear modulus (G*) is defined in equation 1.6 and has the unit Pa.

$$G^* = {^{\tau_A}}\!/_{\gamma_A}$$
(Eq. 1.6)

where τ_A is the shear stress amplitude [Pa] and γ_A is the strain amplitude [%].

The rheometer can measure these parameters during an oscillatory experiment and obtain the G* value. The system also knows the phase shift δ value, which is the time lag between the pre-set and the resulting oscillation movement. Figure 1.9 shows a vector diagram that is used to explain how the rheometer separates the complex shear modulus into the elastic modulus (G'), to describe the solid-state behaviour of the sample, and the viscous modulus (G"), to describe the liquid-state behaviour of the sample.
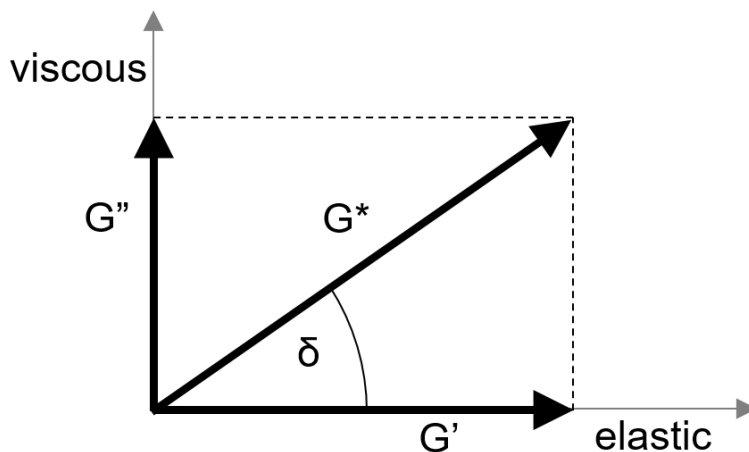
Figure 1.9: Vector diagram illustrating the relationship between complex shear modulus G, elastic modulus G' and viscous modulus G".*

Measuring systems (MS)

Different measurement tools are available to a rheologist in the form of geometries. The three major types are the concentric cylinder, the cone and plate and the parallel plate are illustrated in Figure 1.10. The cone & plate measuring systems are suitable for all types of fluids; however, for suspensions, it has a maximum particle size based on the gap at the tip of the cone. The parallel plate measuring systems are used to test more viscous samples, such as pastes, gels, or soft solids. The concentric cylinder measuring systems are commonly used for tests on low-viscosity liquids (Mezger, 2015). The main types of measuring systems to consider with the concentric cylinder geometry are the bob and the vane, but other types include discs, pins, paddles, and stirrers. For more information on these types, see The Rheology Handbook (Mezger, 2014). Some photos of examples of the geometries are given in Figure 1.11. The diameter of the cone or plate is 25 mm or 50 mm. The parallel plate and concentric cylinder systems are most often used if serration or sandblasting are required to roughen the plate to prevent slip, see section 1.4.7.9.
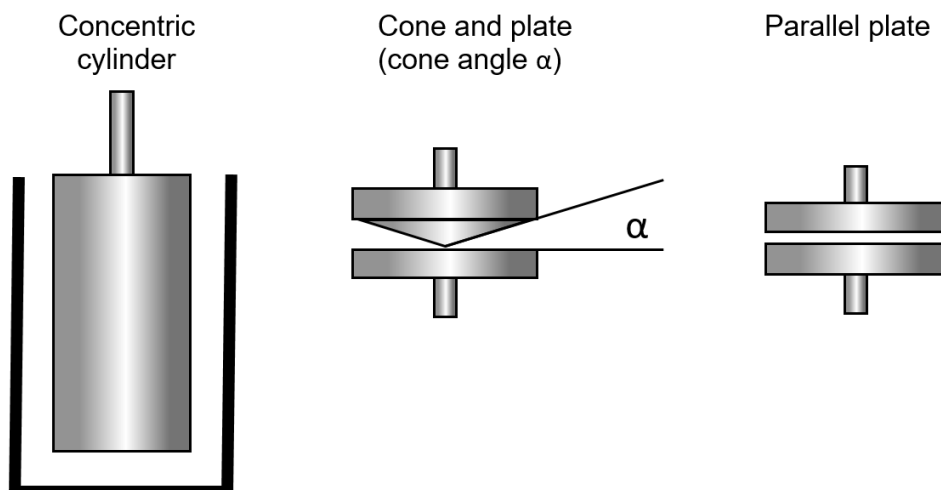
Figure 1.10: Illustration of the three main types of geometry for a rheometer. The cone and plate geometry has an additional parameter which the rheometers software uses in its calculations – the angle of the cone.

Figure 1.11: Photos of some measuring systems (MS). The top photo shows two 50 mm diameter cone MS and one 25 mm diameter plate MS. The left-hand geometry has a black coating that means it can be used for Tru-Gap measurements – the rheometer can adjust the gap during extreme temperature ramp measurements to ensure that the gap remains the same even if the metal expands. The middle cone has a smooth surface, and the 25 mm plate is serrated. The bottom left photo shows a smooth bob, serrated bob and the vane. The bottom right photo shows a starch stirrer.

1.4.7.6.   Shear dependent viscoelastic behaviour

Different types of flow are obtained when the shear rate or shear stress increase and can be shown via a flow curve or viscosity function, see Figure 1.12. Ideally viscous liquids show no change in viscosity when increasing shear rates or stress levels are applied. Materials where the viscosity decreases with increasing shear rate or stress levels are known as shear-thinning. Those where the viscosity increases with increasing shear rate or stress levels are known as shear-thickening.
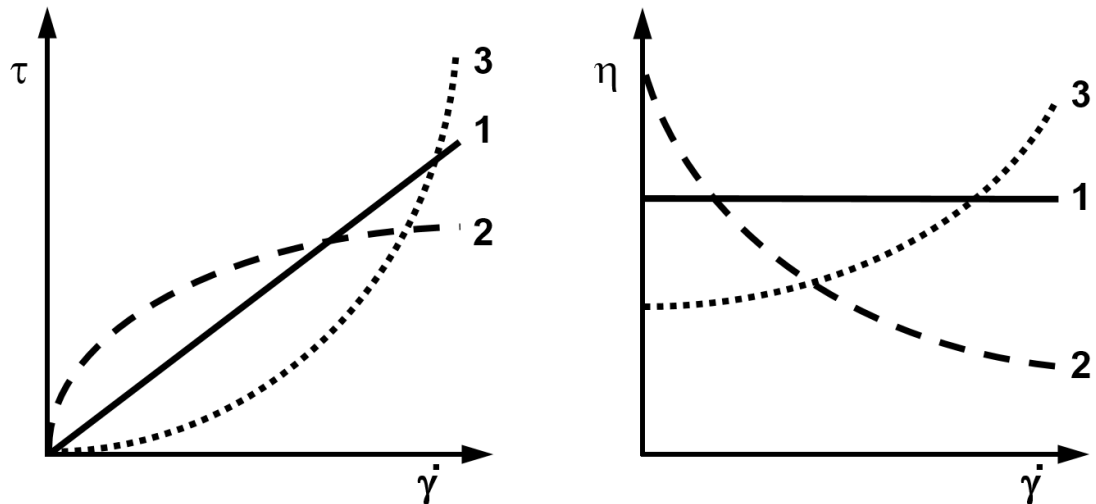
Figure 1.12: Flow curves (left) and viscosity functions (right) showing (1) ideally viscous, (2) shear-thinning, (3) shear-thickening behaviour, based on Mezger, 2014.

1.4.7.7.　Yield stress

A material that has a yield stress starts to flow only if the external forces applied to it are stronger than the material's own internal network of bonds. These bonds are intermolecular forces, for example, dipole-dipole interactions and can even include hydrogen bonds. If levels of shear below the yield stress point are applied, elastic deformation behaviour occurs; the sample can return completely to its original shape when the stress has been removed. Levels of shear above the yield stress point will cause the bonds to break, which may reform upon removal of the shear, and the material will take on viscous characteristics (Mezger, 2017). In other words, applied to chocolate, the yield stress is the point at which the mechanical properties of chocolate alter dramatically from solid-like behaviour to liquid-like behaviour due to the change in shear stress applied to it (Barnes, 1999a).

1.4.7.8.　Measuring yield stress in chocolate

Commonly, the yield stress is measured using rheological methods, such as the application of unidirectional or oscillatory shear. The yield stress value of any given

system measured by a rheometer is impacted by factors such as the mechanical treatment of the sample before rheological measurement, the rheometer's sensitivity, the geometries used, the rheometry protocol and the mathematical model used to evaluate the data and calculate the yield stress value (Dinkgreve et al., 2016, Fernandes et al., 2013, Baker et al., 2006).

To minimise or even eliminate the effect of the treatment of the sample before measurement, known as the "sample history", on the results of the rheological measurement, many protocols include a "pre-shear" step to provide a consistent sample history; for example, 10-15 min at 5 s^{-1} is specified in the standard quality control (QC) chocolate rheology method (IOCCC, 2000). This protocol resulted from a round-robin method development using different laboratories to evaluate the method (Servais et al., 2003). The complete method is described in detail in section 3.2.2. An alternative approach is to start at high unidirectional shear to erase the sample history and then reduce the shear until the yield stress point is reached. This method has previously been applied to chocolate using a shear rate controlled protocol both with a pre-shear step (Dinkgreve et al., 2016) and omitting pre-shear (Arnold et al., 2013).

Unidirectional ramp protocols and bi-directional oscillatory protocols, as well as creep tests, have been used in the past, see Table 1.1. Historically, most protocols that have been proposed are rate controlled rather than stress controlled. However, in this PhD research, shear stress was chosen to control the rheological protocol; this choice is discussed further in section 3.2.2.

All measuring systems discussed in section 1.4.7.5 have been used to measure chocolate viscosity and yield stress, and a review of the literature is shown in Table 1.1. The concentric cylinder geometry has been recommended for use in chocolate viscosity measurements when good laboratory agreement is required (Aeschlimann and Beckett, 2000) and so is often used with chocolate research.

Rheological measurements are often designed to replicate, as much as possible, the conditions that the sample would undergo during processing. During conching, chocolate undergoes very high shear; between 1,000 to 10^7 s^{-1}, dip coating with chocolate moves it at 1 to 100 s^{-1} and pouring chocolate to coat fillings and biscuits requires it to move at 0.01-1 s^{-1} (Mezger, 2011a). The shear imposed during the consumption of chocolate may be relevant for analysis also. The shear rates often used to represent mastication are between 10-500 s^{-1}, whilst 60 s^{-1} corresponds to swallowing and 4 s^{-1} to the movement of particles across the tongue (Gittings et al., 2015, Prinz and Lucas, 1997). In this research, the commencing shear stress of 1000 Pa is generally related to between 500-600 s^{-1}, and the shear rate at the yield stress point was below 0.001 s^{-1}. This means that the values selected encompass most of these practical applications; however, the conching shear stresses could not be reached by the rheometer.

Table 1.1: Review of rheology protocols used on chocolate models and chocolate samples to identify yield stress and/or viscosity or compare samples.

Parameters measured	Geometry	Summary of protocol	Model fitted	Reference
Viscosity of sugar or cocoa powder in medium-chain triacylglycerol	Parallel plate (25 mm)	Shear rate ramp from 0.002-200 s^{-1}	Viscosity at 1 s^{-1}	(Ziegler et al., 2003)
Yield stress of sugar or cocoa powder in medium-chain triacylglycerol	Six-blade vane in a smooth cup with flexible plastic mesh at the wall	Preshear 200 Pa for 30 s, rest 10 min. Shear stress 2 Pa/min until flow observed.	None. The inflexion point between stress and strain curve was taken as the yield stress	(Ziegler et al., 2003)
Yield stress and viscosity of chocolate	Z3 DIN concentric cylinder (25 mm)	Preshear 200 or 150 s^{-1} (depending on the sample) for 6 min. Shear rate reduced to 0.1 s^{-1} within 10 min.	None. Specific points used for both parameters – see paper for details	(Schantz and Rohm, 2005)
Yield stress and viscosity of sugar or fibre in oil	Rough parallel plate (50 mm)	Preshear 50 s^{-1} for 5 min, 0.01 s^{-1} for 5 min. Shear rate 0.01-100 s^{-1} within 30 min, 100 s^{-1} for 2.5 min, 100-0.01 s^{-1} within 30 min	Casson	(Bonarius et al., 2014)
Yield stress and viscosity of chocolate crumb in sunflower oil	Smooth concentric cylinder (25 mm)	0.1-150 s^{-1} over 300 s	Casson	(Carbonell et al., 2004)
Yield stress and viscosity of either chocolate crumb in sunflower oil or sugar in cocoa butter	25 mm DIN concentric cylinder	Preshear 10 s^{-1} for 10 s, rest 10 s. Shear rate 0.0189-1890 Pa, logarithmically over 5 min.	Comparison of Casson and Carreau models.	(Taylor et al., 2009)
	25 or 50 mm serrated parallel plate	Preshear 10 s^{-1} for 10 s, rest 10 s. Shear stress amplitude sweeps 0.01-50 Pa at 1 Hz over approx. 45 min.	Critical shear stress – the end of the linear viscoelastic regime	
Yield stress and viscosity of chocolate made with different sweeteners	Smooth concentric cylinder (Z40 DIN)	Preshear 5 s^{-1} for 10 min. Shear rate 5-60 s^{-1} within 120 s, then 60-5 s^{-1}.	Comparison of Casson, Bingham and Herschel-Bulkley.	(Sokmen and Gunes, 2006)

Parameters measured	Geometry	Summary of protocol	Model fitted	Reference
Yield stress and viscosity of milk chocolate	35 mm parallel plate	Preshear 30 s^{-1} for 300 s. Constant shear rate 15 or 30 s^{-1} while temperature changes (see paper for details)	Casson or Herschel-Bulkley	(Briggs and Wang, 2004)
Yield stress and viscosity of sugar in oil or glass beads in oil	Smooth concentric cylinder (CC27)	Shear rate 1000-0.01 s^{-1} logarithmic ramp over 990 s.	Viscosity at two set shear rates. Herschel-Bulkley for yield stress	(Arnold et al., 2013)
Yield stress and viscosity of milk chocolate with or without lecithin and PGPR	DIN concentric cylinder	"Conditioning step" for 2 min. Shear rate 0.1-100 s^{-1}. No times were given.	Casson	(De Graef et al., 2011)
		"Conditioning step" for 2 min. Shear stress sweep 0.01-50 Pa at 1 Hz. No times were given.	None – end of the linear viscoelastic regime as yield stress	
Yield stress and viscosity of chocolate with different % (vol) sugar	Concentric cylinder	Preshear 50 s^{-1} for 10 s. Shear rate 0.01-1000 s^{-1} or Preshear 50 s^{-1} for 10 s. Shear stress 0.01-400 Pa	Casson or Carreau	(Fernandes et al., 2013)
		Dynamic strain 0.1-100% and stress 0.01-300 Pa at a frequency of 10 rad s^{-1}.	None – solid-liquid transition for yield stress comparison	
Yield stress and viscosity of dark, milk and white chocolate	Concentric cylinder	Preshear 2 s^{-1} for 500 s. Shear rate 2-50 s^{-1} for 180 s then 50-2 s^{-1} for 180 s	Power law, Casson and Windhab models	(Glicerina et al., 2016)
Yield stress of dark chocolate with different volume fractions and lecithin concentrations	Concentric cylinder	Preshear 5 s^{-1} for 15 min. Shear rate 5-50 s^{-1} for 120 s then 50-5 s^{-1} for 120 s	Casson	(Afoakwa et al., 2008)
Yield stress of sugar and fat dispersions in soybean oil	Cone and plate (30 mm diameter, cone angle 5°)	Strain sweeps over a deformation region 0.0001-0.2, torque bar at 3.9g, freq 1 Hz.	G' in the LVR multiplied by the limit of linearity (γ_{lin})	(Johansson and Bergenståhl, 1992b)

1.4.7.9.   Slip phenomenon

The choice of geometry is typically based on several factors, including the reduction of artefacts that may lead to erroneous interpretation. In highly filled suspensions, like chocolate, wall slip can be a problem. At low shear rates, a very narrow (0.1-10 µm) particle depleted region can form at the surface of the moving geometry, causing a lubrication effect (Barnes, 1995), pictorially represented in Figure 1.13. This phenomenon is useful when pumping material through pipes to aid movement but must be considered an artefact during the interpretation of rheological results, as shown in Figure 1.14. Sometimes, even for chocolate, smooth geometries are used successfully, and slip is not a problem (Do et al., 2007, Fernandes et al., 2013). However, often, slip is an issue and then needs to be eliminated, for example, by using serrated or sandblasted geometries (Dinkgreve et al., 2016) or by glueing sandpaper or a plastic mesh onto the geometry to obtain a structured surface (Ziegler et al., 2003). The rough surface can secure more wall adhesion; however, it can disturb the laminar flow conditions, and this effect needs to be taken into consideration when analysing the data (Mezger, 2014). Alternatively, a vane with a cup geometry has been used quite frequently to measure chocolate rheology (Baker et al., 2006, Caton and Baravian, 2008, van der Vaart et al., 2013). The vane is thought to limit disturbance of the structure of the sample during insertion, and that slip would be reduced due to the portion of the sample which is trapped between the blades forming a circular cylinder, so the sheared part of the sample is mostly in contact with the sample within the vane blades during the experiment (Barnes and Nguyen, 2001).
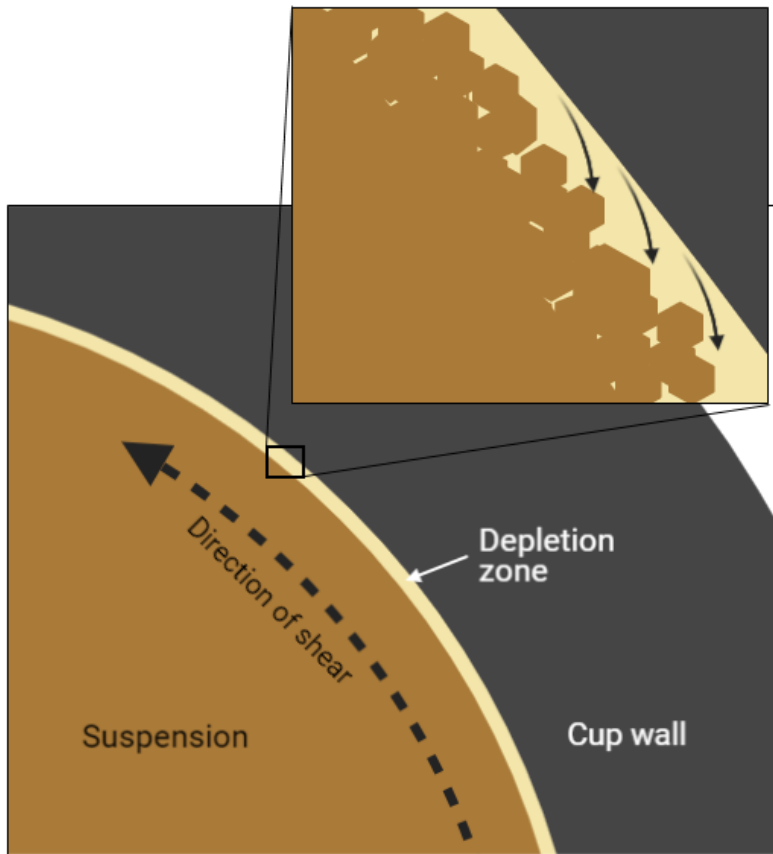
Figure 1.13: An illustration of the depletion effect that causes slip. As the rheometer shears the sample slowly, the particles within the sample start to detach from the geometry wall, which allows the suspension to move more quickly or slip along the wall. Drawn using BioRender.
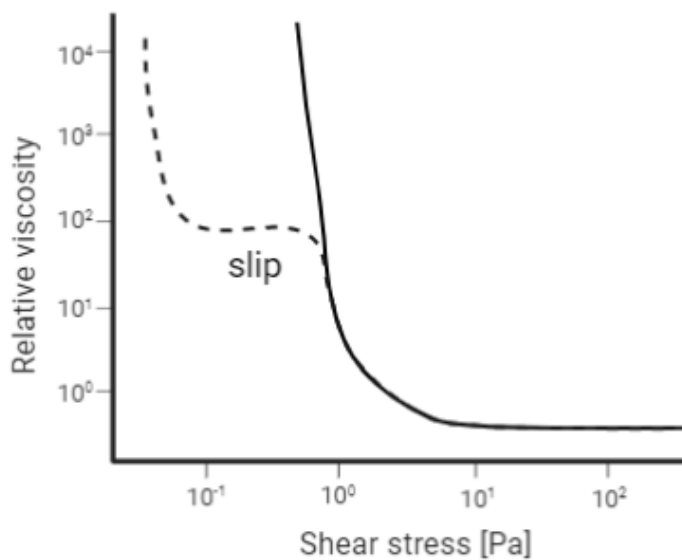
Figure 1.14: Representation of a rheological measurement of a sample without slip (solid line) and with slip (dashed line).

1.4.7.10. Mathematical models used to calculate the yield stress

The purpose of a mathematical model is to express the whole flow curve by a single equation using a small set of parameters. Ideally, these parameters should have a clear physical meaning and explain what happens during the different shear conditions. Models are particularly good when interpolating between measured points, meaning that viscosity or shear stress can be quoted at actual shear rates (IOCCC, 2000). However, the yield stress value is an extrapolated value as shear stress at zero shear rate cannot be measured. Unfortunately, mathematical models are less good at extrapolating values, so the choice of model used is important. However, as the yield stress (at zero shear rate) and viscosity (at infinite shear rate) values that most models provide are the most useful for giving indications of the pressure needed to pump molten chocolate in a factory and how easily chocolate will flow into moulds, it is still helpful to use the models on rheological data to describe the behaviour of the sample (Barbosa et al., 2016).

The first model applied to molten chocolate measurements was the Bingham model (Eq. 1.7), devised in 1916. The Bingham model is a straight-line-with-intercept model applied to results plotted as shear stress against shear rate on a linear scale; the yield stress is the point where the line crosses the ordinate. This method was very useful before computers were widely used for analysis, as all it required was a ruler. It assumes that, once the yield stress is exceeded, the material will flow ideally. It also assumes that the material will return to its original state once the stress falls below the yield value. However, it is not very useful as few actual materials behave in such a manner (Prentice, 1984). In addition, Steiner (1972) observed that there is always a curvature towards the origin below 15 s^{-1}, and this is not accounted for in the Bingham model.

$$\tau = \tau_B + \eta_B . \dot{\gamma} \qquad \text{(Eq. 1.7)}$$

where τ is the shear stress [Pa], τ_B is the Bingham yield value [Pa], η_B is the Bingham plastic viscosity or flow coefficient [Pa.s], and $\dot{\gamma}$ is the shear rate [s⁻¹] (Afoakwa et al., 2009, Mezger, 2011b).

The Herschel-Bulkley model (Eq. 1.8) was published in 1926 (Barnes, 1999b), and it is a modified Bingham model by inserting power-law behaviour for the viscous component.

$$\tau = \tau_{HB} + c.(\dot{\gamma})^p \qquad \text{(Eq. 1.8)}$$

where τ is the shear stress [Pa], τ_{HB} is the "yield point according to Herschel-Bulkley" [Pa], c is the flow coefficient (also known as "Herschel-Bulkley viscosity", η_{HB}) [Pa.sᵖ]; $\dot{\gamma}$, shear rate [s⁻¹] and exponent p which is the Herschel-Bulkley index (Afoakwa et al., 2009, Mezger, 2011b)

The Bingham model was also modified in 1957 by Casson, who used the square root form of the shear rate and shear stress, but the model retained the straight-line-with-intercept form (Eq. 1.9). This model was initially developed for the printing industry for suspensions of pigments. Casson made assumptions about the behaviour of elongated particles which form chains. However, Prentice (1984) noted that some of the substances for which the equation appears to fit the experimental data best are densely packed suspensions of amorphous particles, like chocolate, where the conditions are least like those used by Casson. However, Steiner (1963) reported that the Casson equation could not accurately describe the flow of chocolate below 2 s⁻¹.

$$\sqrt{\tau} = \sqrt{\tau_{CA}} + \sqrt{\eta_{CA}}.\sqrt{\dot{\gamma}} \qquad \text{(Eq. 1.9)}$$

where τ is the shear stress [Pa], τ_{CA} is the Casson yield value [Pa], η_{CA} is the Casson plastic viscosity [Pa.s], and $\dot{\gamma}$ is the shear rate [s⁻¹] (Afoakwa et al., 2009, Mezger, 2011b)

Until the turn of the century, the International Office of Cocoa, Chocolate and Sugar Confectionery (IOCCC) recommended the Casson model with the calculation of the Casson yield value and the Casson plastic viscosity value to be the standard for measuring and comparing the rheological properties of chocolate samples between a shear rate range of 5-60 s^{-1} (Afoakwa et al., 2007, Steiner, 1972, Bouzas and Brown, 1995). In 2000, the IOCCC published an updated analytical method that replaced the earlier advice due to inconsistencies between laboratories when following their earlier guidance. This method was put together following extensive ring tests to ensure consistency between laboratories (Aeschlimann and Beckett, 2000) and involved measuring the chocolate between 2 s^{-1} and, at least, 50 s^{-1}, using the Windhab model (Eq. 1.10) if the laboratory requires curve fitting.

$$\tau = \tau_0 + \eta_\infty \cdot \dot{\gamma} + (\tau_1 - \tau_0) \cdot [1 - \exp{(-\frac{\dot{\gamma}}{\dot{\gamma}*})}] \qquad \text{(Eq. 1.10)}$$

where τ is the shear stress [Pa], τ_0 is the initial yield stress (the value which characterises the "state of rest of the structure"), η_∞ is the high shear viscosity [Pa.s], $\dot{\gamma}$ is the shear rate [s^{-1}], τ_1 is the shear stress that leads to a maximum shear-induced structuring, and $\dot{\gamma}*$ is the Windhab shear stress at a 63.2% defined point [s^{-1}] (Barbosa et al., 2016).

An alternative, much simpler suggestion was made by Servais et al. in 2003. They suggested that just using the value of stress at a shear rate of 5 s^{-1} to represent the yield stress of the sample and using the value of the viscosity at a shear rate of 40 s^{-1} to represent the high shear viscosity would be sufficient as a reference method to compare samples (Servais et al., 2003)

In this research, the Herschel-Bulkley model was applied to the chocolate rheology data, as recommended in several comparisons of the aforementioned models in the literature (Arnold et al., 2013, Sokmen and Gunes, 2006, Briggs and Wang, 2004).

1.4.8. Suspensions used to measure chocolate rheology

In researching the effect of emulsifiers, the suspension used must be carefully chosen because it will affect if the results can be applied to the real system being analysed.

1.4.8.1. Chocolate

Using a batch of chocolate made without emulsifiers and with a reduced fat content allows a researcher to add their chosen emulsifier, dissolved in cocoa butter or another fat, at a later stage. It can be thoroughly mixed in and the effect of the emulsifier compared against samples with different concentrations of the emulsifier, a different emulsifier or only the additional fat. Results of research performed directly with chocolate can be easily applied to a chocolate formulation.

1.4.8.2. Chocolate model

The other method is to use a simplified chocolate model. The model involves typically just one solid particle type and one fat phase. The solid particle can be chosen from those already present in chocolate, e.g. sugar, cocoa particles, milk particles, or not, e.g. glass spheres. In order to reduce the complexity of the formulation, to avoid having to work at raised temperatures and to remove confounding effects of cocoa butter crystal formation (West and Rousseau, 2018, Fernandes et al., 2013) during analysis, oil is often used as a substitute for the continuous phase. A range of chocolate models from the literature is detailed in Table 1.2

Particle phase: Sugar is often selected as the particle phase as it is known that surfactants act primarily at the surface of sugar due to the strong hydrophilic nature of the sugar and the strong hydrophobic nature of cocoa butter. There has been evidence of lecithin interacting with cocoa particles though it is to a much lesser extent than sugar (Minifie, 1980). A comparison of different Lecithin-PGPR blends to reduce the yield stress and viscosity of dark chocolate and milk chocolate has shown that

while the optimum blend for yield stress reduction was the same for both types of chocolate (lecithin:PGPR 30:70), the optimum blend for viscosity reduction was different for the types of chocolate 50:50 for dark and 75:25 for milk chocolate (Schantz and Rohm, 2005). This data implies that milk powder has less interaction with PGPR than cocoa particles or sugar where a reduction in yield stress is concerned, but no direct measurement with milk powder has been made successfully (Ačkar et al., 2014). Most sugar particles have a regular, crystalline shape, and a drying step can be implemented at the start of an experiment to reduce the amount of amorphous sugar. Conversely, cocoa and milk powders have a microstructural nature that includes cavities that trap the fat phase, thus reducing the fat content in the continuous bulk phase, and this can confound results (Attaie et al., 2003, Do et al., 2011). Nonetheless, in this research, cocoa powder was initially investigated to be used as the particle phase but as the temperature of the suspension increased, any remaining cocoa butter still attached to the cocoa particle melted out and mixed with the continuous phase, consequently reducing the volume fraction of the suspenion in an uncontrolled way. Therefore, sugar was selected as the particle phase for this PhD.

Continuous phase: As shown in Table 1.2, a chocolate model suspension can be made with cocoa butter as the continuous phase. In this PhD research, cocoa butter was assessed, and several reasons meant that it was not chosen for the continuous phase. It was difficult to effectively remove all the naturally occurring surface-active molecules in cocoa butter, as it contained a high number of these molecules. The melting points of the triacylglycerol polymorphs necessitated the suspension to be raised to a temperature of 80 °C before lowering to 50 °C: the measurement temperature. Without this step, inconsistent results were obtained; this added complexity to the protocol. In the end, as the goal of the research was to assess the action of different emulsifiers against themselves, sunflower oil was seen as a practical alternative: it is readily available at local supermarkets and does not contain

any solid fat at 20 °C. It also has a history of being used in chocolate models by researchers where rheology was measured (Mohamad et al., 2020, Taylor et al., 2009).

The obvious drawback of using a sugar-in-oil suspension is that the measurements are not directly applicable to chocolate itself. The fatty acids within the oils are different: sunflower oil fatty acids have been measured at around 7% palmitic acid (C16:0), 3% stearic acid (C18:0), 21% oleic acid (C18:1), and 68% linoleic acid (C18:2) (Crapiste et al., 1999) and cocoa butter (from the Côte d'Ivoire) have been measured at 26% palmitic acid (C16:0), 37% stearic acid (C18:0), 33% oleic acid (C18:1), and 3% linoleic acid (C18:2) (Lipp and Anklam, 1998). Babin et al. (2005) performed experiments to measure the influence of lecithin in a sugar suspension using four different food oils: soybean, milk fat, palm kernel oil and cocoa butter, and they found that the continuous phase chosen does make a difference to the rheology of the suspension. Consequently, for research carried out using an alternative continuous phase to cocoa butter, further experiments would be needed to ensure that any findings are carried through into the chocolate formulation to understand how much the other constituents of the chocolate, not just the cocoa butter, interact with the emulsifier, thus altering their behaviour. During this PhD research, some initial steps were taken to assess the impact of PGPR on cocoa butter. Experiments performed using small-angle scattering and wide-angle scattering (SAXS/WAXS) equipment showed that PGPR does not affect the formation of cocoa butter triacylglycerol crystals. However, an impact on crystallisation was seen using differential scanning calorimetry (DSC). Sugar-in-cocoa butter suspension samples containing treated and untreated cocoa butter without or with 0.5% PGPR (Palsgaard 4150) or Lecithin (Adlec™ Non-GMO Lecithin, ADM) were applied. The results indicated that whilst the crystallisation point was not affected by treatment with magnesium silicate or application of emulsifiers, the amount of energy required to

form the crystals was much less for the treated cocoa butter with no emulsifier and treated cocoa butter with 0.5 % PGPR when in suspension with icing sugar, compared to all other sample types. This finding was not pursued further in this PhD research because of time constraints and the decision to use sunflower oil to highlight the differences in the emulsifiers rather than study the interaction with the TAGs within the continuous phase.

Chocolate models are often formulated at phase volume fractions below the maximum packing fraction, which avoids difficulties in sample preparation due to the yield stress character. However, in order to assess the yield stress lowering performance of emulsifiers used in chocolate, a concentrated suspension as a chocolate model was developed for this research.

Table 1.2: Examples of chocolate models used in literature.

Dispersed phase	Continuous phase	Suspension concentration	Particle size [measurement method]	Emulsifiers	Reference
Sugar or non-fat cocoa powder	Medium chain triacylglycerol (NEOBEE M-5)	55% (wt)	<20 µm (>90%) [laser diffraction particle sizer]	Lecithin or PGPR	(Ziegler et al., 2003)
Sugar or fibre rich materials from fruit or vegetable source	Medium chain triacylglycerol (NEOBEE M-5)	5, 10, 20, **30**, 40% (vol)	<71 µm [sieve]	Lecithin	(Bonarius et al., 2014)
Sugar, soda-lime glass or borosilicate glass spheres	Soybean oil or MCT	31% (vol)	Sugar <49.7 µm (>90%) Spheres <21.8 µm (>90%) [laser diffraction]	Lecithin	(Arnold et al., 2013)
Sugar	Cocoa butter equivalent (Illexao 03-61)	70%, 75% and 78% (wt) (56% 62% and 68% (vol))	Two ranges - < 27 µm and <107 µm (90%) [Mastersizer]	Lecithin	(Do et al., 2007)
Sugar	Soybean, milk fat, palm kernel oil, cocoa butter	10-70% (wt)	<36 µm (90%) [Mastersizer]	Lecithin, monoglyceride (Rylo MG 19 Pharma)	(Babin et al., 2005)
Sugar	Sunflower oil	28, 33, 37% (vol)	<80 µm (approx.) (90%) [laser diffraction]	Spinach leaf lipids, lecithin, PGPR	(Mohamad et al., 2020)
Sugar	Cocoa butter, GTO 80 (80% glycerol trioleate)	70% (wt)	<21.35 µm (90%) [particle sizer]	Lecithin or PGPR and together, oat extract	(Vernier, 1997)
Glass spheres, sugar or limestone aggregates	Silicon oil (AK 1000)	Various, up to 65% (vol)	<80 µm (90%) (inferred) [method not specified]	Lecithin	(Windhab, 2000)

Dispersed phase	Continuous phase	Suspension concentration	Particle size [measurement method]	Emulsifiers	Reference
Sugar	Soybean oil	50% (wt)	<30 µm [sieve]	Phosphatidylcholine, lecithin, monoolein, unsaturated MG, saturated MG, polyglycerol EFA, lactic acid EMG, Sorbitan EFA, diacetyl tartaric acid EMG and propylene glycol EFA (MG = monoglycerides; EMG = esters of MG; EFA esters of fatty acids)	(Johansson and Bergenståhl, 1992b)
Chocolate crumb	Sunflower oil	17-75 %(vol)	14 µm (mean) [Laser diffraction particle sizer]	Lecithin	(Taylor et al., 2009)
Sugar	Cocoa butter	17-75 %(vol)	15 µm (mean) [Laser diffraction particle sizer]	Lecithin	(Taylor et al., 2009)
Chocolate crumb	Sunflower oil	60 %(wt)	14.0, 17.2 or 19.6 µm (mean) (three recipes) [Laser diffraction particle sizer]	Sorbitan monolaurate (Span 20)	(Carbonell et al., 2004)

1.5. Literature review: Leaf lipids

The natural alternative to PGPR was proposed to be found amongst leaf lipids, so some background information is also included here.

1.5.1. The internal structure of leaves

The internal structure of a leaf is illustrated in Figure 1.15. Generally, there are three regions in a transversely cut leaf: epidermis, mesophyll and vascular bundles or veins.

The epidermis is a layer of cells covering the surface of the leaf. The upper epidermis of the leaf is primarily there for protection and typically has a coating of cutin and often other waxy substances, which forms the cuticle. The lower epidermis generally has a thinner cutin layer and has numerous tiny pores called stomata ranging from about 1000 to more than 1.2 million per square centimetre of surface (Bidlack and Jansky, 2018b). These pores regulate both gas exchange between the interior of the leaf and the atmosphere, and the evaporation of water that has entered the plant via the root.

The mesophyll makes up most of the leaf body and is where photosynthesis takes place. There are two types of cells in the mesophyll, and sometimes they form two distinct layers, or sometimes they are more heterogeneous. The top layer comprises the palisade cells, compactly stacked, barrel-shaped cells and may contain 80% of the leaf's chloroplasts. The lower region is more the loosely arranged spongy cells, which also contains numerous chloroplasts.

Vascular bundles, or veins, are found in the mesophyll. They consist of the xylem and phloem tissues surrounded by thicker-walled parenchyma cells called the bundle sheath. The veins give the leaf its skeleton. The phloem transports sugars and other carbohydrates, whilst the xylem transports water throughout the plant.
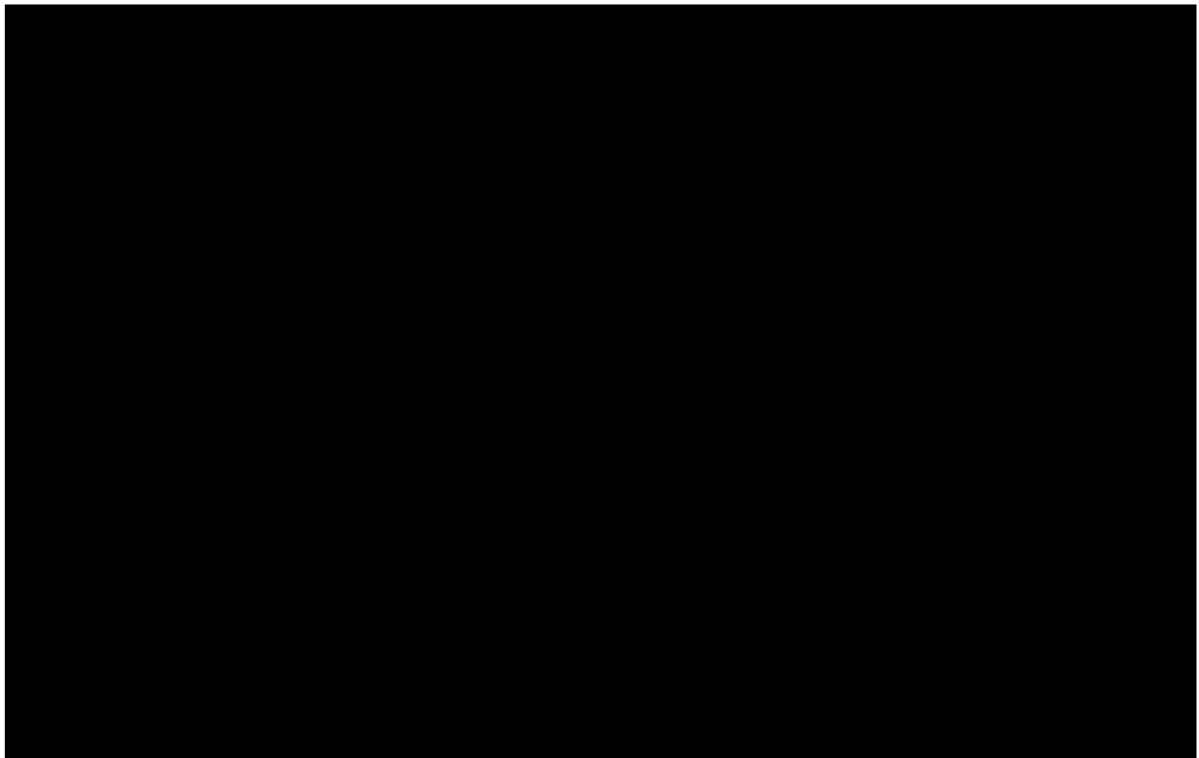
Figure 1.15: Internal structure of leaves, taken from Levetin and McMahon (2016). Figure redacted because the copyright holder cannot be established by the publisher, so permission cannot be granted.

1.5.2. Structure of a leaf cell

The structure of a differentiated mesophyll leaf cell is shown in Figure 1.16, which illustrates the numerous features within the cell, all of which are bound by lipid bilayers or single-layer membranes. The types of lipids and fatty acids that occur in the different membranes can be very particular to the domain of which it is a part. For instance, most plasma membranes consist primarily of phospholipids. In contrast, the plastid membranes consist chiefly of galactolipids, and up to 95% of all α-linolenic acid in a cell is found in the chloroplast (Maréchal et al., 1997). The types of lipids found within a cell are detailed in section 1.5.3, and how these lipids change qualitatively and quantitatively over the lifespan of a leaf is detailed in section 1.5.4.
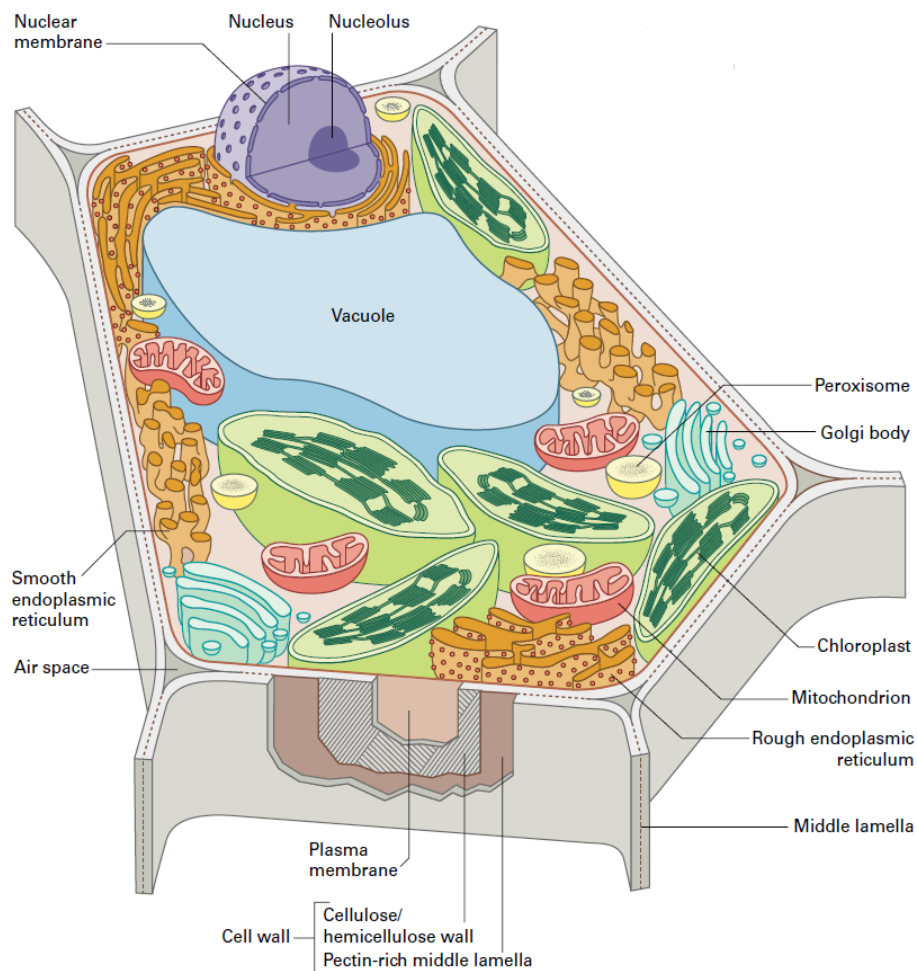
Figure 1.16: Diagrammatic representation of a mesophyll leaf cell, depicting principal membrane systems and cell wall domains of a differentiated plate cell [Republished with permission of John Wiley & Sons Ltd, from Ch 1. Membrane Structure and Membranous Organelles, Staehelin, L. Andrew, from Biochemistry and Molecular Biology of Plants: Second Edition, Eds Buchanan, Bob B, Gruissem, Wilhelm, Jones, Russell L. 2015; permission conveyed through Copyright Clearance Center, Inc.]

1.5.3. Lipid composition in a mature leaf

The composition of leaves is illustrated in Figure 1.17, shown as cellular constituents and lipid types in *Arabidopsis*. This figure shows that around 5.9% of the dry weight of leaves is lipids, and also shows that within the lipid component, the types of lipids found are glycerolipids (53%), chlorophyll (24%), cutin monomers (4%), wax (4%), and other lipids making up the remaining 15%. Lipids have many functional properties within a leaf, which include roles as structural components of membranes (glycerolipids, sphingolipids, sterols), compounds active in electron transfer reaction

from light (chlorophyll, plastoquinone), photoprotection (carotenoids), protection of membranes against damage from free radicals (tocopherols), and waterproofing and surface protection (cutin, surface waxes, very-long-chain fatty acids) (Ohlrogge et al., 2015).
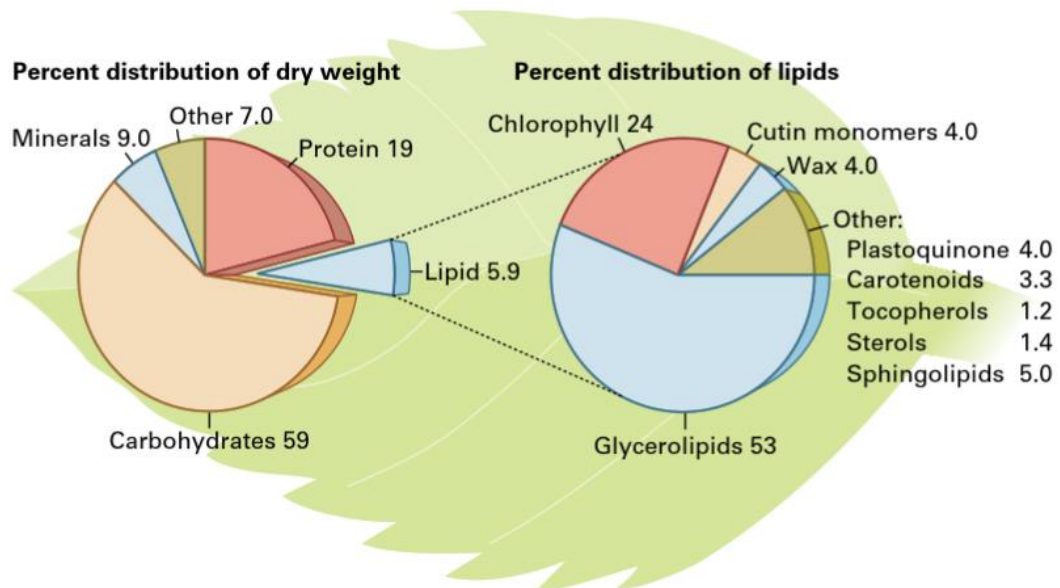
Figure 1.17: Approximate distributions of cellular constituents (as a percentage of dry weight) and lipid types (as a percentage of total lipids by weight) in leaf tissues of Arabidopsis. Some of the values were extrapolated from results obtained with other species. [Republished with permission of John Wiley & Sons Ltd, from Ch 8. Lipids, Ohlrogge, John B., Browse, John, Jaworski, Jan G., Somerville, Chris from Biochemistry and Molecular Biology of Plants: Second Edition, Eds Buchanan, Bob B, Gruissem, Wilhelm, Jones, Russell L. 2015; permission conveyed through Copyright Clearance Center, Inc.].

Glycerolipids consist of fatty acids esterified to derivatives of glycerol. There are four main types in plants: phospholipids, galactolipids, a sulfolipid, and triacylglycerols. Those involved in plant membranes are shown in Figure 1.18. Phospholipids are all molecules based on phosphatidic acid, the structure of which is a glycerol molecule with a phosphoryl group at the *sn*-3 position and fatty acids at the *sn*-1 and *sn*-2 positions. All other phospholipids are synthesised by the esterification of polar groups onto the OH group of this phosphoryl moiety. Glycolipids are similar molecules, but the phosphoryl head group is replaced with galactosyl or sulfovosyl group to form

monogalactosyl diacylglycerol (MGDG – one galactosyl group), digalactosyl diacylglycerol (DGDG – two galactosyl group) or sulfoquinovosyl diacylglycerol (SQDG – one galactosyl with a sulphur trioxide group). These are the main three glycolipids in plants and are primarily found in the chloroplasts and other plastid membranes.

Sphingolipids are concentrated in the plasma membrane and are not esters of glycerol but are long-chain amino alcohols that form an amide linkage to fatty acids. Often the fatty acid in a sphingolipid is longer than C18. They play a significant role in signalling and cell recognition. Some sphingolipids can contain glucose groups, for example, glucosylceramide.

Sterols also play a central role in cell membranes within plants. Sterols have a very large hydrophobic domain and only a hydroxyl group to provide the hydrophilicity needed to be an amphiphilic membrane lipid. However, this makes them able to move rapidly within the membrane bi-layers. This ability enhances the leaves' control of the fluidity of their membrane at extreme temperatures. It disrupts the phospholipids' gelling tendency at low temperatures, and at high temperatures, it interferes with the flexing motions of the fatty acid tails (Staehelin, 2015a). Common free sterols in plant plasma membranes are campesterol, sitosterol and stigmasterol, see Figure 1.18. Sterol esters, sterol glycosides and acylated sterol glycosides are also formed, and the amounts of these differ depending on the plant (Nyström et al., 2012).
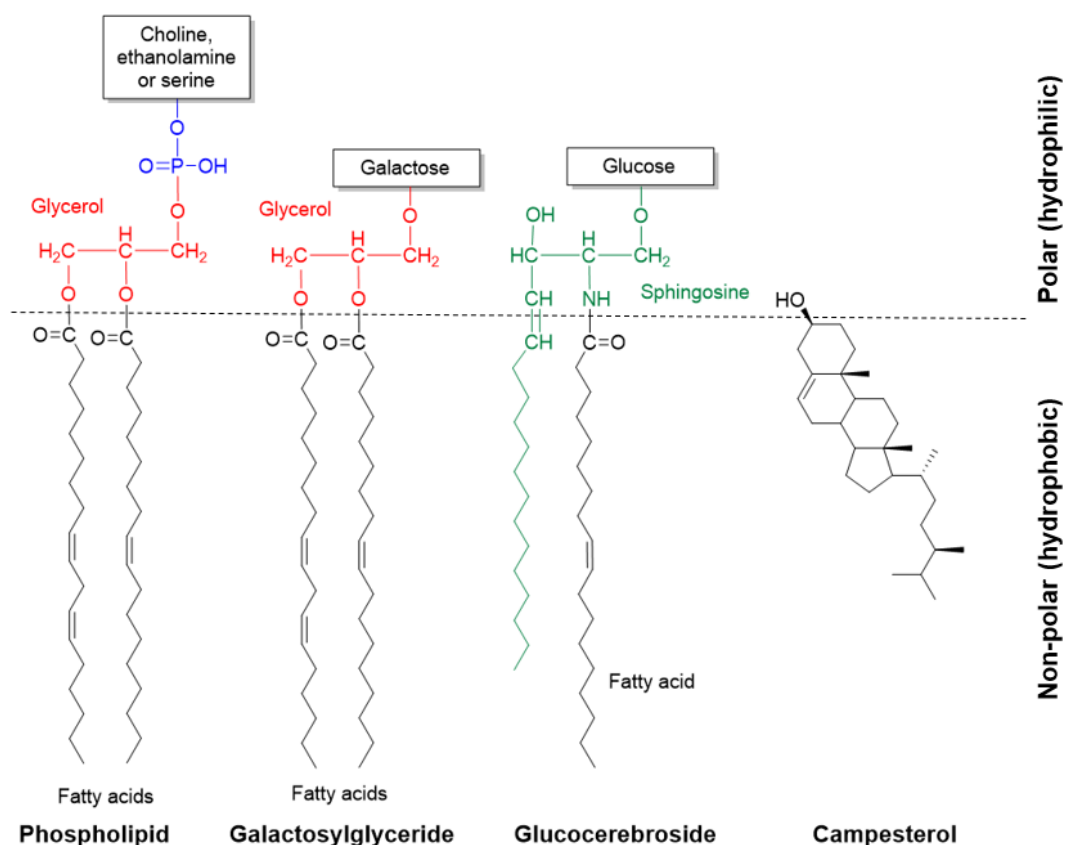
Figure 1.18: Representation of plant membrane lipids

The lipids involved in capturing light energy to enable the plant to convert CO_2 into sugars are **chlorophyll**, **carotenoids** and **plastoquinone**, and these are found in the plastids. The major plastid in green leaves is the chloroplast, where chlorophyll and carotenoids are found. The major plastid in young, red leaves, flowers, and some fruit and vegetables, is the chromoplast, where carotenoids are found (Whatley and Whatley, 1987). Chlorophyll and carotenoids cause the leaves to have a visible colour that changes over the leaf's lifetime. The chlorophylls are located on the thylakoid membranes and absorb light raising the energy level of some of its electrons. This energy is used to split water molecules, releasing oxygen, electrons and protons. The protons enable ATP production, and the electrons pass through the electron transport system, which involves plastoquinone to create NADPH. ATP and NADPH enter the

Calvin Cycle in the stroma of the chloroplast, which enables the conversion of carbon dioxide to sugars for the plant (Levetin and McMahon, 2016, Bidlack and Jansky, 2018c). The pigment lipids absorb light at different wavelengths, allowing for a broad range of energy collection, see Figure 1.19 (Bidlack and Jansky, 2018c). The structure of chlorophyll *a* is shown in Figure 1.20, the structure of lutein, a carotenoid, is shown in Figure 1.21 and the structure of plastoquinione is shown in Figure 1.22.
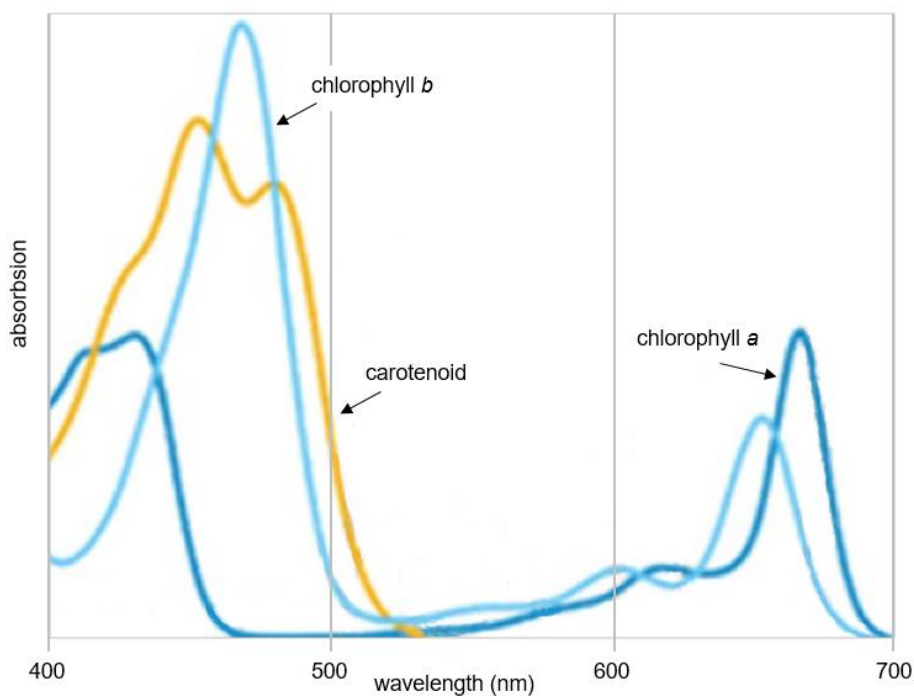
Figure 1.19: The absorption spectra of chlorophyll a, chlorophyll b, and a carotenoid. The maximum absorption of the chlorophylls is in the blue and red wavelengths. The maximum absorption of the carotenoids is in the blue-green to green parts of the visible spectrum.
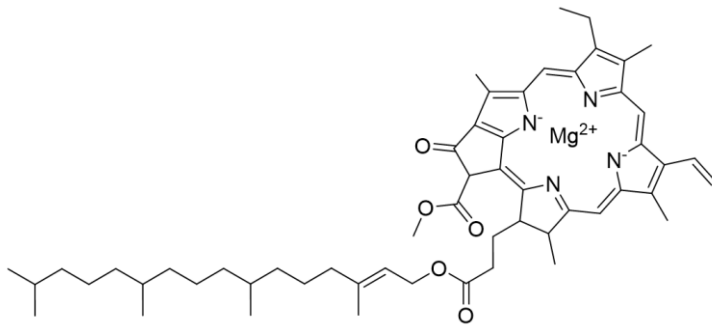
Figure 1.20: Chlorophyll a. There are several types of chlorophyll, but all share the chlorin magnesium ligand, which forms the right side of this diagram.
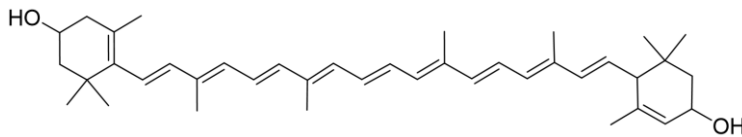
Figure 1.21: Lutein. The general structure of a carotenoid is the polyene tail with double bonds, possible terminal rings
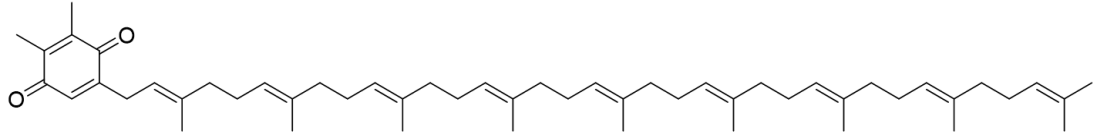
Figure 1.22: Plastoquinone

Four **tocopherols** (α-, β-, γ-, and δ-Tocopherol) are synthesised and stored in plant leaves and seeds. α-Tocopherol (vitamin E) is found in plastoglobules: lipoprotein bodies encompassed by a monolayer of polar lipids attached to the thylakoid membrane. These plastoglobules also store other prenylquinones, carotenoids, neutral lipids and breakdown products of chlorophylls. They vary in size and number during the lifetime of a plastid and become more abundant during stresses, such as high light levels, drought, high salinity, and senescence. During chromoplast development, carotenoid accumulation in plastoglobules confers colour to fruits and petals (Staehelin, 2015a). The primary function of tocopherols in plants is as an

51

antioxidant, although other functions have been described (Azzi, 2018). The structure of α-Tocopherol is shown in Figure 1.23.
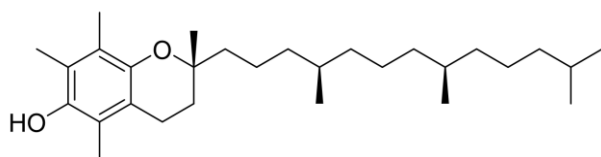
Figure 1.23: The structure of α-Tocopherol, Vitamin E. The other tocopherols' chemical difference consists in the number and position of the methyl groups of the chromanol ring on the left-hand side of the figure

Cutins and **waxes** are lipids formed by epidermal cells and are used on the leaf's surface to provide essential resistance to pathogens, insects, and UV penetration, and a strong barrier to the diffusion of water. The cutin layer of epidermal cells is composed of oxygenated C16 and C18 fatty acids esterified to one another to produce a tough, polyester skin (Ohlrogge et al., 2015). As Figure 1.24 shows, cutin monomers are fatty acids; however, once the cutin layer forms, it does not dissolve in chloroform (Matas et al., 2004). Therefore, only the cutin monomers may be found in a chloroform:methanol lipid extraction such as it was performed in this PhD research.

Cutin alone is not sufficient for determining the barrier/water-retarding properties of the cuticle. The aerial surfaces of plants are covered with a layer of chloroform-soluble, non-volatile lipids, collectively called wax. Wax esters are part of this mixture and are esters of long-chain fatty acids (C26 to C32) and long-chain alcohols, as exemplified in Figure 1.25. In practice, the wax layer is a complex mixture of these hydrocarbon esters with ketones, phenolic esters, terpenes, and sterols (Ohlrogge et al., 2015).
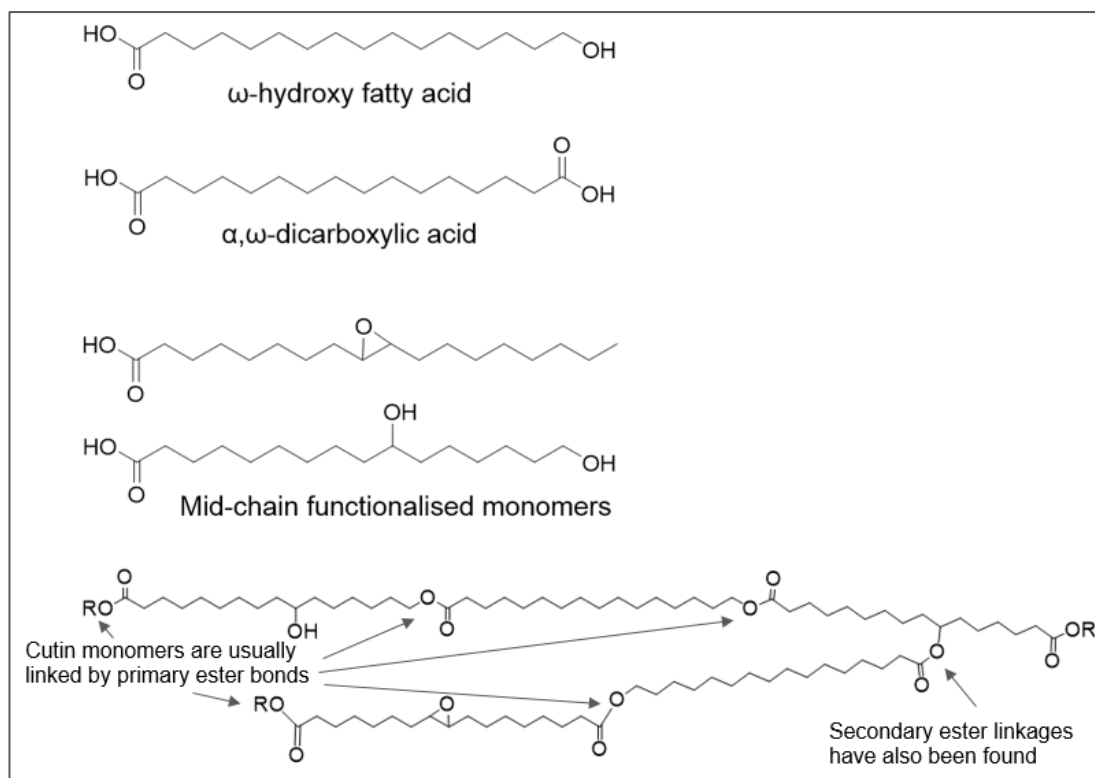
Figure 1.24: Structures of common cutin monomers and hypothetical monomer connectivity patterns. (A) Representative structures within each monomer group. Mid-chain oxygen-functionalised monomers, which include epoxy, hydroxy, vicinal dihydroxy and oxo groups, can be found in addition to normal fatty acids, ω-hydroxy fatty acids and α,ω-dicarboxylic acids. Bottom: A small segment of ω-hydroxy fatty acid-rich polyester is illustrated to show the dominant primary ester linkages that form chains, along with a secondary ester linkage to enable a branch point. More complex structures can be formed with the addition of glycerol (not shown here) (Ohlrogge et al., 2015).
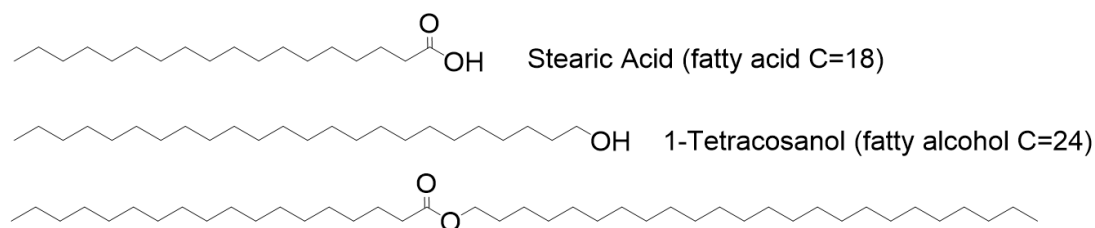
Figure 1.25: Molecular structure for a wax ester found in leaves (Misra et al., 1987).

53

1.5.4. Leaf lipid composition through life stage

As leaves grow, the lipid composition changes. The leaf starts at the meristem, which produces new cells through cell division during an exponential period and stops when the leaf structure is at its predetermined size. During the growth stage, the cells expand and then start to differentiate to create cells adapted to specific functions (Bidlack and Jansky, 2018d) until they achieve the structure illustrated in Figure 1.15.

As the cell matures, the cell wall changes. When new cell walls are formed, a layer of pectin is created between two cells, called the middle lamella. A flexible primary wall consisting of cellulose, hemicellulose, pectin and glycoproteins is laid down on either side of the middle lamella. It continues to grow with the cell during this time. Secondary walls appear inside the primary walls and are derived from the primary walls by thickening and the inclusion of lignin with cellulose microfibrils embedded within them. It is at this point that the cell size is fixed. As the cell ages, the wall thickness increases and can occupy from as little as 5% to as much as 95% of the volume of the cells (Bidlack and Jansky, 2018a). As the cell wall does not contain lipids, no more will be written about this here, though more information can be found in the literature, for example (Carpita et al., 2015).

The plasma membrane is made up of phospholipids arranged in two layers, with proteins interspersed throughout. It is a dynamic structure growing as the cell expands and then can move and flex within the confines of the cell wall. Once the cell wall is formed, it cannot expand further, as already explained, but the lipids are constantly being removed and reformed with time. It can create folds that can be pinched off in the cell, forming a vesicle. Most other membranes within the cell, for instance, the endoplasmic reticulum, also grow as the cell expands, and the lipids within the membrane are replaced as time goes on, but their composition does not change dramatically over the lifecycle of the leaf cell. However, the plastids and the cuticle do change as the leaf cell grows and ages.

Plastids are only found in plant cells and are primarily responsible for photosynthesis, the synthesis and storage of starch and oils, and the creation of fatty acids and lipids. The number of plastids can vary enormously between cells and as a single cell matures. They can reproduce themselves by division within the cell and are found throughout the plant, not just in leaves. As Figure 1.26 shows, plastids have a remarkable ability to differentiate and redifferentiate. The proplastid is the precursor to all types of plastid and is passed on to the next generation of plants through the reproductive process and is maintained in the meristem.

Colourless, unpigmented plastids are often used for storage or are precursors of chloroplasts. The leucoplast produces and stores essential oils in plants that produce these oils, for example, mint leaves or orange skin. The elaioplasts store oil but are found only in cells surrounding developing pollen: they release their oils and sterol esters when the pollen is mature. The amyloplasts store starch granules in plants such as potatoes. The etioplast is a plastid formed when plant tissue that usually contains chloroplasts is kept in the dark. When light is shone on tissue containing etioplasts, they start to develop into chloroplasts.

Chromoplasts and gerontoplasts derive their colour from carotene and xanthophyll pigments. Their presence colours the tissue within which they are located, yellow, orange or red, depending on the combination of these pigments. They are found in fruit, flowers and root vegetables. Chromoplasts can develop directly from the proplastid or by the dedifferentiation of chloroplasts, for example, in ripening tomatoes. When leaves turn green, the chromoplasts will remain, but their colour is masked by the chlorophyll in the developed chloroplasts. Gerontoplasts are formed from chloroplasts that have gone through senescence, and the photosynthetic apparatus has been dismantled. Often large plastoglobules, containing waste lipid materials are present. The proteins are recycled within the plant providing amino acids and nitrogen for the plant.

The chloroplast is the main plastid in green leaves, and a mature leaf cell often contains 75-125 or even several hundred chloroplasts in a few plants (Bidlack and Jansky, 2018a). The formation of a chloroplast is initiated in response to light stimulus and contains a large concentration of thylakoid membranes. Chloroplasts contain specific membrane glycolipids – the galactolipids and SQDG, as already described. The lipids within a leaf can indicate the maturity of a leaf: the total amount of galactolipids present in a plant tissue reflects the expansion of the chloroplast membrane, whereas the total amount of phospholipids such as phosphatidylethanolamine reflects the expansion of the extraplastidial membranes (Douce and Joyard, 1980). Many of the membrane lipids are formed in the chloroplast in conjunction with the endoplasmic reticulum. As well as being the site of photosynthesis which drives sugar and oxygen production, the chloroplast forms most of the leaf's fatty acids, which are exported out to the endoplasmic reticulum to be used for the creation of phospholipids and sterols. The endoplasmic reticulum provides the chloroplasts with acylglycerol backbones to synthesise the galactolipids (Maréchal et al., 1997). As the leaf grows and matures, the demand for these fatty acids in the plasma membranes change over time. In the expanding leaf, fatty acid synthesis is most active, with requirements for fatty acids both in the chloroplast and the other membranes of the cell. However, when the leaf is fully expanded, demand continues at a lower, more stable rate. New lipids are still being formed even though the cell is mature, and existing acyl-lipids require fatty acid replacement, perhaps for thylakoid repair due to the oxidative photochemical processes (Hellgren and Sandelius, 2001). The fatty acids produced in the chloroplasts are also used for the biosynthesis of triacylglycerol in storage cells and, in epidermal cells, they are the basis for the formation of cutin and wax esters in the leaf cuticle (Maréchal et al., 1997).
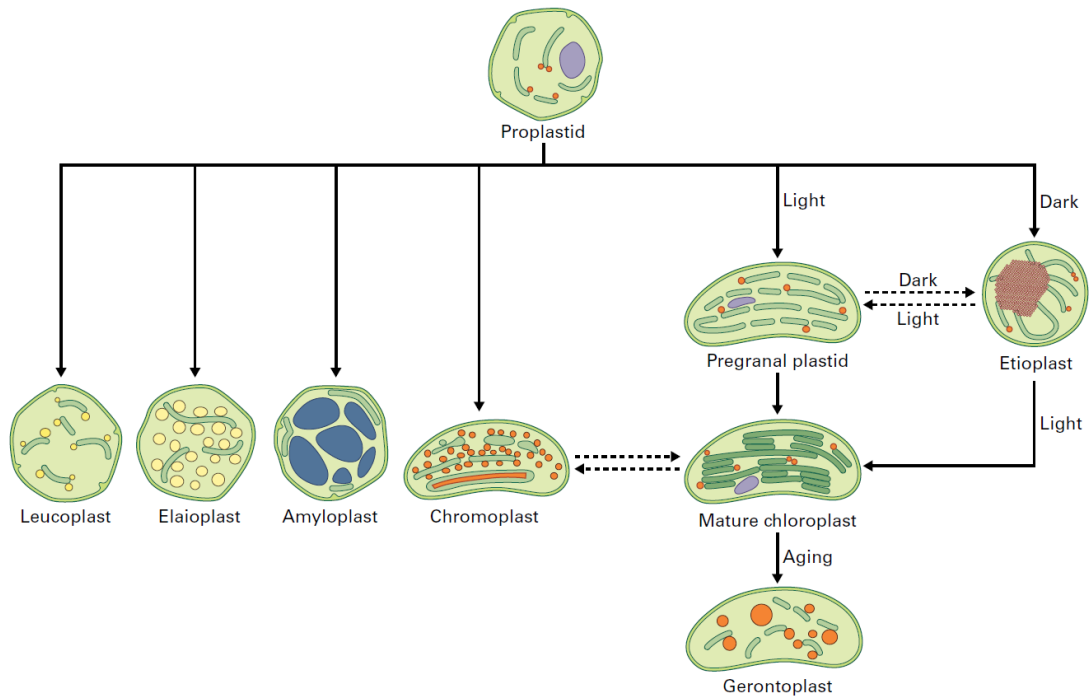
Figure 1.26: Diagram illustrating the developmental relationships between the major types of plastids. All plastids in plants are derived from proplastids, which are maintained in the meristems. Single arrows with solid lines depict normal steps of plastid development; dashed arrows show conversions that occur under special conditions [Republished with permission of John Wiley & Sons Ltd, from Ch 1. Membrane Structure and Membranous Organelles, Staehelin, L. Andrew, from Biochemistry and Molecular Biology of Plants: Second Edition, Eds Buchanan, Bob B, Gruissem, Wilhelm, Jones, Russell L. 2015; permission conveyed through Copyright Clearance Center, Inc.]

The cuticle of the leaf grows and thickens over time, as shown in Figure 1.27. The procuticle found in the young leaf is laid on the outer surface of the epidermal cells. As the leaf expands, waxes and cutin is added, as well as polysaccharides, and there can be the formation of lipophilic globules. As the epidermal cells mature and the secondary wall forms, the cuticle forms discrete layers containing both lipid and polysaccharide components.
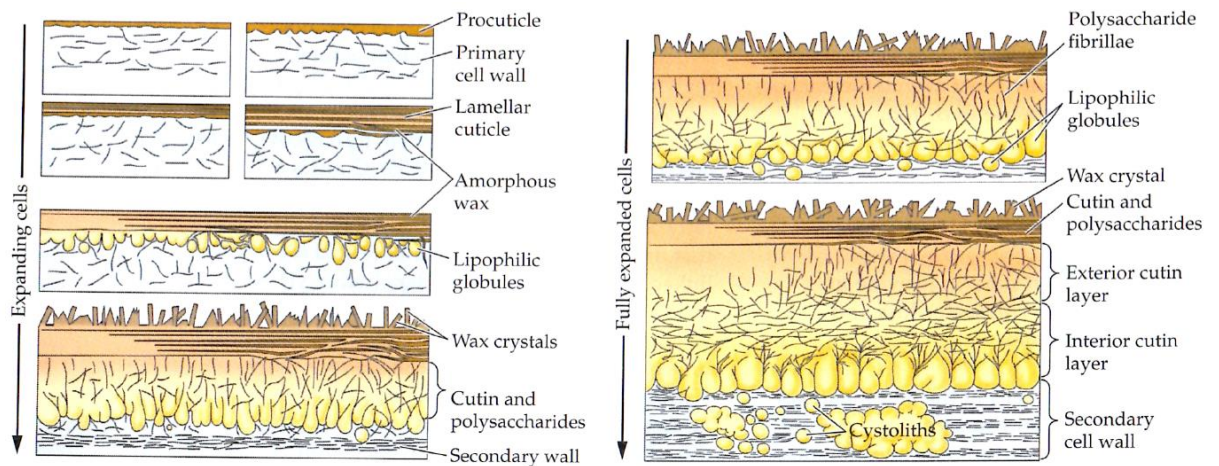
Figure 1.27: Stages in the development of a plant cuticle. At the early stages, the primary cell wall is covered by a thin amorphous layer of wax. As the leaf expands, the amount of wax increases by the agglomeration of secreted globules. Near the time that leaf expansion stops, wax crystals can start to appear on the surface, and the deposition of cutin begins. After leaf expansion, cutin deposition increases, and secondary cell wall deposition starts. The cutin layer may take on a fibrillary appearance, thought to reflect co-deposition of cutin and secondary cell wall materials such as hemicellulose. In the fully expanded mature leaf, distinct zones – the exterior cutin layer and the interior cutin layer – may be visible. [Republished with permission of John Wiley & Sons Ltd, from Ch 10. Lipids, Somerville, Chris, Browse, John, Jaworski, Jan G., Ohlrogge, John B. from Biochemistry and Molecular Biology of Plants Ed Buchanan, Bob B, Gruissem, Wilhelm, Jones, Russell L. 2002; permission conveyed through Copyright Clearance Center, Inc.].

1.5.5.   Measurement of leaf lipids

There are many ways to measure the lipids within leaf matter, and there are many books that outline methods (for example, "Lipid Analysis: Isolation, Separation, Identification and Lipidomic Analysis" by William Christie and Xianlin Han, or "Lipid Analysis, A Practical Approach" by R.J. Hamilton and S. Hamilton) as well as many papers in the literature.

When considering the measurement of lipids in leaves, one must establish the leaves experience between harvesting and lipid extraction. As soon as the leaf has been harvested, lipolytic enzymes within the cells start to hydrolyse the lipids. Therefore, consideration should be given to prevent this from occurring. The leaves could be

frozen in nitrogen immediately after harvesting. However, this can be impractical and will irreversibly damage the cells through osmotic shock and the formation of ice crystals that can cause more significant enzymic degradation unless the tissue is processed at temperatures lower than -20 °C. Other methods used to prevent hydrolysis in spinach include hot water blanching and steam sterilisation (Wattanakul et al., 2019) or submerging in hot isopropanol (Mohamad et al., 2020) before processing. The presence of large amounts of free fatty acids, diacylglycerols and phosphatidic acid within the sample can signify that enzymic degradation of lipids has taken place. However, losses of galactolipids can occur without any evident accumulation of partially hydrolysed intermediates (Christie and Han, 2010a). Polyunsaturated fatty acids will autoxidise very rapidly in air and with strong light. Therefore, care should be taken to keep leaves and lipid extracts away from light and in a nitrogen atmosphere, where possible. After the lipids have been extracted, they are still prone to degradation; they should be kept away from light, stored in a glass vial at -20 °C and in a non-polar solvent to prevent autooxidation.

The second stage is to extract the lipids from the leaf. As already discussed, leaves can contain a high percentage of water, which can be used in the extraction process or, if the lipid extraction protocol requires, removed before extraction takes place. Extraction is more likely to be comprehensive when the leaf cell walls are disrupted. Where leaves are soft and easily homogenised in a blender, for instance, then this is a good choice. Some leaves are tougher and not easily homogenised. In this case, leaves can be dried and ground into fine particles before extraction takes place. Simple lipids in storage vesicles may be easy to extract, whereas complex lipids can be part of membranes and associated with proteins and so are more challenging to extract. The polarity of the lipids themselves will also define which solvents they will dissolve in. Lipids with low polarity, such as triacylglycerol and cholesterol esters, prefer hydrocarbon solvents such as hexane, whereas more polar lipids prefer

solvents such as chloroform. Water is often added to the extraction mixture as it assists extraction by swelling biopolymers in the cell walls and allowing solvents access to lipids (Christie and Han, 2010a). There are several extraction protocols. The one used in this project is a wash protocol that extracts lipids and removes non-lipid contaminants, similar to that devised by Folch, Lees and Stanley (Folch et al., 1957). This method is a fairly easy but relatively efficient method for extracting many common lipid classes (Christie and Han, 2010a). The principle is that the tissue is shaken with chloroform:methanol:weak saline solution (8:4:3). The mixture partitions into two layers – the lower phase is now composed of chloroform-methanol-water in the proportions 86:14:1 (vol) and contains virtually all the lipids. The upper phase consists of the same solvents in the proportions of 3:48:47 (vol) and contains much of the non-lipid contaminants, e.g. sugars, amino acids, salts (Christie and Han, 2010a). Once the lipids have been extracted, they should be treated with care as discussed above.

There are many analytical methods described to analyse lipids or fatty acids, including the use of thin-layer chromatography, gas chromatography, high-performance liquid chromatography, high-resolution ^{1}H, ^{13}C and ^{31}P NMR, light spectroscopy and mass spectroscopy either alone or in conjunction with the chromatographic methods. An explanation of methods used in this PhD is outlined below.

1.5.5.1.   High-performance Thin Layer Chromatography (HPTLC)

Lipid samples from natural sources are a complex mixture of different lipid classes, some of which are listed in section 1.5.3. No single procedure can separate them all, but a combination of knowledge of their polarity and their reactions with specific chemical reagents, and the use of standards, can allow identification and quantification of some or all of these lipids. Chromatography involves the separation

of components in a mixture between a mobile and stationary phase. The components within the mixture have different affinities for these phases and so will migrate at different rates allowing separation to occur. In HPTLC, the stationary phase is silica gel which has adsorptive properties due to its silanol groups (hydroxyl groups) at the surface. The mobile phase is a mixture of solvents, the combination and ratio of which are adjusted according to the polarity of the lipids to be separated. Once separated, some lipids are visible either in the visible light range or in the ultraviolet or infrared wavelength range and so can be photographed and quantified without further steps. However, some lipids have to undergo a further procedure, known as derivatisation, where a reagent that can detect specific functional groups is sprayed on the plate, or the plate dipped into the reagent, and sometimes this is followed by heating to make the bands visible. Chlorophyll and carotenoids do not need derivatisation as they are discernible under visible light. However, in this PhD, two derivatisation solutions were used to visualise other lipids.

Copper acetate-phosphoric acid solution was used to locate molecules with an acyl chain and is a "charring reagent". The chemical mechanisms are shown in Figure 1.28. The methanol, in the presence of phosphoric acid as a catalyst and heat from the oven, esterifies free fatty acids (1) and transesterifies fatty acids from lipids to form fatty acid methyl esters (2). The copper acetate then forms a copper salt, Figure 1.29, with the released fatty acid; this salt chars on heating to give brown or black spots. This method was initially proposed by (Ballance and Crombie, 1958) and has been verified with different lipid fractions (Macala et al., 1983, Fewster et al., 1969).
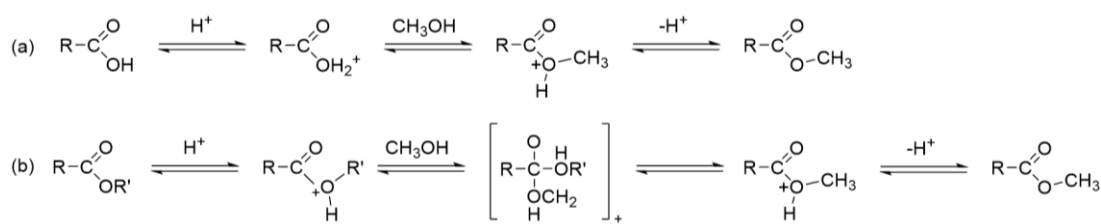
Figure 1.28: Mechanisms for acid catalysed esterification (a) and transesterification (b) with methanol.
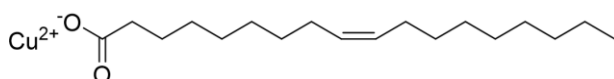
Figure 1.29: Copper salt of a fatty acid (oleic acid)

Thymol solution was used to stain sugars, particularly the galactose ring found on galactolipids, and avoid chlorophyll pigmentation. The reaction that takes place to produce the dark pink spot on the TLC plate is shown in Figure 1.30. The thymol-sulphuric acid solution was developed by Hans Molisch in 1886 to detect carbohydrates (Molisch, 1886) but was adapted for use with TLC in 1965 (Adachi, 1965). Other reagents have been used to detect carbohydrates and are summarised well by Sahaka et al. (2021), but all use the same general mechanism shown in Figure 1.30.
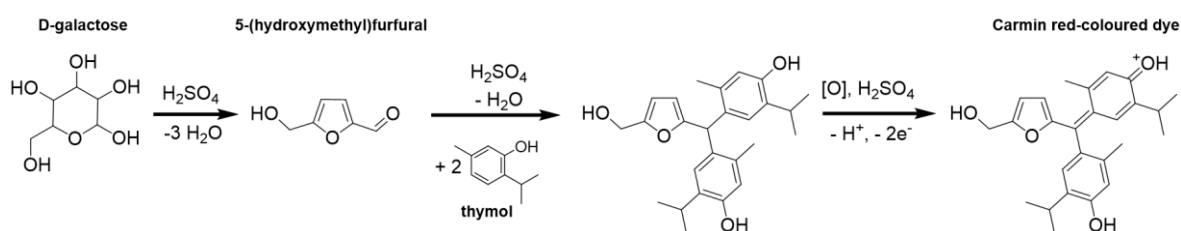
Figure 1.30: Scheme of the reaction of the thymol-sulfuric acid reagent with galactose (Sahaka et al., 2021, Ohta et al., 1985).

1.5.5.2. *Transesterification of fatty acids*

In order to measure the fatty acids in a mixture of lipids by gas chromatographic analysis, they need to be converted into a volatile derivative, usually methyl esters. Some fatty acids may occur as free fatty acids within a sample, but many are esterified to glycerol, cholesterol or alcohols. For a sample containing a significant amount of free fatty acids, acid-catalysed procedures are often utilised. This method involves heating the sample with a large excess of anhydrous methanol in the presence of an acidic catalyst, for example, 5% hydrogen chloride. Often prolonged heating is required under reflux conditions. The mechanism for this reaction is shown in Figure 1.28. Transesterification procedures in the presence of a basic catalyst can be more rapid than acidic reactions; however, they do not methylate free fatty acids: the mechanism is shown in Figure 1.31; the OH$^-$ ion drives the reaction from left to right. Amide bound fatty acids of sphingolipids are also not affected by basic catalysed transesterification.

$$R-C\overset{O}{\underset{OR'}{}} \;+\; {}^-OCH_3 \;\rightleftharpoons\; R-\underset{OCH_3}{\overset{{}^-O}{C}}-OR' \;\rightleftharpoons\; R-C\overset{O}{\underset{O-CH_3}{}} \;+\; {}^-OR'$$
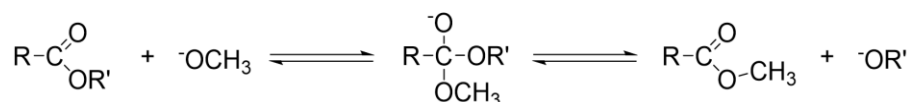
Figure 1.31: Base catalysed transesterification

Many other methods have been developed, some specific for the lipid or sample type that the researchers are studying. William Christie (1993) has extensively reviewed this subject.

In this PhD research, the method used is a pyrolysis reaction using trimethyl sulfonium hydroxide (TMSH), a mild transmethylation reagent (Butte et al., 1982, Yamauchi et al., 1979). The pyrolysis method was initially developed to methylate free fatty acids; however, TMSH also transesterifies acyl lipids through the base-catalysed process explained above (Butte, 1983). TMSH forms a salt with the fatty acid in the initial

preparation and, during application into the GC injection port, the heat causes a reaction that results in methylation of the fatty acid to form fatty acid methyl esters (FAMEs). The mechanism for this reaction with TMSH is shown in Figure 1.32
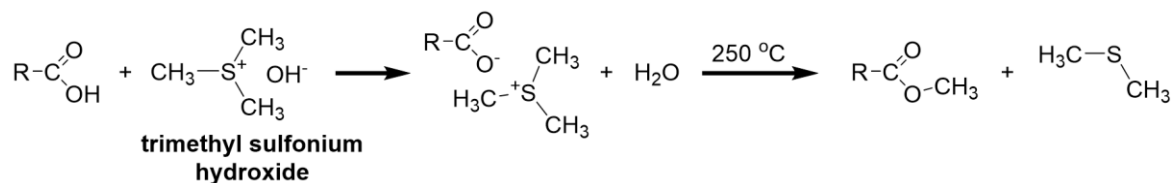
Figure 1.32: Transmethylation reaction with TMSH.

The transmethylation method with TMSH is very convenient; however, it has been shown to have limitations when the lipids contain amino, amide or hydroxyl groups (Vosmann et al., 1998)

1.5.5.3.   *Gas Chromatography-Mass Spectroscopy measurements of FAMEs*

Gas chromatography (GC) is the primary method for fatty acid analysis. Individual fatty acids can often be identified directly from the GC trace due to their retention times, or the GC can be connected to a mass spectrometer or flame ionisation detector to allow further information to be collected to aid identification (Dodds et al., 2005). Fused silica capillary columns use a similar theory to that discussed for HPTLC in section 1.5.5.1. The polarity of the column will determine the elution order of the FAMEs. However, size is a factor with all columns, and shorter fatty acids will elute earlier than longer chain fatty acids. With non-polar columns, unsaturated fatty acids are eluted before saturated fatty acids of the same length, while the reverse is true with polar columns. In very highly polar columns, a very unsaturated fatty acid, e.g. α-linolenic acid (C18:3), will elute after arachidic acid (C20:0). In this work, two columns were used, both highly polar and specially designed to separate FAMEs.

2. Materials and methods

Materials and methods are listed here, where they correspond to more than one chapter in this thesis; otherwise, the material or method is listed within that chapter.

2.1. Polyglycerol polyricinoleate

The polyglycerol polyricinoleate samples used in this research were Admul WOL 1408 (provided by Kerry Ingredients and Flavours EMEA, Netherlands), Grindsted Super and Grindsted 90 Kosher (provided by Danisco, Dupont Nutrition and Health, Denmark), and Palsgaard 4125 and Palsgaard 4150 (provided by Palsgaard A/S, Denmark). The PGPR samples were used as received without further treatment.

2.2. Sunflower oil

Sunflower oil was bought from a local supermarket. To allow interpretation of data as a consequence of the surface-active properties of PGPR alone, the naturally present surface-active components in sunflower oil were removed through treatment with magnesium silicate following the published protocol (Gould et al., 2016).

A mixture of 4% (wt) of magnesium silicate (Florisil®, <200 mesh, fine powder, bought from Sigma-Aldrich, Germany) and sunflower oil was stirred for 30 min at 600 rpm and 22 ± 1 °C on a magnetic stirrer (Carousel Tech Stirring Hotplate, Radleys, UK). The magnesium silicate was then removed by centrifugation at 2700 g and 20 °C for 30 min (Jouan CR3i multifunction Centrifuge, Thermo Fisher Scientific, Massachusetts, USA). This method is illustrated in Figure 2.1. The treatment was verified as successful using a pendant drop tensiometer (Profile Analysis Tensiometer PAT1, SINTERFACE Technologies, Germany) as described in Section 2.7. The treated sunflower oil was stored in amber glass bottles in the dark at room

temperature (22 ± 1 °C) for no more than two weeks to reduce the risk of oxidation which would create new surface-active molecules, for example, free fatty acids. The absence of surface-active molecules was validated at least every three days using the tensiometer.

Mix sunflower oil with 4% magnesium silicate for 30 min at 600 rpm.

Pour into 50 mL centrifuge tubes.

Centrifuge at 2700 g for 30 min at 20 °C.

Collect supernatant.

Check treatment is successful using tensiometer.

Store in an amber duran bottle in the dark at 22 ± 1°C for no more than two weeks.
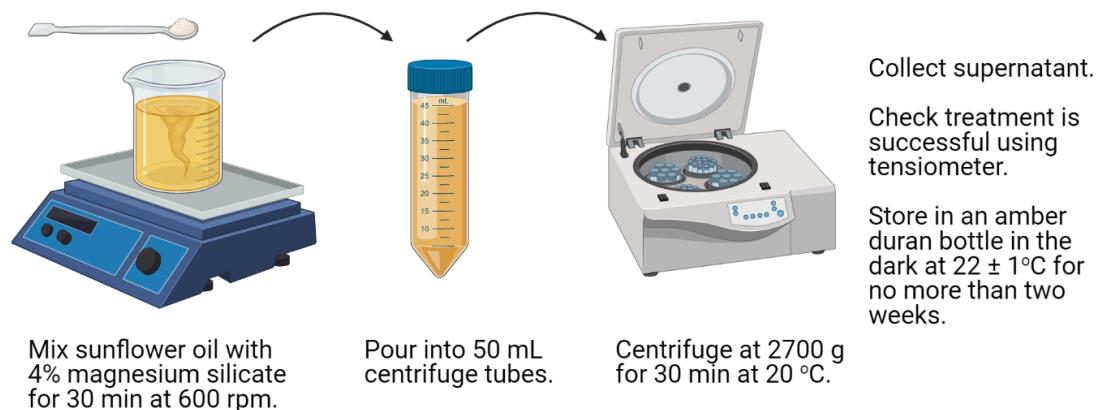
Figure 2.1: Illustration of the treatment of sunflower oil to remove surface-active components. Graphic drawn in Biorender.

2.3. Incorporation of PGPR into the treated oil

PGPR was added to the oil at the required concentration by weighing the PGPR, then the oil, into a beaker. The mixture was stirred gently for 60 min (100 rpm and 22 ± 1 °C) using a magnetic stirrer (Carousel Tech Stirring Hotplate, Radleys, Essex, UK), as described in the literature (Ziegler, Garbolino, & Coupland (2003)).

2.4. Sugar

Icing sugar (containing less than 1.5% calcium phosphate as a free-flowing agent, British Sugar) was bought online from a wholesaler (LCO Trading Ltd Store, UK).

When sugar crystals are fractured during grinding, soft amorphous layers are formed. These amorphous layers account for 2-3% weight of total sugar and are very hygroscopic (i.e. they quickly absorb water from the environment) (Garbolino, 2002).

This moisture would cause changes to the rheology of the sugar-in-oil suspension. Therefore, before use in the chocolate model, the sugar was dried overnight in batches of around 100 g in a vacuum oven (Gallenkamp, Fistreem International, Loughborough, UK) at 60°C and then left to cool in a desiccator before preparing the suspensions.

The sugar particles' size was measured in sunflower oil using laser diffraction equipment (Mastersizer 2000, Malvern Instruments Ltd, UK). The icing sugar was dispersed in sunflower oil, which included a small amount of PGPR (around 0.5%) to aid dispersion. It was then manually mixed and sonicated before measurements took place. The volume-weighted mean was 35.16 μm, and the volume-based diameter indicated that 90% of the particles were smaller than was 87.09 μm. These values are slightly larger than those expected in chocolate, where the maximum particle size is often 35 μm (Ziegler and Hogg, 2017). However, in research using a chocolate model, sometimes the particle size is slightly larger than this (Bonarius et al., 2014, Mohamad et al., 2020), as shown in table Table 1.2.

2.5.   Chocolate model

Sugar-in-oil suspensions (65% (wt) or 53% (vol)) for rheological assessment were prepared from treated sunflower oil, PGPR and dried icing sugar.

The oil was treated to remove surface-active components as described in section 2.2. If required, PGPR was added to the oil at the required concentration following the instructions in section 2.3. Before being utilised as the suspension particle phase, the icing sugar was dried as outlined in section 2.4.

One part dried icing sugar was combined with one part treated sunflower oil or prepared PGPR/oil mixture on a weight basis. The mixture was stirred manually with a spatula until all sugar particles appeared wetted by the oil phase. Thorough mixing

was accomplished using a high shear overhead mixer (SilversonL5M, Silverson Machines Ltd, UK) for 4 min at 8000 rpm. The sample batch size was kept constant at 190 g and contained in a 250 mL beaker with an internal circumference just wider than the mixer head. The beaker was placed in an ice bath to ensure that the temperature of the mixture did not reach values above 47°C, to avoid the risk of oxidation (Crapiste et al., 1999). The samples were stored for 39 ± 2 h at 22 ± 1 °C, away from light, before adjusting the solid phase fraction to 65% (wt), as follows: The samples were transferred to centrifuge bottles and centrifuged (Beckman Model J2-21 centrifuge, with JA-14 fixed angle motor) for 10 min at 3836 g and 10 °C. Subsequently, the appropriate amount of supernatant (calculated as 23% of the total weight of the sample) was removed using a Pasteur pipette. The sample was manually stirred with a spatula and left to stand for at least 10 min before briefly stirring again and applying to the rheometer. Manual stirring was required at this point due to the very high concentration of the suspension: an automated system would be unable to achieve good dispersion at this point because of the consequent rheology of the sample and the challenge of redispersing the centrifuged pellet.
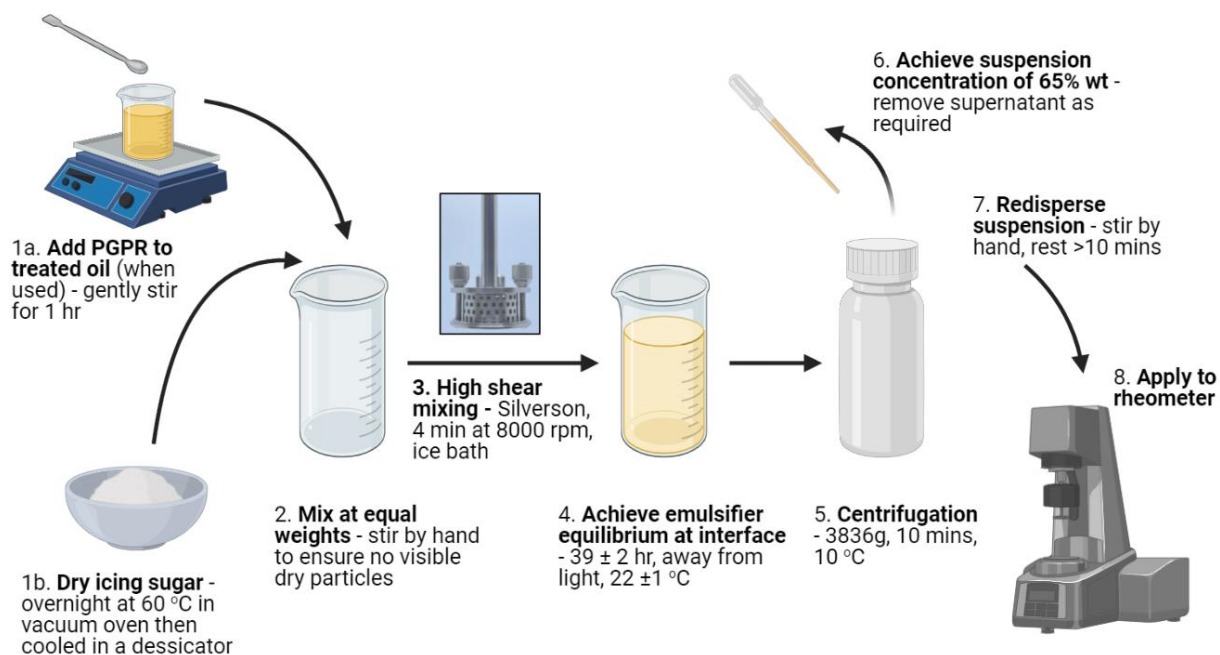
Figure 2.2: Illustration of the chocolate model preparation. Graphic drawn in Biorender.

2.6. Rheological protocol

Two rheological protocols were devised in order to measure the yield stress in the samples. They were found to give similar yield stress values for the samples, and so in most of this thesis, only the data from the unidirectional stress controlled ramp were reported. However, where the samples had a high yield stress, for example, where the yield stress was close to that of the sample with no added emulsifier, the oscillatory stress sweep was more applicable. Rotational tests measure the flow of a material and demonstrate the yield stress of a material when the force applied breaks the bonds causing the measured viscosity to reduce to a place where the sample can flow. The oscillatory test is an amplitude sweep where the particles are moved against each other with increasing force. The rheometers' results reveal how strong the bonds are between particles. When the stress applied is at a level where the bonds break, the material yields causing the elastic modulus to fall.

2.6.1. Unidirectional stress controlled ramp

The shear rheological properties of the prepared suspensions were evaluated on a stress controlled rheometer (Anton Paar Physica MCR 302 Rheometer, Graz, Austria) fitted with a serrated cup (C-CC27-SS-P) and serrated bob (CC27-0-40/P6) inserted into a Peltier holder (C-PTD200). The sample was applied to the geometry, and the measurement started immediately, at 20 °C. The rheological protocol consisted of a unidirectional stress ramp from 1000 Pa to 0.1 Pa, collecting ten logarithmically spaced data points over each decade. Each stress was applied for 10 s, and then the data was collected. Finally, utilising the rheometer's software package (Anton Paar RheoPlus, and, in later experiments, Anton Paar RheoCompass 1.21), the data were fitted to the Herschel-Bulkley model to obtain (Herschel-Bulkley) yield stress values, see equation 1.8, section 1.4.7.10.

2.6.2. Oscillatory stress sweep

This stress sweep was programmed from 0.1 Pa to 100 Pa, with ten logarithmically spaced data points acquired per decade. Each stress was applied for 10 s, and then the data was collected. The oscillatory stress sweep was performed at a frequency of 10 rad/s. Using an excel spreadsheet, the data was processed, and the yield stress was obtained using a method popularised by Walls et al. (2003). Here, the elastic stress ($G' \gamma$) is plotted as a function of the strain amplitude. The maximum in the elastic strain curve is interpreted as the yield stress of the material.

2.7. Interfacial tension and critical micelle concentration

A pendant drop tensiometer (Profile Analysis Tensiometer PAT1, SINTERFACE Technologies, Germany) was utilised for the analysis. Treated sunflower oil ± PGPR was contained in a quartz glass cuvette kept at 20°C using a water bath (Grant

Instruments, UK). A drop of ultrapure water was pendant from a straight capillary (stainless steel, 2 mm outer diameter) into the oil; the cross-sectional drop area was set to 25 mm^2. Images were taken every second until equilibrium was achieved, which was taken to be no change in the interfacial tension value ± 0.1 mN/m over 400 seconds. The value used to report the equilibrium value was the average of the last 400 s data.

The critical micelle concentration (CMC) is the concentration at which the amphiphilic molecules start to form micelles or reverse micelles. This process is critical to an emulsifier as, when micelles form, the amphiphilic molecules are not free as unimers to adsorb at the interfaces: interfacial tension measurements are constant above the CMC value. The CMC value is calculated by measuring the equilibrium interfacial tension of a system using increasing concentrations of the amphiphilic molecule. The equilibrium values are plotted as the interfaction tension values [mN/m] versus the logarithm of the concentration. Two gradients will be formed – the gradient will be zero above the CMC, and below, there will be a decrease in interfacial tension as the concentration of emulsifier in the system increases. The point where these two lines intersect is designated the CMC value.

2.8.   Production of ultra-pure water

Ultra-pure water was obtained through a Select FUSION water purifier (Purite Ltd, UK). The process of purifying water in this device is outlined below (Purite, 2008):

Potable feedwater enters the unit via an external 5 μm carbon-impregnated pre-filter. The filter removes up to 95% of all particles > 5 μm and will dechlorinate to < 0.1 ppm on 0.5 ppm feedwater supply. The pre-filtered water enters the reverse osmosis modules, where 85-95% of salts are removed. This water is known as the permeate. Water containing the rejected salts is drained from the machine.

The permeate is further purified by a Puripac PP8 cartridge containing mixed ion-exchange resin and activated carbon. The deionised water then feeds directly into a storage tank and at this point at Grade 2 standard. To produce Grade 1+ quality water at the point of use, the water is drawn from the tank by a recirculation pump at a rate of up to 1 litre/min and polished via an NCP media pack containing high purity semiconductor grade nuclear grade resin and activated carbon. The polished water is then irradiated by dual-wavelength ultraviolet light (185/254nm) that photo-oxidises any dissolved organics, thus reducing the Total Organic Carbon content of the water and deactivating any living bacteria present. The high purity water is dispensed through a sterile 0.2 μm filter.

2.9. Lipid analysis using high-performance thin-layer chromatography (HPTLC)

HPTLC was used to identify and, where possible, quantify the lipids within the sample. Polar and non-polar lipids could be separated using distinct conditions as outlined below. The solvent mixtures were optimised by Dr Jutarat Wattanakul during her secondment to the University of Marseille as part of her PhD research (Wattanakul, 2020). Appropriate amounts of the samples were spotted onto a plate with lipid standards. The standards were used to either locate the lipid of interest or applied at different volumes to create a standard curve so that the concentration in the sample could be deduced. The volume of sample applied had to be optimised over consecutive plates so that the band colour density fit within the range of the standard curve.

The general method was as follows: the samples and standards were spotted as 8 mm bands onto a thin-layer silica plate (60 F_{254} glass TLC plates (10x20 cm), Merck) using a Linomat 5 semi-automatic sample application system (CAMAG®, Switzerland) equipped with a 100 μL Hamilton syringe, controlled by VisionCATS software (version

2.5, CAMAG®, Switzerland). The chosen development solvent was poured into the elution tank (Twin Trough Chamber, CAMAG®, Switzerland) at least 30 min before the separation was to take place, and a sheet of filter paper was placed against the inside of the tank on the side that would not be used by the plate. The filter paper enabled better saturation of the air within the tank to ensure optimum performance. The separation of the lipids was performed by placing the plates in the tank and allowing the solvent front to progress up the plate until it was 75 mm from the bottom of the plate. The plate would then be removed and allowed to dry in a fume cupboard. This step may be repeated if the separation of components was shown to be challenging.

If the lipid types require derivatisation to reveal the bands, the plate would then be dipped into the chosen derivatisation solvent using a Chromatogram Immersion Device 3 (CAMAG®, Switzerland). After allowing the plate to dry, it was placed in an oven (Elgento™ E14025 Compact Mini Oven, 9 Litre, made in China for RKW Ltd, UK) at the required temperature and time, or until the bands were developed. Images of the plates were taken by a TLC Visualiser 2 (CAMAG®, Switzerland). The data from the plates were analysed using the VisionCATS software.

2.9.1. Development solutions

For polar lipid separation, with an emphasis on the galactolipids, the mobile phase was made using chloroform (Honeywell, USA), methanol (Fisher Scientific, USA) and water in the proportions: chloroform:methanol:water (47.5:12:1.25, vol).

For non-polar lipid separation, the detection of fatty acids, or for separation of carotenoids, the mobile phase was heptane (ACROS Organics™, Belgium), diethyl ether (Honeywell, USA) and acetic acid (ACROS Organics™, Belgium) in the proportions: heptane:diethyl ether:acetic acid (55:45:1 (vol)). For the best separation

73

of these lipids, the plates would often need to be applied to the mobile phase twice, ensuring the plate was thoroughly dried between steps.

2.9.2. Derivatisation solutions

For galactose ring staining, thymol with sulphuric acid was used. The solution was made as follows: 1 g thymol (Sigma Life Science, Germany) was dissolved with 190 mL ethanol (Fisher Scientific, USA). The container was put on ice, and 10 mL sulphuric acid (96%) (VWR Chemicals, France) was added with care. Once the plate was dipped in this solvent and dried, it was heated at 110 °C in the oven for 4 min or until the colour had developed; see section 1.5.5.1 for the chemical reaction which occurs.

For general acyl group staining, copper acetate-phosphoric acid solution was used. This solution was made by heating 300 mL of distilled water to 80 °C using a magnetic stirrer on a heated plate. Copper acetate (50 g) was gradually added to the hot water. The heat is then switched off to allow the solution to return to room temperature whilst the stirring continues. The solution is vacuum filtered and made up to 435 mL using distilled water, then 40 mL phosphoric acid (85%) is added and shaken until the white precipitate disappears. Finally, 25 mL of methanol is added. Once the plate is dipped in this solvent mixture and dried, it is placed in the oven at 180 °C for 7 min or until the charred bands appear, see section 1.5.5.1 for the chemical reaction which occurs.

Once made, the derivatisation solutions were stored in sealed Duran bottles at room temperature and reused for up to six months.

2.10. Transmethylation of fatty acids using trimethyl sulfonium hydroxide (TMSH)

The PGPR samples or dried leaf lipid samples were dissolved in chloroform as described in the relevant results chapter, then 1 mL of this dissolved lipid was measured into a clean glass bijou bottle. Methyl pentadecanoic acid (100 µL; internal standard) (Sigma Aldrich, Germany) was added, followed by 200 µL Trimethylsulfonium hydroxide (TMSH), 0.25M solution in methanol (ACROS Organics™, Belgium). The lid was applied to the bijou bottle, vortex mixed and left for at least 10 min to ensure complete conversion. The mixture was then filtered into amber glass vials through 0.45 µm PTFE filter membranes (Whatman, GE Healthcare Life Sciences).

2.11. Fatty acid analysis using gas chromatography-mass spectrometry (GC-MS)

Due to the availability of equipment within the laboratory with the COVID-19 shut down and gradual reopening, the fatty acids within the two types of samples analysed in this PhD were performed on two different GC-MS, as described below.

PGPR: The fatty acid methyl esters (FAMEs) created from the PGPR samples that had undergone the transesterification process outlined in section 2.10 were analysed using gas chromatography coupled to mass spectrometry detection (GC-MS) (Thermo Scientific, DSQ) using a modified method based on Bahrami et al. (2014). After filtering the dissolved FAMEs through a 0.45 µm PTFE filter membrane into an amber glass vial, the samples (1 µL) were injected into a Phenomenex Zebron ZB-FFAP (30 m × 0.25 mm) column using a vaporising injector with a split flow of 50 mL/min of helium. The oven temperature was maintained at 120 °C for 1 min and then increased to 250 °C at a rate of 5 °C/min and held for 2 min. Detection was conducted

using a mass spectrophotometer. The identification of individual fatty acids was achieved using a mass spectrum library by comparing retention time and molecular mass to FAME standards. Blanks containing 2 mL of chloroform were included every six samples to minimise any carry-over between samples.

Cocoa leaves: The FAMEs created from the leaf lipid samples that had undergone the transesterification process outlined in section 2.10 were analysed using gas chromatography coupled to a mass spectrometer/flame ionisation detector (GC-MS/FID) (ISQ™ 7000 Single Quadrupole GC-MS System, Thermo Scientific). The dissolved FAMEs were filtered through a 0.45 μm PTFE filter membrane into an amber glass vial. The sample (1 μL) was injected into an Agilent J&W Cp-Sil 88 (100m x 0.25 mm) column using a vaporising injector with a split flow of 30 mL/min of helium. The oven temperature was maintained at 140 °C for 5 min and then increased at a rate of 4 °C/min to achieve a final temperature of 240 °C that was held for 10 min: a 40 min measurement time. The mass spectrometer was run in SIM (Selected Ion Monitoring) and SCAN (35-550 amu) modes simultaneously. The SIM mode was developed by selecting ions of interest (a quantifying and two confirming ions) from spectra collected by running the Supelco 37 Component FAME Mix Standard (Sigma Aldrich, Germany) using the same instrument, improving selectivity and sensitivity for the 37 FAME compounds contained within the standard. The FID was heated to 260 °C, lit with a constant flow of 35 mL/min Hydrogen and 350 mL/min air, and allowed time to equilibrate before the analysis was started. A serial dilution of the FAME Mix Standard was used to create a standard curve from which the amount of each component contained in the samples was calculated. Additional vials containing the FAME Mix Standard were included for quality control at the start and end of the analytical run, and blanks containing 2 mL of chloroform were included for every six samples to minimise carry-over between samples.

3. Development of a chocolate model and yield stress protocol

3.1. Introduction

In section 1.4, chocolate was introduced as a concentrated suspension material that, when fully conched, generally exhibits the rheological characteristics of a marked yield stress followed by shear thinning (Wolf, 2017). The high volume particle fraction can mean that during conching, the chocolate can experience times of frictional jamming and dynamic shear thickening (DST). This phenomenon is caused by a fluid-solid phase transition occurring due to system spanning networks of particle contacts, which can occur by mechanisms such as hydroclustering (particles are pushed together under high shear and cannot break away because of drag forces) or dilatancy (dilation of granular shear flows is frustrated by its container, resulting in addition normal forces) (Brown and Jaeger, 2014). However, for chocolate, continued shearing, and with the addition of emulsifiers, produces molten chocolate with the desired rheological characteristics (Blanco et al., 2019).

In sections 1.4.7.8 and 1.4.8.2, a review of model systems and rheological parameters that have been used in literature as the methods to measure the yield stress of chocolate and chocolate models was included. These protocols address the aims for which they were devised, which is often viscosity as well as yield stress measurement. The main advantage that PGPR presents to chocolate manufacturers is in the adjustment of the yield stress, and any natural alternative would need to replicate this functionality. As this was so important, the first objective in this PhD research was to develop a chocolate model for a sugar-in-oil suspension of a high packing fraction and a rheological protocol to assess the yield stress reducing efficacy of the PGPRs and the prospective alternative emulsifier. The aim was to achieve good reproducibility of yield stress data acquired on repeat batches of prepared chocolate

models so the different efficacies of the five PGPR samples could be reliably compared. There are different ways that variation can occur between samples. These include system variation due to the measuring equipment; and process variation due to human error, uncalibrated machines or confounding issues within the process. Variation in the results can cause erroneous conclusions to be drawn about the experimental results. All equipment used was regularly inspected, and the inertia and motor adjust checks were performed on the rheometer each day before the experiments took place. The methodical steps were written down and followed carefully each time the experiment took place to limit human error. The main issue foreseen with a sugar-in-oil suspension was the break up the sugar aggregates. If the method did not perform the shearing required to separate these aggregates in a consistent manner, then the variable sugar aggregate sizes would affect the rheological properties and lead to inaccurate results.

To ensure that the final rheological protocol gave realistic results, the data were compared and verified against data acquired following the International Office of Cocoa, Chocolate and Sugar Confectionery (IOCCC) Analytical Method 46 (2000), described in 3.2.2. This method had been evaluated using five ring-tests in more than 32 laboratories in eight countries to confirm that the protocol was reliable (Aeschlimann and Beckett, 2000). However, the method relies heavily on the extrapolation of the yield stress value from a small data set, which is not desirable for a detailed exploration of the yield stress reducing power of emulsifiers. The ring tests performed gave results that had a coefficient of variation of 8% between laboratories for most chocolate samples used, however the results for the white chocolate sample had a coeffcient of variation of 13%. Therefore, these variations were used as a benchmark for the protocol developed for this thesis.

The protocol development was attempted first, and it was performed on commercial dark chocolate; then, the chocolate model was developed. The final, validated

rheological protocol and chocolate model preparation method are outlined in sections 2.5 and 2.6, and these are used in chapters four, six and seven of this thesis.

3.2. Materials and methods

3.2.1. Materials

Dark chocolate (G&B's Dark 70%, Green and Black's, UK) and sunflower oil were purchased from a local supermarket. Icing sugar was purchased online from a wholesaler; see section 2.4 for details. PGPRs are listed in section 2.1.

The commercial dark chocolate consisted of cocoa mass, raw cane sugar, cocoa butter, emulsifier (soya lecithin) and vanilla extract. The nutritional information lists the fat content as 42 g per 100 g chocolate, from which it is assumed that the solid content is around 58% (wt). Dark chocolate was used because of its small number of ingredients, making it a simpler suspension than milk chocolate. Unfortunately, no commercial dark chocolate could be obtained in the supermarket that contained PGPR to coincide with the chocolate emulsifier system studied in detail in this PhD research. PGPR was only found in Cadbury's Dairy Milk chocolate and the supermarket's budget milk chocolate.

3.2.2. Methods

The surface-active components were removed from the sunflower oil following the method in section 2.2. Icing sugar was dried before use as outlined in section 2.4.

It was decided that the concentric cylinder method would be used in this research, as discussed in 1.4.2. The geometries used in the protocol development are shown in Figure 3.1.

Smooth bob (CC27): diameter 26.7 mm, length 40.0 mm
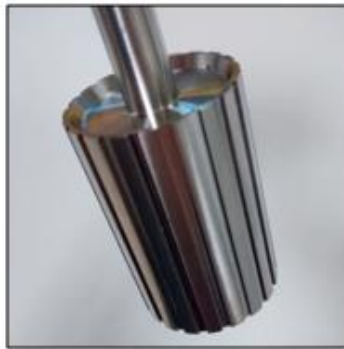
Serrated bob (CC27-0-40/P6): diameter 26.7mm, length 40.0 mm
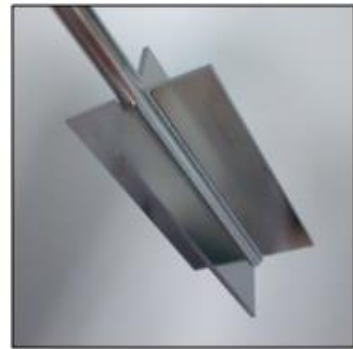
Vane (ST22-4V-40): diameter 22.0 mm, length 40.0 mm

Smooth cup (C-CC27-SS): diameter 28.9 mm

Serrated cup (C-CC27-SS-P): diameter 28.9 mm

Figure 3.1: Geometries used in the development of the protocol. The smooth cup and bob were used together, and the serrated cup and bob were used together. The vane was used with both cups.

The pairs of geometries (smooth bob & smooth cup, serrated bob & serrated cup, vane & smooth cup, and vane & serrated cup) were used to measure the rheology silicone oil with a viscosity of 10,000 cSt to ensure there were no problems with the rheometer or the geometries. They all measured the viscosity as expected, as shown in Appendix 1.

The protocol developed for this PhD research used the concept of Arnold et al. (2013), which started with a high shear rate and used a decreasing ramp to measure the yield stress; the viscosity rises sharply as the yield stress point is reached. This initial high

shear mitigates any effects of the sample history, which means a pre-shear step is not required.

In the literature, many protocols used to examine the rheology of chocolate or other highly filled suspensions, including the paper by Arnold et al. (2013), employ shear rate control that imposes the deformation, especially if they measure the viscosity of the sample. If yield stress data is also to be obtained, then it is extrapolated using a mathematical model. Some of the protocols in the literature are summarised in Table 1.1. However, as previously discussed in section 1.4.7.7, if yield stress is to be examined closely, the rheological protocol should be controlled by the shear stress. Using shear stress could allow for the yield point to be determined directly by defining it as the shear stress where the shear rate is the lowest measured (Mezger, 2014) or more conventionally by applying a mathematical model to the data. Some researchers have used a shear stress controlled protocol to measure the yield stress (Fernandes et al., 2013, Ziegler et al., 2003) or a stress controlled oscillatory protocol (De Graef et al., 2011, Fernandes et al., 2013, Taylor et al., 2009). Therefore, a shear stress-controlled protocol was developed.

Many protocols, especially those that use a continuous shear ramp, employ a mathematical model to their rheological data to obtain the yield stress value. Some explanations and the equations for these models were described in section 1.4.7.10. The Casson model (equation 1.9 in section 1.4.7.10) is used often in chocolate research; however, it has been shown to be unrepresentative of the behaviour of chocolate rheology, especially at low shear rates (Taylor et al., 2009, Briggs and Wang, 2004), and even the IOCCC (2000) has recommended discontinuing its use. The Carreau, Herschel-Bulkley, and Windhab models have been suggested as alternatives; see Table 1.1. In this research, as aforementioned, the Herschel-Bulkley model (equation 1.8, section 1.4.7.10) was used based on the recommendation in the literature (Arnold et al., 2013, Sokmen and Gunes, 2006, Briggs and Wang, 2004).

The IOCCC protocol (2000) is as follows: the sample is brought to 40 °C under constant shear rate, preferably 5 s^{-1} for standard chocolates or 2 s^{-1} for "very thick ones" (a precise definition of "very thick" is not made within the protocol). The pre-shearing stage should continue until the viscosity remains stable within a range of less than 2 % over two minutes. The measurement protocol should then begin at 2 s^{-1} and increase to 50 s^{-1} over three minutes. The shear rate should then be held at 50 s^{-1} for one minute before decreasing again from 50 s^{-1} to 2 s^{-1} over three minutes.

The sample preparation method was initially based on Mohamad et al. (2020). In this method, the sugar-in-oil suspension was mixed at 1000 rpm using an overhead impeller stirrer for 1 hour at room temperature (22 ± 1 °C). It was then put in an end-over-end mixer in a sealed container to stop sedimentation until it was measured on the rheometer. This method was for a sugar-in-oil suspension with a maximum dispersed volume fraction of 0.37 (50 %(wt)). In this PhD research, to ensure the range of particle-particle interaction forces encountered in densely packed chocolate systems is present in the model systems to assess the action of the emulsifier comprehensively, a model system that reflects the volume fraction found in chocolate, around 0.56 (70% (wt)) (Do et al., 2007) was developed. The relevant interaction forces include intermolecular forces between close neighbouring particles, which could be Van der Waals forces (Mezger, 2014), hydrogen bonding (James et al., 2019), Keesom forces (rotating dipoles), Debye forces (permanent dipoles-induced dipoles), London forces (fluctuating dipole–induced dipole interaction) or even capillary forces, if water has been absorbed (Koos and Willenbacher, 2011). Interparticle friction also comes into play at high volume fractions (Richards et al., 2020). Therefore, the proposed method (Mohamad et al., 2020) had to be adjusted to allow for this, as described below.

3.2.3. Statistical analysis

The results shown in Figure 3.3 were analysed in pairs based on the method and geometries used. A two-tailed independent t-test was employed for each pair using SPSS (Statistics v 27, IBM Corp, USA). The significance level was set at $p < 0.05$, and three measurements were made per batch produced.

The results shown in Figure 3.9 were analysed in groups based on the amount of PGPR added to the sample. A one-way analysis of variance (ANOVA) followed by a Tukey post-hoc using SPSS (Statistics v 27, IBM Corp, USA). In order to ensure that the ANOVA test was applicable, the homogeneity of variance was evaluated within the three batches representing the types of samples, as assessed by Levene's test for equality of variances. The significance level was set at $p < 0.05$, and three measurements were made per batch produced.

3.3. Results and discussion

3.3.1. Development of the rheological protocol

The first objective was to devise a methodology to determine the impact PGPR has on yield stress. This method needed to be reproducible and should give data in the low shear region such that comparisons of the yield stress reductions caused by the PGPRs, and any other emulsifiers, could be made. The development of the rheological protocol was performed using commercial dark chocolate as the sample, which was broken into pieces, placed in a wide-mouthed Duran bottle (500 mL capacity) and melted in a convection oven (MOV-112F, Sanyo Electric Biomedical Co, Ltd, Japan) at 50 °C for at least one hour before use. The use of a commercial

reference sample enabled the protocol to be assessed without being confounded by any sample inadequacies.

As discussed in section 3.1, a high-to-low shear stress ramp method was chosen. This was run from the highest shear stress available for the geometry, according to the limits of the rheometer: 2700 Pa for the smooth bob or 3000 Pa for the vane or serrated bob. Shear stress was decreased stepwise and logarithmically to 0.1 Pa, or lower if the sample displayed a very low yield stress, collecting ten logarithmically spaced data points over each decade. Each stress was applied for 10 s, and then the data was collected. The temperature was kept at a constant 20 °C by the Peltier of the rheometer.

The different geometries assessed are shown in Figure 3.1. The geometries were paired as follows: Smooth bob & smooth cup, serrated bob & serrated cup, vane & smooth cup, and vane & serrated cup. Data from the proposed protocol was compared to data obtained using the IOCCC standard method (2000) using just the smooth bob & smooth cup and the vane & serrated cup. The results obtained are shown in Figure 3.2. For all data sets, there was a Newtonian region of low viscosity at high shear stress. As the shear stress was decreased, there was an increase in the viscosity as the particles in the chocolate started to form the intermolecular bonds that caused the yield stress. The data obtained from different aliquots of the same batch of molten chocolate measured with the same geometry and protocol were very similar to each other for the whole data range until slip was observed after the yield stress region was reached. The reproducibility of these data acquired in these samples both within and between groups is discussed in the next paragraph. The phenomenon of slip was introduced in section 1.4.7.9, and arrows highlight it in Figure 3.2.

The data were evaluated to compare the two methods, and the results are shown in Figure 3.3. The data obtained using the IOCCC standard method were analysed using the Windhab model (equation 1.10, section 1.4.7.10), as recommended in the

standard procedure (IOCCC, 2000), to attain the yield stress. As a comparison, the data for the smooth bob & cup and the vane & serrated cup generated using the protocol developed for this PhD research were analysed using the Herschel-Bulkley model (equation 1.8, section 1.4.7.10). These two geometries were evaluated as they were those used in the IOCCC protocol measurements. For both protocols, the viscosity measured at 40 s^{-1} was taken as chocolate viscosity, following the recommendation by Servais et al. (2003), as the Herschel-Bulkley model does not provide an infinite shear viscosity value as the Windhab model does.

It can be seen from Figure 3.2 that the data acquired with the new protocol developed for this PhD research compares very well to the data collected using the IOCCC model. Regarding the yield stress data, the data from the smooth bob & cup using the two protocols gave yield stress values that were not significantly different from each other ($t_{(4)}$ = -0.959, p = 0.392). There is a difference between the protocols as far as the yield stress values were concerned when the vane & serrated cup was used ($t_{(4)}$ = 29.029, p < 0.05), but only a 7% change. For the viscosity at 40 s^{-1}, the values from the two protocols were not significantly different for either of the geometries used (for smooth bob & cup ($t_{(4)}$ = -0.315, p = 0.769), for vane & serrated cup ($t_{(4)}$ = -0.532, p = 0.623)). There were differences in viscosity value between the two geometries; however, this can be explained by the fact that 40 s^{-1} was at around 110 Pa when the vane & serrated bob was used, whereas it was around 75 Pa when the smooth bob & cup were used. Referring back to Figure 3.2 shows that at 110 Pa, the vane & serrated bob viscosity data were already starting to rise, however at 75 Pa, the viscosity data from the smooth bob & cup were just starting to deviate from the plateau region. This data confirmed that using the method developed would give equivalent values to the IOCCC method but more data in the low shear region, which is important for greater detail if the yield stresses are very similar.

The data within geometries/protocols were also very reproducible. The coefficient of variation shown in

Table 3.1 confirms that the data within the sets of results are very similar, 3.79 % being the largest variation.

The next area to consider with the method developed is the elimination or, at least, reduction of slip which can cause errors in the interpretation of the results. Slip occurs at around 7 Pa with the geometry pairs that include the smooth and serrated bob, and at around 11 Pa in the geometry pairs with the vane. It appears, visually, in Figure 3.2 that the measurements collected by the vane & serrated cup showed the least slip.

However, an anomaly can be seen when comparing the data measured with the smooth cup & bob and the serrated cup & bob, with the geometry pairs that include the vane. As shown in Figure 3.2, the same chocolate sample starts to show an increase in viscosity value towards its yield stress value at different shear stresses. Suppose the viscosity of 100 Pa.s is taken as an arbitrary point. In that case, one can see that the chocolate in the serrated cup & bob has that viscosity at about 8 Pa. In contrast, the chocolate in the vane & serrated cup reaches the same viscosity at about 12 Pa. This difference must be due to the geometries, so it was investigated further.

As shown in Figure 3.1, the diameter of the vane (22 mm) was different from the diameter of the bob (26.7 mm), which meant that the gap size was different; 3.46 mm for the vane & cup, and 1.125 mm for the serrated bob & cup. A larger gap can lead to inhomogeneous deformation behaviour (Mezger, 2014), which could perhaps encourage a higher yield stress due to the Van-der-Waals forces already being built up in the stationary layer of the suspension (Shamu and Håkansson, 2019). Therefore, the experiment was repeated with a vane of a larger diameter (26 mm) but otherwise the same design as the previously used vane. The data obtained by running aliquots of the dark chocolate in the serrated cup using the two vanes and the serrated

bob is shown in Figure 3.4. The vane with the larger diameter produced a lower yield stress value than the smaller diameter vane; however, it was not comparable with the measurements collected with the bobs.

The difference between the two types of geometry appeared to be an issue with the flow field. A review of the chocolate rheology literature did not seem to provide the answer; however, an explanation was found in the literature for another highly filled suspension system; concrete and grouts. Traditionally, the vane is thought to trap the sample within a cylindrical shape, as was observed with automotive greases (Keentok et al., 1985) and hence thought to reduce slip (Barnes and Nguyen, 2001). However, when a sample of non-colloidal particles in a shear stress fluid (at 40% (vol) fraction) was sheared in a rheometer connected to a magnetic resonance imaging device, a particle depleted layer is observed, as seen in Figure 3.5. Ovarlez et al. (2011) noticed that the blades cause this depleted layer, "a kind of wall slip near the blades", which arises almost immediately on commencement of shear and would lead to an incorrect rheological measurement. However, this layer would presumably lead to the measurement of a lower yield stress in a sample rather than a higher one, so this cannot be the whole story. Recent experiments on cement grouts using different bobs, including the vane, have shown a higher yield stress with the vane in some cases (Shamu and Håkansson, 2019). Their explanation for this phenomenon starts with the finding by Ovarlez et al. (2011) but adds that the unsheared stationary particles within the blades and in the cup flocculate during the measurement, even during high shear, so that structural bonds build up between particles. As the stresses applied decrease, further interparticle bonds can more easily form across the sheared area, which leads to the higher yield stress measurement. Although experiments since the observation of Ovarlez et al. (2011) have shown that a vane is acceptable in some circumstances, for example, if the sample is measured at a low strain (Feneuil et al., 2020) or with lower volume fractions (Pierre et al., 2017), it is clear that it is not appropriate to use

the vane with the protocol developed in for this PhD research. Therefore, as the measurement of the chocolate with the smooth bob and cup resulted in very obvious slip, the serrated bob and cup were selected as the geometry pairing to be used in this PhD research. Care would be taken to ensure that any slip was noted and mitigated in the analysis.

Figure 3.2: Viscosity curve showing the rheology of the dark chocolate sample using the proposed protocol with the four pairs of geometries: smooth bob & cup ◆, serrated bob & cup ▲, vane & smooth cup ●, vane & serrated cup ■. Open and closed shapes indicate different batches of the sample using the same geometry. The results from the proposed protocol are shown in black, and those from the IOCCC method are in red. The blue arrows indicate the onset of slip.
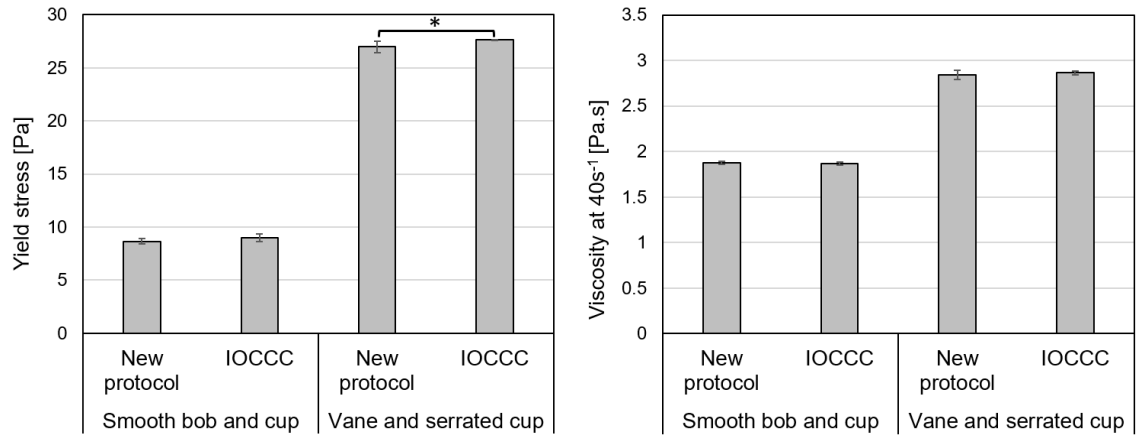
Figure 3.3: Yield stress [Pa] and viscosity at 40 s^{-1} [Pa.s] of the data shown in Figure 3.2 for both protocols where the smooth bob & cup were used, and the vane & serrated cup were used. The data bars represent three data points, and the error bars are the standard deviation of the means. The pairs of data were compared using an independent t-test, and any significance found between the pairs are shown with an asterisk (p<0.05).

Table 3.1: Values for the data shown in Figure 3.3 with the coefficient of variation included. The sample size for each data set is three. A t-test was applied to the pairs of means, and the p-value is shown here.

Measure	Geometry	Protocol	Mean	Std dev	%CV	p-value
Yield stress [Pa]	Smooth bob and cup	New protocol	8.67	0.26	2.99	0.392
		IOCCC	8.99	0.34	3.79	
	Vane and serrated cup	New protocol	26.99	0.55	2.03	< 0.05
		IOCCC	27.63	0.02	0.09	
Viscosity at 40s^{-1} [Pa.s]	Smooth bob and cup	New protocol	1.88	0.02	0.93	0.769
		IOCCC	1.87	0.02	0.87	
	Vane and serrated cup	New protocol	2.84	0.05	1.86	0.623
		IOCCC	2.86	0.024	0.84	

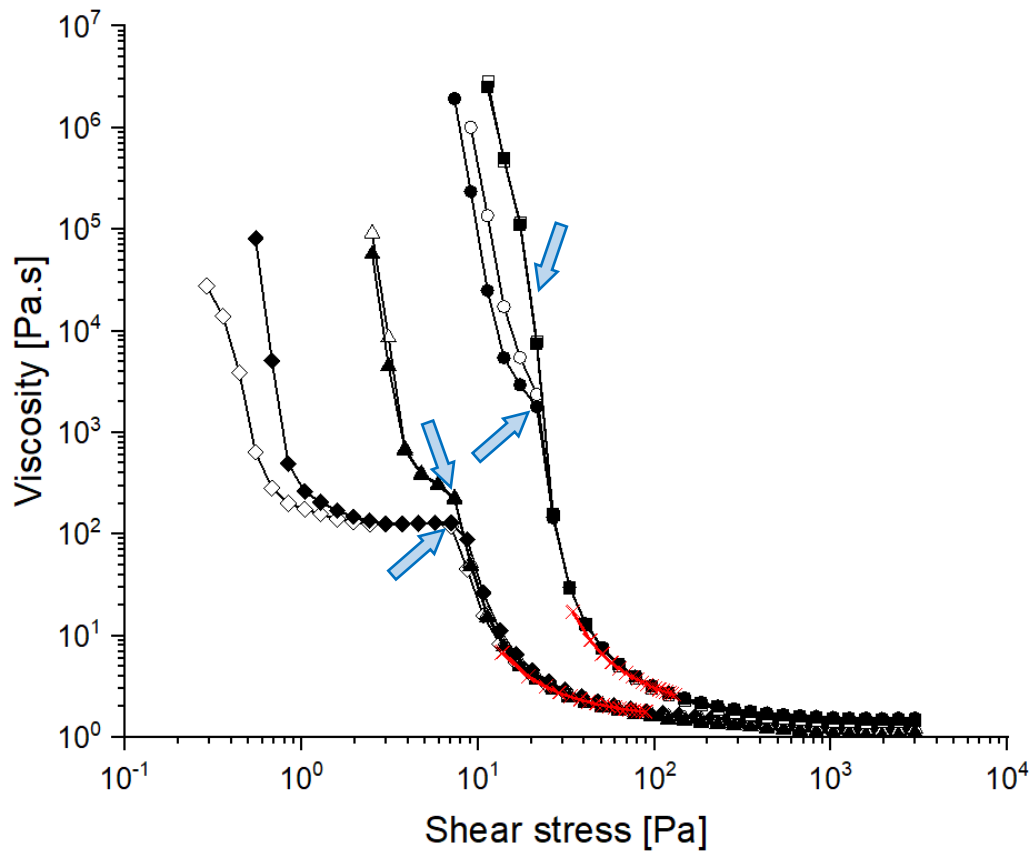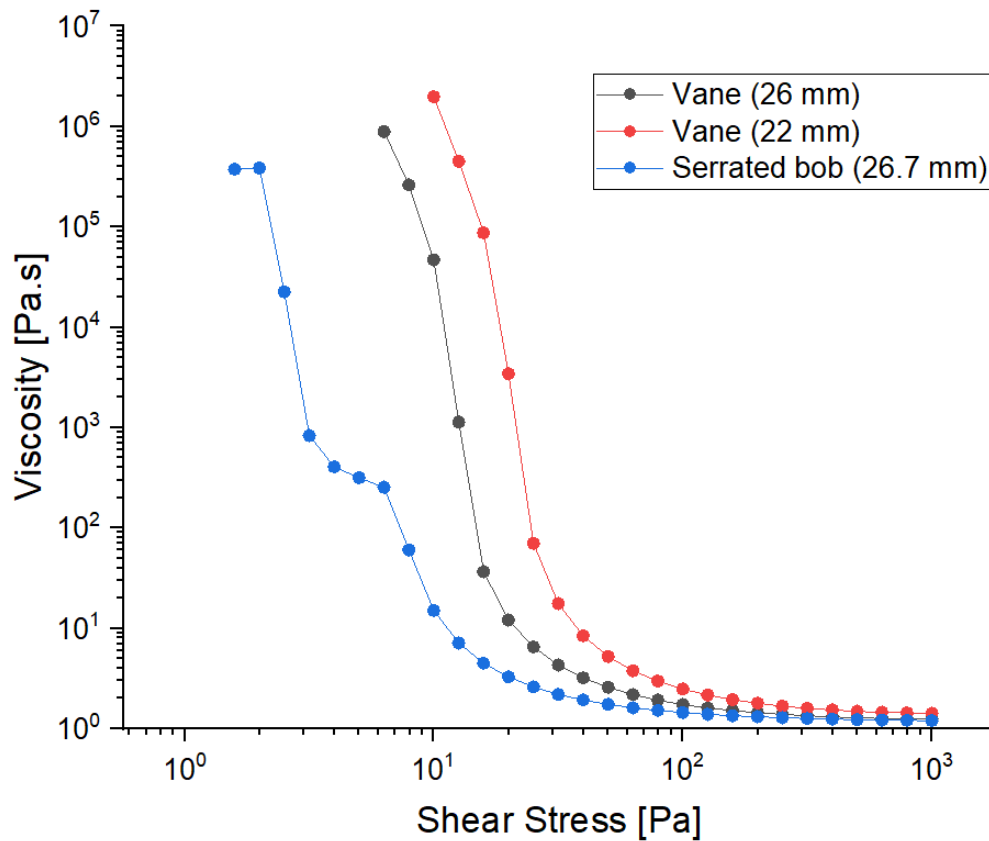*Figure 3.4: Viscosity curve showing the rheology of the dark chocolate sample using the proposed protocol with the serrated cup (28.9 mm), with the two vanes and the serrated bob.*
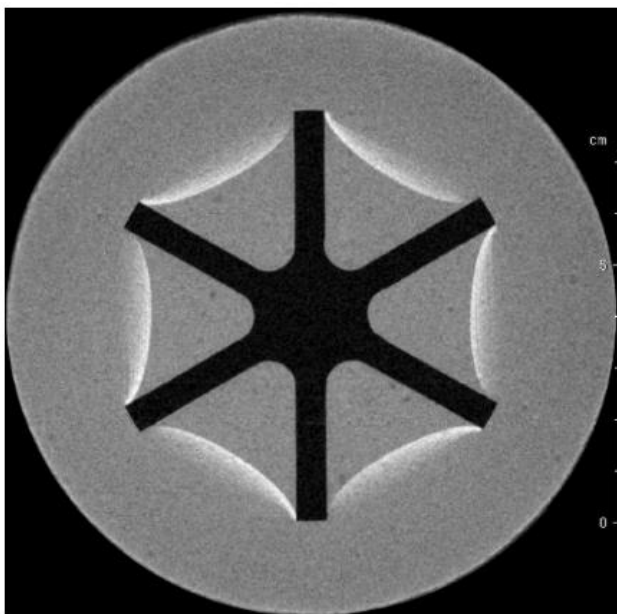
Figure 3.5: Two-dimensional magnetic resonance image of a 40% (vol) suspension of monodisperse polystyrene beads (diameter 250 µm) in a yield stress fluid (dodecane oil containing 7% Span 80 emulsifier into which a 100 g/l CaCl$_2$ solution was dispersed using a Silverson mixer: the droplets are around 1 µm in size and droplet concentration in the emulsion is 75%) after shear in a vane-in-cup geometry. The vane has a diameter of 8.04 cm, the outer cylinder diameter is 12 cm, and the height is 11 cm. This image shows a particle depleted area extending from the edges of the vane blades in a concave curve. Taken from Ovarlez et al. (2011)

3.3.2. Chocolate model

The chocolate model was to be created using sunflower oil and icing sugar at a volume fraction as close to chocolate as possible. The icing sugar had a volume-weighted mean particle size of 35 µm, and 90% of the particles were smaller than 87 µm.

The purpose of this step of the PhD research was to develop a sample preparation method with a high solid fraction (around 70 % (wt)), as already discussed. The sugar-in-oil sample should be reproducible within batches, and to assess this, the Herschel-Bulkley yield stress would be obtained for each data set and compared within and between batches. The Herschel-Bulkley model would be applied to the data from 0.1-100 s^{-1} to avoid the slip region. This range is also used in literature (Arnold et al., 2013). The criteria for a reproducible method were set as the yield stress within a batch, and between batches of the same type, should not be significantly different using a one way ANOVA test. The coefficient of variation would not be more than 10 %, which was based on the coefficient of variation of the results obtained during the method development of the IOCCC method as an average of the variances seen in this work (Aeschlimann and Beckett, 2000).

As aforementioned, the method of Mohamad et al. (2020) was used as a starting point for the chocolate model preparation method, see section 3.2.2. The method had previously been used for samples with a maximum packing fraction of 50% (wt) (0.37% (vol)) to reflect the amount of sugar found in a chocolate sample rather than the packing fraction of the total solids. Preparing a suspension of sugar-in-oil at 70% (wt) (no PGPR) before applying to the overhead mixer resulted in a suspension that was so concentrated that jamming occurred during hand mixing and so was considered unsuitable for the overhead stirrer. Therefore, the method was attempted at 65% (wt). However, the concentration was such that the mixer motor struggled to

stir at 1000 rpm. Therefore, instead of 1000 rpm for 1 hour, the sample was mixed at 200 rpm overnight before applying it to the rheometer.

Figure 3.6 shows the results of two batches, each of 65% (wt) sugar-in-oil suspensions without or with added PGPR, as listed in section 2.1, at a concentration of 0.3% (total suspension weight). The colours represent each sample type (Light brown – no PGPR; black – Admul WOL; green – Grindsted 90; blue – Grindsted Super; red – Palsgaard 4125; purple – Palsgaard 4150), and open and closed symbols represent the two batches. As can be seen from Figure 3.6, there was significant variability between the batches. This variation could be due to an agglomeration of sugar particles. Therefore, a higher shear was applied to break them up; breaking up sugar aggregates is one of the purposes of the conche shearing in chocolate processing (Beckett et al., 2017).
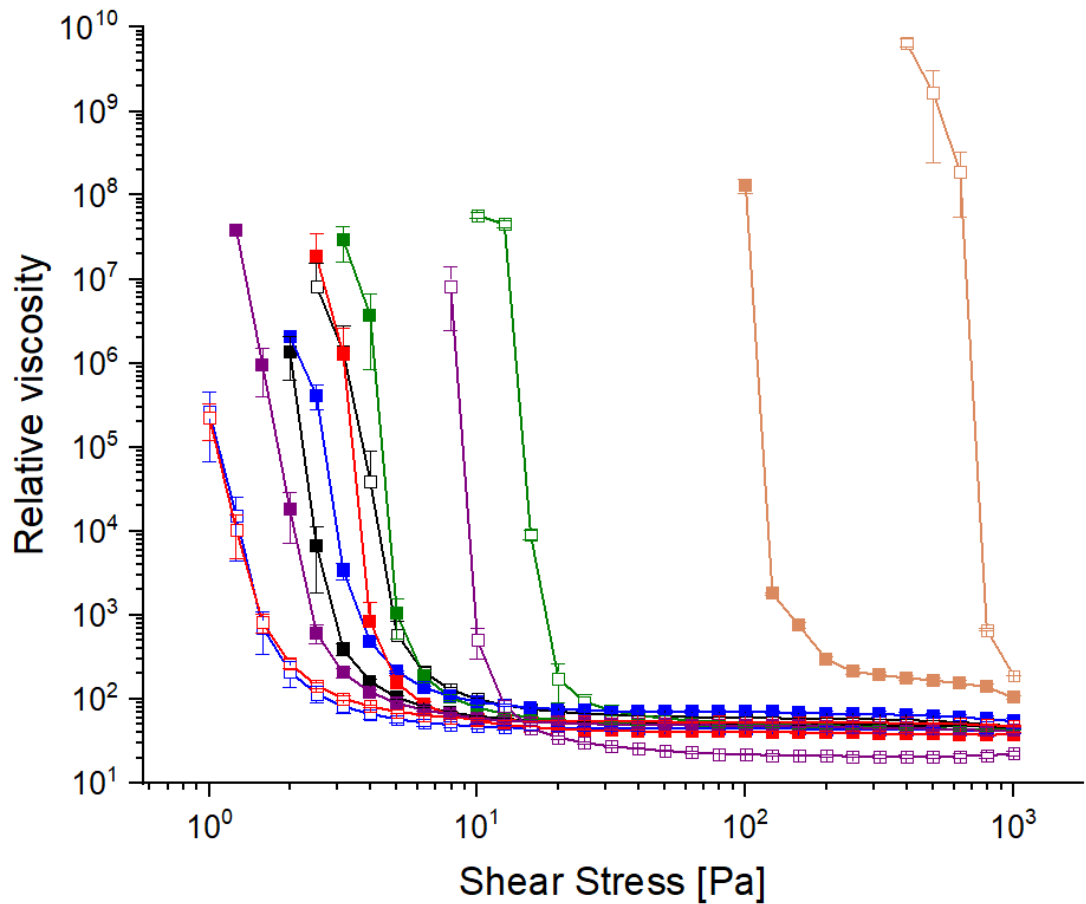
Figure 3.6: The viscosity curves of two batches of samples for each PGPR at 0.3% concentration and no PGPR. The batches types are as follows: Light brown – no PGPR; black – Admul WOL; green – Grindsted 90; blue – Grindsted Super; red – Palsgaard 4125; purple – Palsgaard 4150. The open and closed symbols denote the two batches. The error bars show the standard deviation between three replicates of each sample.

High shear mixing was applied using a square hole high shear screen attached to the head of a Silverson mixer. High shear mixing functions as follows: The high-speed rotation of the rotor blades within the workhead exerts a powerful suction, drawing the suspension upwards into the centre of the workhead. The centrifugal force created then forces the suspension towards the edge of the workhead, where it is subjected to a milling action in the clearance between the ends of the rotor blades and the inner wall of the screen. This is followed by intense hydraulic shear as the materials are forced, at high velocity, out through the perforations in the screen and circulated into

the main body of the suspension. The materials expelled from the head are projected radially at high speed towards the sides of the mixing vessel. At the same time, fresh material is continually drawn into the workhead, maintaining the mixing cycle.

High shear mixing is an efficient mixing method; however, it raises the temperature of the sample due to the friction generated. It is known that elevated temperatures increase the risk of oxidation of sunflower oil (Crapiste et al., 1999); therefore, the beaker containing the sugar-in-oil suspension was placed in an ice bath, and pauses in the mixing were incorporated if the temperature reached 47 °C. Crapiste et al. (1999) found in their experiments that this temperature did not lead to significant hydrolytic alteration and release of free fatty acids that might affect the interpretation of results in this PhD research. Four, six or eight minutes of mixing at 8000 rpm were evaluated to ascertain the optimum mixing time.

Emulsifiers need time to adsorb at the surface of the sugar crystals, at which point they create an equilibrium between the molecules at the surface and those in the oil. Therefore the samples were allowed to rest for at least 24 hr after mixing (Johansson and Bergenståhl, 1992a).

As Figure 3.7 reveals, there was still no reproducibility between batches with this method, whether the attempt was made without emulsifier (a) or with 0.3% PGPR (b).
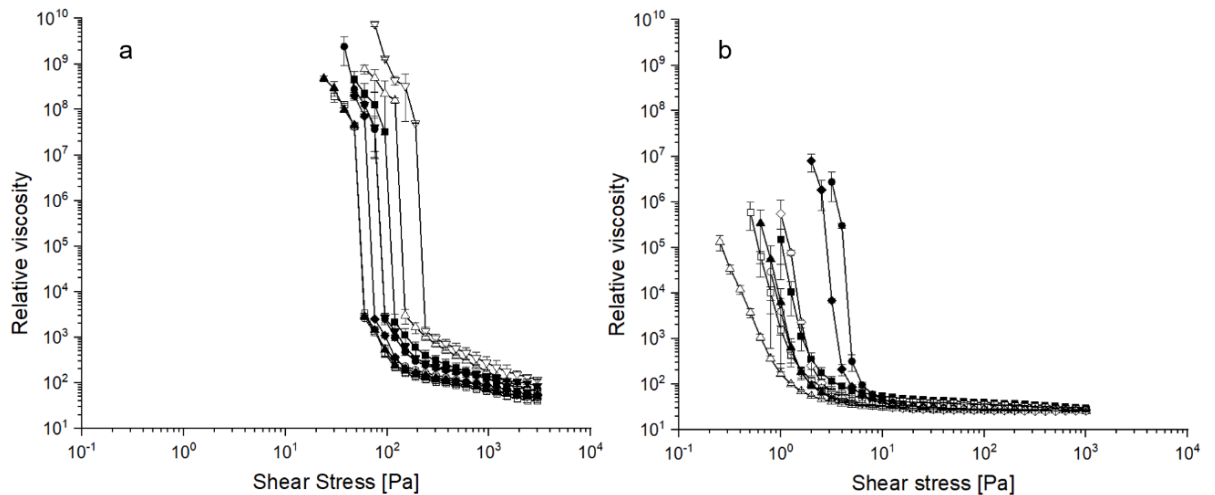
Figure 3.7: Variations are shown following the first attempt with the high shear mixer of 65% (wt) icing sugar in sunflower oil: (a) without and (b) with 0.3% PGPR. Five different methods were planned with different lengths of time shearing (4 min, wait, 2 min wait, 2 min ■, 2 min, wait, 2 min wait, 4 min ●) and different external strategies (2 min, wait, 2 min wait, 2 min with ice sleeve▲, jacketed vessel ▼ or on ice ◆). Graph a has no PGPR included, and graph b has 0.3% P4150 added. The error bars represent the standard deviation within the batch using three measurements.

Therefore, the high shear method was amended to reduce the particle concentration during the mixing stage to 50% (wt). As the heat had been an issue previously, which meant long pauses between mix steps, this stage was performed with the beaker in an ice bath and with the lowest evaluated mixing time; four min at 8000 rpm. These changes meant that the temperature of the suspension never went above 47 °C during the mixing, so pauses were no longer required. Once the samples had rested for 24 hours at 20 °C in the dark, they were centrifuged for 10 min at 3836 g and 10 °C, and the appropriate amount of clear supernatant was removed using a Pasteur pipette (23% of the suspension's total weight) to achieve a final concentration of 65 % (wt) sugar-in-oil suspension. The suspension was stirred by hand to disperse the sugar particles in the oil, and then it was rested for at least 10 min before applying to the rheometer. No visible sedimentation occurred during this time.

Figure 3.8 shows the results of this iteration of the method development. The data in 3.8a were obtained with the 65% (wt) sugar-in-oil suspension without PGPR, and the

data in 3.8b were obtained with the 65% (wt) sugar-in-oil suspension with 0.3% PGPR. From this figure, when PGPR is added at a concentration of 0.3%, this method appears to deliver very good results. However, there is still some variation in the viscosity curves for the sample with no PGPR. Figure 3.9 displays this more clearly by showing the Herschel-Bulkley yield stress values calculated from the data and the error bars within each batch. A one-way ANOVA was conducted to identify if there were significant differences between the yield stress values between batches of each type of sample. There was homogeneity of variances within the three batches representing the types of samples, as assessed by Levene's test for equality of variances (for no PGPR: $F = 1.984$, $p = 0.218$; for 0.3% PGPR: $F = 0.134$, $p = 0.733$). There was no significant difference between the three batches within sample types (for no PGPR: $F = 0.349$, $p = 0.719$; for 0.3% PGPR: $F = 0.356$, $p = 0.720$). This requirement was the first criterion for a robust method described at the beginning of this section. The second criterion was that the variation within and between each batch would be less than 10 %. As shown in Table 3.2, for the samples containing PGPR, the variation between batches and within batches was within the 10 % limit (batch 1: 7.54%, batch 2: 8.13% and overall: 7.81%). However, in the batches without PGPR, there was a much more considerable variation. Only one batch came close to this limit (batch 3 with a variation of 10.46%), and overall, the variation was 27%. The variation is probably due to the aggregation of sugar crystals where no emulsifier is present.

Figure 3.10 shows microscope images of sugar crystals in treated sunflower oil without and with PGPR mixed using the method described. A small amount of the suspension was removed and diluted with the same continuous phase with which they were initially mixed. A small amount was placed on a glass microscope slide without a coverslip. The sample without PGPR shows that aggregates remained, which are not as apparent in the sample with PGPR. Preparing a suspension void of PGPR at

an initially lower particle fraction did not improve the results. Therefore, this method was taken forward to be used with the rheology protocol for the rest of the PhD research, and 1000 Pa was selected as the starting shear stress for all samples; it was found not necessary to start at 3000 Pa. The results of any samples with low or no emulsifier content were to be interpreted with care, considering the results of these experiments.
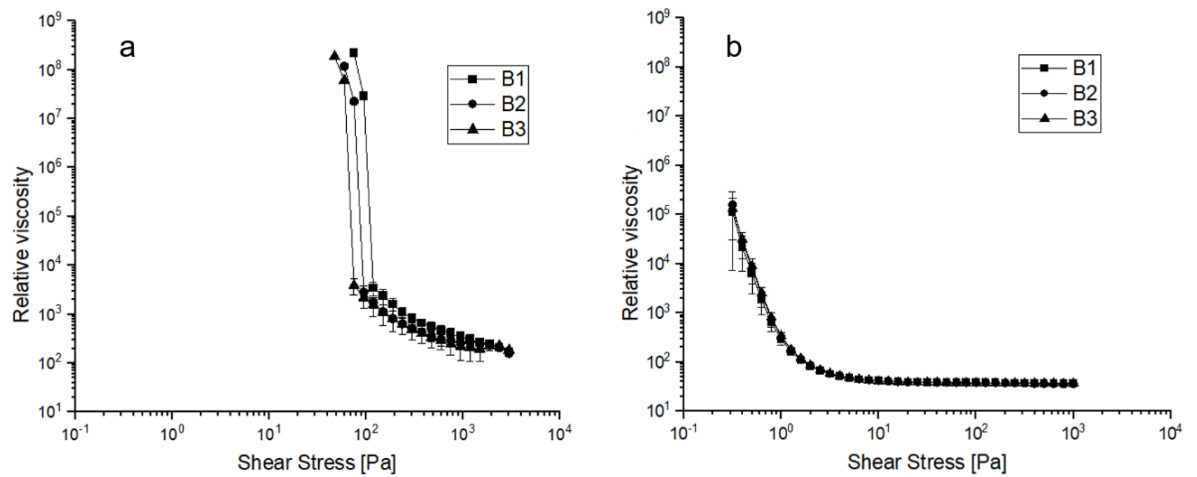
Figure 3.8: Viscosity curves showing 65% (wt) sugar-in-oil suspensions (a) without and (b) with 0.3% PGPR when the suspensions were made starting at 50 % (wt) concentration and then removing supernatant before rheological measurement to create a 65 % (wt) sugar-in-oil suspension. The error bar is the standard deviation of the mean based on three replicates. See Figure 3.9 for further discussion on the yield stress.
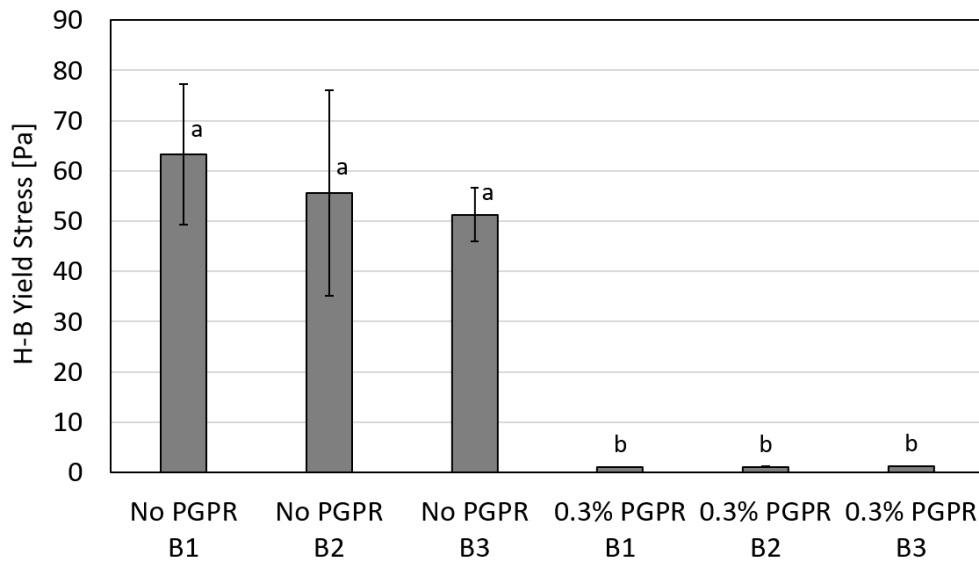
Figure 3.9: Herschel-Bulkley yield stress values for three batches of 65 %(wt) sugar-in-oil suspension without and with 0.3% PGPR. Each of the three batches was not significantly different from the others. The error bars shown for the suspension without PGPR are large and reflect probable sugar aggregates that cannot be removed without the application of an emulsifier. The error bar is the standard deviation of the mean based on three replicates. The data for each sample type were compared using ANOVA, followed by a Tukey post-hoc test to evaluate the differences. The letters represent significantly different results ($p < 0.05$), a>b.

Table 3.2: Average, standard deviation and coefficient of variation values for the Herschel-Bulkley yield stress values (to 2 decimal places) recorded for each batch and as a total across all batches of the same type of sample. Due to time constraints, only one data point was collected from 0.3% PGPR B3. The number of data points is made clear in the sample column. The p-value shown was calculated using ANOVA.

Sample	Average H-B yield stress [Pa]	Std Dev	% CV	p-value
No PGPR B1 (3 data points)	63.32	13.99	22.10	
No PGPR B2 (3 data points)	55.55	20.43	36.79	0.719
No PGPR B3 (3 data points)	51.26	5.36	10.46	
0.3% PGPR B1 (3 data points)	1.04	0.08	7.54	
0.3% PGPR B2 (3 data points)	1.08	0.09	8.13	0.720
0.3% PGPR B3 (1 data point)	1.13			
No PGPR (all) (9 data points)	56.71	15.46	27.26	
0.3% PGPR (all) (7 data points)	1.07	0.08	7.81	
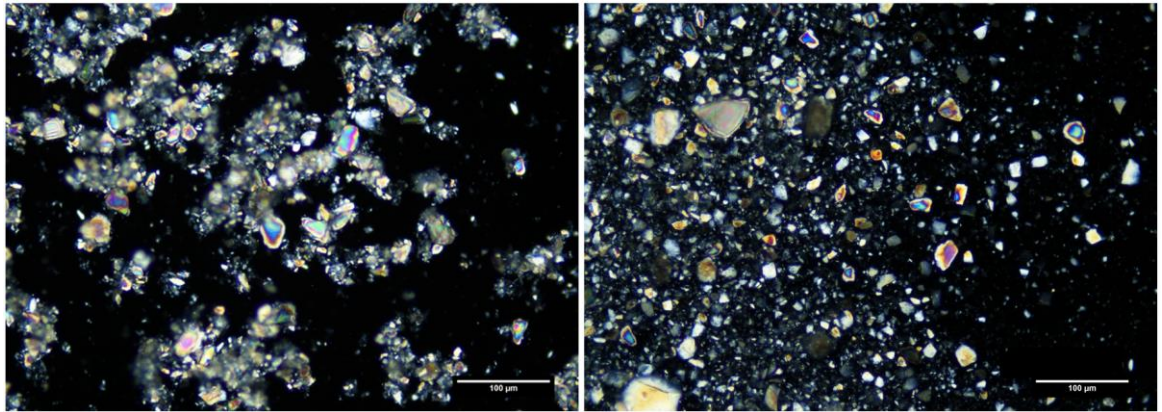
Figure 3.10: Microscope images of sugar crystals in treated sunflower oil without (left) and with (right) PGPR, measured at x20 magnification; the bar represents 100 µm. These were mixed using the finalised chocolate model method, then a small amount was removed and diluted with the same continuous phase with which they were initially mixed. A small amount of this mixture was then applied to a glass microscope slide without a coverslip. These images show that aggregation occurs in the sugar samples without PGPR which could explain the inter-batch variation seen in Figure 3.8 and Figure 3.9.

The slip effect was not as severe when using the chocolate model compared with the commercial chocolate using the same geometry; compare Figure 3.2 (squares) with Figure 3.8. As discussed earlier in sections 1.4.7.5 and 1.4.7.9, roughening the surfaces of a geometry reduces the amount of slip experienced by the sample. However, the surface chemistry between sample and geometry has also been proposed as a way to tune a system to reduce or eliminate slip (Cloitre and Bonnecaze, 2017). The amount that the particles within the sample are attracted or repulsed by the wall of the geometry has been shown to impact the amount of slip observed – the more attracted the particles are to the wall, the less slip is observed (Seth et al., 2008, Walls et al., 2003). The geometries used in the proposed method for this PhD are made from stainless steel, which is naturally hydrophilic. In samples where no PGPR is used, the sugar would be attracted to the cup and bob walls as both are hydrophilic. However, when the emulsifier is included in the suspension, the hydrophilic parts of PGPR molecules will be attracted to the stainless steel surface of the geometry as well as the sugar. This effect is exploited in industrial applications.

Cationic surfactants are used to prevent corrosion of stainless steel by acids in industrial applications (McCafferty, 2010, Hegazy, 2015). Non-ionic surfactants have also been shown to have corrosion prevention capabilities by adsorbing at the surface of the metal surface (Fuchs-Godec and Pavlović, 2012). In the samples analysed in this PhD, the surface-active molecules from PGPR would initially have been in equilibrium between the surface of the sugar and the bulk phase, perhaps in micelles. Once the sample had been applied to the cup, the PGPR molecules would start adsorbing to the cup and bob surfaces as well as the sugar. Perhaps the effect of creating hydrophobic walls means that the hydrophobic suspension can adhere to the wall of the cup and bob, as desired for laminar flow (Mezger, 2014). A critical factor for a surfactant to protect stainless steel, highlighted by McCafferty (2010), is good adherence to the metal surface by the hydrophilic part of the molecule. Although the chocolate sample used in these experiments did contain surfactants, these were lecithin molecules rather than PGPR, so perhaps the larger headgroup possessed by PGPR increases its adsorpsion to the stainless steel. In addition, the lecithin used within the chocolate would presumably be the lowest required to achieve the desired rheological properties. This may mean that there were less molecules available in the bulk to adhere to the geometries.

If emulsifier concentrations were applied to a suspension below the critical micelle concentration, introduced in section 2.7, this effect may affect the rheology of the sample, as the geometry wall would now compete with the sugar for the emulsifier. This proposed phenomenon was not investigated further during this PhD thesis; however, it may be beneficial to assess the effects of surfactant attraction to the geometry walls in future research. A consistent washing and drying protocol was used for cleaning the geometry between samples to minimise any emulsifier carryover on the geometries. This consisted of washing the geometry in warm soapy water with a soft toothbrush. It would then be rinsed in warm water and dried using a paper towel

followed by compressed air to ensure full dryness. The geometries were allowed to cool to 20 °C in the rheometer before the next test was started.

3.4. Conclusions

A sugar-in-oil (65% (wt)) suspension as a chocolate model was developed using high shear mixing, initially at a lower particle fraction than the final product. After leaving the mixed suspension for at least 24 hours, it was concentrated by centrifuging the sample and removing supernatant until a 65% (wt) suspension was achieved. The rheological protocol of the shear stress ramp from 1000 Pa to 0.1 Pa gave reliable results, unaffected by the sample history when the emulsifier was applied to the sample. This method was shown to be reliable when the emulsifier was applied; however, when no emulsifier was used, it was not possible to generate batches that did not show variability as the emulsifier was needed to disrupt the aggregates. Nonetheless, the yield stress values of the batches without any emulsifier were not significantly different to each other, so the method was accepted with the limitation this presents.

This suspension creation method and rheological protocol, outlined in detail in sections 2.5 and 2.6, were then used to compare the yield stress reducing capacity of PGPRs in chapter 4.

4. Functionality assessment of commercial polyglycerol polyricinoleate samples using a chocolate model

4.1. Introduction

As introduced in section 1.4.4, polyglycerol polyricinoleate (PGPR) is a yield stress reducing emulsifier often used together with lecithin, a viscosity reducing emulsifier, to control the rheological properties of chocolate. PGPR is made using the fatty acids found naturally in castor oil; these are primarily ricinoleic acid, whose hydroxyl groups allow the acid group from other fatty acids to link by esterification to form poly-fatty acid chains. These polyricinoleate chains are further esterified to a polyglycerol chain, which results in an amphiphilic molecule with a strong hydrophobicity. It dissolves readily in oil or cocoa butter or in highly dispersive, non-polar organic solvents such as chloroform. The appearance of PGPR is similar to honey – transparent, yellow and viscous.

There are several PGPR products on the market, and many manufacturers have at least two versions of PGPR – often a "high performing" version and a "regular" version. However, the amount by which the PGPRs' performance varies between manufacturers is unknown. Staff in new product development departments and at the processing lines of large scale chocolate manufacturers are well aware of differences in the yield stress lowering performance of various commercial PGPR products (personal communication, Vieira, J.), but this is based on experience rather than measured yield stress data. Utilising this empirical evidence was the beginning of this PhD journey, as it was hypothesised that linking yield stress performance to molecular characteristics would provide knowledge for the targeted exploration of natural resources to find an alternative to replace PGPR. The performance of the PGPRs is reported in this chapter, and in chapter 5, the results of the molecular characterisation of the PGPRs are described.

As aforementioned, chocolate is a concentrated suspension of solid particles, including sugar, in a fat phase formed chiefly of cocoa butter. Sugar, being hydrophilic, does not disperse well in the fat phase and forms aggregates. The emulsifiers in chocolate aid this dispersion: the emulsifiers' hydrophilic head group adsorbs to the sugar; its hydrophobic tail groups extend into the oil/fat. The emulsifier displaces fat immobilised at the sugar surface, which increases the fat in the mobile phase. Perhaps more importantly, the emulsifier allows the sugar crystal to act as if it was hydrophobic. This change allows sugar aggregates to be broken down, and any cocoa butter trapped within the aggregate is released, further increasing the fat available in the mobile phase.

To measure the variation in the yield stress reducing performance of different PGPR products, five commercially available samples were incorporated into the chocolate model and assessed using the rheology protocol, the development of which is described in chapter 3. In order to understand whether the surface hydrophobicity that the PGPR imparts to the sugar, which in turn affects dispersion behaviour in the fat phase, can be linked to the interfacial tension at the oil/water interface, measurements were made on a pendant drop tensiometer to find the critical micelle concentration (CMC) for each PGPR. It is hypothesised that there would be a correlation between the outcomes of the two techniques, which will mean that knowledge of how the molecular structures of surfactants alter the interfacial tension between oil and water could be applied to give insights into the PGPRs molecular structure.

4.2. Materials and methods

This section covers only materials that have not already been introduced in sections 2.2 and 2.4. The chocolate model method and rheology protocols are outlined in sections 2.5 and 2.6. The background to the interfacial tension method is outlined in section 2.7, but the settings are noted here.

4.2.1. Polyglycerol polyricinoleate

Five commercially available polyglycerol polyricinoleate samples were used in this research, as listed in section 2.1.

4.2.2. Incorporation of PGPR into the chocolate model

The chocolate model method is described in section 2.5, including the flow diagram shown in Figure 2.2. Regulations allow PGPR to be used in chocolate formulations at a maximum of 5 g/kg (Directive, 1995), which equates to no more than 0.5%. However, it is generally used at 0.2 or 0.3%, depending on the recipe (personal communication, Vieira, J.). Throughout this chapter, where the concentration of PGPR in a suspension is given, it is based on the total suspension weight. Concentrations of 0.1%, 0.3% and 0.5%, which correspond to 0.29%, 0.86% and 1.43% in the oil phase, respectively, were chosen for these comparisons to give a collection of data within the regulations.

The chocolate model method provides a 65% (wt) (53.4% (vol)) sugar-in-oil suspension, using dried icing sugar and sunflower oil that has been treated to remove naturally occurring surface-active components. If PGPR is included in a suspension, it is added to the oil before high shear mixing.

At least two batches of sugar-in-oil suspension were created for each PGPR and concentration. Suspensions with no PGPR were also made as a comparison.

4.2.3. Rheological protocol

The unidirectional shear protocol described in section 2.6.1 was applied. Three aliquots were taken from each batch created and measured on the rheometer. As discussed in section 3.3.1, the Herschel-Bulkley model was chosen to apply to the data, and the Herschel-Bulkley (H-B) yield stress was recorded. This calculation was

performed using the rheometer software (RheoCompass v 1.21, Anton Paar). The results for each section are presented as a viscosity curve and a bar graph illustrating the H-B yield stress values. Relative viscosity, which is the ratio of the viscosity of the suspension to that of the continuous phase, was used because it negates differences found due to the continuous phases. The viscosity of the treated sunflower oil was found to be 62.8 mPa.s (± 0.12 mPa.s, n = 3). When 1.43% of PGPR was added, the maximum used in this research, the viscosity was slightly reduced: 59.8 mPa.s (± 0.29 mPa.s, n = 3). A one-tailed t-test was applied to these results, and they were found to be significantly different ($t_{(4)} = 45.7, p < 0.01$). Therefore, using the relative viscosity meant the impact of the change in the viscosity of the continuous phase, made by the addition of the PGPR, was negated.

4.2.4. Interfacial tension

The interfacial tension was measured between the oil phase, without and with added PGPR, and ultrapure water. PGPR was initially added to treated sunflower oil at a concentration of 5%, utilising the same mixing protocol as described in section 2.3. From this, serial dilutions were made from 2.5% down to 0.02%. After preparation, the samples were kept for a maximum of three days at 22 ± 1 °C in the dark. A pendant drop tensiometer (Profile Analysis Tensiometer PAT1, SINTERFACE Technologies, Germany) was utilised for the analysis. The method is described in section 2.7. Samples were analysed in duplicate.

4.2.5. Statistical analysis of data

A one-tailed t-test was applied to the viscosity measurements for treated sunflower oil with and without PGPR to confirm whether the conversion from absolute to relative viscosity measurements should be used, see section 4.2.3.

The results shown in Figure 4.2 and Figure 4.4 were analysed using a one-way analysis of variance (ANOVA) followed by a Tukey post-hoc using SPSS (Statistics v 27, IBM Corp, USA). In order to ensure that the ANOVA test was applicable, the homogeneity of variance was evaluated within the batches representing the types of samples, as assessed by Levene's test for equality of variances. In Figure 4.4, two batches failed the test for homogeneity and so were excluded from the analysis. The significance level was set at $p < 0.05$, and three measurements were made per batch produced

In Table 4.1, the interfacial tension values for the low concentration PGPR solutions were compared to the equation of the line of best fit using MS Excel software using a one-way ANOVA calculation for the values where the PGPR concentration was below the CMC value. The significance level was set at $p < 0.05$. The high concentration PGPR solutions data were not expected to correlate with the interfacial tension measurements above the CMC value; therefore, the standard deviation values are given.

The comparison between the CMC value and the H-B yield stress values in Figure 4.6, and the comparison between lowest interfacial tension measurements and the H-B yield stress values mentioned in the text were made using a Pearson product-moment correlation calculation on SPSS (Statistics v 27, IBM Corp, USA).

4.3. Results and discussion

In this chapter, the second project objective was realised: to quantify the yield stress effects of five commercially available PGPRs. The third objective was started with the interfacial tension measurements to start to collect information to determine the molecular characteristics of the PGPRs.

4.3.1. Rheology

The first experiment was to compare the PGPR samples. They were included in the 65% (wt) sugar-in-oil suspension at 0.3% concentration, and the viscosity was measured as a function of shear stress. The results are shown in Figure 4.1. The viscosity curve shows that all the PGPRs reduce the yield stress compared to the sample with no PGPR, as expected. The data also show a difference between the efficacies of the PGPR samples to lower the yield stress. There is a period of Newtonian behaviour at the high shear region for all samples containing PGPR from 1000 Pa to around 20 Pa. At this point, the Grindsted 90 batches start to increase in viscosity. The other PGPR batches start to increase in viscosity at around 8 Pa. It is difficult to distinguish between them at this point; however, Palsgaard 4125 does diverge from the remaining PGPRs, as can be seen at the higher viscosity region. The inter-particle forces discussed in section 3.2.2 start to come into play as the shear stress is reduced, and the samples start to act more like a solid as the yield stress point is passed.
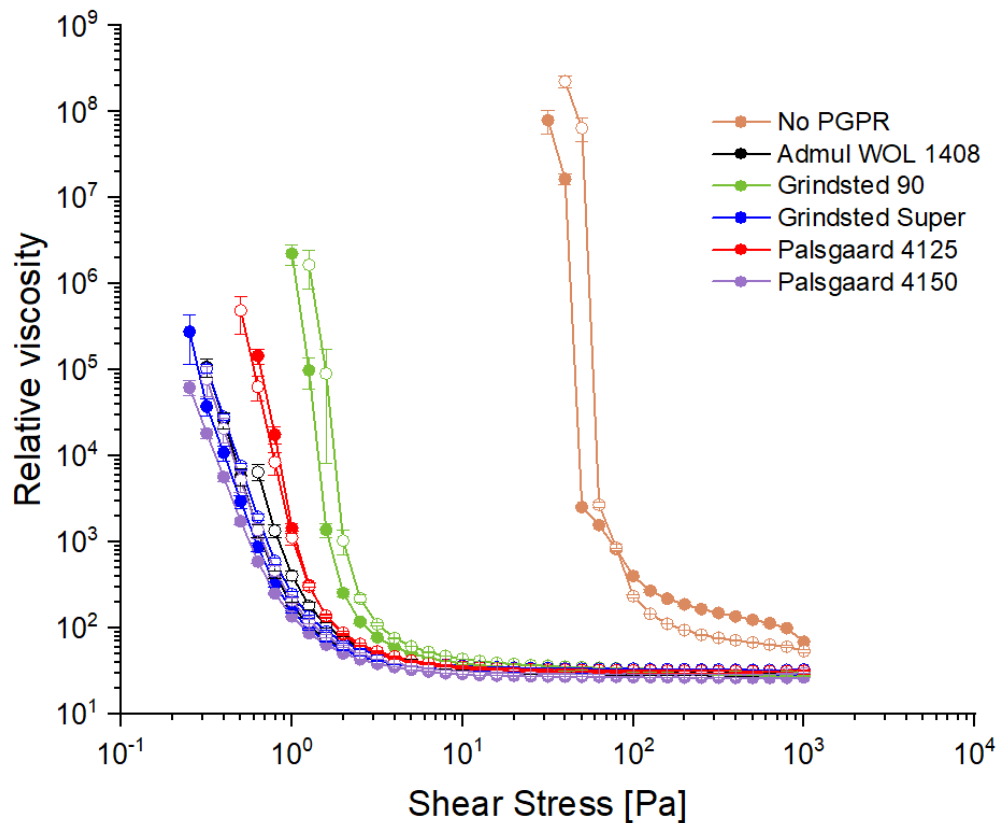
Figure 4.1: Viscosity curve for 65% (wt) sugar-in-oil suspension with all PGPRs at 0.3% concentration. Two batches are shown (filled and unfilled circles), with three replicates per batch. The error bars (standard deviation) are shown for each point unless the bar is within the symbol.

Figure 4.2 shows the H-B yield stress values of the data shown in Figure 4.1 (batches combined to give six data points per bar), omitting the samples with no PGPR. The statistical differences between the means are shown using letters. As discussed above, Grindsted 90 was the least efficient at reducing the yield stress, with a mean H-B yield stress value of 1.9 Pa, and Palsgaard 4125 was slightly better, with a mean H-B yield stress of 1.3 Pa. However, Admul WOL, Grindsted Super and Palsgaard 4150, with mean H-B yield stresses of 1.0 Pa, 0.9 Pa and 0.9 Pa, respectively, were not significantly different from each other and were the best at reducing the yield stress from the five PGPRs analysed. These three PGPRs are stated to be the

manufacturers' "high performing" versions of their PGPRs, and there seems to be very little which separates their yield stress lowering performance measured here.
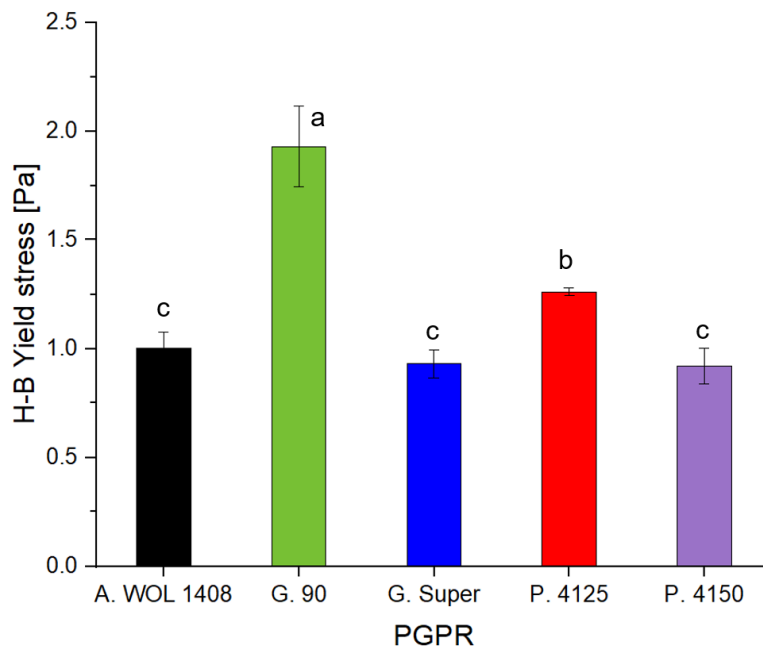
Figure 4.2: The Herschel-Bulkley yield stress values calculated from the data shown in Figure 4.1. Two separate batches were created for each sample type, analysed three times (to give six data points). The data were analysed using post-hoc analysis of variance (ANOVA) according to a Tukey post-hoc test with statistical significance at p<0.05, a>b>c.The error bars represent the standard deviation of the mean. Note that the H-B yield stress value for the samples with no PGPR was 57.6 Pa (± 15.8 Pa), as shown in Figure 4.4. It is not shown, so the differences between the PGPRs are more easily visualised.

Grindsted 90 (the PGPR with the least effect) and Palsgaard 4150 (one of the PGPRs with the greatest effect) were chosen for further investigation. Palsgaard 4150 was selected from the group with similar efficacies because this PGPR is advertised to be created especially for chocolate; however, any of these PGPRs could have been chosen. These two PGPRs were then applied to the 65% (wt) sugar-in-oil suspension at 0.1% and 0.5% concentrations. As before, two batches were produced, and, from these batches, three aliquots were taken and applied to the rheometer. The data for the two batches were combined, giving six data points for each position in the graph. The results are shown together with those already collected for 0.3% PGPR in Figure

4.3. Again, all PGPR concentrations show a reduction in the yield stress compared to that with no PGPR. Adding 0.1% of either Palsgaard 4150 or Grindsted 90 is not enough to give a Newtonian plateau region – the viscosity rises slightly from 1000 Pa to 100 Pa before increasing more markedly until reaching its yield stress. However, there is a difference between the yield stresses of these two PGPRs even at this low concentration. The 0.3% concentrations have already been discussed, but it is interesting to note that the yield stress point of 0.5% Grindsted 90 is very similar to that of 0.3% Palsgaard 4150. From this, it could be inferred that a manufacturer would need to use around 66% more of Grindsted 90 compared to Palsgaard 4150 to achieve the same yield stress reduction. However, this is only a rough estimate, and further experiments to check this claim for chocolate should be performed. The addition of 0.5% Palsgaard 4150 reduced the yield stress even further. Rector (2000) observed that, depending on the recipe of the chocolate, PGPR added at a concentration of 0.5-1.0 % can reduce its yield stress to zero.
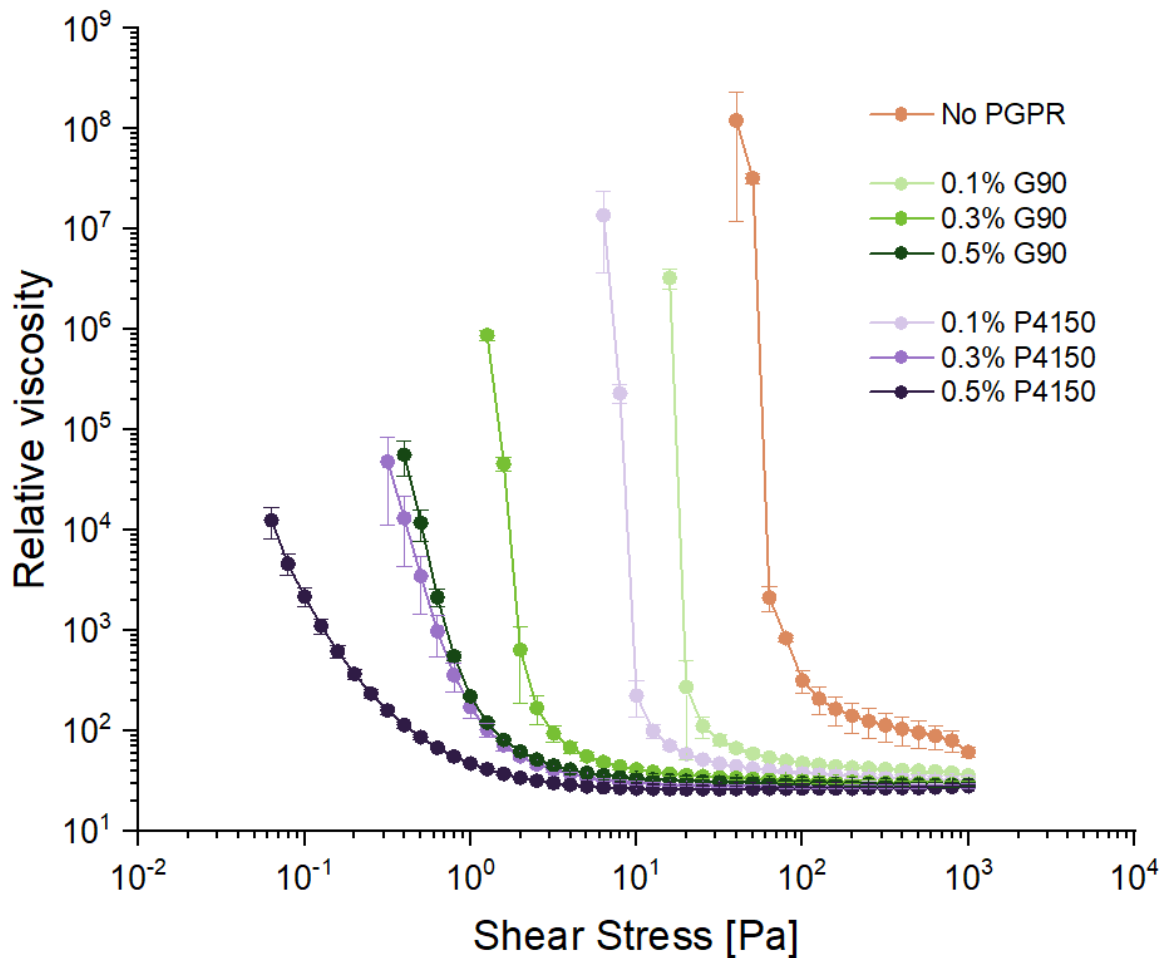
Figure 4.3: Viscosity curves for 65% (wt) sugar-in-oil suspensions containing Grindsted 90 or Palsgaard 4150 at 0, 0.1%, 0.3% and 0.5% concentration. Two batches were created for each type of PGPR/concentration and, from each, three replicates were measured. The bars represent one standard deviation from the mean. The two batches have been combined in this graph, giving six data points per mean value.

Figure 4.4 makes the differences and similarities more evident; again, it shows the H-B yield stress values of the data shown in Figure 4.3 (two batches combined to give six data points per bar). The large error bars for the samples with no PGPR and 0.1% Grindsted 90 meant that these data sets could not be included in the post-hoc analysis; however, for the other sample types, the statistical differences between the means are shown using letters.

The mean H-B yield stress where no emulsifier was present was 57.6 Pa. As expected from the discussion in section 3.3.2, the error bars are large as it is not possible to eliminate sugar aggregation in the absence of added emulsifier. At the concentration of 0.1%, Grindsted 90 lowered the H-B yield stress to 15.5 Pa, and the concentration of 0.1% Palsgaard 4150 lowered the H-B yield stress to 8.0 Pa. The concentration of 0.3% Grindsted 90 lowered the H-B yield stress to 2.0 Pa. These four appear different from each other. The latter two were statistically significantly different from each other and from the remaining suspensions. These three suspension types gave yield stress values that did not differ significantly from each other (p=0.14). In order of yield stress reducing efficacy improvement, these were 0.5% Grindsted 90, 0.3% Palsgaard 4150 and 0.5% Palsgaard 4150, which reduced the yield stress of the chocolate model to 0.95 Pa, 0.92 Pa and 0.42 Pa, respectively.
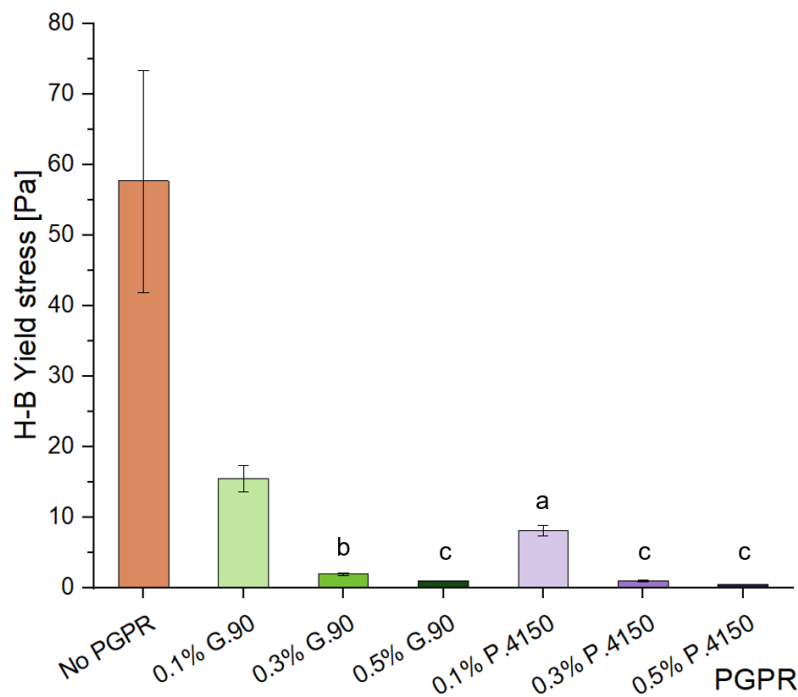
Figure 4.4: The Herschel-Bulkley yield stress values calculated from the data shown in Figure 4.3. The data are presented as a mean ± standard deviation. Two separate batches were created for each sample type, analysed three times (to give six data points). Statistical analysis was performed using analysis of variance (ANOVA); however, the samples with no PGPR and 0.1% G 90 were removed from the post hoc analysis because the data were not homogenous enough. The results of a post-hoc Tukey test, which was applied for the remaining five data sets, are shown using letters. Different letters show a statistical significance at p<0.05, a>b>c.

4.3.2. Interfacial Properties

The equilibrium interfacial tension values plotted against the log of the concentration of each PGPR in treated sunflower oil are shown in Figure 4.5. As expected, there was an initial region of decreasing interfacial tensions, and then a plateau region as the concentrations of PGPR increased. Regression lines were applied to each region. The critical micelle concentration (CMC) was calculated as the intercept point of the two regression lines (Barnes and Gentle, 2011). As only two batches were assessed, standard deviation bars cannot be used on the mean values. However, the two batches showed very good agreement, with 44% of all data pairs showing the same equilibrium value, and the greatest variation was by 0.4 mN/m, which represented only two sets of pairs. The values are given in Appendix 2. The regression lines for the low concentration values were applied using Microsoft Excel software and fit with a good correlation of R^2 higher than 0.97 for all data sets. ANOVA was applied to these values using MS excel software. The regression lines fit significantly well ($p <$ 0.05) for all of the lower concentration values. The higher concentration values did not correlate with the interfacial tension values, as expected, but the standard deviation of the points from the means were not greater than 0.18 for all data. The equations for each regression line are given in Table 4.1, and the R^2 values and their p-values are given for the low PGPR concentration measurements, with the standard deviation given for the high PGPR concentration measurements. The CMC values and the lowest interfacial tension measurements are given in Table 4.2.
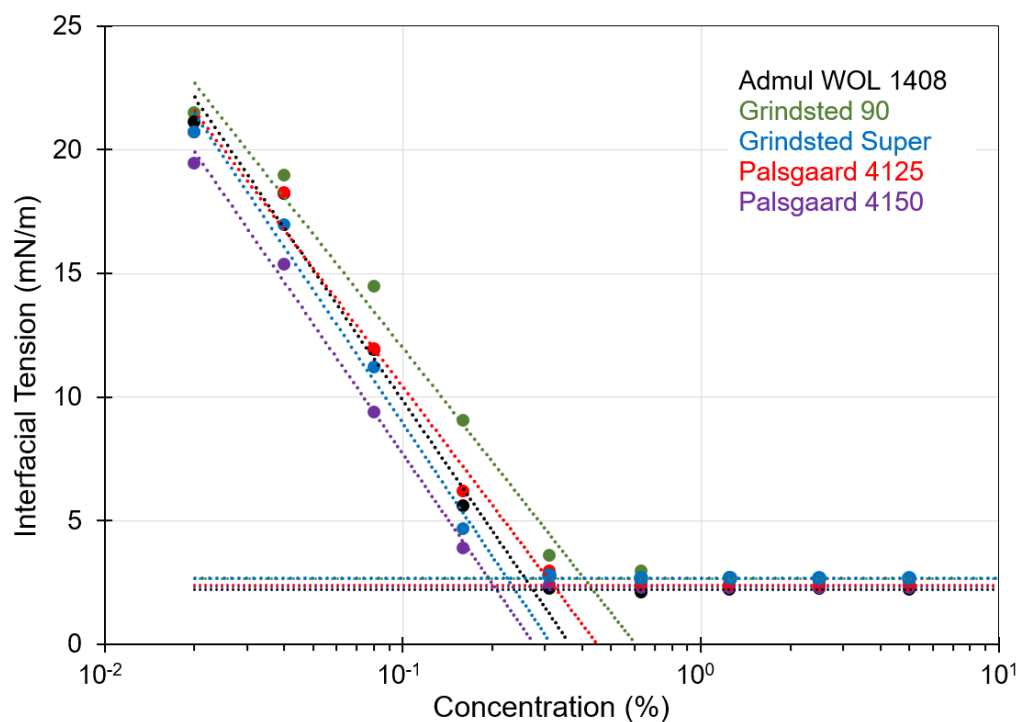
Figure 4.5: The equilibrium interfacial tension values plotted against the log of the concentration of the PGPR samples. Values were obtained in duplicate, and the average of the two points was used to create the trendlines.

Table 4.1: Equations of the lines and R^2 and p values or standard deviations for each line are shown in Figure 4.5. These were produced using Microsoft Excel software.

PGPR	Low concentration region			High concentration region	
	Eqn of line	R²	*p*-value of correlation	Eqn of line	*Standard deviation*
Admul WOL 1408	y = -17.54 log(x) - 7.68	0.98	0.012	y = 2.2	0.06
Grindsted 90	y = -15.31 log(x) - 3.32	0.98	0.001	y = 2.63	0.18
Grindsted Super	y = -17.91 log(x) - 8.96	0.99	0.007	y = 2.7	0.04
Palsgaard 4125	y = -15.95 log(x) - 5.53	0.98	0.001	y = 2.41	0.03
Palsgaard 4150	y = -17.47 log(x) - 9.77	0.99	0.003	y = 2.32	0.06

Table 4.2: The critical micelle concentration of the five PGPRs calculated using the intercept of the two regression lines shown in Table 4.1. The lowest interfacial tension measured, taken as the data from the three highest concentrations (six data points), is also displayed.

PGPR	Critical micelle concentration (%)	Lowest interfacial tension (mN/m)
Admul WOL 1408	0.27	2.22
Grindsted 90	0.41	2.58
Grindsted Super	0.22	2.70
Palsgaard 4125	0.31	2.40
Palsgaard 4150	0.20	2.30

The interfacial measurement results of the PGPRs show that these samples had different CMC values. Palsgaard 4150 had the lowest CMC value, and Grindsted 90 had the highest CMC value. The results also show that the amount by which the PGPRs lower the interfacial tension differed, though the differences were slight. Admul WOL1408 reduced the interfacial tension the most, and Grindsted Super reduced it the least.

Figure 4.6 shows the CMC values plotted against the H-B yield stress values. The trendline has an equation of y = 0.189x + 0.0536,. The data were analysed using the Pearson product-moment correlation using SPSS and the $r_{H\text{-}BYS\text{-}CMC}$ = 0.96, with a coefficient of determination of 0.92 and significance at the 0.01 level (two-tailed test). This shows a very strong positive relationship between the measured H-B yield stress and the CMC value, with 92% of the variation shared between the two groups. Therefore, it can be said with confidence that the yield stress reducing capacity of the PGPRs relates to the CMC values. The data for the lowest interfacial tension (L-IFT) was also plotted against the H-B yield stress (data not shown), and the correlation was only $r_{H\text{-}BYS\text{-}L\text{-}IFT}$ = 0.33, with a coefficient of determination of 0.11. This is a weak relationship, and the variation shared between groups was only 11%, so it can be concluded that the molecular structure features known to be important in reducing the

interfacial tension, compared to molecules of a similar structure, are not relevant to this discussion.
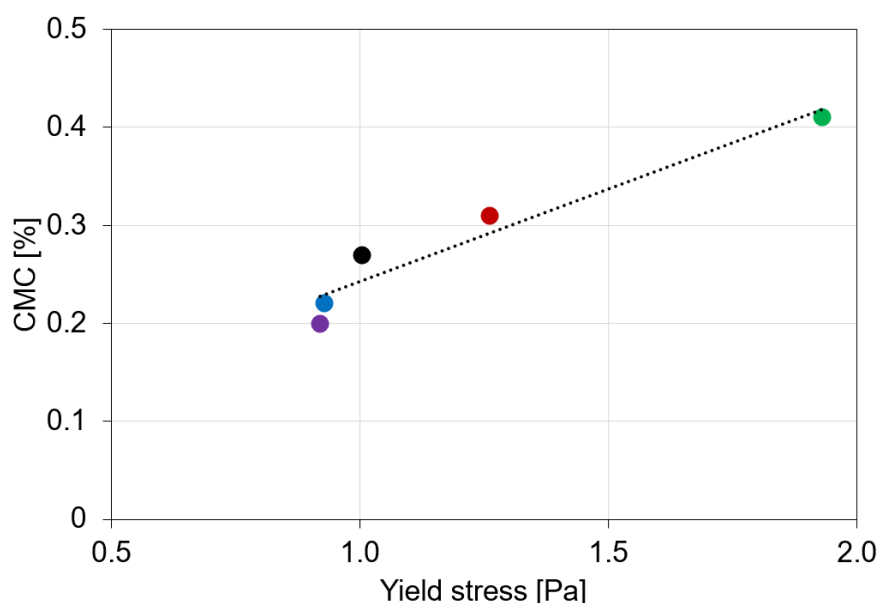
Figure 4.6: CMC values plotted against yield stress values. The regression line was y = 0.189x + 0.0536 and the values correlated with $r_{H-BYS-CMC}$ = 0.96, p < 0.01, using the Pearson product-moment correlation.

The CMC data were based on interfacial tension measurements taken once the system reached equilibrium. The system consisted of a drop of water pendant in a cuvette of oil containing the amphiphilic PGPR molecules. During the initial stages of the measurement, the PGPR molecules move in the oil, attempting to position themselves so that the phase boundary has the lowest free energy possible within the system. The free energy of a mixture of molecules, in this case, in a liquid, is controlled by both entropy and enthalpy. The enthalpy contributions are determined by molecular interaction energies, such as covalent, electrostatic, and Van-der-Waals interactions. Entropy contributions are determined by the tendency of a system to adopt its most disordered state.

In order to lower the free energy in an oil-in-water system containing an amphiphilic molecule like PGPR, the hydrophilic portion of the molecules will adsorb at the water's

surface, with the hydrophobic tails extending into the oil. The molecules alone in the

oil increase the system's free energy as the hydrophilic head is exposed. Therefore,

at a particular concentration, the CMC concentration, the molecules themselves come

together to form reverse micelles where the hydrophilic heads turn together where

they are protected from the oil, see Figure 4.7. Once this concentration is met, the

interfacial tension of the drop is no further reduced. Equilibrium is not a static phase;

however, molecules can leave the reverse micelles, return to the bulk phase, and

adsorb to the water-oil interface and vice-versa. This movement frequently occurs

with residence times within micelles and presumably reverse micelles, typically

shorter than milliseconds (Kronberg et al., 2014a). Therefore, characteristics that

would discourage an amphiphilic molecule from forming micelles would give a higher

CMC value.
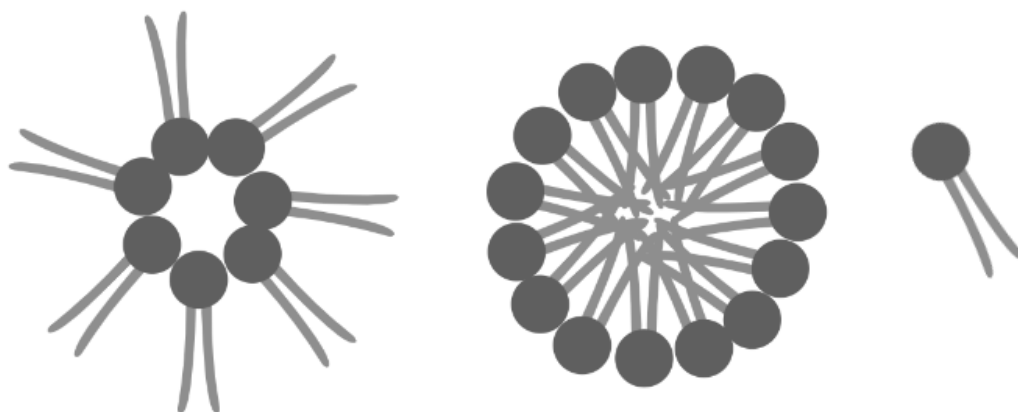
Figure 4.7: Graphic showing a reverse micelle (in oil) on the left and a normal micelle (in water) in the middle. A unimer molecule is shown on the right. The hydrophilic head group is shown as a circle, and the hydrophobic tail groups are shown as curved lines. Drawn using BioRender.

A long hydrophobic chain length is known to result in a low CMC value where the

emulsifier is suspended in water (Kronberg et al., 2014b). In water, the hydrophobic

tail causes the system's energy to increase, which pushes the unimers to form

micelles. In oil, the opposite would be true, and a larger hydrophilic head group would

encourage reverse micelle formation. It can be inferred then that PGPRs with lower CMC values have longer polyglycerol headgroups. A bulky tail group may also reduce the PGPR molecules' ability to form reverse micelles; therefore, it could also be inferred that the polyricinoleate chains are likely to be straight and not branched.

4.4. Conclusions

This research described in this chapter set out to ascertain whether the differences observed by chocolate formulators between PGPRs could be shown in controlled experiments and, if so, what could interfacial tension measurements tell us to aid understanding the molecular structure of the PGPR molecules themselves. Rheological measurements were taken in order to compare the yield stress values of the five PGPR samples. These measurements showed that the PGPRs do indeed have different efficacies. Interfacial tension measurements were made to ascertain the critical micelle concentration value of the PGPRs. Differences were found in the CMC value, and a slight difference was found in the amount to which the PGPR can lower the interfacial tension after the CMC point. The efficacy of the PGPRs to reduce the yield stress of the chocolate model related well to the CMC value: the PGPR with the lowest CMC value corresponds to the PGPR that reduces the yield stress of the chocolate model the most and vice versa. It is known that when molecules of a similar structure are compared in water, a lower CMC value is often due to the longer alkyl length of the hydrophobic group (Kronberg et al., 2014c). It can be inferred that when an emulsifier is in oil, it is the length of the hydrophilic head that is important. Vernier (1997) concluded that the best functionality of PGPR and PGPR-like emulsifiers came when the molecules had both longer acyl chains and when the molecules adhered tightly to the sugar crystals. A larger headgroup on the PGPR may provide better adsorption at the sugar surface.

In chapter 5, several different methods were used to assess the size and composition of the PGPR molecules. Electrospray Ionisation-Mass Spectrometry, Size Exclusion Chromatography and Nuclear Magnetic Resonance were used to evaluate the size of the molecules. Calculations based on the hydroxyl, iodine and saponification value ranges imposed on PGPR batches by food regulatory bodies were applied to theoretical PGPR molecules to visualise the types of molecules that would create a PGPR to meet these guidelines. Finally, the composition of the fatty acids within the PGPR was inspected using a transmethylation reaction followed by analysis by gas chromatography-mass spectroscopy. It was expected that the data collected from these experiments would give further comprehension of the chemical properties that provide an efficient PGPR.

5. Molecular characteristics analysis of the PGPR samples

5.1. Introduction

The data presented and discussed in chapter 4 show that there appears to be three different yield stress reducing efficacies within the five commercially available PGPRs tested. Grindsted 90 had the lowest potential for lowering the yield stress, Palsgaard 4125 was better, but Admul WOL 1408, Grindsted Super and Palsgaard 4150 gave the best yield stress lowering functionality. These last three were very similar in their efficacy. Interfacial tension measurements, made on a pendant drop tensiometer with ultrapure water in the drop and PGPR in treated oil in the cuvette, were made and showed that the critical micelle concentration (CMC) values obtained were proportional to the ability of the PGPR to reduce the yield stress. In other words, the better a PGPR molecule was at lowering the CMC value, the better it seemed to be at lowering the yield stress of the chocolate model. This knowledge implies some structural differences between the PGPRs. When an emulsifier is dissolved in oil, a lower CMC is achieved when an amphiphilic molecule has a more hydrophilic head group than molecules of a similar structure to encourage reverse micelle formation. It is clear that the chemical structure of the PGPR molecule is of importance to its action. The third, fourth and fifth objectives for this PhD project, listed in section 1.2, are the aim of this chapter. The goal is to determine the size and molecular characteristics of the PGPRs and determine which of these characteristics are responsible for the yield stress modification. Given this information, a more focused search for a novel natural alternative can be planned.

5.1.1. Polyglycerol polyricinoleate molecular structure

5.1.1.1. Manufacture

The production of PGPR is described in section 1.4.5 but summarised here. PGPR is synthesised by first hydrolysing the fatty acids from the triacylglycerols in castor oil (around 80-90% are ricinoleic acid) (Wilson et al., 1998). These fatty acids are then condensed into poly-acyl chains, formed with estolide bonds connecting the acid part of one fatty acid to the hydroxyl group on a ricinoleic acid. The chain length is limited by the incorporation of a fatty acid that does not contain a hydroxyl group; for example, oleic, linoleic and stearic acid have been found, at 3-8%, 3-7% and 0-2% respectively, in castor oil (Wilson et al., 1998). The manufacturer can also control the chain length by the amount of time allowed for the poly-acyl reaction to take place. The polyglycerol chains are created separately by condensing glycerol and forming ether bonds. Finally, the polyglycerols are added to the poly-acyl chains, a further condensation reaction occurs, and ester bonds link the two groups of chains together (Wilson et al., 1998). The poly-acyl groups can esterify to any hydroxyl group on the polyglycerol; however, they most often react with the end group(s) due to their availability. Figure 5.1 shows two theoretical diagrams of the PGPR molecule, both with a tri-glycerol chain. The top molecule has two poly-acyl chains at both ends of the polyglycerol chain and a stearic acid acting as a capping fatty acid, although this chain can be much longer than two fatty acids. It is possible to have a ricinoleic acid molecule at the end of the poly-acyl chain, as shown in the lower chain of the molecule. The bottom molecule shows a PGPR with only one poly-acyl chain.
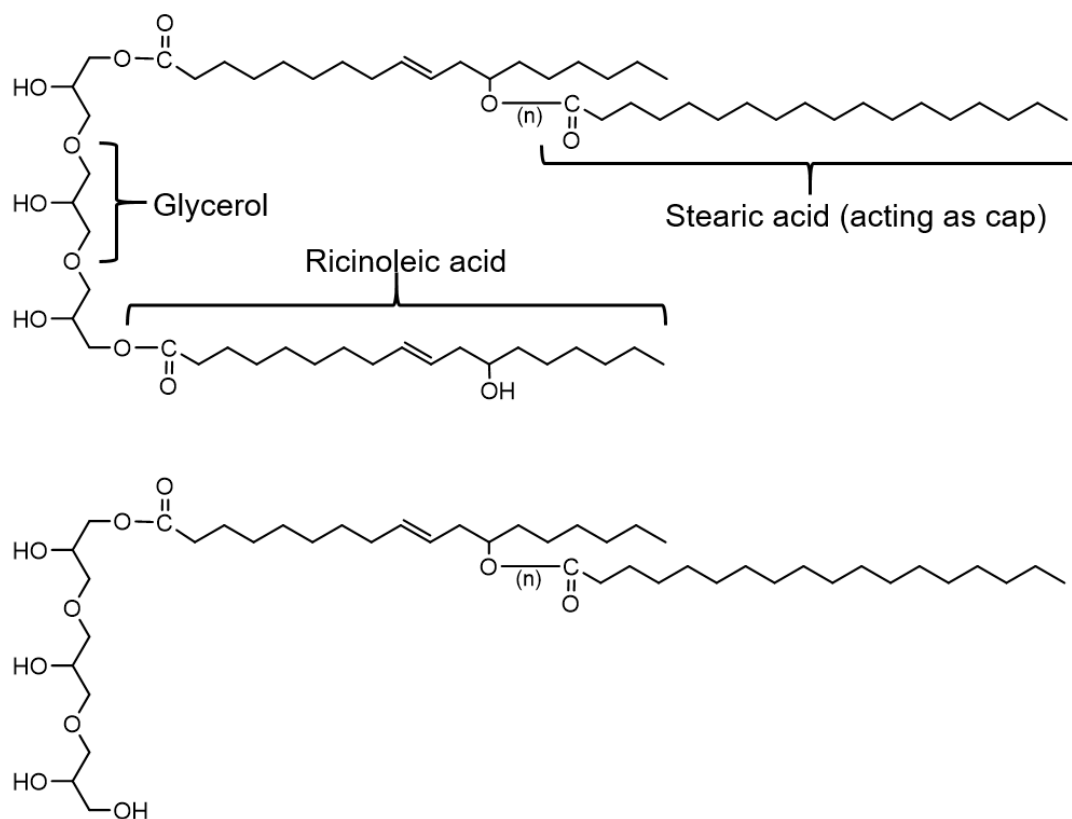
Figure 5.1: The molecular structure of Polyglycerol Polyricinoleate. The polyglycerol chain is shown as a triglycerol chain; however, more or fewer glycerols can form the polyglycerol in the PGPR. "n" indicates that more ricinoleic acids can be included in the poly-acyl chain. The top molecule shows two poly-acyl chains esterified to the polyglycerol, and the bottom molecule shows one poly-acyl chain.

5.1.1.2.   Size

There is some debate in the literature about the molecular size and character of PGPR. Bastida-Rodríguez (2013) stated that the average number of glycerol molecules in the polyglycerol chain is three, and the average number of fatty acids in each of two polyricinoleate chains is between five and eight. A PGPR molecule with three glycerol molecules and ten ricinoleic acid molecules (i.e. two chains of a five-chain polyricinoleate) would have a molar weight of 3045 g/mol. Personal communication Kerry, the manufacturer of Admul WOL 1408, stated that the average molecular mass of their PGPR is 2000 g/mol. Two PGPR samples that have been measured using Electrospray-Ionization Mass Spectrometry (ESI-MS) had molar

weight values averaging at around 1170 g/mol, ranging between 400 and 2000 g/mol (Orfanakis et al., 2012).

5.1.1.3.   Restrictions

As PGPR is classified as food-grade, it is restricted by food safety regulations. Again, this is discussed in section 1.4.5 but summarised in Table 5.1.

Table 5.1: Summary of the permissible ranges imposed on PGPR by Food Regulatory bodies.

Criteria	Range	Purpose of test	Regulatory body
Acid value	≤ 6 mg KOH/g	Free fatty acids	CEC (2008) FAO/WHO (1992)
Hydroxyl value	80-100 mg KOH/g	Hydroxyl groups	
Iodine value	72-103 g I/100g	Olefinic double bonds	FCC (2016)
Saponification value	170-210 mg KOH/g	Fatty acids in the molecule	
	> 75 % di-,tri- and tetraglycerols, and < 10% polyglycerols equal to or higher than heptaglycerol	Polyglycerol chain length	CEC (2008) FAO/WHO (1992)

5.1.2.   Summary of the experiments in this chapter

In order to elucidate potential differences in the chemical structure of the five PGPR samples introduced in section 2.1, electrospray ionisation-mass spectroscopy (ESI-MS), size-exclusion chromatography (SEC) and nuclear magnetic resonance (NMR) spectroscopy were employed. A large number of possible molecular conformations of PGPR molecules were screened against theoretical calculations for the hydroxyl, iodine, and saponification value ranges to evaluate those that would meet the regulatory requirements imposed on PGPR and give further information about the size and structure of the PGPR molecules within the samples. Finally, the fatty acid profile

of the PGPRs was characterised using transesterification followed by gas chromatography-mass spectroscopy (GC-MS).

5.2. Materials and methods

The polyglycerol polyricinoleate samples used in this research were outlined in section 2.1. The transesterification reaction and analysis with GC-MS were described in sections 2.10 and 2.11.

5.2.1. Electrospray ionization-mass spectrometry

Electrospray ionisation-mass spectrometry (ESI-MS) was applied to all PGPR samples, following literature protocol with slight modification (Orfanakis et al., 2012). PGPR samples were mixed with acetone (1% (wt)), and 250 µL of this was mixed with 60% methanol/40% water containing 0.2% formic acid (50 µL). They were then injected into the electrospray source of a mass spectrometer (Micromass Quattro Ultima, Massachusetts, USA) using a 250 µL glass syringe (SGE Analytical Science, Australia) fitted to a syringe pump (Harvard Apparatus 22, Massachusetts, USA) set at 100 µL/min. The source was in positive ion mode, 4.2 kV capillary voltage, 250 °C desolvation temperature, desolvation gas at 188 L/h. The experiments were performed at low resolution to enable the size of the polymeric PGPR molecules to be seen. The cone voltage was 25 V. The spectra were recorded from m/z 200 – 3000 using MassLynx version 4.0.

5.2.2. Size exclusion chromatography

Size-exclusion chromatography (SEC), also known as gel permeation chromatography, was used to separate molecules by their size and obtain molar mass averages. An Agilent Infinity II MDS instrument featuring differential refractive index

(DRI), viscometry (VS), dual-angle light scatter (LS) and two-wavelength UV detectors was equipped with 2 x PLgel Mixed C columns (300 x 7.5 mm) and a PLgel 5 μm guard column. The eluent was chloroform. Samples were run at 1 mL/min and 30 °C. Poly(methyl methacrylate) (PMMA) and polystyrene standards (Agilent EasyVials) were used for calibration. Analyte samples were filtered through a PTFE filter with 0.22 *μ*m pore size before injection. Molecular weight averages and dispersity values were determined by third-order PMMA conventional calibration (1,568,000 – 960 g/mol) using Agilent GPC/SEC software.

The data are presented as a raw data curve and a molecular mass distribution calculated using a standard curve from the PMMA standards. The raw data SEC curve is a molecular size-distribution curve and is useful for relative sample comparison when samples have been run under the same sample conditions (Striegel et al., 2009). On the molecular mass distribution graph, the intensity on the y-axis is related to both the concentration and refractive index increment of the material. For a material of the same composition, the refractive index should not change across the distribution; therefore, the y-axis should be solely determined by concentration. The normalised y-axis is named dwdlogM.

All GPC experiments were performed and analysed by Dr. Daniel W. Lester in the Polymer Characterisation Research Technology Platform at the University of Warwick.

5.2.3. Nuclear magnetic resonance

Nuclear magnetic resonance (NMR) spectroscopy was applied to compare the length of the fatty acid chain (polyricinoleate chain) between Palsgaard 4150 and Grindsted 90. This was done by comparing the peaks' heights in the alkene region. The material was dissolved in deuterated chloroform (Aldrich Chemistry, USA) (1:1 by weight) and around 600 mL placed into clean NMR tubes. Spectra were then acquired at 25 °C

on a Bruker Avance III 800 MHz spectrometer using a 5 mm QCI Cryoprobe. 128 scans of 32K points with a spectral width of 13 ppm were collected. The free induction decays were multiplied by an exponential weighting function with a line broadening of 0.3 Hz before the Fourier transformation. Phasing and baseline correction was performed, and the spectra were processed using Bruker Topspin Software. No further analysis was performed on the spectra as the purpose was to compare the two samples only.

All NMR experiments were performed by Dr. Huw E. L. Williams at the Centre for Biomedical Sciences at the University of Nottingham.

5.2.4. High-performance thin-layer chromatography

The samples for high-performance thin-layer chromatography (HPTLC) were prepared as follows. PGPR was added into chloroform at a ratio of 1:20, gently shaken and then stored in a capped bijou bottle in the dark at -20 °C until analysis. An α-linolenic acid standard was used to calibrate the free fatty acids and was dissolved to a concentration of 1 mg/mL in chloroform/methanol (2:1 (vol)). The mobile phase used was chloroform:methanol:water (47.5:10:1.25 (vol)), and the derivatisation solution used was the copper acetate-phosphoric acid solution, the preparation of which is described in section 2.9.2. The derivatisation solution stains molecules with an acyl group when charred; see section 1.5.5.1 for more details. The experimental procedure for the separation of lipids using HPTLC is described in section 2.9.

5.2.5. Fatty acid analysis

The PGPRs were initially dissolved in chloroform at a ratio of 1:5. They then underwent transesterification using trimethyl sulfonium hydroxide (TMSH), and the fatty acid methyl esters (FAME) were analysed using gas chromatography-mass spectrometry detailed in sections 2.10 and 2.11.

5.2.6. Statistical analysis of data

The results shown in Figure 5.15 were analysed using a one-way analysis of variance (ANOVA) followed by a Tukey post-hoc using SPSS (Statistics v 27, IBM Corp, USA). The significance level was set at $p < 0.05$, and one measurement of each of three true replicates were used in the mean value of each data point.

5.3. Results and discussion

5.3.1. Molecular size distribution

5.3.1.1. Electrospray Ionisation-Mass Spectroscopy

The chemical structures of the PGPR samples were analysed using Electrospray Ionisation-Mass Spectroscopy (ESI-MS). This method was chosen because it has been used previously to characterise PGPR samples (Orfanakis et al., 2012). In this protocol, the researchers appear to be able to obtain peaks in the mass spectrometer when the PGPR was dissolved merely in the acetone. However, no peaks were shown when this was tried, indicating that the PGPR in acetone alone could not ionise. Therefore, a portion of the dissolved PGPR in acetone (250 µL) was removed and mixed with a mixture of 60% methanol/40% water containing 0.2% formic acid (50 µL). This addition has previously been shown to assist the ionisation of samples in the ESI-MS equipment because formic acid is a proton donator. Ionisation then occurred, and the peaks are shown in Figure 5.3-Figure 5.6.

The ability of the PGPRs to dissolve, initially in the acetone, and then with the inclusion of the methanol/water mix, was an issue, as can be seen in Figure 5.2. Unfortunately, the purity of the acetone was not recorded at the time of the experiment; however, two bottles of acetone were available at the time of this

experiment and could have been used, with purities of 98% (VWR Chemicals, France) and >99.9% (Honeywell, Germany). If the 98% purity acetone was used, the PGPR might have formed an emulsion with the 2% water in the solvent, causing the cloudy appearance; PGPR is known to create spontaneous water-in-oil emulsions (Bahtz et al., 2016). However, if the very pure acetone was used, perhaps adding the PGPR at the 1 % concentration was too high for this solvent, causing PGPR aggregates or reverse micelles to form. After the methanol/water solution was added, there were visible insoluble particles in the sample. These particles could be reverse micelles or emulsion droplets. This question could be investigated in future by measuring the sample using a particle sizer or zeta sizer. Orfanakis et al. (2012) do not discuss ionisation or solvation issues in their paper.
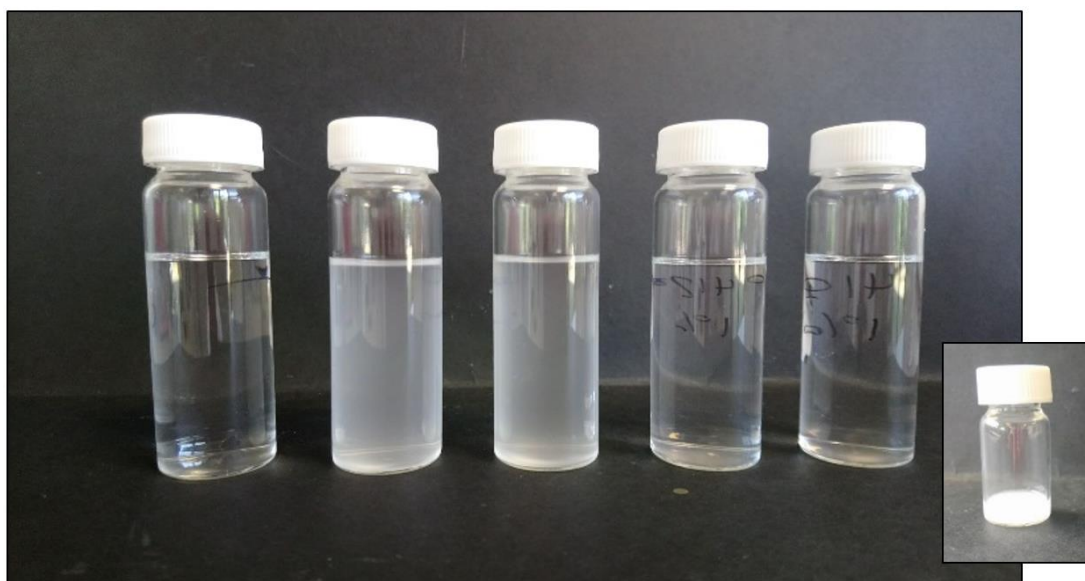
Figure 5.2: The five PGPRs at a concentration of 1% in acetone. The inset shows one sample where 250 μL of PGPR in acetone is mixed with 60% methanol/40% water containing 0.2% formic acid (50 μL).

During analysis, MS-MS techniques were used on the highest peak (544 m/z) to ensure that the molecules were not doubly charged. When a molecule is ionised and obtains a single charge, the mass to charge ratio is equivalent to the molecular weight of that molecule. However, if a molecule becomes doubly charged, then the mass to

charge ratio will be half the molecular weight, leading to interpretation errors. Where double charging has occurred, the MS-MS spectra focussing on a single MS peak will reveal fragments higher than the peak selected.

Figure 5.3 showed that double charging was not occurring in these samples.
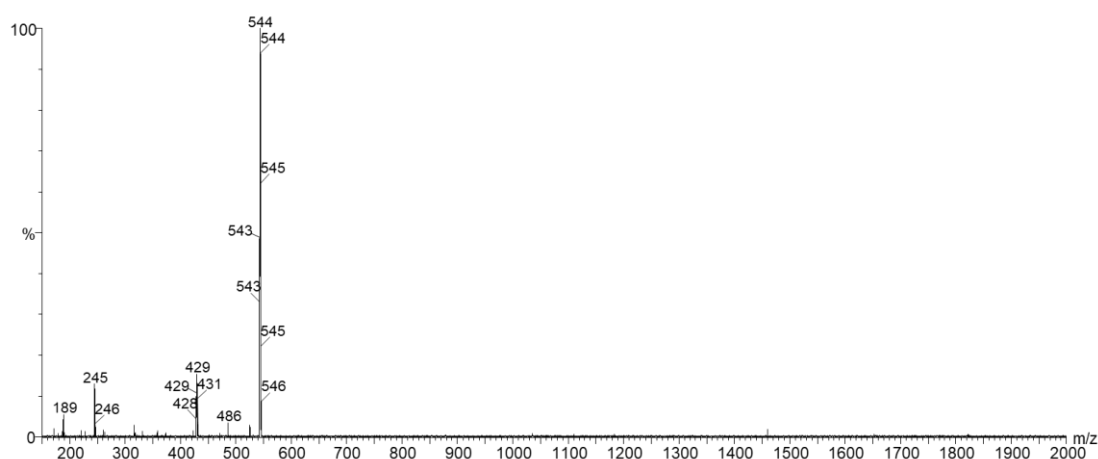
Figure 5.3: MS-MS analysis of the peak at 554 m/z showing that no fragments connected to this peak are larger than 544 m/z.

Figure 5.4 shows the spectrum obtained of Grindsted Super in acetone. The highest peak is set at 100%, and the abundance of all other molecules are relative to that peak. PGPR samples are not expected to contain molecules with random molecular weights; as already discussed, they are made up of a mixture of molecules with units of glycerols and ricinoleic acids. Therefore, it is relatively easy to designate the molecule peaks found in the spectra. There will be several peaks on the spectra related to each molecule due to adducts of hydrogen, sodium, potassium or water, which are formed during ionisation. In this analysis, most of the adducts were sodium or potassium.

In the following discussion, PG denotes a polyglycerol chain, and the number following it is the number of glycerol molecules in the chain. Similarly, PR denotes a poly-acyl chain, here assumed for simplicity to be a chain containing only ricinoleate

fatty acids, followed by a number representing the number of fatty acids in the chain. For example, PG3-PR10 would be the notation for a PGPR with three glycerol molecules and ten fatty acid molecules linked by ester and ether bonds, as applicable.

A repeating pattern of peaks can be seen several times in the spectra. The highest peaks in each repeat (i.e. with their highest peak at 544, 825, 1105, etc. m/z) relate to a molecule containing a PG3 and an increasing number of PRs as the pattern repeats up the m/z range (e.g. PG3-PR1, PG3-PR2, etc.). This peak pattern is followed by a combination of a PG4:PR increasing and PR alone, again increasing in length throughout the repeats (e.g. PG4-PR1 & PR2, PG4-PR2 & PR3, etc.). The PG4-PR(x) and PR(x+1) molecules overlap because their charged states overlap. Figure 5.5 focuses on the spectrum between 775-1350 m/z to show two sets of the repeating pattern, and the molecule to which the peak pattern refers is noted.
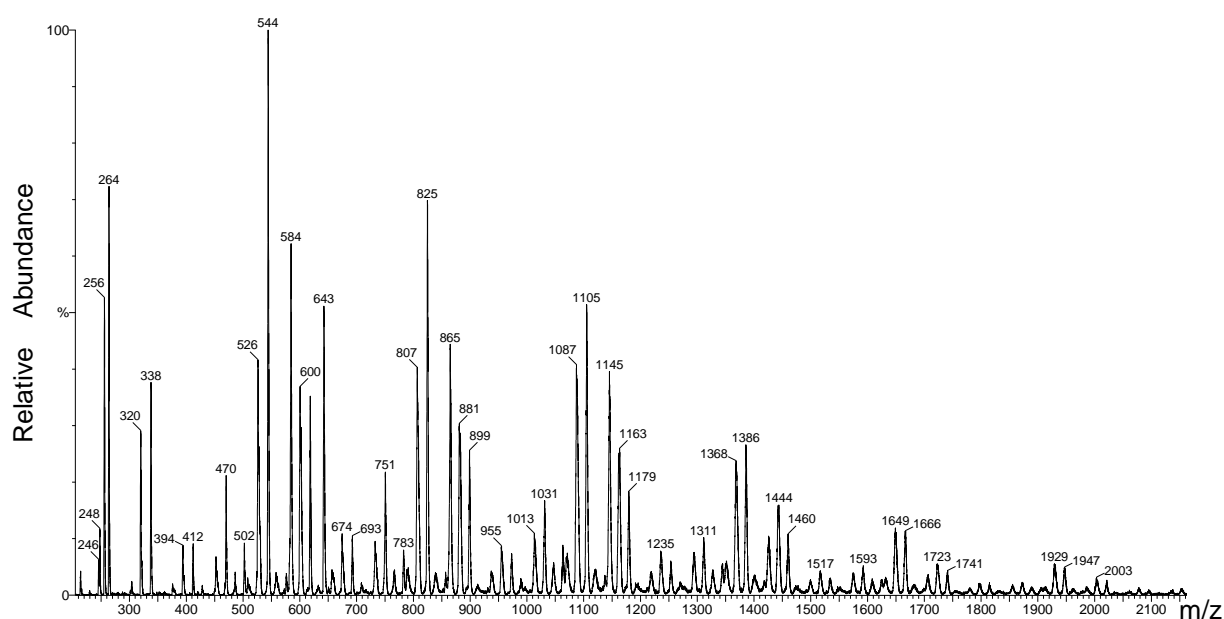
Figure 5.4: The spectrum obtained by Grindsted Super. This experiment was run in duplicate, and very similar results were obtained with both samples.
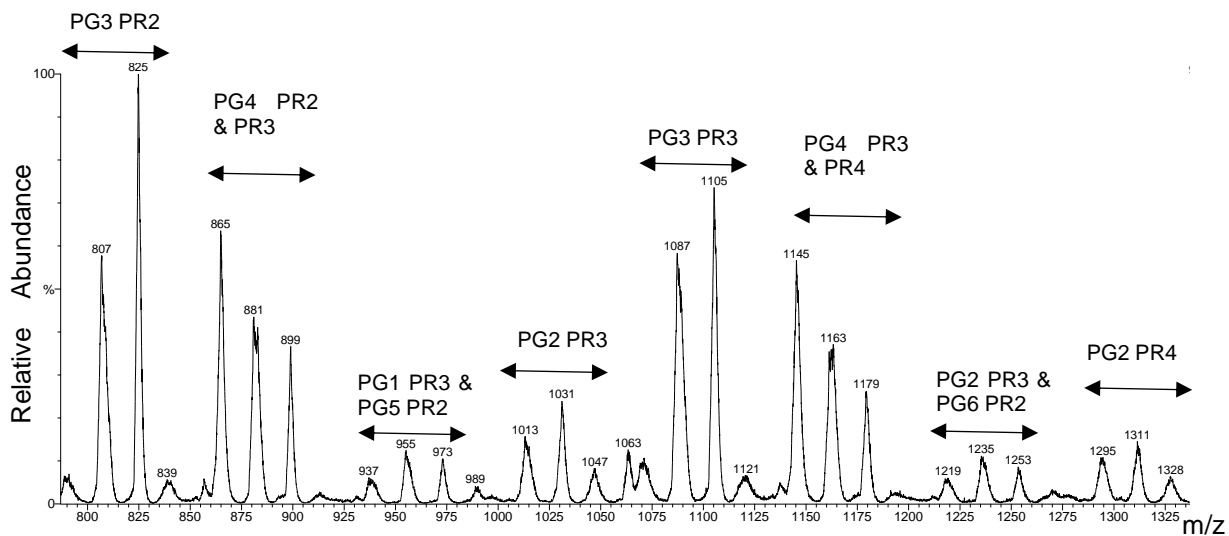
Figure 5.5: The spectrum shown in Figure 5.4 but focussed to 775-1350 m/z (PG = a number of glycerol units linked with ester bonds, PR = a number of ricinoleate units linked with ether bonds. The number following the code denotes the number of units in that molecule)

All PGPR samples were run in duplicate, and they all gave a very similar profile to Grindsted Super. These spectra are displayed in Figure 5.6. The data indicate that the molecular weight range of all the PGPRs was between 200-1600 m/z. The masses form a skewed curve, with a peak at 544 m/z, relating to a PGPR molecule of PG3-PR1.
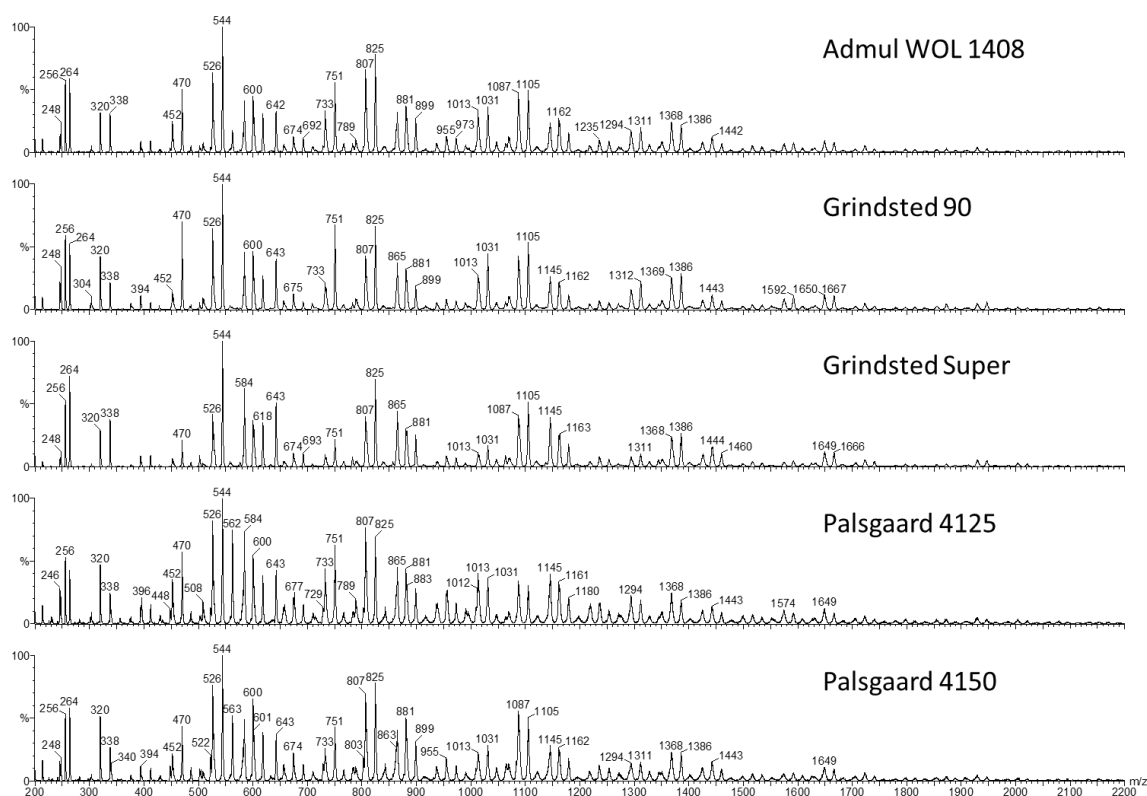
Figure 5.6: Spectra from all samples of PGPRs shown together. The spectra are all very similar, with a skewed curve ranging from 200-2000 m/z and the most abundant peak is at 544 m/z.

The data is different from the molecular weight expectations of an average of 3045 g/mol (Bastida-Rodríguez, 2013) or 2000 g/mol (personal communication, Kerry). The range of molecular weights of the molecules within the PGPRs is more similar to the data shown by Orfanakis et al. (2012), who found their data ranged from 400-2000 g/mol. They also found that the regular recurring pattern emerged. However, their data showed a bell-shaped curve with a peak at 1030 m/z, which would relate to a PGPR molecule of PG2-PR3.

In 1998, Nestlé commissioned an analysis of several PGPRs (Rousset and Bertoli, 1998). One of the experiments performed was ESI-MS of PGPRs dissolved in isopropanol. This data also showed a similar skewed profile with a lower molecular weight profile than was expected within the sample. However, in their results, the peaks did not show the regular pattern that the data here and Orfanakis et al. (2012)

show, so they concluded that the ESI-MS had fragmented the molecules during the measurement.

Rousset and Bertoli (1998) did, however, find evidence of cyclically esterified ricinoleic acids. As discussed above, during PGPR production, ricinoleic acids must be esterified to chains with a length as long as required for the PGPR functionality. It is intended that the esterification reaction forms linear chains; however, it has been predicted (Wilson et al., 1998) that cyclic polyricinoleate can be formed, Figure 5.7. Wilson et al. (1998) do not envisage that the cyclic polyricinoleate will cause detriment to the final product, except that it will not be able to react with polyglycerol. A cyclicly esterified bi-ricinolate would have a molecular weight of 561 g/mol. A substantial peak at this m/z was visible for the two Palsgaard PGPRs, and it is not present for the other PGPRs, as shown in Figure 5.6. This finding indicates that the method used by this manufacturer may encourage this cyclicly esterified bi-ricinolate to form.
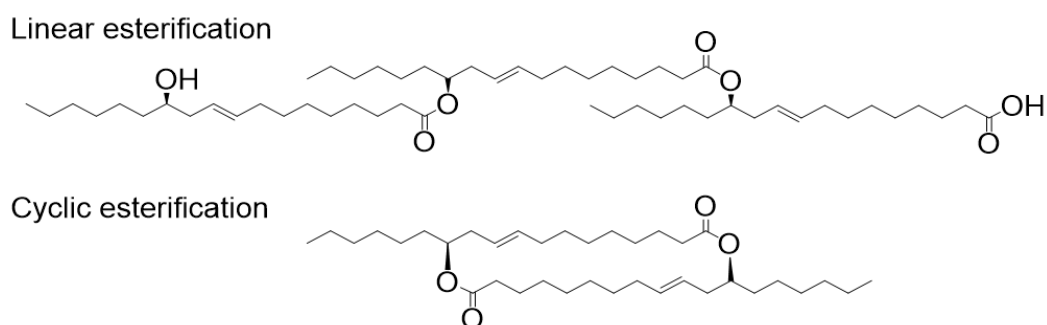
Figure 5.7: Predicted products of the esterification reaction with ricinolate proposed by Wilson et al. (1998).

The smaller-than-expected molecules found in this analysis may be a product of the addition of methanol:water which forced some molecules out of solution. It could be expected that the more hydrophobic molecules would be most likely to come out of solution as the polarity increases as "like dissolves like". Only molecules dissolved in

the solvent will be measured by the ESI-MS, which may be why only the smaller, slightly less hydrophobic molecules are observed in the mass spectra. Even though the data may show the incomplete range of molecules within the samples, it is still important to note that the spectra for all the PGPRs are so similar to each other.

5.3.1.2. Size-exclusion chromatography (SEC)

A size-exclusion technique was chosen to explore this further.

Figure 5.8 is a chromatogram showing the molecular weight distribution of the samples. This data implies a range of molecules within the PGPR samples, and this range has sizes between 100 and 30,000 g/mol, with a peak between 6,000 and 7,500 g/mol. This range is much greater than expected. There are several reasons that this could be. Calibration curves are only accurate if the chemistry and architecture of the analyte are identical to that of the calibration standard (Striegel et al., 2009). The poly(methyl methacrylate) (PMMA) standards used to make the standard curve may be inappropriate for the PGPR. PMMA is generally used for larger polymers, and the expected size of the PGPR molecules was at the bottom end of its range. With SEC, the folding of the molecule is important as the method separates the molecules by their size, immaterial of their molecular weight. If the PGPR molecules fold less than the standards do and take up a larger space, they may imply a larger molecular weight. Alternatively, the PGPR molecules themselves may be aggregating together, which would mean that the particles measured by the SEC would have a larger molecular weight than expected for single PGPR molecules. An examination of the particle sizes using a Zeta Sizer with different concentrations of PGPR in chloroform could be performed to see if there was a change as the concentration increased. This experiment would clarify whether there was any aggregation.

The other point of note, perhaps most apparent, is that the molecular weight ranges for all PGPRs are very similar. This result means that either the PGPR molecules

have a very similar range or that the aggregates, if formed, have a similar range. Therefore, although these data cannot be used as an indication of the molecular weight, they are still useful as they are informative for illustrating comparisons between the sizes of the molecules with the five samples.
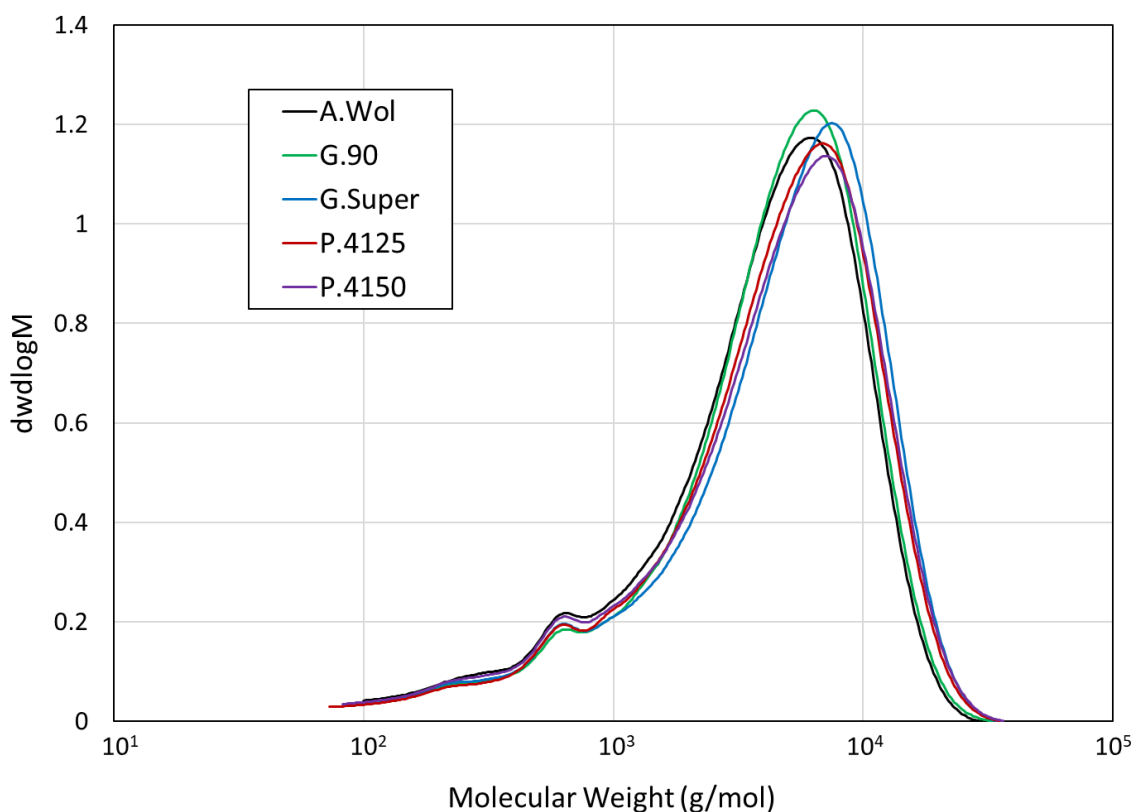
Figure 5.8: Overlaid multi-detector chromatogram of the molecular weight distributions of the five PGPR samples.

The intensity of signal vs retention time is shown in Figure 5.9; this is the raw data without calibration for molecular weight using the standards. Each PGPR shows a progressively higher baseline signal due to the typical baseline shift as the samples were run one after the other on the same day. However, it is helpful when overlaying samples to compare them, and the peak retention times can be seen as the same for all PGPRs. As discussed in section 5.2.2, looking at the raw data for samples run under the same conditions is a good way of comparing the molecules within the samples. The molecular content of all PGPRs appears to be similar.
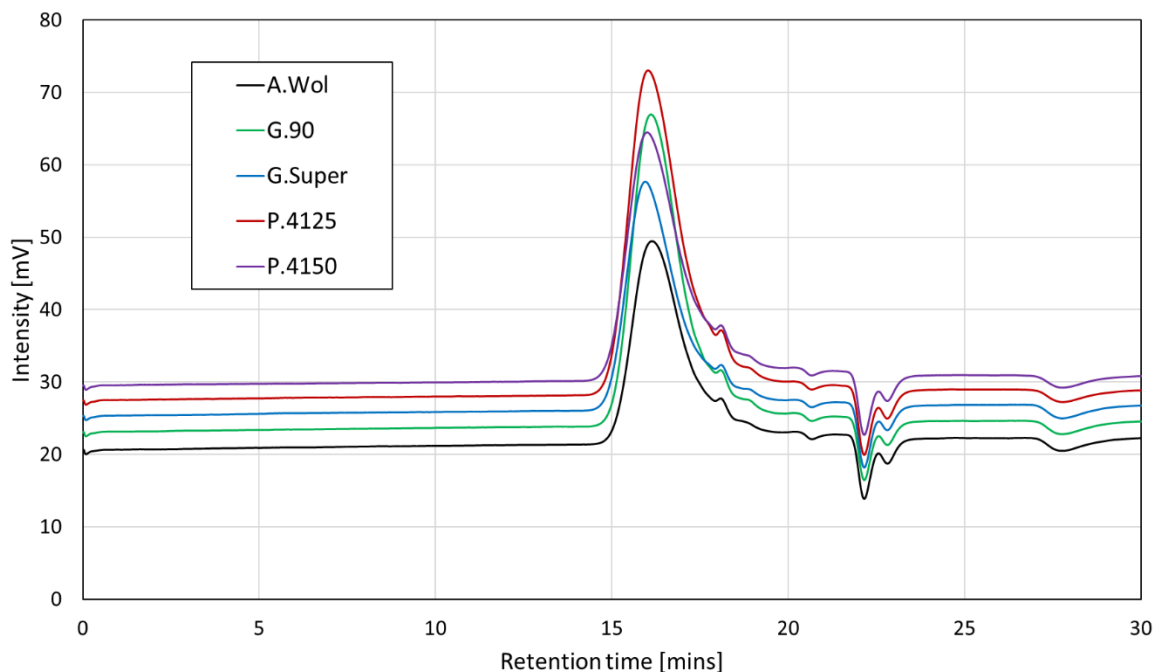
Figure 5.9: Intensity of the signal to the refractive index detector vs retention time (min) of the PGPRs. The molecules within the PGPRs all elute at very similar times.

The SEC data obtained by Rousset and Bertoli (1998) for one PGPR is shown in Figure 5.10. Unfortunately, they do not reveal the column or instrumentation or the solvent used to dissolve the PGPRs in their report. Comparing raw data between two experiments without this information is problematic, which is why transformation from the raw data size distribution into molecular mass distribution using an accurate calibration is generally performed (Striegel et al., 2009). However, even though a detailed comparison cannot be made, a general, visual comparison is possible. It can be seen that the curve shape is similar to that obtained in Figure 5.9: there is a sharp peak, with multiple distributions implied towards the endset of the main peak.
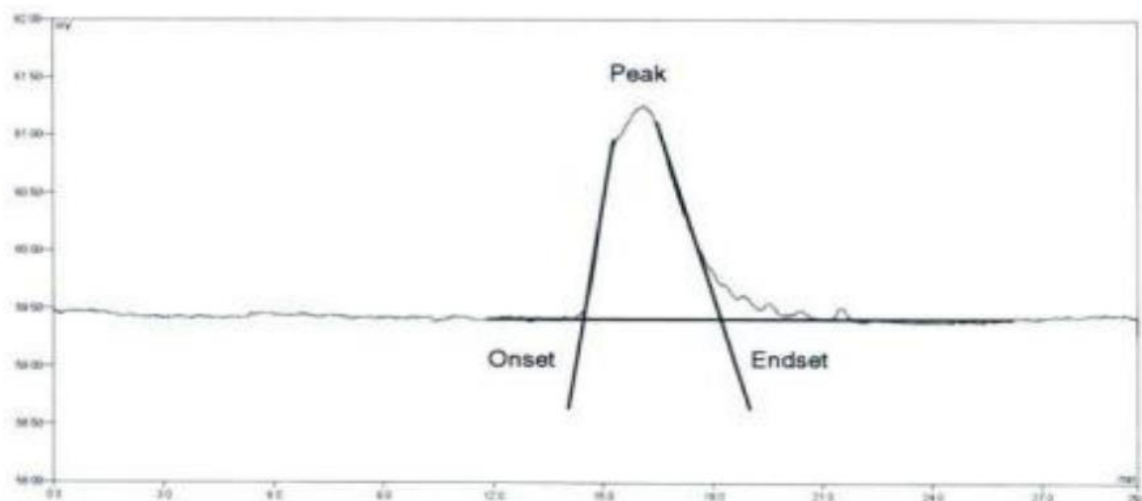
Figure 5.10: Intensity of the signal to the refractive index detector vs retention time for the PGPR tested by Rousset and Bertoli (1998). The retention times are unclear on this copy, but the peak shape is similar to Figure 5.9. Unfortunately, it was not possible to obtain an image with a higher resolution.

Although Rousset and Bertoli (1998) do not reveal the method they used in their report, they calibrate the results, giving peak molar masses of their PGPR samples in a more expected range. Of the samples they tested, three are the same as those used in this research. Table 5.2 shows a comparison of the peak molar masses measured in this PhD research and the data obtained by Rousset and Bertoli (1998).

Table 5.2: Peak molar mass [g/mol] for each PGPR measured in this PhD with the peak molar mass for those measured by Rousset & Bertoli (1998). Both were measured using size exclusion chromatography. The method for Rousset & Bertoli is unknown, but they calibrate to achieve a peak molar mass for their samples, which is more in the expected range for PGPRs. Two batches of Grindsted 90 were used by Rousset & Bertoli, and both are given here.

PGPR	Peak molar mass [g/mol] (present research)	Peak molar mass [g/mol] (Rousset & Bertoli)
Admul WOL 1408	6000	2700
Grindsted 90	6220	2800 (B1) 2700 (B2)
Grindsted Super	7441	
Palsgaard 4125	6804	2900
Palsgaard 4150	7052	

In other literature, SEC is also credited as characterising PGPR with a molecular weight "ranging from several hundred to over four thousand g/mol". (Dedinaite and Campbell, 2000). However, no method was given in this paper either.

5.3.1.3. Nuclear Magnetic Resonance (NMR) Spectroscopy

As a final attempt to find a difference in the sizes of the PGPR molecules, particularly the polyricinoleate chain, NMR spectroscopy was utilised. A difference in the alkene region between two PGPR samples would indicate a difference in the number of double bonds in the polyricinoleate chain and infer a different polyricinoleate chain length. The two PGPRs selected in section 4.3.1 for further review were also chosen here. These were Grindsted 90, the PGPR that was least efficient at lowering the yield stress, and Palsgaard 4150, one of the PGPRs which was most efficient at lowering the yield stress of the sugar-in-oil chocolate model suspension.

The results of the NMR spectroscopy are shown in Figure 5.11. The alkene region is at 123-135 ppm (part per million): no difference was revealed between the two PGPRs. The finding was a surprise given that Vernier (1997) suggests that the length

of the polyricinoleate chain was essential to the functionality of a PGPR or similar emulsifier; the longer the chain, the better the yield stress-reducing functionality. However, as with ESI-MS and SEC, the NMR results also showed that the range of molecular sizes within the two PGPRs shown are very close.
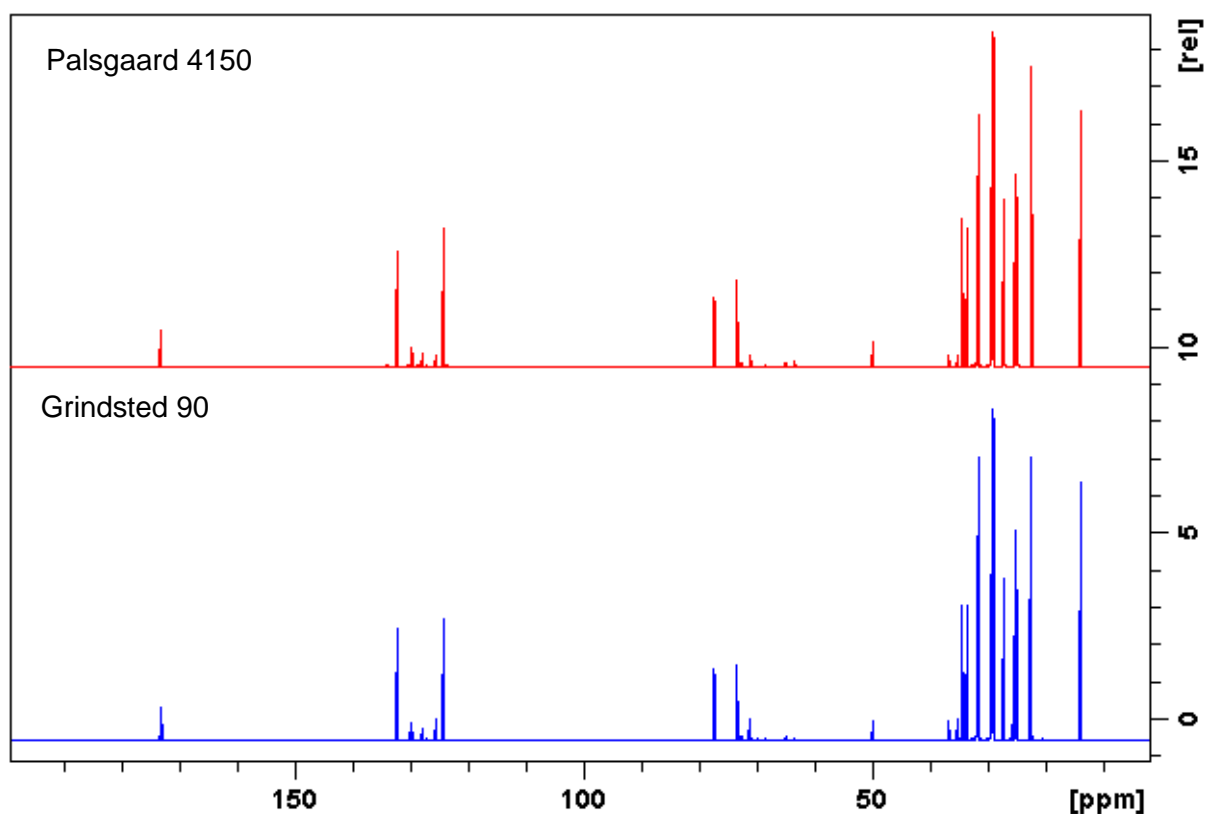
Figure 5.11: ¹³C-NMR spectra of Palsgaard 4150 and Grindsted 90 in d-Chloroform. Differences in the alkene region (123-135 ppm) would indicate different polyricinoleate chain lengths; however, both spectra are very similar.

5.3.1.4.   Interim review of data and next steps

Bringing together the results of the three methods, it is not possible to state a specific molecular weight range for the PGPR samples in this research. However, molecules' size range can be identified as being essentially the same between PGPR samples. Nevertheless, the fact remains that the research outlined in chapter 4 shows a functionality difference between the PGPR samples.

To further investigate the likely size of the PGPR molecules and give some further insights into the expected structure of the molecules, a large number of possible molecule structures were screened against the ranges given by the Food Regulators using calculations. This screening process would reveal the PGPR molecule structures that would give the sample the correct iodine values, hydroxyl values and saponification numbers. This process is described and discussed in section 5.3.2.

As the hydrophobic polyricinoleate chain's length is not the cause of the differences found between the functionality of the PGPR samples, the fatty acid composition of the PGPRs was analysed using transesterification and gas chromatography-mass spectrometry (GC-MS) methods. The results of this analysis are examined in section 5.3.3.

5.3.2. Composition of PGPR molecules based on theoretical calculations

As stated in section 5.1.1.3 and explained in 1.4.5, regulators require that the PGPR samples meet various criteria before they are allowed to be used in food. The manufacturers test their PGPRs against these values using standard analytical methods. However, it is possible to calculate these values if the molecular structure is known.

As described in section 5.1.1, the fatty acids used in PGPR come from castor oil, a collection of triacylglycerols (TAGs) whose fatty acids are primarily ricinoleic acid (80-90%). This fatty acid is critical in the condensation reaction due to its hydroxyl group, see Figure 5.12. Other fatty acids said to be present in castor oil TAGs are oleic acid (3-8%), linoleic acid (3-7%) and stearic acid (0-2%) (Wilson et al., 1998). These fatty acids act as "capping" fatty acids to halt the extension of the polyricinoleate chain further, as is seen generally in estolide production (Chen et al., 2020, Isbell, 2011, Zerkowski, 2008). The polyricinoleate chains can be esterified to the polyglycerol

molecules at any of its hydroxyl groups (Wilson et al., 1998); however, the end hydroxyls are the most likely candidates due to accessibility, see Figure 5.1.
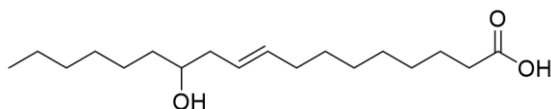
Figure 5.12: Chemical structure of ricinoleic acid

When selecting the range of theoretical molecules to be screened, it was decided that molecules with a polyglycerol chain from one to seven molecules would be included, as the regulations discourage the use of polyglycerols over heptaglycerol. The polyricinoleate chain was not so restricted, so chains from one to 20 were selected. It is unlikely that chains longer than 20 would be made due to the time it would take to generate a chain this length.

The presence of the "capping" fatty acids within the castor oil adds complexity to the theoretical calculations, particularly the hydroxyl value – i.e. whether the PR chain's end fatty acid has an OH group strongly impacts this value. The alternative "capping" fatty acids considered in the screened molecules were stearic acid and linoleic acid, as these make a difference to the hydroxyl and iodine values. To summarise the molecular structures considered at the end of the chains, they are all C18 fatty acids but ricinoleate: one double bond and an OH group, linoleate: two double bonds and no OH group, and stearate: no double bonds and no OH group. Their structures are shown in Figure 5.13. Whether there are one or two PR chains in the PGPR also impacts the hydroxyl value, a lone PR chain leaves an extra OH group on the PG chain; see the lower molecule in Figure 5.1.
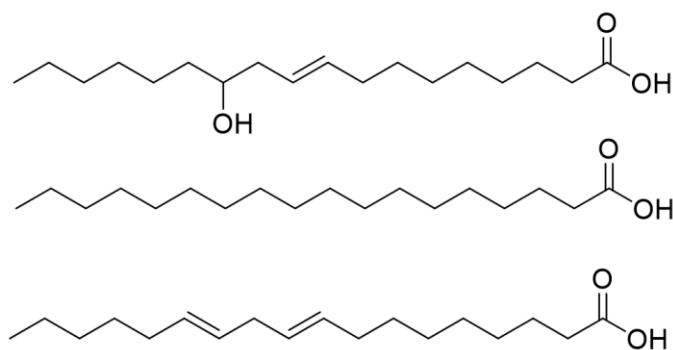
Figure 5.13: Structures of the capping fatty acids considered in the screened molecules: ricinoleic acid (top), stearic acid (middle) and linoleic acid (bottom)

On an industrial scale, a range of PGPR molecules is generated that average out to the values needed. Therefore, molecules within the range for two of the criteria by out by 5% for the third were included as "successful" molecules. This level was chosen as an arbitrary value but to reflect the natural variation that occurs in the real-world situation.

5.3.2.1. Theoretical calculations used

Hydroxyl value: This is a measurement of hydroxyl groups in an organic material (2007a). Experimentally, it can be measured by acetylating the sample with a solution of acetic anhydride in pyridine in a pressure bottle at 98°C, or under reflux. The excess reagent is hydrolysed with water, and the acetic acid is titrated with a standard sodium hydroxide solution. The hydroxyl content is calculated from the difference in the titration values of the blank and sample solutions (ASTM, 2017).

However, when the chemical structure is known, this can be estimated theoretically

$$HV \ (mg \ KOH \ per \ g \ sample) = \frac{MW_{KOH} * n_{OH}}{MW_{PGPR}} * 1000$$

Where MW_{KOH} is the molecular weight of potassium hydroxide, n_{OH} is the number of hydroxyl groups on the PGPR and MW_{PGPR} is the molecular weight of the PGPR molecule.

In PGPR, hydroxyl groups are expected on the glycerol carbons and the end of the PR chain, in the case of a ricinolate fatty acid.

Iodine value: This is a measure of the proportion of unsaturated linkages, or olefinic double bonds, present on the fatty acids (2007b). Experimentally, the sample can be dissolved in carbon tetrachloride and then iodine bromide is added. It is shaken and then stored in the dark for 30 min. Potassium iodide and water are added, and the contents are gently shaken while being titrated with sodium thiosulphate, adding starch as an indicator towards the end. In tandem, a duplicate experiment should be run but without the sample. The difference in the amount of sodium thiosulphate required to neutralise the liberated iodine in each flask is used to calculate the iodine value (ECSPP, 2019).

Again, when the chemical structure is known, it can be calculated theoretically:

$$IV \ (g \ iodine \ per \ 100 \ g \ sample) = \sum \omega_i * \frac{253.81 * n_i}{MW}$$

Where ω_i is the percentage of the fatty acid component (in this theoretical case, this is taken as 100% for each molecule individually), n_i is the number of olefinic double bonds of the molecule, MW is the molecular weight of the PGPR molecule, and 253.81 is the molecular weight of the iodine molecule (I_2) (BSI, 2018)

Saponification number (SN): The SN is a measure of the alkali-reactive groups, for example, ester bonds, within a sample (2007c), which reflects the number of fatty acids in the molecule compared with the size of the entire molecule. Experimentally, the sample can be refluxed with ethanolic potassium hydroxide solution for 1-2 hours. A colour indicator is then added and the solution titrated against hydrochloric acid until

the colour changes. A blank test should also be performed, and the difference in the volumes of hydrochloric acid is used to calculate the saponification number (BSI, 2020a).

The SN can be theoretically calculated by

$$SN \ (mg \ KOH \ per \ g \ sample) = \frac{n_{FA} * 1000 * 56.1}{MW}$$

where n_{FA} is the number of fatty acids in a molecule, and *MW* is the molecular weight of the molecule (BSI, 2020a).

The **acid value** is a measure of the free fatty acids within the sample (BSI, 2020b). As free fatty acids were not detected in the HPTLC experiment, and a measured low acid value indicates the completion of the PGPR batch during production (Wilson et al., 1998), this calculation was not performed on the theoretical molecules.

5.3.2.2.   Discussion

A total of 819 molecules were screened. These were molecules with 1-7 glycerols in the polyglycerol chain (PG1 to PG7) and 1-20 fatty acids in a polyricinoleate chain (PR1 to PR20). PG7 was chosen as the largest glycerol chain to be screened as regulations state that 90% of all PGPR molecules must be below this number. PR20 was chosen as the largest polyricinoleate chain to be screened as an arbitrary but large number. Except for the molecules with PR1, the number of fatty acids was considered as either a single chain (e.g. PR6) or two chains (e.g. PR3 x 2) on the polyglycerol chain. More than two PR chains may be found on a PGPR molecule; however, only these two scenarios have been considered here as they are considered the most common in PGPRs, as discussed in section 5.1.1.1. Finally, the PR chains were considered with different end fatty acids: a ricinoleic acid molecule (one double bond, one OH group), a stearic acid molecule (no double bonds, no OH group) or a linoleic acid (two double bonds, no OH group). The structures are shown in Figure

5.13. These fatty acids were chosen arbitrarily but based on the expected fatty acids within castor oil. Other fatty acids could have been considered here as oleic has been found in castor oil (Wilson et al., 1998). However, as this screening approach was considered to be a guide and not an exhaustive list, merely these three fatty acids were selected.

The equations in section 5.3.2.1 were put together in the spreadsheet, and a segment of this is shown in Figure 5.14. From analysing the results of the calculations, it became clear that only a small percentage of possible molecules meet the criteria.

Screened molecule details

Results of the calculations

Three ranges combined here

Red shaded cells indicate values within

Red text indicate values within range ± 5%

Red cells indicate that all ranges are satisfied

Yellow cells indicate two values are within range and one ± 5%

																													PG		
PG			4	4	4	4	4	4	4	4	4	4	4	4	4	4	4	4	4	4	4	4	4	4	4	4	4	4	4	4	4
PR			1	2	2	3	3	4	4	5	5	6	6	7	7	8	8	9	9	10	10	11	11	12	12	13	13	14	14	15	16	16
PR chains			1	1	2	1	2	1	2	1	2	1	2	1	2	1	2	1	2	1	2	1	2	1	2	1	2	1	2	2	1	2

Figure 5.14: A section of the spreadsheet used to screen the theoretical molecules, showing the PG4-PR1 to PG4-PR16 molecules. The theoretical structures are outlined at the top with the number of PG molecules, the number of PR molecules and the number of PR chains on the PGPR; however, only 1 or 2 were considered here. The "Range calculations" section shows the calculations for each of the ranges for the three types of PGPR capping molecules. Red cells meet the criteria, and cells with red text are in the ± 5% extra window. The "Meets all three criteria" section shows the structure of the molecules that would pass the Food Regulatory requirements and, in orange, those in the ± 5% range. It can be seen that out of the 93 molecule structures shown in this fragment of the spreadsheet, only 13 meet the criteria, with five more in the extended range.

146

It is relatively easy for the molecules to meet the saponification number criteria (75% met the SN, 82% with the extended range) and the iodine value criteria (71% met the IV, 78% with the extended range). However, meeting the hydroxyl value is more challenging (13% met the HV and 18% with the extended range). Applying the results of the three equations to the molecules screened shows that the capping fatty acids made a difference to the PGPRs allowed by the regulatory bodies. Only 15% (20% with extended range) of molecules with ricinolate ends, 10% (16% with extended range) with linoleate ends, and 5% (11% with extended range) with stearate ends meet all these criteria. The percentage of molecules screened that met all the criteria for all 819 molecules reviewed was only 10% (15% extended range).

As the regulatory criteria state that at least 75% of all PGPR molecules must have a PG chain of di-, tri-, and tetraglycerols, it is valuable to look at this subset. Only 38 molecules meet the criteria, equating to almost 11% of all molecules within this subgroup (351 molecules). It is easy to see how difficult it is to alter a PGPR manufacturing method from an established one in order to improve it. From this subgroup, presumably, where the PGPR manufacturers want to create most of their molecules, the molecular weight range of criteria-meeting molecules was 1831-4223 g/mol.

Personal communication with consultants in the field of commercial surfactants and with industrialists who make PGPR reveals that synthesising it is not a precise art. Quality control involves pragmatic performance-in-chocolate model tests and the wet chemical tests outlined above, rather than the analysis of PGPR chemical structure.

In the results of the calculations performed here, the optimal ratio of PG length to PR length was found to be 1:3 to 1:4 for those molecules where a ricinoleate was the end of the chain, and it was 1:2 to 1:3 for the other molecule types. This difference was due to the presence or absence of a hydroxyl group at the ends of the PR chain. In PGPR manufacture, it may be wise to assess the fatty acids in the castor oil feedstock

before processing commences. The percentage of non-ricinoleate fatty acids within the feedstock will make a difference in how long the PG and PR chains should be and may impact the initial condensation reaction times.

5.3.3. Fatty acid profile of PGPRs

The cause of the differences between the functionality of the PGPR samples shown in Chapter 4 was not found in the experiments performed in section 5.3.1; the molecular weight distributions were remarkably similar between samples. Therefore, the research continued with an analysis of the fatty acids within the PR chains. The fatty acids discovered using the transmethylation with the TMSH method are shown in Figure 5.15. Ricinoleic, stearic, oleic and linoleic acids were expected (Wilson et al., 1998) as well as "small amounts of other fatty acids" (Christiansen, 2015). In all the PGPR samples analysed, palmitic, stearic, oleic, linoleic and α-linolenic acids were discovered. There are three C18:2 fatty acids peaks found on the gas chromatogram shown in Figure 5.16. The peak at 18.69 min is in the position amongst the fatty acids where linoleic acid elutes typically, so it can be said with reasonable certainty that this is the identity of this peak (Christie and Han, 2010c). The other two C18:2 eluted later, so they need further consideration before they can be identified, and these are discussed later. A peak which appears to be glycerol was also found using this method: it is presumed that this is free glycerol within the sample, rather than the glycerol in the PGPR molecule itself; if the reaction released all embedded glycerol, then the results from all PGPR samples would show a much more significant glycerol peak.

The total fatty acids measured by GC-MS were only around 100 mg/g PGPR, which is 10% of the weight of all molecules within the sample. This amount is too low to be all the fatty acids within the sample; literature (Wilson et al., 1998) and the calculations made in section 5.3.2 agree that the total should be in the region of 80-90% by weight

(70-75% of the total molecules in the sample). Therefore, it is presumed that the transmethylation method used with TMSH only removed the fatty acids at the ends of the PGPR molecule, which were previously described as the capping fatty acids in section 5.3.2. The TMSH reaction is known to be a very mild reaction (El-Hamdy and Christie, 1993) and, together with the opinion of Isbell et al. (2001) that "the secondary ester linkage of the estolide is more robust to hydrolysis than triglycerides", it is assumed to be the case in this analysis.
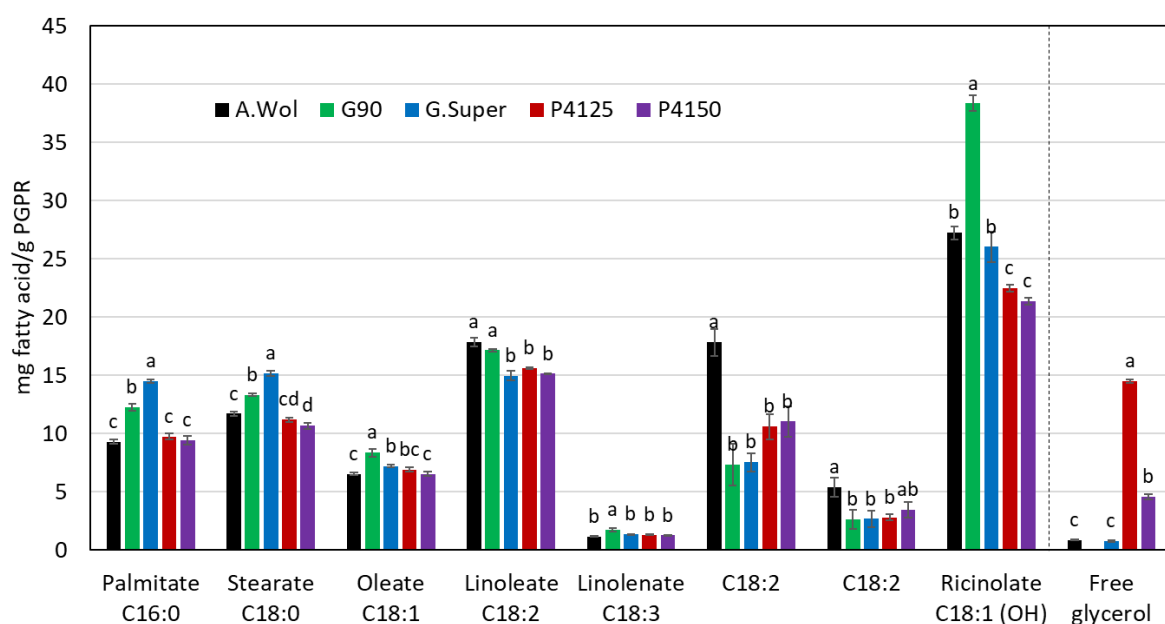

Figure 5.15: Fatty acid results from the transesterification method with TMSH followed by GC-MS. The statistical differences between each substance detected is shown using letters with a>b>c>d. Values were obtained as a mean and standard deviation from three samples of extracted lipids.

It can be seen in Figure 5.16 that two unidentified C18:2 fatty acids are eluted from the GC after α-linolenic acid. This elution order is unusual, but Δ5 linoleic acid molecules have been found to elute at a later retention time (Wolff et al., 1999). Wilson et al. (1998) suggest that dehydration of ricinoleic acid is possible during the condensation reaction that produces the polyricinoleate chains, and this would produce two different C18:2 molecules, see Figure 5.17.

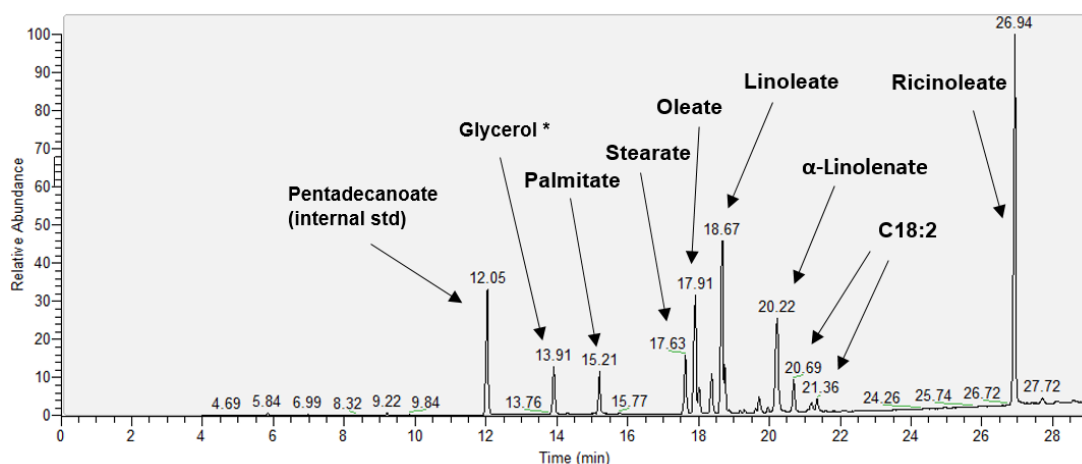One or both of these could be the unknown C18:2 molecules.

*Figure 5.16: The gas chromatographic trace following transesterification of Palsgaard 4125. *The glycerol peak is only found in the Palsgaard PGPRs.*
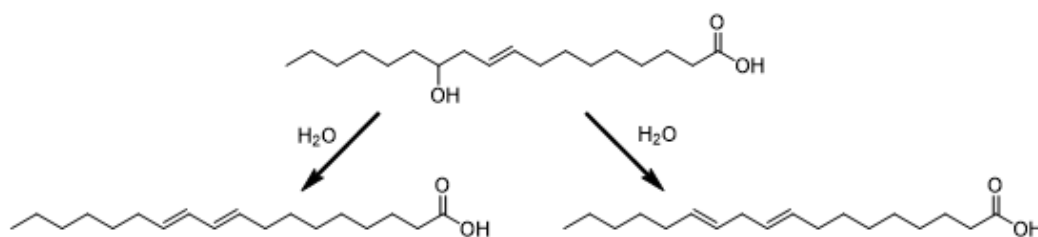

Figure 5.17: Possible molecules following dehydration of ricinoleic acid (Wilson et al., 1998).

Another suggestion could be that the TMSH reaction has been known to methylate the hydroxyl group of the ricinoleic acid as well as the acid group, forming a methoxy fatty acid methyl ester, see Figure 5.18 (Vosmann et al., 1998). This molecule could be an alternative suggestion for the unknown C18:2 molecules.
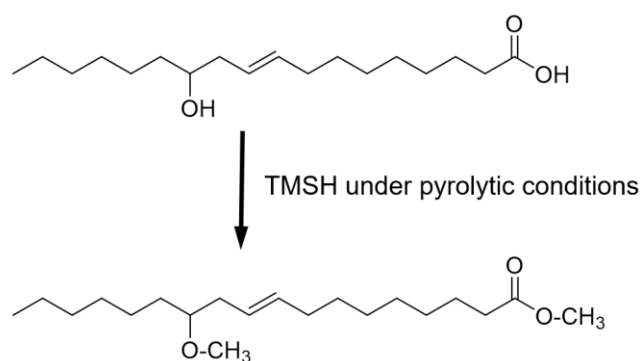
Figure 5.18: Possible formation 12-methoxy octadec-9-enoic acid methyl ester from 12-hydroxy octadec-9-enoic acid (ricinoleic acid), following pyrolysis with TMSH.

The fragmentation patterns generated by the mass spectrophotometer are shown in Figure 5.19, which highlights that the fragments for all three peaks are very similar. The prominent peak for all is at 67, which would be a C_5H_7 di-ene fragment – this confirms the presence of two double bonds and the molecular weight fragment is at 294, which suggests a linoleic acid molecule. If either of these C18:2 molecules were the methoxy fatty acid methyl ester, then there should be fragments at *m/z* 294 $[M-CH_3OH]^+$, 129 $[C_8H_{17}O]^+$ and 97 $[129-CH_3OH]^+$ (Vosmann et al., 1998). Unfortunately, apart from the fragment at 294, which is also the molecular weight fragment of linoleic acid, there are no significant peaks that would indicate the presence of 12-methoxy octadec-9-enoic acid methyl ester.

Many peaks surrounding the smaller fragments could indicate fatty acid isomers or that the double bonds are undergoing rearrangement due to conjugation. Therefore, instead of being formed from the dehydration of ricinoleic acid during processing, they could have arisen from linoleic acid double bond rearrangement.

If the total fatty acid content of the PGPR samples could be measured, it may be possible to calculate where the most likely origin for these fatty acids could be, given that the amount of ricinoleic acid in castor oil is around 90% and linoleic acid is present at between 3-7% (Wilson et al., 1998). This might be possible if the transesterification

reaction was repeated using a different method (Christie, 1993) and the results were compared. A stronger reagent, or more vigorous reaction, may hydrolyse all the fatty acids from the PGPR molecule, so a more thorough investigation into the fatty acid content of the sample can be performed.
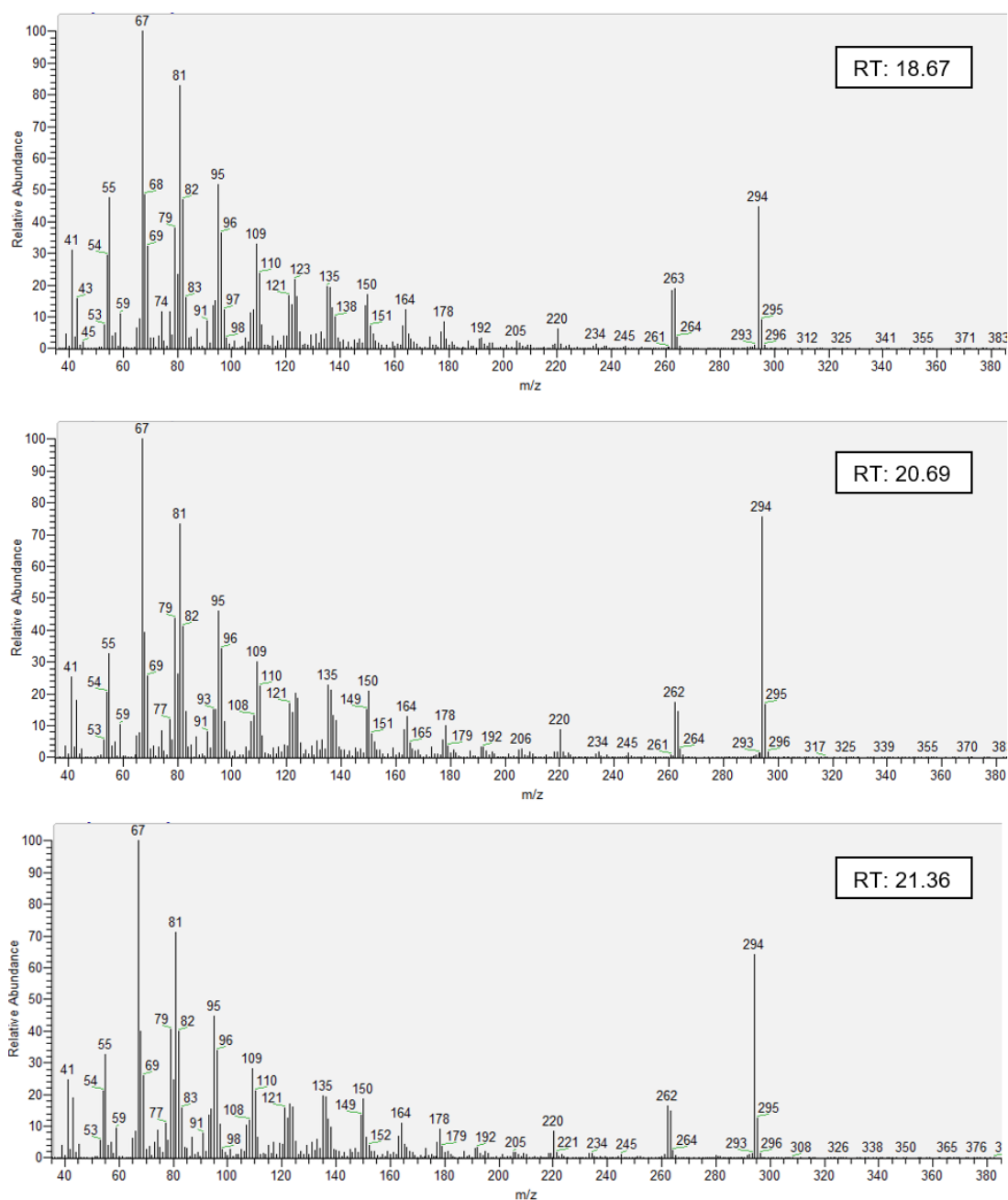

Figure 5.19: Fragmentation pattern of the three C18:2 molecules found in PGPR

However, the most important finding is that the fatty acid analysis indicated that Grindsted 90 has significantly more PR chains with a ricinoleate capping group than

152

the other PGPRs, as shown in Figure 5.15. Grindsted 90 is the PGPR that had the lowest capacity for reducing the yield stress in the chocolate model, so perhaps this is the key to understanding the issue. The hydroxyl group on the ricinoleate at the end of the chain makes it more hydrophilic, so it may be that the chain folds back and adsorbs to the sugar, thus reducing the power of the PGPR molecule to extend its long hydrophobic tails into the fat phase. The length of the polyricinoleate chain has been linked to its effectiveness (Vernier, 1997) and reducing its ability to extend into the continuous phase may limit its effectiveness. A graphic representation of this theory is shown in Figure 5.20.
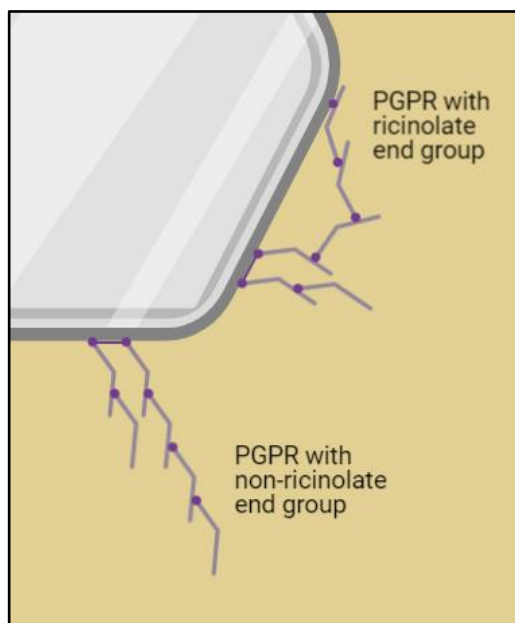

Figure 5.20: Illustration to describe the possible result of a hydroxyl group on the end fatty acid of the polyricinoleate chain, using the traditional adsorption theory. The grey area denotes a sugar crystal. The darker purple circles represent the presence of the hydrophilic hydroxyl parts of the PGPR. Created using BioRender.

Middendorf et al. (2015) found evidence using Atomic Force Spectroscopy which suggested the PGPR molecules form pillow-like deposits on the surface of the sugar with cocoa butter. The illustration used in their paper is shown in Figure 5.21. The limitation for the Grindsted 90 PGPR could still be valid using this alternative theory, as demonstrated in Figure 5.22.
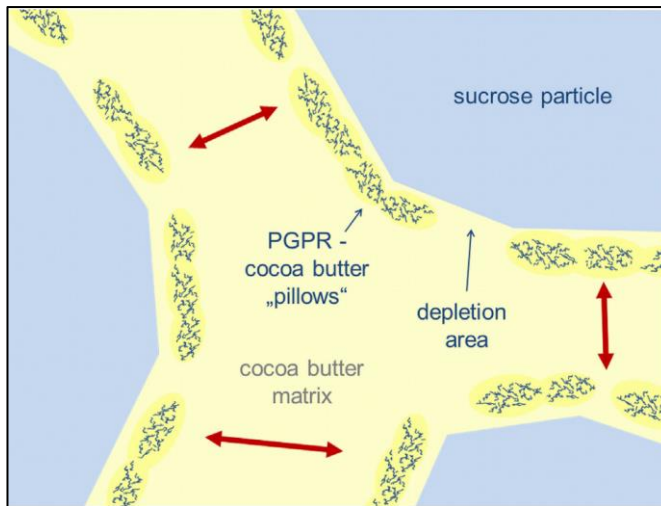
Figure 5.21: Illustration of pillow-like deposits consisting of cocoa butter and PGPR polymers associated with ground sucrose particles, pillows act like spacers and loosely bound buffers between sucrose molecules leading to an enormous decrease in yield value (Middendorf et al., 2015).
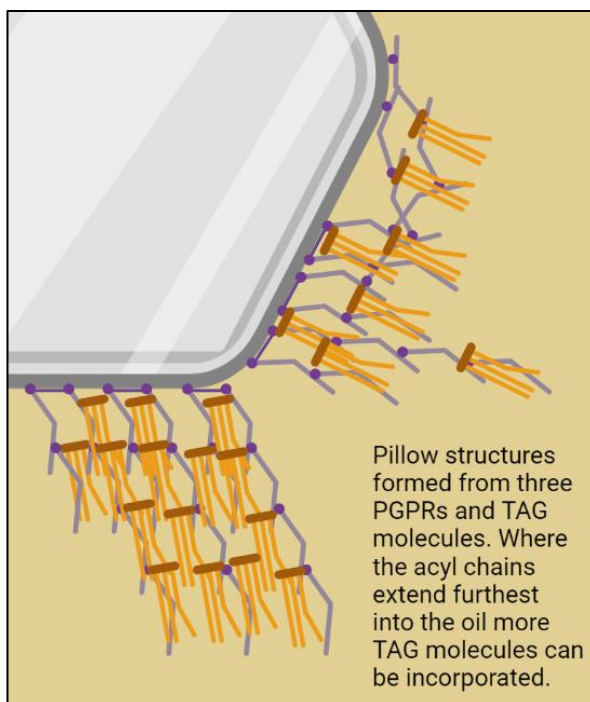
Figure 5.22: Illustration to describe the possible result of a hydroxyl group on the end fatty acid of the polyricinoleate chain, using pillow theory. The grey area denotes a sugar crystal. The darker purple circles represent the presence of the hydrophilic hydroxyl parts of the PGPR. The orange groups are triacylglycerol (TAG) molecules from the oil. It should be noted that the mechanism for the interaction between TAG and PGPR have not been elucidated; however, it is presumed that the glycerol groups may interact between each molecule. The TAG molecules shown are not representative of actual cocoa butter TAGs or their crystallisation. Created using BioRender.

Finally, the presence of free glycerol is of interest, especially as this is highest in Palsgaard 4125, which was found to have less capacity for reducing yield stress than the best three PGPR samples. If true, perhaps the hydrophilic glycerol takes up space at the sugar surface so that the PGPR molecules have less space to occupy. However, the presence of such a high amount of glycerol seems questionable because the theoretical hydroxyl value of glycerol is 1827 mg KOH/g. When the information used to create Figure 5.15 was recalculated to show the mol%, the glycerol molecules comprised 23% of the total molecules in the Palsgaard 4125 sample. If the remaining fatty acids are assumed to be capping fatty acids, and if one assumes that each of these represents just one PGPR molecule, which has a hydroxyl value of 0 (not possible in reality), the overall hydroxyl value of the PGPR sample would still be 420 mg KOH/g. This value is still very elevated and would not be allowed by the regulators: the authorised range is 80-100 mg KOH/g (CEC, 2008, JECFA, 1992). Therefore, this free glycerol measurement should be verified using a standard industry method to ensure that this is a "real" finding.

5.4. Conclusions

This phase of the research set out to discover what it is about the structure or chemistry of the PGPR molecules that caused the functional differences measured in chapter 4. It was challenging to evaluate the molecular size of the PGPRs. The ESI-MS gave molecular mass range values that were too small, and the size exclusion chromatography gave values that were too large to be true when compared to the values determined by the theoretical screening process. These calculations showed that PGPRs that meet these regulations are within a molecular weight range of 1831 to 4223 g/mol. The manufacturers create a PGPR with a range of molecules and evaluate the hydroxyl, iodine and saponification values experimentally; therefore, a pragmatic view must be taken; some molecules within the samples themselves may

be above or below the ranges, but different molecules could balance each other to give an overall value within the range.

However, a conclusion can be drawn about the molecular weight range of the samples. The ESI-MS and SEC results, taken with the NMR values, show that the PGPRs all have a very similar range profile, leading to the conclusion that the functionality difference is not due to the length of the polyricinoleate chains as this provides the greatest molecular weight contribution.

The fatty acid profile, by transesterification of the capping fatty acids (those at the end of the polyricinoleate chains) followed by analysis on a GC-MS, was considered. Here, the PGPR that reduced the yield stress the least (Grindsted 90) was shown to contain a significantly higher amount of ricinoleic acid capping fatty acids, suggesting that the hydrophobic tail ends of this PGPR were more polar than the other PGPRs. This increase in hydrophilicity appears to interfere with its functionality. From this information, it was proposed that any PR chains with a ricinoleate at the end might fold back to interact with the sugar, rather than extending into the fat/oil, which means that the long hydrophobic chain is not as effective, as illustrated in Figure 5.20. Additionally, if the pillow theory action of PGPR suggested by Middendorf et al. (2015) is considered, illustrated in Figure 5.21, perhaps this polar region makes it less effective at incorporating the triacylglycerols into the pillows, as imagined in Figure 5.22. The effect of the capping fatty acid on the performance of the PGPR could indicate that an assessment of the fatty acid content of the castor oil used for making the polyricinoleate is important for PGPR manufacturers.

In the PGPR that reduced the yield stress more than Grindsted 90 but less than the three best PGPRs (Palsgaard 4125), there was a significant increase in free glycerol, which may compete for adhesion at the surface of the sugar. The issue of the free glycerol would need to be looked at more closely before firm conclusions can be drawn – a standard method of measuring free glycerol should be employed to ensure

the values are "real", and methods are provided in the literature (for example, Mercer and Halalweish (2010)). If this free glycerol value is found to be correct, experiments could be planned to use Grindsted Super or Admul WOL 1408, add to it increasing levels of glycerol and assess the new sample's performance in the chocolate model. These experiments could show the effect of the presence of free glycerol in the PGPR. It implies that removing any free glycerol molecules from the PGPR would also help achieve a more highly functioning PGPR.

The final aim of this PhD is to find a natural alternative to PGPR. The information in this chapter was applied to the decisions made: Generally, PGPR molecules have a PG chain of between two and four molecules to abide by regulations. The results of the theoretical calculations discussed in section 5.3.2.2 generally showed that the number of polyglycerols to poly-fatty acids in acceptable PGPR molecules was 1:3 (linoleate or stearate capping fatty acid) or 1:4 (ricinoleate capping fatty acid). The results of the GC-MS showed that the PGPR had a better efficacy if the polyricinoleate chain was as non-polar as possible.

A review of known natural molecules that would replicate a long acyl chain showed that waxes and wax esters are formed of very-long-chain fatty acids. However, waxes are poorly miscible in oil (Broughton et al., 2018), may increase the viscosity of the fat phase when they do dissolve and may give a waxy mouth feel to the chocolate. Alternately, naturally occurring estolides could be used. These molecules are relatively rare, although estolides linked to digalactosyl diacylglycerol (DGDG) have been found in oats and tested as a PGPR alternative with some success (Kaimainen et al., 2012, Lindecrantz et al., 2015). Estolides have also been found in seed oils, for example, *Dimorphotheca pluvialis* (African daisy) (Hayes et al., 1995a), *Lesquerella* (Hayes et al., 1995b, Kleiman et al., 1972, Lin and Chen, 2013), *Apocynaceae* (dogbane family) (Smith and Zhang, 2016) and, of course, *Ricinus communis* (Castor) seed (Lin et al., 2006). They have also been found in the secretions of caterpillars

(Smedley et al., 2002) and possum (McLean et al., 2015). Vernier (1997) looked at various naturally occurring lipids, including phospholipid and oat lipid extracts, and fractions of these lipid types. Although surface-active properties within these lipid groups were identified, a yield stress lowering effect comparable to PGPR was not found.

Therefore, an alternative theory was proposed: to evaluate the importance of PGPR's larger headgroup for its functionality; this has not been investigated before. The action of PGPR may depend on both the large head group and the extended acyl groups, as suggested by the interfacial tension findings in Chapter 3. Digalatosyl diacylglycerol (DGDG), found in leaves, has previously been shown to be surface-active in sugar-in-oil suspensions (Mohamad et al., 2020). However, lipids with larger headgroups, and more particularly, space between the acyl groups attached to the headgroup, have not yet been evaluated as an emulsifier in literature. This molecular structure is found naturally as acylated monogalactosyl diacylglycerol (acyl-MGDG). Therefore, this molecule was chosen as the candidate to take forward and assess for yield stress reducing properties. This molecule is not commercially available; thus, the following approaches were taken to obtain this molecule: using recombinant protein expression technology to obtain a pure fraction of acyl-MGDG (details in chapter 6), and by stressing a leaf to create this molecule naturally, to study a route of obtaining acyl-MGDG that industry might take (details in chapter 7). Chocolate is the product in which this new emulsifier would be used, so it was decided to use cocoa leaves as a starting point for this analysis.

6. Acyl-MGDG as an alternative for PGPR

6.1. Introduction

In Chapter 5, different analytical techniques were employed to ascertain the structure of PGPR and compare this knowledge with the differences in functionality found in Chapter 4. The aim was to find the structural characteristics of the best performing PGPR that could be leveraged when proposing a natural alternative. The results of these analyses showed that the PGPRs molecular weight ranges were remarkably similar to each other. However, a larger polyglycerol chain and an increase in the prevalence of hydroxyl groups at the end of the polyricinoleate chains seemed to reduce the effectiveness of the PGPR at reducing yield stress. Calculations on theoretical PGPR molecules, using the regulatory ranges for hydroxyl, iodine and saponification values (CEC, 2001, FCC, 2016, JECFA, 1992), indicated that the molecules must have a high number of fatty acids in the molecule compared to the glycerol – around three to four fatty acids for every one glycerol. In addition, almost all PGPR molecules must have at least two glycerols in their polyglycerol chain; however, the longer the polyglycerol chain, the more flexibility there is with the theoretical length and configuration of the polyricinoleate chain within the ranges given. However, the regulations restrict the length of the polyglycerol chain from two to four glycerols for 75% of PGPR molecules within the product.

In this Chapter, the natural alternative proposed at the end of Chapter 5 is discussed and then created using recombinant protein expression technology. As stated in objective six, the impact of the assay mixture on the yield stress of the 65% (wt) sugar-in-oil chocolate model was to be assessed to compare its functionality with that of PGPR. As previously reported, the choice taken was to focus on the head group portion of the molecule: to find a lipid where the acyl groups were separated further

than customarily found, for example, in a diacylglycerol, to mimic the polyglycerol backbone.

Phospholipids, often under the name lecithin, are used widely in food products because of their surface-active properties. The action of lecithin is described in more detail in section 1.4.4, and although it shows good viscosity reducing properties, it does not affect the yield stress of chocolate as much as PGPR. The surfactant properties of galactolipids found in leaves, such as spinach, have been evaluated (Mohamad et al., 2020). While galactolipids do show surface-active properties, the extent to which they affected the yield stress was difficult to assess given the volume fraction of the chocolate model used in this research (up to 50% (wt)). From the literature, it appears that no one has assessed the surfactant properties of a lipid molecule that has an extended space between acyl groups to see if it may mimic the significant yield stress lowering effect of PGPR.

Such a molecule exists in nature in the form of acylated monogalactosyl diacylglycerol (acyl-MGDG), an MGDG molecule with an additional acyl group at the C-6 position of the galactose ring (Heinz, 1967a). Figure 6.1 shows the chemical structures of phosphatidylcholine, one of the phospholipids found in lecithin; monogalactosyl diacylglycerol (MGDG); and acyl-MGDG, with the structures in red highlighting the structure between acyl groups.
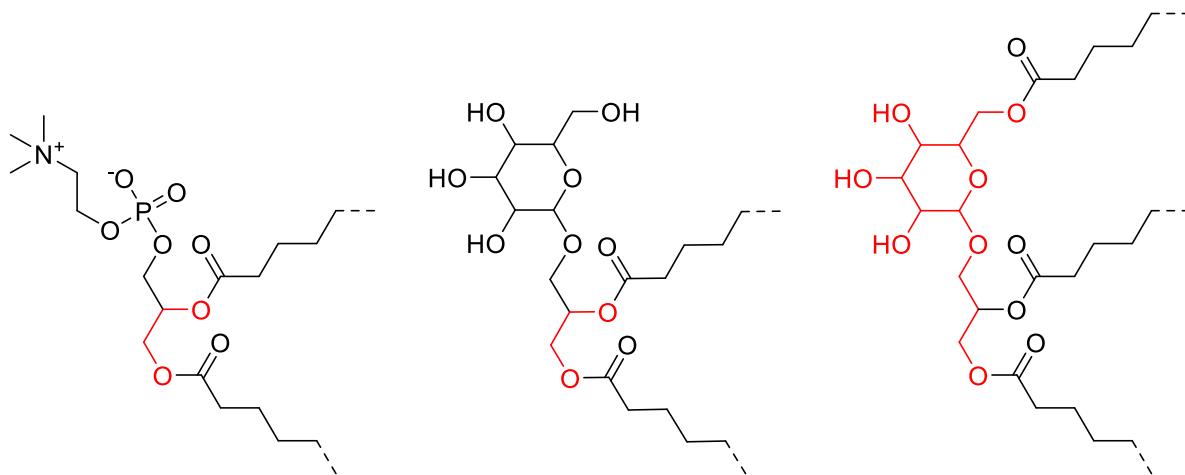
Figure 6.1: Chemical structures of phosphatidylcholine, MGDG and acyl-MGDG, in this order, with the part of the glycerol structure between acyl groups, highlighted in red. In this illustration, the fatty acid chains are shortened, and dotted lines show where the molecule would continue.

Acyl-MGDG was initially found in spinach (*Spinacia oleracea*) (Heinz, 1967a) but has since been found in daffodil (*Narcissus pseudonarcissus*) (Liedvogel and Kleinig, 1977), *Arabidopsis thaliana* (Andersson et al., 2006, Ibrahim et al., 2011), wheat (*Triticum aestivum*) and tomato leaves (*Solanum lycopersicum*) (Vu et al., 2014a) and tobacco leaves (*Nicotiana tabacum*) (Matsuzaki et al., 2014). Nilsson et al. (2015) suggest that acyl-MGDG is, in fact, ubiquitous in the plant kingdom after leaves have undergone stress. Using freeze-thaw methods, they tested the leaves of plants from species representing the major groups of land plants and detected acyl-MGDG in all these plants to a lesser or greater extent. They went on to isolate the enzyme responsible for this acylation process. As this enzyme belongs to a family of phospholipases, they proposed the name Acylated Galactolipid Associated Phospholipase 1 (AGAP-1), and it appeared to be located in the cytosol or the outer envelope membrane of the epidermal cells. It was not found in the chloroplasts, so Nilsson et al. (2015) postulate that the enzyme only has access to the galactolipids when the chloroplasts are broken during trauma. They also discuss what the purpose of acyl-MGDG might be to the cell. They found evidence suggesting that head group

acylated galactolipids were produced to protect the leaf rather than, as had been postulated previously, stimulating cell death, and propose that the process might sequester de-esterified polyunsaturated fatty acids to avoid the effects of lipid stress (Farmer and Mueller, 2013). AGAP-1 transfers an acyl group, often from a DGDG molecule, to the galactose head group of an MGDG (Heinz, 1967b, Vu et al., 2014a). Acyl-MGDG fits the criteria for a molecule with acyl groups spaced out further than a standard glycolipid.

Acyl-MGDG cannot be bought commercially at present, so two methods to obtain acyl-MGDG were devised. In this chapter, the AGAP-1 enzyme was grown from a vector kindly supplied by the team who first identified it (Nilsson et al., 2015). Recombinant protein expression technology was used to create an amount of AGAP-1 protein grown up in *Escherichia coli*, which was then purified and used in an assay with MGDG and DGDG bought as purified powder samples. The presence of acyl-MGDG in the resultant assay material was verified through high-performance thin-layer chromatography (HPTLC). Once the presence of acyl-MGDG was established, the assay material was assessed for yield stress reducing properties using the chocolate model. In chapter 7, cocoa leaves were stressed using different methods to see if acylated MGDG might be induced to occur naturally, and the lipid extract from these leaves was applied to the chocolate model for the assessment of yield stress reducing properties. These results are discussed in chapter 7.

6.2.   Materials and Methods:

6.2.1.   Reagents and materials

Details of the sugar, sunflower oil and treatment of both for the chocolate model are detailed in sections 2.2 and 2.4. The PGPRs are detailed in section 2.1.

All reagents for the recombinant protein expression, purification and assay were purchased from Sigma-Aldrich unless otherwise stated in the text.

Sterilisation of all media and flasks was performed with a square chamber autoclave (Astell Scientific Ltd, UK). The cultures were grown in 2 L Erlenmeyer flasks, in a shaking incubator, at 37 °C (Certomat BS-1 shaking incubator, Sartorius Stedim Biotech, Germany) and 16 °C after induction (Floor Shaker Incubator MaxQ 5000, model 4358, Thermo Scientific, USA). All cells were harvested using a J2-21 Centrifuge (Beckman, IN, US) and a Jouan CR3i multifunction Centrifuge (Thermo Fisher Scientific, Massachusetts, USA). Soniprep 150 Plus (MSE, UK) was used to lyse the cells.

6.2.2. *E. coli* growth, maintenance and media

6.2.2.1. E. coli strains

Commercially available chemically competent *E. coli* BL21-CodonPlus (DE3)-RP cells were obtained from Agilent Technology (Texas, USA)

6.2.2.2. Growth media

Media components were sterilised by autoclaving (121 °C, 20 min, 15 psi), or where stated in the text by filtration (0.2 µm filter), and mixed when cooled. Media solutions were prepared in deionised water (dH$_2$O) and stored at room temperature unless otherwise stated. Where solid medium was required, agar (15 g/L) was added to the medium prior to autoclaving. Where applicable, antibiotics were added to growth media. Chloramphenicol solutions (25 mg/mL) were prepared in ethanol (100 %) and Carbenicillin (100 mg/mL) solutions were filter sterilised and stored at -20 °C. All cultivations were performed at 37 °C, 200 rpm and in baffled Erlenmeyer flasks, with nominal volumes five times the culture volume unless otherwise stated.

For general growth and maintenance, *E. coli* strains were cultured in lysogeny broth (LB), as per the Miller formulation, which contained peptone (Oxoid, UK) (10 g/L), yeast extract (Oxiod, UK) (5 g/L) and sodium chloride (10 g/L). Strains were routinely stored as glycerol stocks at -80 °C. Glycerol stocks were prepared by picking a single colony of the strain and culturing it overnight in LB (100 mL) supplemented with carbenicillin (100 µg/mL) and chloramphenicol (25 µg/mL). Cultures were harvested by centrifugation (5000 rpm, 10 min, 4 °C) and resuspended in LB supplemented with glycerol (20 % (vol)) to an OD_{600} of 6.

6.2.2.3. Expression strains

Plasmid pGS21α containing the gene sequence encoding AGAP-1 cloned between the *Hin*dIII and *Bam*HI restriction sites was obtained from the Department of Biological and Environmental Sciences, University of Gothenburg, Sweden and was named pGS21α::agap1. Commercially available chemically competent *E. coli* BL21-CodonPlus(DE3)-RP cells (Agilent Technology (Texas, USA)) were transformed with the pGS21α::agap1 plasmid, according to the manufacturer's instructions. Briefly, the plasmid (3 µL) was added to the cells (100 µL) and incubated on ice for 30 min. A heat shock of 42 °C for 10 seconds was applied, and the cells were cooled on ice for 5 min. SOC medium (950 µL) was then added, and the cells were shaken for 60 min at 37 °C. The resulting culture was plated and incubated overnight at 37 °C.

Transformed cells were plated on LB agar supplemented with carbenicillin 100 µg/mL and chloramphenicol 25 µg/mL and incubated for 16 h at 37 °C. A single colony was used to inoculate 30 mL of LB medium supplemented with carbenicillin (100 µg/mL) and chloramphenicol (25 µg/mL), and this was cultured for seven hours at 37 °C, 180 rpm before cryostocks of cells were prepared and stored at -80 °C in 20% glycerol. To confirm the presence of the correct plasmid in the production strain, the plasmid

was extracted and sequenced with T7 promoter forward and reverse primers. The protein and gene sequences for AGAP-1 can be found in Appendix 3.

6.2.2.4. Protein expression

A colony of *E. coli* BL21-CodonPlus(DE3)-RP transformed with pGS21α::agap1 was used to inoculate LB medium (30 mL) containing carbenicillin (100 µg/mL) and chloramphenicol (25 µg/mL), in a conical flask (250 mL volume). The resulting culture was incubated for 16 h at 37 °C and 180 rpm. This starter culture (2.5 mL) was used to inoculate fresh LB medium (500 mL) supplemented with carbenicillin and chloramphenicol in an Erlenmeyer flask (total volume 2 L). The resulting cultures were incubated at 37 °C and 200 rpm until the OD_{600} reached 0.8 (Jenway 7315 Spectrophotometer, Bibby Scientific Ltd, UK). Protein expression was induced by the addition of 1 mL isopropyl β-D-1-thiogalactopyranoside (IPTG; 0.5 M stock in deionised water sterilised by filtration). Induced cultures were incubated for 24 h at 16 °C and 150 rpm, after which the cells were harvested by centrifugation (6000 rpm – 4354 x *g*, 10 min, 4 °C) and stored at -20 °C.

6.2.3. Protein purification

Cell pellets were resuspended in buffer A (Table 6.1) at 4 °C supplemented with cOmplete™ protease inhibitor cocktail (1 tablet/10 mL) at a volume of 5 mL per gram wet cell mass. The suspension was sonicated on ice (Soniprep 150 Plus, MSE, UK) for 2 minutes (22 microns amplitude) in 20 s bursts, with intervals for cooling. Cell debris was removed by centrifugation at 3200 rpm – 1,500 x g at 4 °C for 30 minutes.

TALON® Superflow™ histidine-tagged protein purification resin (GE Healthcare Biosciences AB, Sweden) was added to a 2 mL Eppendorf tube and washed with buffer A, which was then removed once the resin had settled. The cell-free extract was added to the Eppendorf tube, then incubated for 40 mins on a rocking roller bed

at room temperature. The supernatant was removed, the resin was resuspended in buffer A and then transferred to a 1 mL gravity-flow column. The resin was washed three times using 8-10 bed volumes of buffer A. The fourth wash was done with buffer C. The polyhistidine-tagged protein was removed from the column by washing five times with five bed volumes of buffer D.

Table 6.1: Buffers used in section 6.2.3 and 6.2.4.

Buffer A	50 mM Tris HCl, 300 mM NaCl, pH 8.0
Buffer B	50 mM Tris HCl, 300 mM NaCl, pH 7.5
Buffer C	50 mM Tris HCl, 300 mM NaCl, pH 8.0, 15 mM Imidazole
Buffer D	50 mM Tris HCl, 300 mM NaCl, pH 8.0, 150 mM Imidazole

6.2.4.   Protein analysis

6.2.4.1. SDS-PAGE

Protein samples from each stage (10 µL) were mixed with 10 µL of Laemmli sample buffer (20:1 2x Laemmli Sample Buffer with 50 µL 2-mercaptoethanol, both Bio-Rad, USA) and incubated at 90 °C for 5 minutes. Precision Plus Protein™ Dual Color Standards (Bio-Rad Laboratories Inc, USA) 10 to 250 kDa (2.5 µL) and samples (5-9 µL) were loaded onto a 4-15%, 15-well comb, Mini-PROTEAN® TGX™ Gel (Bio-Rad Laboratories Inc, USA) and ran at 200 V, 400 mA for 35 min, with Tris-Glycine-SDS running buffer (10x TGS (TrisGlycine/SDS buffer), Bio-Rad Laboratories Inc, USA, diluted 1:10 with distilled water).

The gel was stained with Coomassie staining solution (Coomassie Brilliant Blue R-250 (161-0436), Bio-Rad). After rinsing the gel, the destaining solution (Coomassie Brilliant Blue R-250 Destaining Solution, Bio-Rad) was applied.

Imidazole was removed from the purified protein solution using dialysis cassettes, allowing the removal of buffer salts and small contaminants less than 10 kDa (Slide-a-Lyzer® Dialysis cassette G2 10,000 MWCO, 3 mL capacity, Thermo Scientific, USA). The eluate from the column showing the highest protein concentration, as found using the SDS-PAGE analysis, were combined and pipetted into a dialysis cassette. The cassette was floated in a beaker of buffer B, which was gently stirred for 48 hours. The volume of the sample was approximately 3 mL, and the beaker contained 500 mL of buffer B. This buffer was replaced with fresh buffer three times during the dialysis period to allow the complete exchange into buffer B. It was essential to remove all the imidazole from the sample to prevent the enzyme from being inactivated; this had been a problem in the past (personal communication with Mats Andersson, named correspondent (Nilsson et al., 2015)). The dialysed mixture was then carefully removed from the cassette, and the protein concentration was measured using a protein assay (Pierce™ BCA Protein Assay Kit, ThermoScientific, USA).

6.2.4.2. Protein concentration by Bicinchoninic acid assay

A set of bovine serum albumin (BSA) standards was prepared via serial dilution in a range of 25 to 2000 µg/mL. The working reagent was prepared by mixing 50 mL of reagent A (sodium carbonate, sodium bicarbonate, bicinchoninic acid and sodium tartrate in 0.1M sodium hydroxide) with 1 mL of reagent B (contains 4% cupric sulfate). Assays were performed in test tubes in triplicate by mixing 2 mL working reagent with 100 µL of either AGAP-1 sample, BSA standard, or sample buffer (control). Samples and standards were incubated at 37 °C for 30 minutes and then cooled to room temperature before measuring the absorbance at 562 nm (Genesys 10S VIS spectrophotometer, ThermoScientific, USA). The absorbances of BSA standards were used to generate a standard curve from which the protein concentration in the sample was estimated.

6.2.5. Creating acyl-MGDG

The assay method was based on that devised by Nilsson et al. (2015). However, the assay method, as stated, used only 2 or 4 µg of MGDG, so the concentration of resultant acyl-MGDG would be very low. The original assay method was merely aimed at proving that the enzyme was responsible for the acylation reaction. Therefore, the concentration of the substrates and the enzyme were increased to encourage a higher final concentration of acyl-MGDG. The published method also only used MGDG as the substrate for the assay as the goal of this research was to assess the types of fatty acids preferentially used by the AGAP-1 enzyme (C-18 or C-16). Research has shown that the enzyme appears to favour the removal of an acyl group from DGDG and its addition to the galactose ring of MGDG (Heinz, 1967b, Vu et al., 2014a), so the substrate was changed to a mixture of MGDG and DGDG, to encourage maximum yield.

The paper did not state the concentration of enzyme required to convert the MGDG to acyl-MGDG, so an initial assay plan was devised to assess this question. MGDG and DGDG were dissolved in 10 mM sodium deoxycholate buffer (pH 7.2) and thoroughly mixed with a vortex mixer. A volume containing 10 µg each dissolved galactolipid (MGDG 1 mg/mL and DGDG 1 mg/mL) was added to five 2 mL microtubes. Volumes of dissolved AGAP-1 were added to the substrates as shown in Table 6.2, and finally, 80 µL of 250 mM Sodium acetate buffer (pH 5.3) was added. All were mixed with gentle agitation (70 rpm in an orbital incubator (SI500 Stuart®, Bibby Scientific Ltd, UK)) at 22 °C for 60 mins. The reaction was terminated by adding 200 µL ice-cold butanol:methanol (3:1 (vol)) supplemented with 0.05% (w/v) butylated hydroxytoluene, and the tube left on ice for 30 mins. 200 µL heptane:ethyl acetate (3:1 (vol)) and 200 µL of 5% (vol) acetic acid in water were then added, and the tube was capped and inverted several times. The upper (organic) phase was removed and set aside. 300 µL heptane:ethyl acetate (3:1 (vol)) was then added, mixed by

inversion, the top phase removed, and the organic phases pooled. The assay mixture was then dried under nitrogen and frozen at -80 °C until use. This lipid extraction method is very similar to the BUME method (Löfgren et al., 2012)

Table 6.2: Amounts of MGDG, DGDG, enzyme and sodium deoxycholate added to each microtube to detect the optimal concentration for the production of acyl-MGDG. The enzyme was produced but then had to be used in a hurry due to circumstances beyond our control, and there was no time for statistical study design. Therefore, the enzymes were used in the assay at increasing volumes chosen on the day based on the amount of enzyme available.

Sample name	MGDG (µg)	DGDG (µg)	Enzyme (µg)	Sodium deoxycholate (µg)
S. Deoxy	0	0	0	0.25
Assay 0 enzyme	10	10	0	0.25
Assay 50 µL enzume	10	10	12.85	0.25
Assay 75 µL enzyme	10	10	19.28	0.25
Assay 100 µL enzyme	10	10	25.70	0.25
Assay 150 µL enzyme	10	10	38.55	0.25

Once the optimal enzyme concentration was evaluated, a second assay set was devised using a new batch of enzyme produced using the glycerol stock created in section 6.2.2.3 and following the processes described in sections 6.2.2.4, 6.2.3 and 6.2.4. This time, a volume containing 50 µg of each dissolved galactolipid (MGDG 1 mg/mL and DGDG 5 mg/mL) was added to a 2 mL microtube. The correct amount of enzyme was applied based on the results of the first assay set.

It was noted that sodium deoxycholate was extracted with the galactolipids in the assay. It has also been shown that MGDG and DGDG have surface-active properties (Mohamad et al., 2020). Therefore, several control samples were also created to ensure that the rheology results were not influenced by the inclusion of sodium deoxycholate or any unreacted galactolipids, see Table 6.3.

Table 6.3: A summary of the samples made to control for variation due to different components in the assay mixture. The amounts used in the assay are included in the row "Acyl-MGDG". An additional sample with 1 mg each MGDG and DGDG was included as a higher lipid content sample.

Sample name	MGDG (µg)	DGDG (µg)	Enzyme (µg)	Sodium deoxycholate (µg)	Lipid content (mg)
MGDG/DGDG 50 µg	50	50	0	0	0.1
S. Deoxy	0	0	0	0.25	0
S. Deoxy + MGDG/DGDG	50	50	0	0.25	0.1
Acyl-MGDG	50	50	TBC	0.25	0.1
MGDG/DGDG 1 mg	1000	1000	0	0	2

6.2.6. High-performance thin-layer chromatography (HPTLC) analysis

The assay samples were run on the HPTLC after dissolving them in chloroform:methanol (2:1 (vol)) to verify the presence of acyl-MGDG. Appropriate amounts of the samples were spotted onto a plate with standards to show the locations of MGDG and DGDG. The plates were run in a mobile phase of chloroform:methanol:water (47.5:12:1.25 (vol)) and developed using the thymol solution or copper acetate-phosphoric acid solution as the derivitizer solvent. The general method for using the HPTLC is given in section 2.9.

The samples were then transferred to 5 mL bijou bottles and stored at -80 °C until use.

6.2.7. Chocolate model preparation

The chocolate model to assess the yield stress reducing performance of the novel emulsifier was similar to the method reported in section 2.5 that was applied to the commercial PGPR samples but scaled down to allow for a smaller quantity of lipid. As a first step, the assay mixture, which had been dried in a glass bijou bottle, was

dissolved in 4.5 mL of treated sunflower oil (see section 2.2 for method) using an orbital incubator (SI500 Stuart®, Bibby Scientific Ltd, UK) at 30 rpm for one hour at 22 ± 1 °C. The oil and assay mixture was transferred to a 50 mL centrifuge tube, and the same amount of dried icing sugar was added to it. The suspension was mixed using a high shear mixer (UltraTurrax, Yellowline DI 25 basic, IKA-WERKE GmbH & Co, Germany) using a dispersing tool (S25N-10G, IKA-Werke GmbH & Co, Germany) for 4 min at 22000 rpm in an ice bath. The rotational speed was calculated to replicate the tangential velocity imposed on the sample by the Silverson in the original method; see section 2.5. The samples were then placed in an incubator (MIR-153, SANYO Electric Co., Ltd, Japan) in the dark for 39 hours (± 2 hr) at 20 °C. The solid phase fraction was adjusted to 65% (wt) by centrifuging the tubes for 10 min at 3836 g and 10 °C (Jouan CR31 multifunction centrifuge, Thermo Electron Corporation) and removing the appropriate amount of supernatant using a Gilson pipette (23% of the total sample weight). The sample was manually stirred with a spatula and left to stand for at least 10 min before briefly stirring again and applying it to the rheometer.

Two batches for each sample type were made.

6.2.8. Rheological Measurements

The rheological protocol was modified due to the small sample volume and the fact that the unidirectional shear method led to the top plate spinning through at shear stress values that were not much higher than the yield value. Hence, the oscillatory protocol alone, introduced in 2.6.2, was applied in combination with parallel plate geometry. An oscillatory pre-shear step (100 Pa, 10 rad/s, 2 min) was applied to eradicate sample history. A serrated parallel plate geometry of 25 mm diameter and 1 mm gap height fitted to a Peltier heating system was used, as shown in Figure 6.2.

This time, the rheometer used was an Anton Paar Physica MCR 302 Rheometer (Graz, Austria) as the laboratory had had an upgrade. The results were found to be equivalent to the MCR 301 rheometer used in chapter 4.

From each sample made in section 6.2.7, three replicates were measured.

Figure 6.2: Serrated parallel-plate geometry used in the small sample volume protocol. These were: Top plate (PP25/P2: Diameter 24.948 mm) with a serrated bottom plate (SS/P2) attached to a Tru-Gap Peltier plate (P-PTD200/62/TG).

6.2.9. Statistical analysis of data

The results shown in Figure 6.9 were analysed using a one-way analysis of variance (ANOVA) followed by a Tukey post-hoc using SPSS (Statistics v 27, IBM Corp, USA). The significance level was set at $p < 0.05$, and one measurement of three true replicates was used in the mean value of each data point.

6.3. Results and discussion

6.3.1. Recombinant protein expression and purification

The recombinant AGAP-1 protein containing a polyhistidine tag was successfully expressed in *E. coli* and purified by affinity chromatography. The expressed protein was present primarily in the insoluble fraction, as was found by Nilsson et al. (2015). However, enough soluble protein was present to perform the enzymatic assay, as can

be seen in the soluble phase lane in Figure 6.3. Purification of the soluble fraction by immobilised nickel affinity chromatography produced 1.5 mL of protein solution at 0.257 mg/mL concentration, which was exchanged and stored in Tris-HCl buffer pH 7.5. The total yield of purified protein was 0.4 mg protein / 500 mL culture.

As the amount of enzyme needed per weight of substrate was not yet known, an assay of increasing amounts of the enzyme was performed as described in 6.2.5. The assay mixtures from the samples were applied to a TLC plate using the methods described in sections 2.9 and 6.2.6. Figure 6.4 and Figure 6.5 show the results of this experiment. As increasing concentrations of the enzyme are used, so the bands for MGDG and DGDG fade, and a strong band appears, which has a higher retention time than MGDG. Literature shows us that this band is likely to be acyl-MGDG (Heinz et al., 1974). Other, more faint bands on the plate can be identified as acyl-diacylglycerol monoacylglycerol and diacylglycerol monoacylglycerol (Heinz et al., 1974, Sahaka et al., 2021). For reference, a graphic showing the locations of galactolipids found in spinach homogenates by Heinz et al. (1974) is shown in Figure 6.6.

It can be seen, from this experiment, that the lowest concentration of protein that gives conversion to a new band was 19.28 µg. This means that the amount of protein required for the second assay, which would be applied to the chocolate model, was approximately the total amount of MGDG+DGDG together by weight. It must be noted here that the protein comprised not only AGAP-1 enzyme after the purification process; Figure 6.3 shows there are also proteins at about 30, 23, 17 and 12 kDa. Nilsson et al. (2015) also found these impurities and performed size exclusion chromatography to remove them. However, this further purification step was not performed in this project, and enzymic activity occurred irrespective of the impurities.

The second round of recombination and purification produced 2.4 mL of protein solution at 0.208 mg/mL concentration, and the total yield of purified protein was 0.5

mg protein / 500 mL culture. This protein concentration was used to calculate the amount to be added to the MGDG and DGDG substrates. Each galactolipid was applied to the assay at 50 µg of each substrate, and 100 µg of protein was added.

The assay was performed, and the resultant assay mixture was dried and dissolved in chloroform:methanol (2:1). This was run on HPTLC as described in sections 2.9 and 6.2.6. This plate was derivatised using copper acetate/phosphoric acid solution rather than thymol, highlighting acyl groups rather than galactose ring. Figure 6.7 shows that the plate revealed two new bands and the disappearance of MGDG and DGDG bands. These bands could be acyl-MGDG and acyl-MGMG if Figure 6.4 is referenced. These two molecules had three or two acyl chains, respectively, to create copper salts in the reaction with the derivitizer for subsequent charring. The band for DGMG was not observed on this second plate. If thymol only visualised the band of DGMG with its two galactose rings, there were probably not enough acyl groups in the band present for the copper acetate/phosphoric acid to detect it. The identity of the bands on the plates have been achieved by comparing the retention times of the molecules to TLC plates in literature. To positively confirm the identity of the two bands in future, LC-MS/MS should be applied (Nilsson et al., 2014).

The initial paper was reviewed to get an idea of the yield of acyl-MGDG that might have been obtained. Nilsson et al. (2015) used 2 or 4 µL of spinach MGDG with fatty acids of either 16:3 and 18:3 or both fatty acids of 18:3. They discovered that both types of MGDG were equally good substrates for head group acylation but that the enzyme strongly preferred to transfer the 18:3 fatty acid. They obtained a maximum of 250-300 pmol acyl-MGDG from their assay. A rough calculation of the yield can be made if a presumption that the assay used 2 µg MGDG, and this MGDG was an equal mixture of 18:3,16:3-MGDG (MW 747.01 g/mol) and 18:3,18:3-MGDG (MW 775.06 g/mol), so the average molecular weight was around 761 g/mol. Therefore, in 2 µg of the substrate, there would have been 2,628 pmol MGDG, so the yield of acyl-MGDG

was approximately 10%. Unfortunately, the amount of enzyme applied in this assay is not identified in the paper, so it is not clear if the low yield of acyl-MGDG is due to the inefficiency of the enzyme or the concentration of enzyme used.

Although the identity of the molecules within the assay mixture could not be confirmed using LS-MS/MS, due to time constraints, successful production of acyl-MGDG was assumed based on the HPTLC results. Its functionality was evaluated by adding the mixture to the chocolate model and assessing its effect on the rheology.
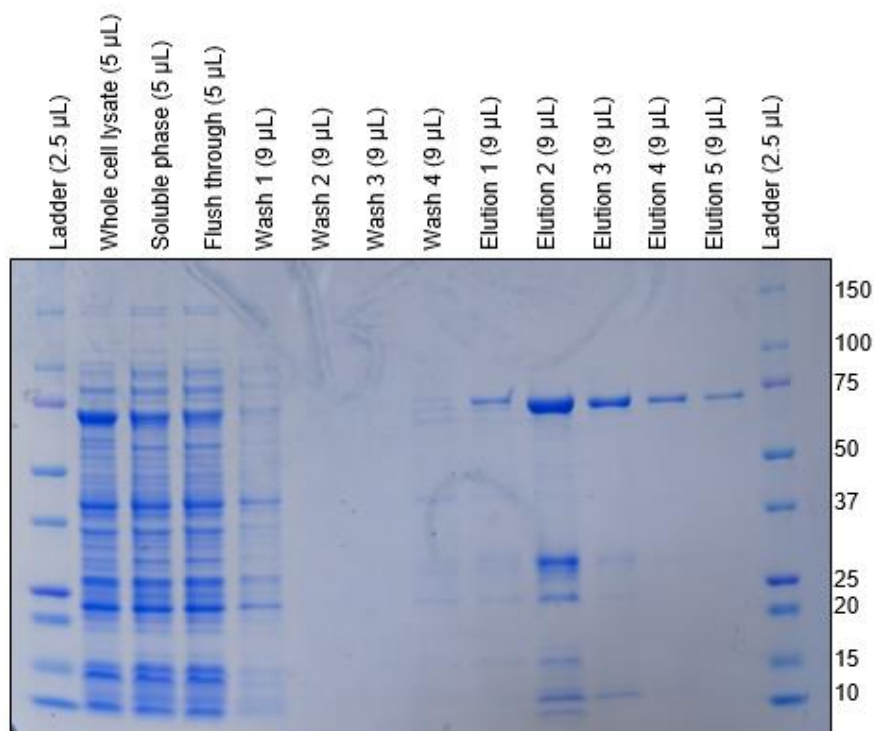
Figure 6.3: SDS gel of the fractions from the purification process. The sample descriptors are shown at the top of the gel, and the molecular weight scale is shown in kDa on the right side of the gel. The AGAP-1 enzyme appears at about 73 kDa (note, the expected mass is around 77 kDa). The elution samples show some additional protein impurities at 30, 23, 17 and 12 kDa.
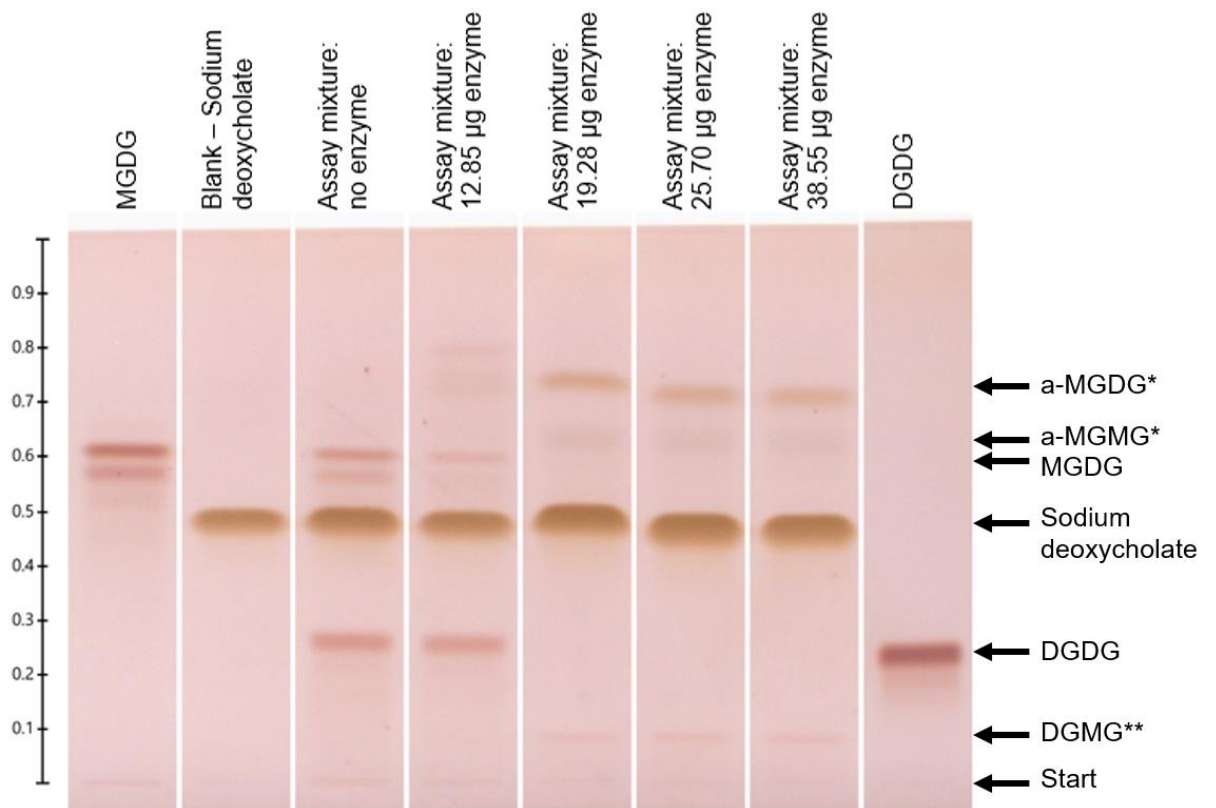
*Figure 6.4: Initial analysis using the enzyme at different concentrations in the assay. In this experiment, 10 µg each of MGDG and DGDG were used as the substrate. The assay using 19.28 µg of the enzyme is the lowest concentration where the MGDG and DGDG are no longer present, and there is the appearance of a new band with a retention time of 0.72 mm. The thymol derivatizer solution was used. Band identifiers indicated by * refer to (Heinz et al., 1974), see also Figure 6.6, and ** refers to (Sahaka et al., 2021). Graphic generated using the CAMAG software.*
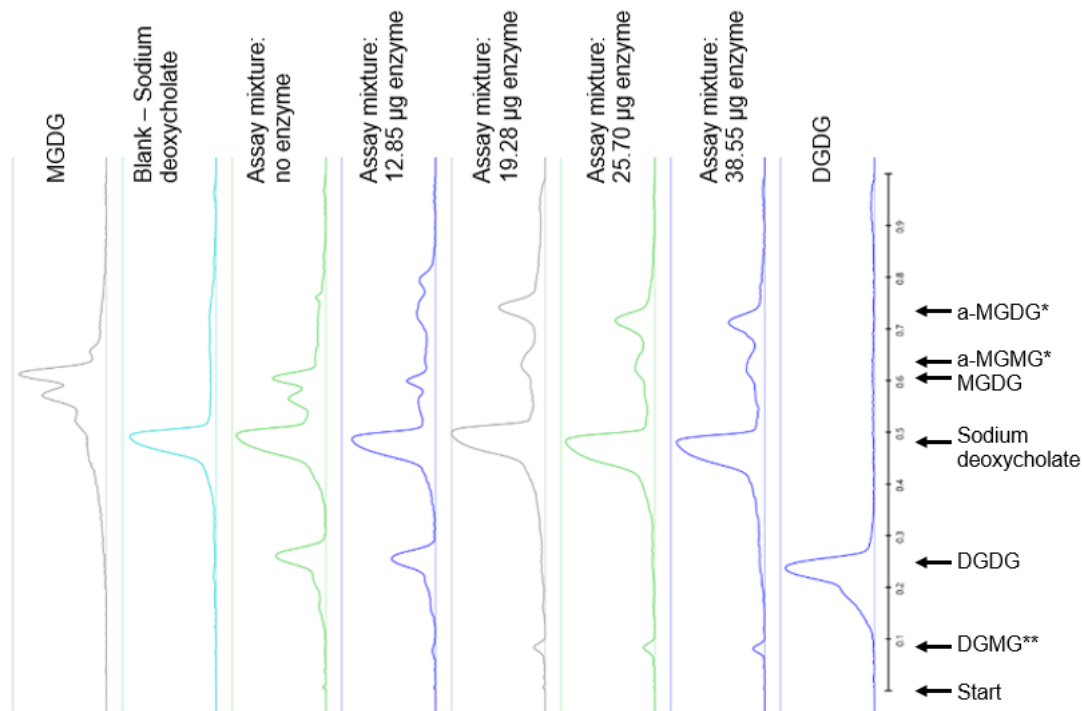
Figure 6.5: Profile of lanes shown in Figure 6.4, which aids the identification of some of the smaller peaks. Graphic generated using the CAMAG software.
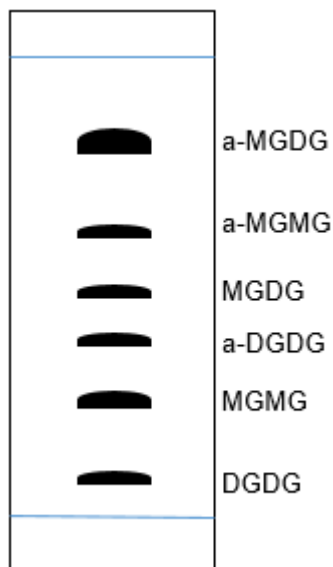

Figure 6.6: Graphic based on the TLC plate generated by Heinz et al. (1974) showing the galactolipid bands found in homogenised spinach.
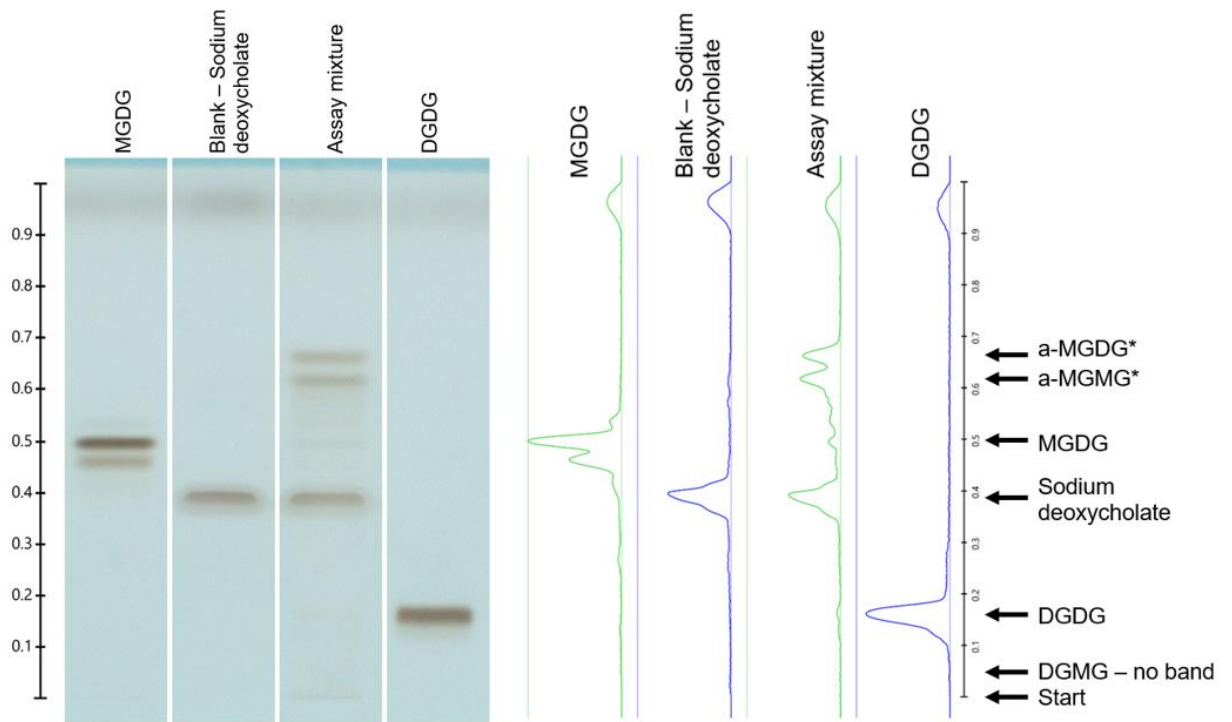
Figure 6.7: HPTLC lanes on the plate (right) and the profiles (left) showing bands of MGDG (lane 1), blank showing band for sodium deoxycholate (lane 2), the assay mixture (lane 3) and DGDG (lane 4). It appears that the assay has converted the MGDG and DGDG into acyl-MGDG and acyl-MGMG, but no DGMG can be seen, perhaps because of the derivatizer solution used. Graphic generated using the CAMAG software.

6.3.2. The effect of Acyl-MGDG on the rheology of the chocolate model

Figure 6.8 shows the results of the oscillatory measurements conducted on the 65% (wt) sugar-in-oil suspensions containing the assay mixtures outlined in Table 6.3, plus two samples with no addition and one with 0.3% Palsgaard 4150. The data was displayed as the elastic modulus (G') versus shear stress. Only one batch was shown for all sample types except for the samples with no addition and the assay mixture samples; the batches from the other sample types produced very similar data. There was a period where the elastic modulus was high at low shear stresses for all samples – a linear viscoelastic region (LVR). For all samples except the one with PGPR, this region was at about 200 kPa. For most samples, this continues until a shear stress of

about 8-9 Pa, where a sharp decrease in the elastic modulus to about 10-15 Pa occurs. This sharp reduction in the elastic modulus was where the yield stress occurs, and the sample starts to flow, behaving in a more viscous manner. The curves for most of these samples overlap, but one of the assay mixtures ends the LVR at a slightly lower shear stress, approximately 6 Pa. The sample containing 1 mg each of MGDG and DGDG showed an LVR at an elastic modulus of around 80 kPa and started the decrease in G' at an even lower shear stress – around 4 Pa. The error bars were most pronounced at the very low shear stress region, where seemingly random measurement artefacts occur, and also at the sharp reduction in elastic modulus where some replicates yielded slightly earlier or later than others. These differences were not unexpected given that sugar aggregates have already been implied in samples with no emulsifier during the chocolate model method development, section 3.3.2. These aggregates could cause differences in the yield stress between batches and could also be the cause of the variable elastic modulus measurements found at low shear stress.

The sample containing PGPR shows a similarly structured curve, but the initial high stage elastic modulus was much lower at around 300 Pa, with the reduction decreasing to a storage modulus under 1 Pa at a shear stress of around 4-5 Pa. The error bars for this sample were generally small. However, they become slightly larger around the lowest G' point, probably because the logarithmic scale shows up the differences more at such low values.

The yield stress for the curve was calculated using the method developed by Walls et al. (2003) and is described in more detail in section 2.6.2. The results were shown in Figure 6.9, and statistically significant differences were identified by letters. The sample with only sodium deoxycholate did not increase or decrease the yield stress, which means that the inclusion of this substance at this concentration does not need to be considered during the analysis of the yield stress measurements for the other

samples. It appears that one of the batches of assay mixture did decrease the yield stress slightly, but the other showed no significant difference. This could mean that either acyl-MGDG does not reduce the yield stress or that there was insufficient lipid to make a noticeable difference. Table 6.4 shows the approximate amount of lipids in each sample. By relating Figure 6.9 and Table 6.4, it can be seen that when a higher concentration of lipids was used in the sugar-in-oil suspension, there was a higher yield stress reduction, meaning that it may simply be that there was not enough acyl-MGDG adsorbing to the surface of the sugar crystals to make a difference to the yield stress.
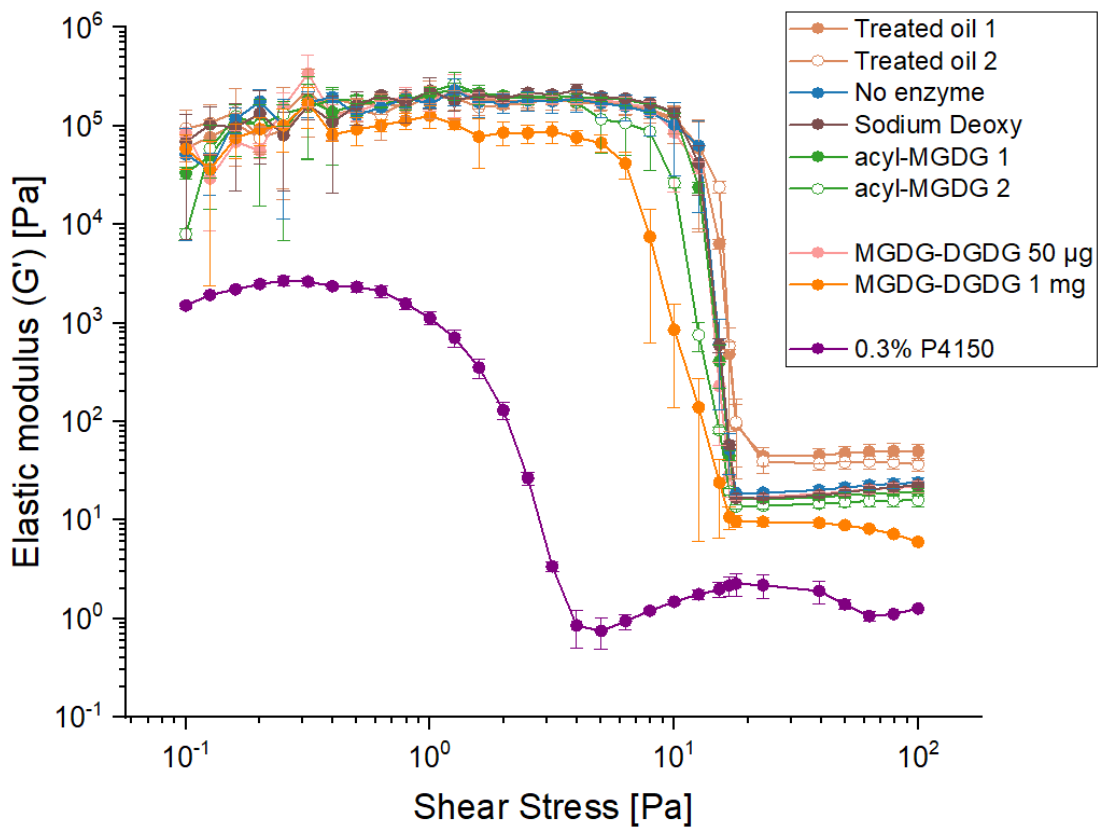

Figure 6.8: Storage modulus as a function of shear stress showing the sample yielding shown as the G' falls. All samples were analysed in triplicate. Only one batch is shown for most samples, but both batches of 65 % sugar-in-oil without emulsifier and assay mixture replicates are shown.
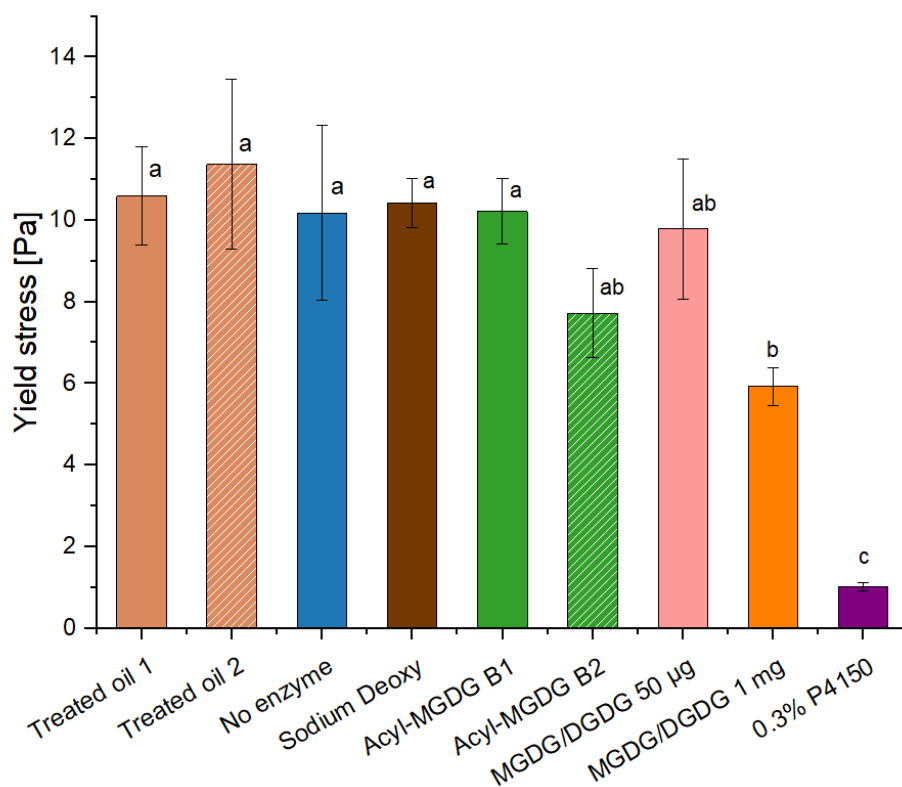
Figure 6.9: Yield stress values of samples shown in Figure 6.8 using the method devised by Walls et al. (2003). The error bars show the range of yield stress values found for each batch (3 data points). As found in section 3.3.2, where there is no emulsifier present, the sugar crystals aggregate, causing a larger variation in the yield stress to be measured. The amount of lipid available to adsorb to the sugar is low for most of these samples; see Table 6.4.

Table 6.4: Approximate amount of lipid in each sample. For PGPR, this assumes the whole sample was lipid. For the "acyl-MGDG" assay mixture, the lipid was assumed to be the weight of the MGDG and DGDG applied to the assay – some will be converted to acyl-MGDG and some acyl-MGMG and possibly DGMG; however, it was assumed that no lipid was degraded.

Sample	Lipid (mg)
MGDG/DGDG 50 µg	0.1
S. Deoxy	0
S. Deoxy + MGDG/DGDG	0.1
Acyl-MGDG	0.1
MGDG/DGDG 1 mg	2
0.3% PGPR	43

6.4. Conclusions

The AGAP-1 protein obtained from the laboratory in Sweden altered the MGDG and DGDG substrates to create at least two new, different molecules. These were shown to be present in the assay mixture using HPTLC, and literature was referred to confirm that the position of these bands on the plate matches bands apportioned to be acyl-MGDG and acyl-MGMG (Heinz et al., 1974). The band thought to be acyl-MGDG was not confirmed as such using LC-MS/MS (Nilsson et al., 2014) due to time constraints, but this should be included in the future. When added to the chocolate model, the assay mixture did not significantly alter the yield stress, which could mean that acyl-MGDG has no yield stress lowering functionality in the chocolate model or that the concentration was too low. Due to time constraints, it was not possible to reproduce these experiments at higher enzyme and substrate concentrations; however, it would be interesting to perform the assay again but using 1 mg MGDG, 1 mg DGDG and 2 mg of enzyme, amounts which are viable using the method outlined in section 6.2.5. The results could be compared to the yield stress reduction caused by the sample with 1 mg of each of the galactolipids to see how the alteration to acyl-MGDG affects the yield stress compared to unaltered galactolipids. It would also be interesting to compare with a sample containing 1 g of PGPR; after all, one of the aims of this PhD is to replace PGPR with a natural alternative.

Even though the initial experiment with acyl-MGDG did not show a conclusive result for its yield stress reducing power, it was decided to proceed to the leaf experiments regardless, as more acyl-MGDG may be available using this second method. Having created the acyl-MGDG by recombinant protein expression technology and applied it to the chocolate model, the final area to pursue was to stress cocoa leaves to cause them to synthesise acyl-MGDG *in vivo*. Therefore, in chapter 7 of this thesis, cocoa leaves, obtained from the Eden Project, UK, had different stress protocols applied

upon them to see which would create acyl-MGDG. The most promising leaf lipids were applied to the chocolate model to assess their rheology altering capabilities.

7. Assessing cocoa leaves as a natural source of yield stress reducing surfactants

7.1. Introduction

This Chapter describes the final stage in the journey to seek a natural alternative to polyglycerol polyricinoleate (PGPR). In Chapter 6, acylated monogalactosyl diacylglycerol (acyl-MGDG) was produced in the laboratory. The enzyme responsible for the addition of an acyl group to the head group of monogalactosyl diacylglycerol (MGDG) in nature, Acylated Galactolipid Associated Phospholipase 1 (AGAP-1), was donated by the research group who first identified it (Nilsson et al., 2015). Recombinant protein expression technology was used to create an amount of AGAP-1 protein using *Escherichia coli*. The protein was purified and used in an assay with commercially available monogalactosyl diacylglycerol (MGDG) and digalactosyl diacylglycerol (DGDG) to create acyl-MGDG. The resulting assay mixture was presumed to contain acyl-MGDG based on analysis with high-performance thin-layer chromatography (HPTLC) when the results were compared with the literature. LC-MS/MS could have been applied to confirm the results, but this was not done due to time constraints. This assay mixture was applied to the chocolate model, and its effect on the sample's yield stress was assessed. Unfortunately, the rheological assessment of one batch of assay mix showed only a very small change from the baseline sample that contained no additional lipid. The other batch of assay mixture showed no change. As discussed in chapter 6, it could be that acyl-MGDG does not work as an emulsifier, or it was not at a sufficient concentration to affect the yield stress of the chocolate model. In this Chapter, the alternative route of obtaining acyl-MGDG from leaves was applied.

As early as the 1960s, it was shown that leaves perform head-group acylation of MGDG under stress (Heinz, 1967b). It was then established that this acylation was

achieved by an enzyme removing an acyl group from DGDG and adding it to the C6 of the galactose moiety of MGDG (Heinz, 1967a). Acyl-MGDG was found initially following the homogenisation of spinach leaves in buffer, but other types of stresses applied to leaves have been shown to have the same effect. These methods include mechanical wounding of *Arabidopsis thaliana* leaves on the plant (Ibrahim et al., 2011), freeze-thaw treatment of discs of *A. thaliana* leaves (Nilsson et al., 2012), infection with bacteria and freezing treatment of whole plants of *A. thaliana*, and mechanical wounding of *A. thaliana*, wheat (*Triticum aestivum*) and tomato (*Solanum lycopersicum*) plants (Vu et al., 2014a). In this chapter, these methods have been adapted and implemented to stimulate the cocoa leaf to create acyl-MGDG: mechanically wounding the cocoa leaves on the plant, or once they were in the laboratory, and freeze-thaw treatment. Senescent leaves and leaves with evidence of damage from *Nipaecoccus nipea* (coconut mealybug) were also collected for analysis.

The methods used to stress the leaves are listed, with their references, in 7.2.2. The lipids from these different leaf samples were then assessed using HPTLC, and a candidate that appeared to have accumulated acyl-MGDG was applied to the chocolate model and compared with lipids from an unstressed leaf. The rheology of the chocolate models was measured, and the impact that the lipids have on the yield stress compared to that of PGPR itself; completing objective six of this PhD.

7.2. Materials and methods

7.2.1. Cocoa leaves

Cocoa leaves were generously donated by the Eden Project, Cornwall, UK. The *Theobroma cacao* plants were given to the Eden Project by Reading University, but unfortunately, records of their specific cultivar details were lost before donation.

Leaves at different life stages: young pink leaves, healthy mature green leaves, and senescent leaves were collected, along with those to be stressed. One tree had many fresh, green leaves that were similar in size and age: these were collected in number to be stressed or used as control leaves. Another batch of cocoa leaves was generously donated by Nestlé cocoa farms in Côte d'Ivoire. Figure 7.1 shows photos of some of the leaves used in this project.

The leaves from the Eden Project were harvested, wiped with 75% ethanol and dried before removing them from the Biome. They were placed between the pages of an A4 spiral-bound notebook and wrapped in plastic film wrap before transporting them back to the laboratory in a car, which took around 7.5 hours. The use of the notebook and film wrap for the leaves from the Eden Project was to mimic that experienced by the leaves sent by a courier from Côte d'Ivoire to the UK. It took approximately six days between harvesting the leaves and their delivery to the laboratories; however, this time delay was not replicated for the Eden Project leaves.

Other materials used in this research are listed in sections 2.1, 2.2 and 2.4.

Figure 7.1: Photos of some of the cocoa leaves used in this analysis. From top left and clockwise: the tree where control and stressed leaves were collected showing the green leaves and some young pink leaves collected from the Eden Project Biome; leaves received from Côte d'Ivoire (note some leaf senescence during transport); leaves impacted by coconut mealybug from the Eden Project (from now on referred to has 'insect' leaves); a single mature leaf from the Eden Project.

7.2.2. Cocoa leaf stress methods

The control cocoa leaves were stressed in the following ways:

7.2.2.1. Freeze trauma.

Approximately 9 hours after harvesting, the leaves were frozen at -20 °C for 2 hours and then left to defrost for 24 hours (similar to the method used by Vu et al. (2014a)) before freezing at -80 °C and processing as described in section 7.2.3.

7.2.2.2. *Mechanical trauma 'perforated'.*

The leaves were cleaned whilst still on the tree with 75% ethanol and dried. They were wounded by rolling a Mikki™ hard pin slicker brush (A good hair day, Mikki, UK) over selected leaves backed with a wad of blue-roll (similar to the method used by Bailey et al. (2005)). Figure 7.2 shows the leaves following harvesting showing the perforations.

7.2.2.3. *Mechanical trauma 'crushed'.*

Approximately 7.5 hours after harvesting, the leaves were firmly rolled over for 10 seconds using a rolling pin and then left for 30 minutes. This method is similar to the method used by Ibrahim et al. (2011); however, the rolling pin was used for crushing the leaves, rather than squeezing with forceps, as the cocoa leaves are more rigid than *A. thaliana* leaves.

Figure 7.2: Cocoa leaves showing perforations.

7.2.3. Cocoa leaf processing

As soon as possible after harvesting (8 hours ± 30 mins) or after applying the stress as described in 7.2.2, the leaf's stem was cut off at the leaf; the remaining leaf was weighed and then frozen at -80 °C for 24 hours. The leaves were then put into a freeze-dryer (Super Modulyo, Edwards, UK) for five days. Once the freeze-drying process was complete, the leaves were ground (Cookworks Coffee and Herb Grinder, made in China, imported by Argos, UK, 150 W) and sieved to ensure the particles were <125 μm. Lipid extraction was performed as described in section 7.2.5. A summary of the leaves' appearance while fresh and freeze-dried, and as a lipid extract made from 0.1 g of freeze-dried, ground leaf dissolved in 1 mL acetone, is shown in Figure 7.3 and Figure 7.4.
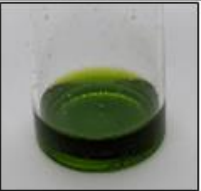
Sample type	Fresh leaf	Freeze dried	Lipid extract
Côte d'Ivoire			
Eden "control"			
Eden "young"			
Eden "mature"			

Figure 7.3: Unstressed leaves as fresh and freeze-dried leaves, and the lipid extract dissolved in 1 mL acetone.
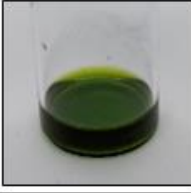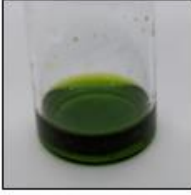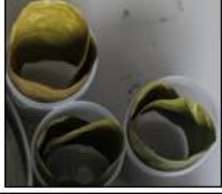
Sample type	Fresh leaf	Freeze dried	Lipid extract
Eden "Punctured"			
Eden "Crushed"			
Eden "Insect"			
Eden "Freeze-thaw"			
Eden "Dead"			

Figure 7.4: Stressed leaves as fresh and freeze-dried leaves, and the lipid extract dissolved in 1 mL acetone.

7.2.4. The moisture content of leaves

In order to assess the moisture content of the cocoa leaves, the Côte d'Ivoire leaves were dried until a constant weight was achieved in an oven at 105 °C (Memmert, LN110, Germany). The leaves from the Eden Project were weighed when received in the lab and again once freeze-drying was complete.

7.2.5. Lipid extraction

Lipid extraction was performed based on the method of Folch et al. (1957), modified by Bligh and Dyer (1959). Accurately weighed freeze-dried, ground leaf (approx. 0.1 g for lipid analysis or 0.3 g for NMR analysis or to assess for yield stress reduction capabilities) was mixed with chloroform:methanol (2:1 (vol)) (1.2 mL (0.1 g leaf) or 2.4 mL (0.3 g leaf)). This was vortexed for 1 min, then 0.9% sodium chloride solution (1 mL (0.1 g leaf) or 3 mL (0.3 g leaf)). was added, and the sample vortexed again for 1 min. The samples were centrifuged (1,750 g, 30 mins, 4 °C, Jouan CR3i multifunction Centrifuge, Thermo Fisher Scientific, USA), and the lowest phase was removed using a glass pipette into a fresh centrifuge tube. Further chloroform:methanol (1.2 mL/2.4 mL) was added, then the tube was vortexed, centrifuged, and, again, the lowest phase was removed. This step was repeated to obtain three volumes of lipid extract, which were pooled in the fresh centrifuge tube. This tube was then centrifuged (1,750 g, 10 mins, 4 °C). The lowest phase was filtered (0.45 µm polytetrafluoroethylene (PTFE) filter membrane, Whatman syringe filter, GE Healthcare Life Scientific) and dried under nitrogen.

7.2.6. Lipid analysis

The lipid samples were analysed using high-performance thin-layer chromatography (HPTLC), after being dissolved in chloroform:methanol (2:1 vol), to separate and reveal the lipids within the leaves and assess the presence of acyl-MGDG. Appropriate amounts of the samples were spotted onto a plate, and MGDG and DGDG standards were either used as locators or at different concentrations to create a standard concentration curve. The plates were run in a mobile phase of chloroform:methanol:water (47.5:12:1.25 (vol)) and visualised using thymol solution as the derivatizer solvent to highlight the galactolipids and acyl-MGDG. The thymol solution stains the galactose moiety of the galactolipids. The presence of free fatty

acids and non-polar lipids within the leaves was measured by separating the leaf lipid samples using heptane:diethyl ether:acetic acid (55:45:1 (vol)) and derivatising using copper acetate/phosphoric acid solution.

The general method for HPTLC is given in section 2.9. More information about the derivatising solutions is given in section 1.5.5.1.

7.2.7. Rheological analysis using the chocolate model

The yield stress reducing properties of the lipid extract most likely to contain acyl-MGDG and the unstressed, control leaf were evaluated using the chocolate model system described in chapter 6.2.7. The chocolate model samples contained the dried lipid extracts, which had been dissolved in the treated sunflower oil before mixing with the sugar. These samples were then measured on the rheometer using the 25mm serrated parallel plates geometry used in section 6.2.8. These samples' yield stress and viscosity were such that the original rheological protocol method could be applied as described in section 2.6.1; however, the ramp protocol was started at 100 Pa rather than 1000 Pa.

7.2.8. Fatty acid analysis

The lipids' fatty acid profile was evaluated to more fully understand the changes that the leaves had undergone after stress or during ageing. The method described in sections 2.10 and 2.11 were employed: transmethylation with trimethyl sulfonium hydroxide solution (TMSH) followed by GC-MS analysis.

7.2.9. Chlorophyll and Carotenoids analysis

The chlorophyll *a*, chlorophyll *b* and total carotenoids levels were analysed following a spectrophotometric method (Lichtenthaler and Buschmann, 2001). The lipids are

dried and dissolved in 1 mL acetone and then vortex mixed for 1 minute. All samples except the 'dead' leaf lipid were further diluted to 1:100. In a quartz cuvette, the absorbance of the samples was measured at 662 nm, 645 nm and 470 nm on a UV VIS spectrophotometer (Genesis 10S VIS, Thermo Fisher, US). The density of light absorbance is then converted to a concentration of each type of molecule using the following calculations (Lichtenthaler and Buschmann, 2001):

$$Chlorophyll\ a\ (\mu g\ ml^{-1}) = (11.24\ \times A_{661.6}) - (2.04\ \times A_{644.8})$$

$$Chlorophyll\ b\ (\mu g\ ml^{-1}) = (20.13\ \times A_{644.8}) - (4.19\ \times A_{661.6})$$

$$Total\ carotenoids\ (\mu g\ ml^{-1}) = \frac{(1000\ \times A_{470}) - (1.90\ \times Chl\ a\ ) - (63.14\ \times Chl\ b)}{214}$$

These values were converted to mg/g whole leaf (dry weight) using the following calculation:

$$Concentration\ (mg\ g^{-1}) = \frac{concentration\ (\mu g\ ml^{-1})}{(DW\ leaf\ (mg)) \div (volume\ of\ acetone\ (ml))}$$

Additional tests were run to evaluate the qualitative presence of two carotenoids: lutein and β-carotene. Three separate samples of ground, freeze-dried leaves, each weighing between 0.1000 and 0.1099 g, underwent lipid extraction following the method described in section 7.2.5. These were then applied to the HPTLC plates (10 μL) and were run against lutein and β-carotene standards as location markers. The plate was developed using heptane:diethyl ether:acetic acid (55:45:1 (vol)) twice, with a drying step of 10 minutes in between. Once dried, the plate was photographed without derivatisation.

7.2.10. Statistical analysis of data

The results shown in Figure 7.8, Figure 7.9, Figure 7.10 and Figure 7.14 were analysed using a one-way analysis of variance (ANOVA) followed by a Tukey post-

hoc using SPSS (Statistics v 27, IBM Corp, USA). The significance level was set at p < 0.05, and one measurement of each of three true replicates was used in the mean value of each data point.

7.3.   Results and discussion

7.3.1.   Analysis for the presence of acyl-MGDG

Lanes from the HPTLC plates are shown in Figure 7.5. The two galactolipids verified using standards are indicated with arrows – MGDG with the grey arrow and DGDG with the black arrow. The first eight lanes in this figure are the lipids from different leaf samples. The final lane shows the results from the assay mixture formed when the AGAP-1 enzyme was added to purified MGDG and DGDG as described in section 6.2.6. Different volumes of the leaf lipids were applied to the plate in an attempt to create a band density that fell between the ranges of MGDG and DGDG standards that made a standard curve, see section 7.3.3.3. In this figure, most leaf lipid extract samples were applied at a volume of 15 µL; however, the 'crushed' and 'young' were applied at 20 µL, and 'frozen' was applied at 25 µL. As varying amounts of lipid was extracted, the calculated mass of lipid applied to each lane is included in Figure 7.5.

In Figure 7.6, an attempt is made to identify the bands which appear on the plate. Given that the thymol derivatisation solution visualises the position of molecules with galactose rings, the bands which are red must have this moiety. Literature is used to propose the molecules found in the leaves on the HPTLC plate.

The acyl-MGDG band is visually present in many of the lipid samples shown in Figure 7.5, as shown by a red band around 10 mm above the MGDG band. The treatments inflicted on the leaves do not seem to have created an increased acyl-MGDG band

compared to the untreated leaves. It could be that chlorophyll breakdown started as soon as the leaves were harvested from the tree, and during transit from the tree to the laboratory, the enzymes had started working to sequester free fatty acids onto the headgroups of MGDG as proposed in the literature (Nilsson et al., 2015). This was a surprising finding as it was supposed that the chloroplasts would need to be physically broken before the enzyme, located in the cytosol, would come into contact with the galactolipids (Nilsson et al., 2015).

It had previously been planned that one of the treated leaves would be chosen to be added to the chocolate model for the measurement of yield stress. As the freeze-thaw treatment is most often used in literature to create acyl-MGDG, it was decided that the freeze-thaw leaf sample should be put forward alongside the control leaf. Lipids were extracted from 0.3 g of ground dried control leaf (two replicates) and 0.25 g ground dried freeze-thaw treated leaf (one replicate). This was the entirety of the remaining freeze-thaw treated leaf sample.
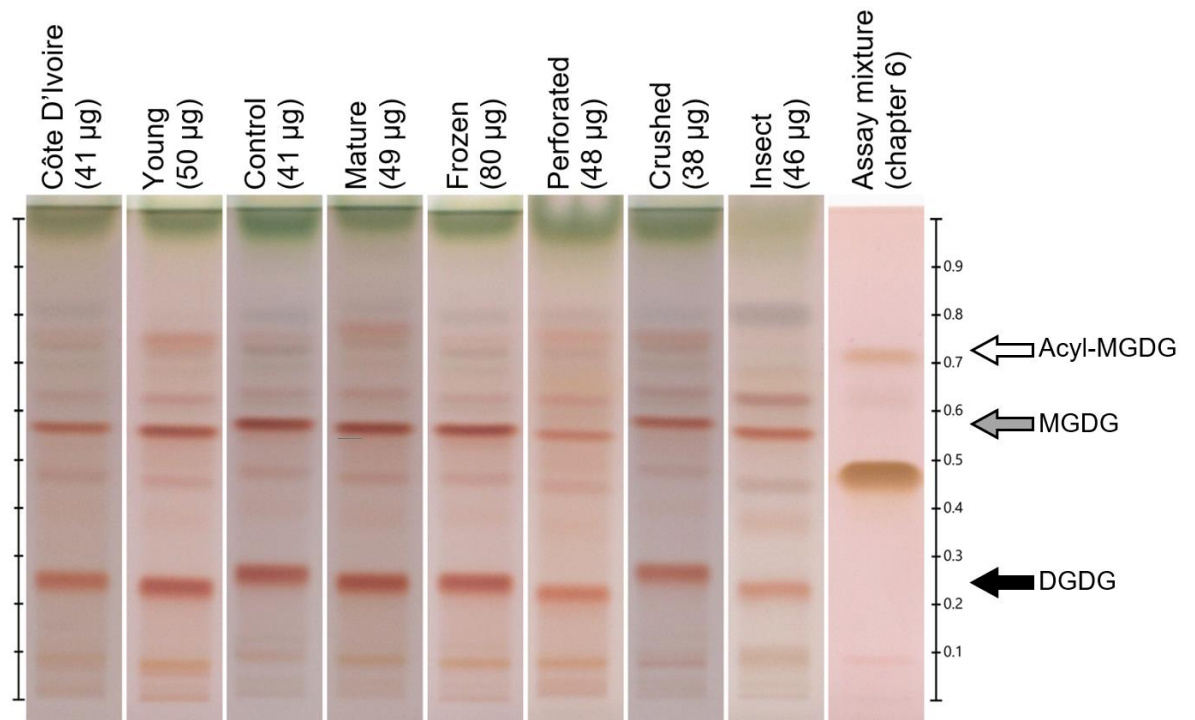
Figure 7.5: Lanes from the HPTLC analysis of the leaf types and the acyl-MGDG created and discussed in chapter 6. The acyl-MGDG thought to be found in the assay is highlighted with a white arrow and coincide with the red bands with the highest retention times in the leaf samples. The MGDG retention time is indicated with a grey arrow, and the DGDG bands are indicated with the black arrow. The large brown band found on the acyl-MGDG sample is sodium deoxycholate.
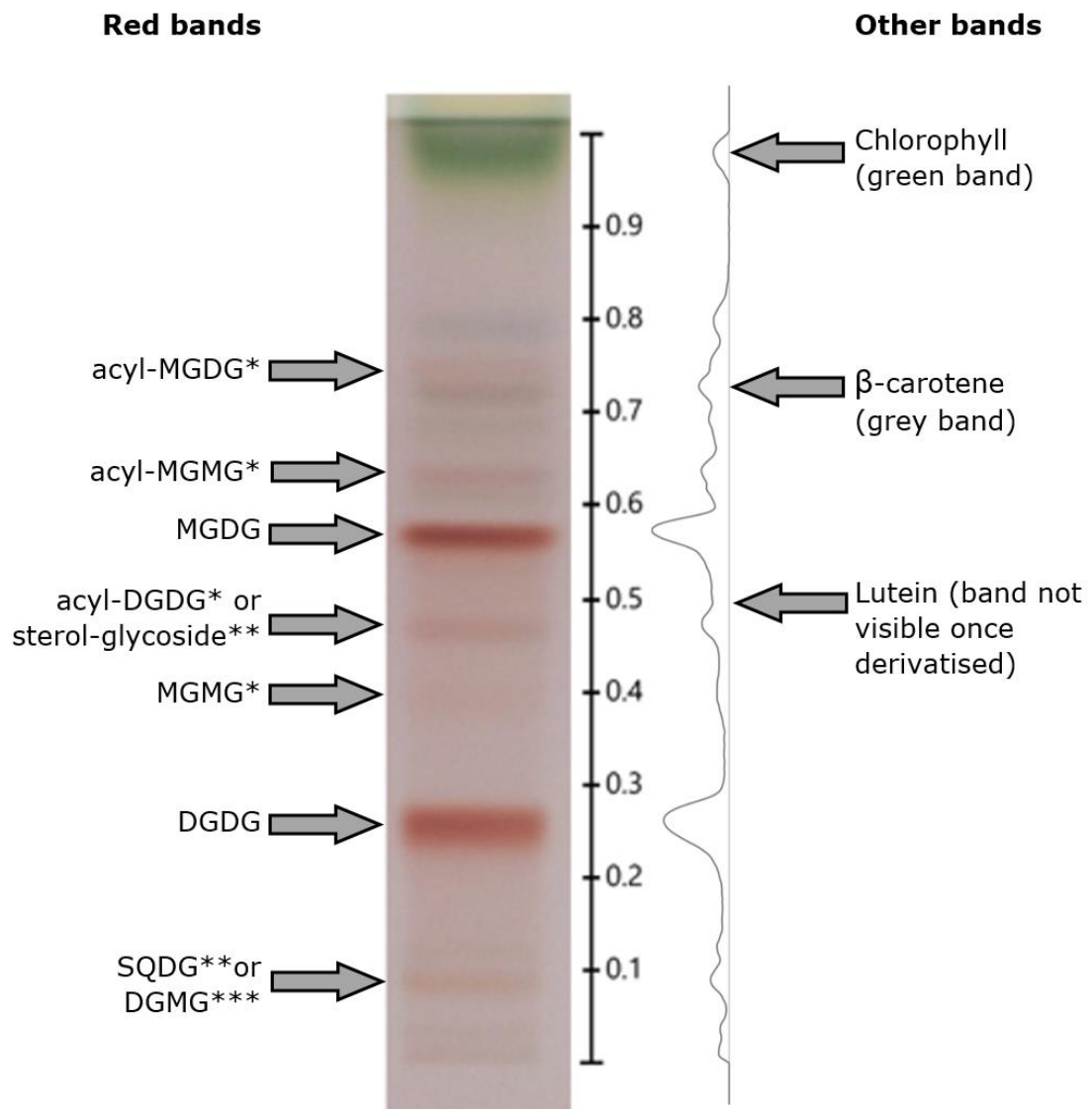
Figure 7.6: One HPTLC plate lane showing the lipids found in the "control" leaf with definite or putative identification. The density profile has been included in this figure to aid the visualisation of the bands. Standards have confirmed the bands where the labels are without asterisks. Labels identified with * refer to lipids identified by Heinz et al. (1974). Lipids identified with ** are identified by Christie et al. (2010b), and lipids identified with *** were identified by Sahaka et al. (2021) and are alternative possibilities. The red bands identify lipids containing a galactose group due to the reaction taking place with the thymol solution (Sahaka et al., 2021).

197

7.3.2. Rheological analysis

The results of the rheological analysis are shown in Figure 7.7. The curves show the same profile as seen with the rheology of the PGPR samples measured in section 4.3.1, with a low viscosity Newtonian stage at high shear stress, followed by a sharp increase in viscosity at the yield stress point. The viscosity of the frozen leaf samples is never reduced as much as the PGPR at the higher shear stress rates, and the yield stress is higher than that shown by PGPR. However, the addition of control leaf lipids (around 20 mg in the 9 mL suspension) to the chocolate model system does show a similar yield stress reduction as the addition of 0.3% Grindsted 90 PGPR (around 43 mg in the 9 mL suspension). Figure 7.8 shows that the yield stress of the chocolate model sample with the cocoa leaf lipids is not significantly different from either Grindsted 90 or Palsgaard 4150 when they were used at 0.3% of the total weight of the chocolate model. The objective of this chapter was to see if acyl-MGDG, created by causing stress to a leaf, could reduce the yield stress of a chocolate model in a similar way to PGPR and become a natural alternative. The lipids from a cocoa leaf, which had been stored for eight hours after harvesting, might be a good natural alternative to PGPR.

It is unfortunate that the amount of lipids extracted from the different leaf samples varies. It would be revealing to further explore this by repeating the experiment with the same amount of lipid in each sample to understand more fully if the difference in the yield stress reduction caused by the control lipid than the freeze-thaw lipids was due to concentration rather than content. However, 0.25 g freeze-thaw treated leaves yielded 14 mg of lipid, which means the lipid content was 0.1% (wt) of the chocolate model, and 0.3 g control leaves yielded 20 mg of lipid, meaning the lipid content was around 0.15 % (wt) of the chocolate model. When spinach leaf lipids were added to a 50% (wt) sugar in oil suspension at a concentration of 0.1 % and 0.3%, the yield stress did not alter substantially – approximately 2.4 Pa (0.1%) compared to 2.2 Pa (0.3%)

(Mohamad et al., 2020). These results were obtained using a less concentrated suspension than the 65% sugar-in-oil suspension on this project. Nevertheless, it is possible that the difference in the concentration of the lipids here is not crucial: it is the lipid content within the sample that makes the difference. Therefore, detailed analysis and discussion of the lipids in the leaves follow.
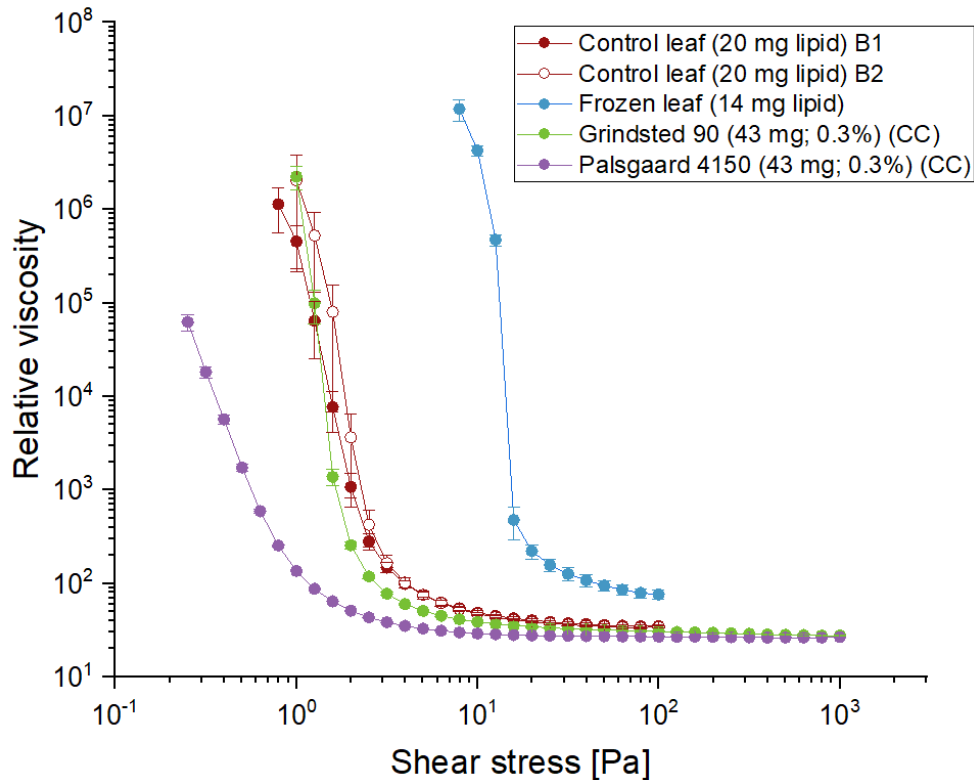
Figure 7.7: Relative viscosity against shear stress of the 65% dried icing sugar in treated sunflower oil with leaf lipid, evaluated using a 25 mm parallel plate. The 0.3% PGPR samples are shown, which were run previously (see section 4.3.1) using a concentric cylinder. The PGPR results have been included as a comparison. The presumed amount of lipid within each sample is shown in the legend. Even though the error bars look large for the control leaf samples, they do not translate to too much variation in the calculated Herschel Bulkley yield stress, see Figure 7.8. Each point reflects the mean value of three replicates, the error bars represent one standard deviation.
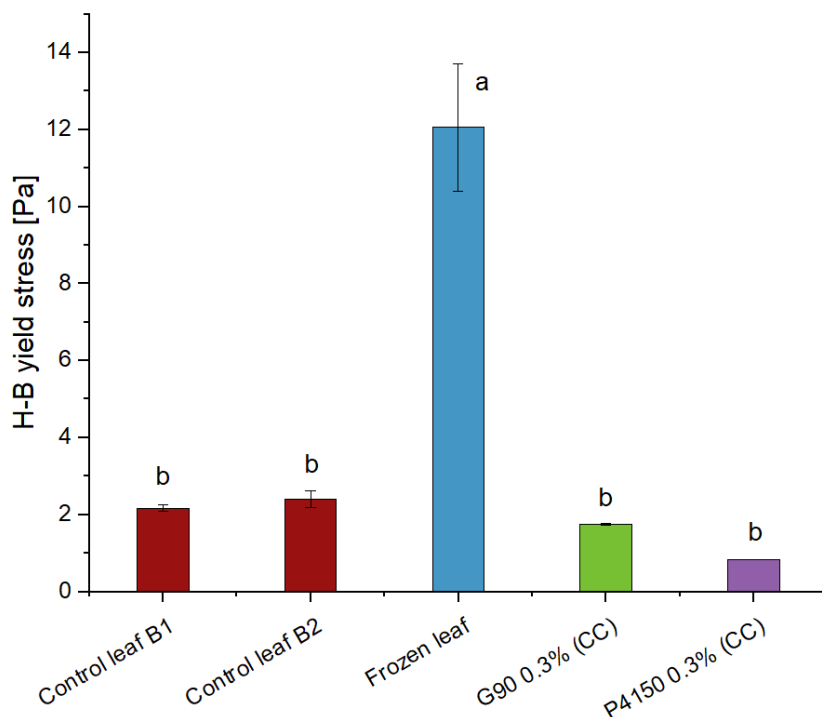
Figure 7.8: The calculated Herschel Bulkley yield stress values for the viscosity curve data shown in Figure 7.7. The bars represent three replicates from one batch produced. The error bars are the standard deviation. The data were analysed using ANOVA followed by a Tukey post-hoc test. The letters represent significantly different results a>b.

7.3.3.   Composition of cocoa leaves

The leaves' lipid composition must first be analysed so that an understanding can be made as to the importance of each of the cocoa leaf lipids in reducing the yield stress. Consideration should also be made into any nutritional benefits to be gained from these lipids, or indeed, any antinutrients within the leaf.

7.3.3.1.   Moisture content

Figure 7.9 shows the moisture content of some of the cocoa leaves used in this analysis. The moisture content of spinach, kale and nettle leaves was assessed in literature was found to be 94%, 82%, and 77%, respectively (Gedi et al., 2017). Avocado leaves have been found to have a moisture content of 60-70%, depending

on their variety (Haas, 1938). Leaves from the creosote bush have been shown to vary their moisture content depending on the water available to the plant, the species, the leaf's position on the stem compared to other leaves, and the time of day (Runyon, 1936). This is why, in reported analysis, it is recommended that the lipid values are related to the dry weight of the leaf rather than fresh leaf, as this should make any values quoted relatable to other work. In Figure 7.9, it can be seen that the water content also varies by the age of the leaf; the 'young' leaf was soft and had a higher moisture content than the 'control' green leaf, which in turn had a higher moisture content than the tougher mature leaf. While the leaf is young, the cells are still expanding, and so the cuticle which protects the leaf in maturity is not formed; merely a thin layer of wax is present. As the leaf develops, the cuticle expands and incorporates globules of wax, cutin, polysaccharides, hemicellulose and cellulose (Ohlrogge et al., 2015). This increase in the rigid structure of the leaf may be the reason for the apparent decrease in moisture content compared to the dry weight of the leaf.

A one-way ANOVA was conducted to identify what significant differences were present between the moisture content of each type of leaves. The 'young' and 'control' leaves were excluded from the analysis as there was only one replicate. As assessed by Levene's test for equality of variances, there was homogeneity of variances ($F = 2.828$, $p = 0.065$). There was a significant difference between the groups as determined by the one-way ANOVA ($F = 171.752$, $p < 0.001$). A Tukey post-hoc test revealed where the differences lie and are illustrated by letters in Figure 7.9.
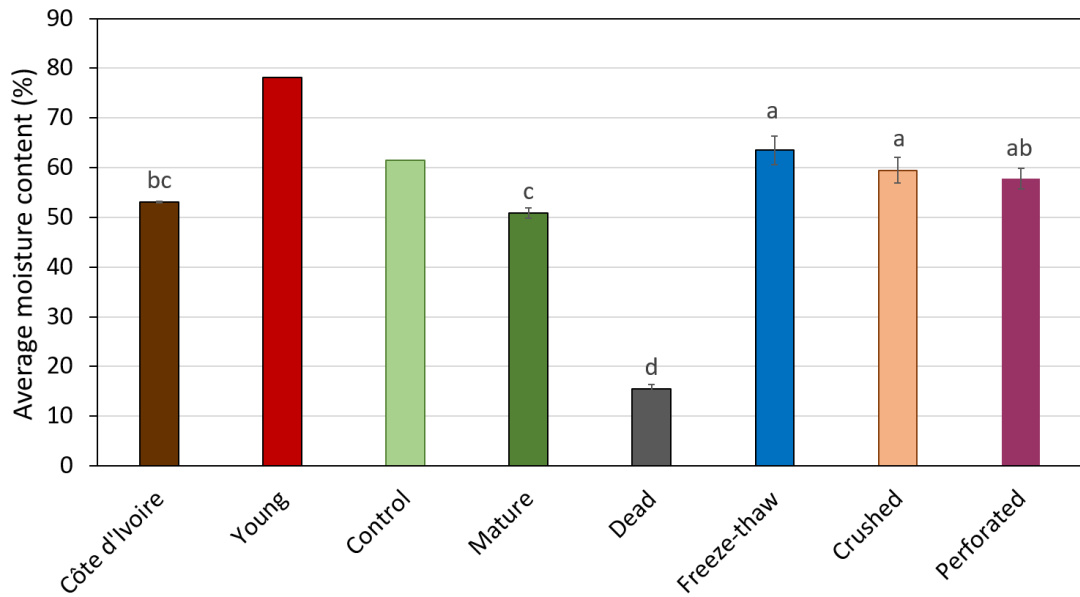
Figure 7.9: Average moisture content of the different types of leaves. 'Insect' leaves were omitted due to a weighing error. Each bar represents the results of three separate samples, except for 'young' and 'control', where all the leaves were dried together, so only one result is obtained. For all other leaf types, the bar is the standard deviation of these results. The data (except for 'young' and 'control') were compared using ANOVA, followed by a Tukey post-hoc test to evaluate the differences. The letters represent significantly different results a>b>c>d.

7.3.3.2. Lipid extract

About 6% of the dry weight of leaves are lipids, and around 53% of the lipids are glycerolipids which are generally found in the membrane structural components, for example, the chloroplasts (Ohlrogge et al., 2015).

The evaluation of the leaf lipids showed that the amount of lipid obtained was around 5-6% of the leaf's dry weight, as shown in Figure 7.10. The mass of lipids obtained is reasonably constant; however, the 'Côte d'Ivoire' and the 'Frozen' leaves had the highest amount of lipid when compared to the leaf's weight, but they were not significantly different from the 'Control', 'Mature' and 'Perforated' leaves. The 'Young', 'Dead' and 'Insect' leaves were not significantly different from the 'Control' and 'Mature' leaves. The 'Crushed' leaves had the least lipid extracted though this was not significantly different to the 'Young', 'Dead' and 'Insect' leaves.

202

The amount of lipid extracted from the 'Dead' leaves is surprising as it is known that the total fatty acid content of *Arabidopsis*, *Brachypodium* and switchgrass leaves decrease by at least 80% after senescence (Yang and Ohlrogge, 2009). Chlorophyll breakdown is one of the first responses of the leaf to senescence (Thompson et al., 1998), and it has been found that *Arabidopsis* leaves lose on average 93% of their chlorophylls during this time (Himelblau and Amasino, 2001). When the leaf has completely senesced, most of the remaining biomass is cell wall polysaccharides, lignin, and cuticular lipid that cannot be dissolved in chloroform, as discussed in section 1.5.3 (Troncoso-Ponce et al., 2013). It is possible that the unexpectedly high level of lipids in the 'Dead' sample was due to weighing errors resulting from the very low masses of lipids being measured.
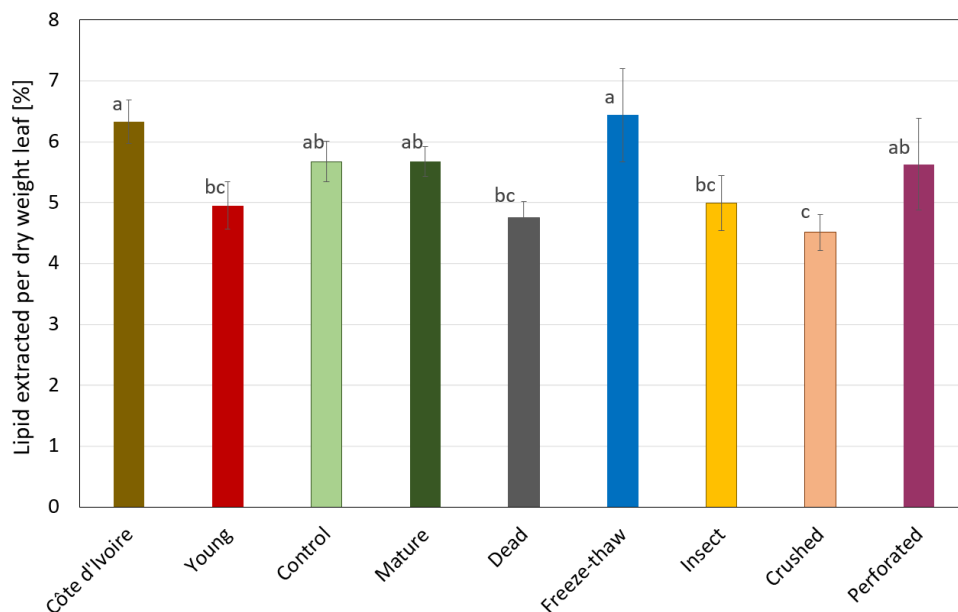
Figure 7.10: Lipid extract from leaf samples per dry weight of leaf as a percentage, showing that, as expected, the extract is around 6% (Ohlrogge et al., 2015). The amount of lipids obtained is reasonably constant; however, the leaves from the 'Côte d'Ivoire' and the 'Frozen' leaves had the highest amount but were not significantly different from the 'Control' and 'Mature' leaves. The 'Young', 'Dead', and 'Insect' leaves were not significantly different from the 'Control' and 'Mature' leaves. The 'Crushed' leaves had the least lipid extracted though this was not significantly different to the 'Young', 'Dead' and 'Insect' leaves. The data bars represent six data points, and the error bars are the standard deviation of the means. The data were compared using ANOVA, followed by a Tukey post-hoc test to evaluate the differences. The letters represent significantly different results a>b>c.

Before discussing the lipid content detail, it is important to note that an enzyme deactivation step was not utilised on the leaves within this research. As discussed in section 1.5.5, a deactivation step is often performed to prevent lipid degradation, including fatty acids from being broken down by hydrolytic enzymes, after the leaves are harvested; this would give misleading results. This step was omitted because the cocoa leaves from Côte d'Ivoire had already travelled for several days before they reached the laboratory, so it was presumed that any enzymatic degradation had already occurred. The leaves collected from the Eden Project were frozen at -80 °C as soon as possible after harvesting (around 7.5 h), which would halt enzymatic action and autooxidation at that point (Christie and Han, 2010a). However, many degradation processes occur as soon as the leaf is harvested, including acylation of galactolipids, as shown in Figure 7.5.

7.3.3.3. Glycerolipids

The levels of MGDG and DGDG in the leaves were measured using HPTLC, shown in Figure 7.11. There was some variation between the values produced by the different plates run for this analysis, as seen in the error bars; however, the data is presented for discussion.

This data shows unexpectedly low concentrations of MGDG and DGDG in all leaves. As discussed in section 1.5.3, glycerolipids make up 53% of the lipids in an average mature, unharvested leaf (Ohlrogge et al., 2015). MGDG makes up approximately 40-50% of total glycerolipids, with DGDG making up approximately 15% (Dörmann, 2013). The values measured are a fraction of these expected levels. The leaves' phospholipid profile was measured by ^{31}P NMR, using a method based on literature (Cremonini et al., 2004), and it revealed that phosphatidic acid was the major phospholipid in the sample (data not shown). HPTLC analysis of non-polar lipids within the leaves also showed high levels of 1,2 diacylglycerol – around 100-120 mg/g

lipid extract for most samples. No free fatty acids were evidenced in any samples except for a small amount in the 'insect' and 'dead' leaves, 8 mg and 2 mg/g lipid extract, respectively. The presence of these lipid types is a strong indicator of glycerolipid breakdown (Christie and Han, 2010a).
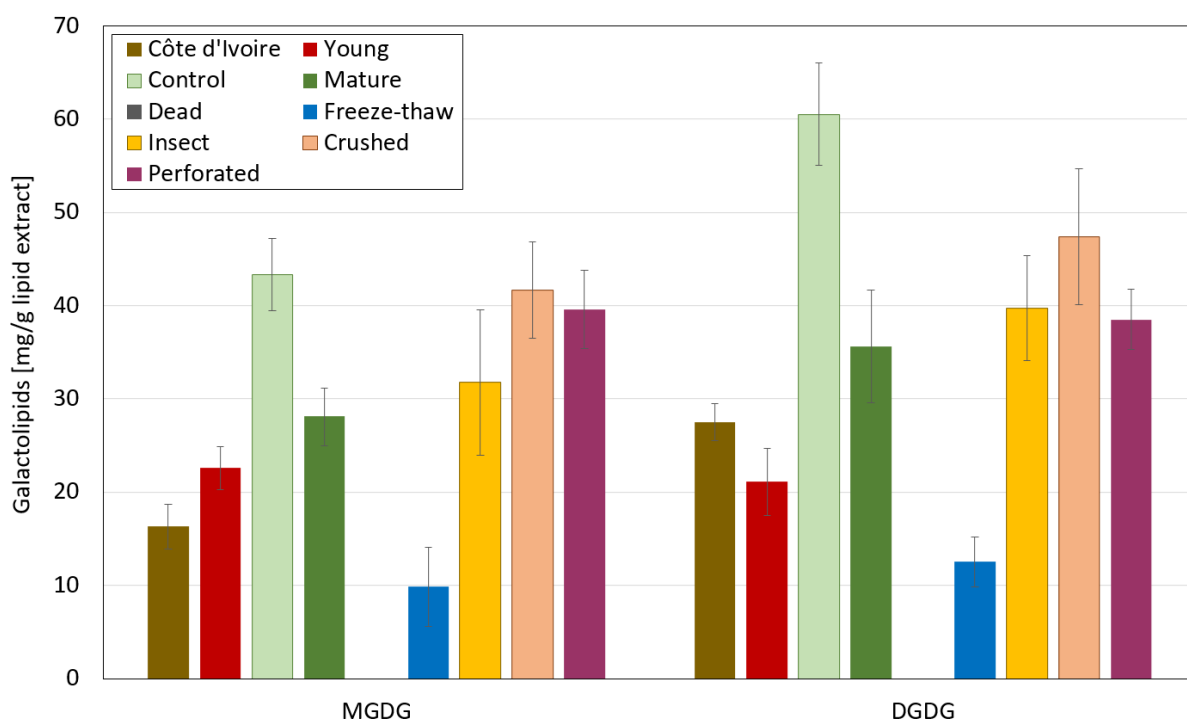
Figure 7.11: Concentration of MGDG and DGDG found in the different leaf samples. No MGDG or DGDG was found in the dead leaves. Three different lipid extracts were used for each bar, each measured on four plates, giving 12 data points per measurement given in this figure. The data for 'Côte d'Ivoire' and 'Control' represent only three plates due to a plate failure; therefore, these bars were calculated with nine data points. The error bars, calculated as standard deviation, are quite large and reflect variation on the plates rather than the replicates. Therefore, the data is given as a general representative of the concentrations within the leaves and statistical analyses were not applied to this data.

7.3.3.4. Fatty acids

Figure 7.12 shows the amounts of fatty acids within the samples, presented as mg fatty acid per g lipid. It can be seen that the five fatty acids routinely found in leaves: palmitate, stearate, oleate, linoleate and α-linolenate (Ohlrogge et al., 2015), are present in cocoa leaves.

It appears that insect interference of the leaf changes the fatty acid profile to form short-chain saturated fatty acids. Generally, short-chain fatty acids are found in leaves as storage lipids (Ohlrogge et al., 2015). Saturated fats, on the whole, are seen as unhealthy in the diet, leading to an increased risk of coronary heart disease. However, when diets rich in short-chain or medium-chain saturated fatty acids were compared to those rich in oleic acid in Malaysian adults, there was no increased concentration of inflammation markers (Voon et al., 2011).

In Figure 7.13, the fatty acid levels found in the extracted lipids are shown as the molar percentage. This format is helpful when comparing samples. The most apparent observation is between young, control and mature leaves. The young leaves were pink or red, indicating that chromoplasts are present that have not yet matured to green chloroplasts (Staehelin, 2015b). The fatty acids of the lipids in chromoplasts are often linoleic acid, whereas chloroplasts' lipids contain high amounts of α-linolenic acid; 90% of fatty acids in the chloroplast can be α-linolenic acid (Ohlrogge et al., 2015). The desaturation process that is expected to occur can be seen clearly in the decrease of linoleic and the increase in α-linolenic acid as the leaf ages in these three leaf lipid samples.
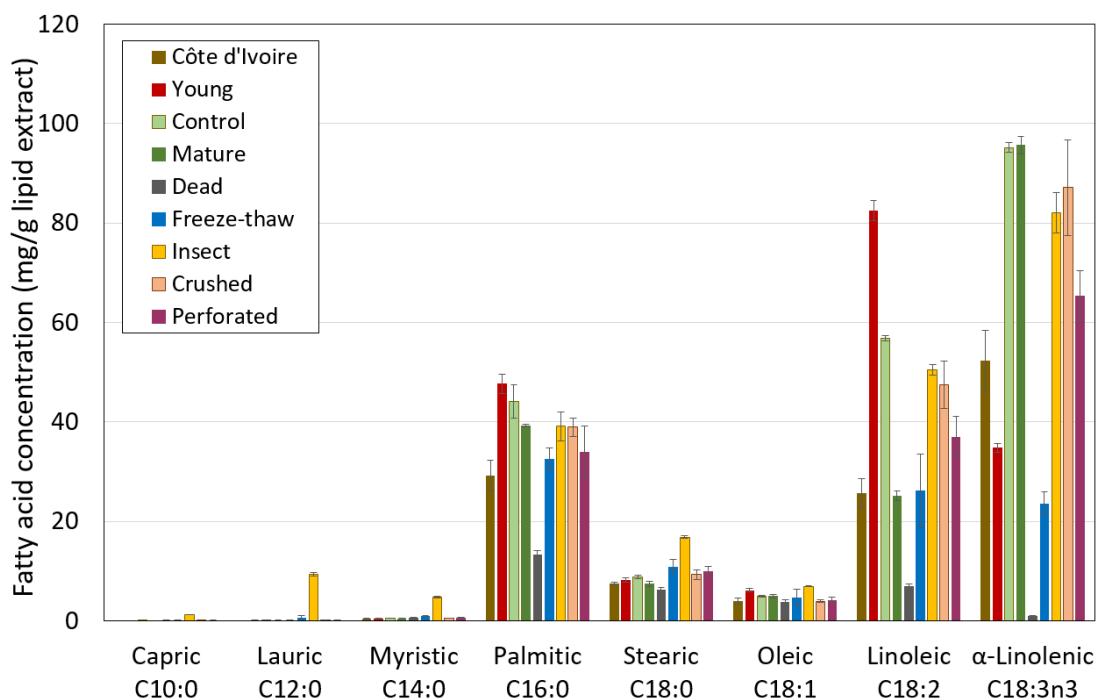
Figure 7.12: Fatty acid concentration of the leaf samples, shown as mg of each fatty acid per gram of lipid extract. Each bar represents three true replicates, and the error bars are the standard deviation of the means.
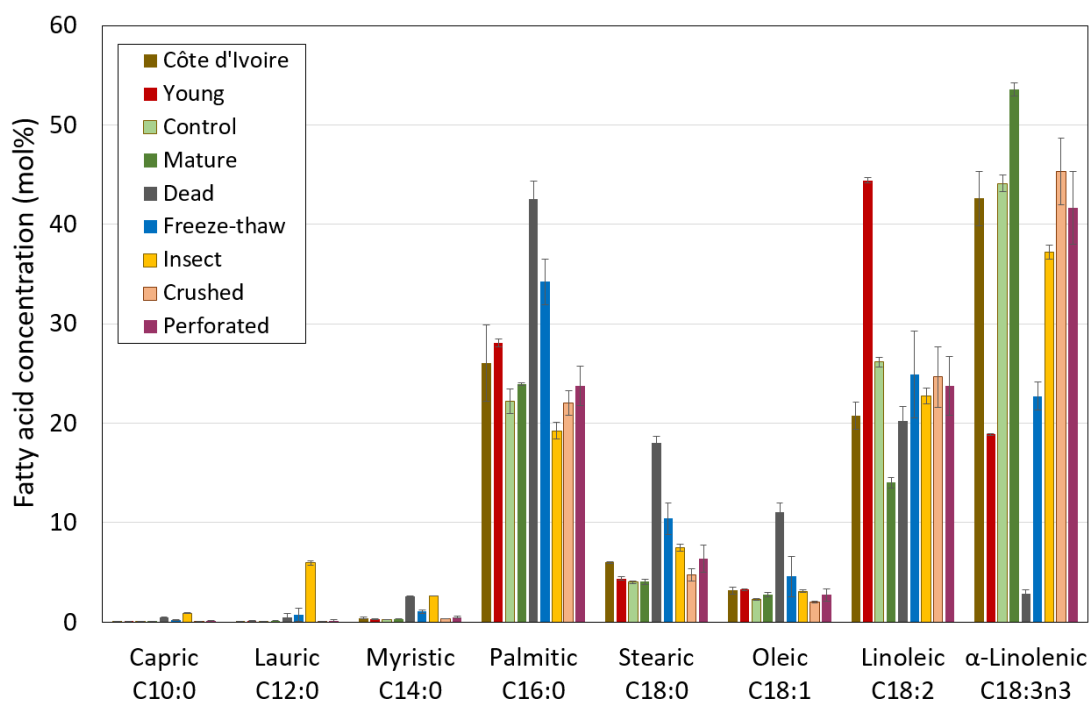
Figure 7.13: Fatty acid concentration of the leaf samples, shown as the molar percentage. Each bar represents three true replicates, and the error bars are the standard deviation of the means.

7.3.3.5. *Chlorophyll and carotenoids*

Figure 7.14 shows the amount of chlorophyll *a* (Chl a), chlorophyll *b* (Chl b) and carotenoids in the leaves. As outlined in Section 7.2.1, all the leaves were prepared for transport in a similar way by picking the leaves, placing them between the pages of a spiral-bound notebook, and finally wrapping the notebook in cling film. The representatives at the Nestlé farms in Côte d'Ivoire used this method, so the leaves were prepared for transport from the Eden Project in the same way. At the time, this method was thought to have the advantage of protecting the leaves from sunlight, which can cause the breakdown of chlorophyll in harvested leaves (Mangos and Berger, 1997). However, darkness can cause stress-induced senescence in the leaves, as discussed in literature (Buchanan-Wollaston, 1997, Lipton, 1987, Troncoso-Ponce et al., 2013). The highest amounts of chlorophyll and carotenoids appear in the 'control', 'mature' and 'perforated' leaves obtained from the Eden Project. There is significantly fewer ($t_{(4)}$ = 5.52, p < 0.01) of Chl *a* + *b* in the mature leaves obtained from Côte d'Ivoire compared to the mature leaf from the Eden Project, which is the leaf that is most similar to it in life stage and appearance. The reason for this reduction could be the time in unrefrigerated transit from Africa to the UK, as peroxidase breakdown of chlorophyll has been shown to increase substantially after three days of storage at 25 °C (Yamauchi and Watada, 1991). Other reasons could include the fact that Côte d'Ivoire has more sunlight than the UK: it has been found that *Acer*, *Fagus* and *Tilia* leaves grown in the sun have less chlorophyll than those in the shade (Lichtenthaler et al., 2007), or it could be that these are different cultivars of *Theobroma cacao* plant and so the genes determine the difference in the amount of chlorophyll present. Generally, applying stress to the leaves appears to reduce the chlorophyll and carotenoids levels by a similar amount. As stated in the introduction, the 'young' leaves have not yet developed chloroplasts and so have low levels of chlorophylls. The 'dead' leaf has much less chlorophyll and carotenoids.

Having said this, the values of Chl a, Chl b and carotenoids are low compared to literature. Table 7.1 shows some data from *Populus nigra*. By comparing this data with that in Figure 7.14, it can be seen that these leaves are closer to the green senescent leaf values in the table. This concurs with the hypothesis already raised that, during the transport time, these leaves have been significantly broken down by the endogenous lipases and other enzymes.

Table 7.1: Chlorophyll and carotenoid levels in <u>Populus nigra</u> (Lichtenthaler and Buschmann, 2001)

Leaf type	Chl a+b [mg/g dw]	Carotenoids [mg/g dw]
Dark green sun leaves	8.03	1.81
Dark green shade leaves	12.41	2.39
Green senescent leaves	5.00	1.24
Yellowish-green senescent leaves	1.99	1.13

When considering individual types of carotenoids, Figure 7.15 shows that β-carotene and lutein are present within cocoa leaves from the Côte d'Ivoire; lutein to a greater extent than β-carotene. Although the levels of the different carotenoids were not quantified in this research, HPLC measurements could be done to evaluate the actual amounts within the leaves (Bunea et al., 2008, Kidmose et al., 2001).
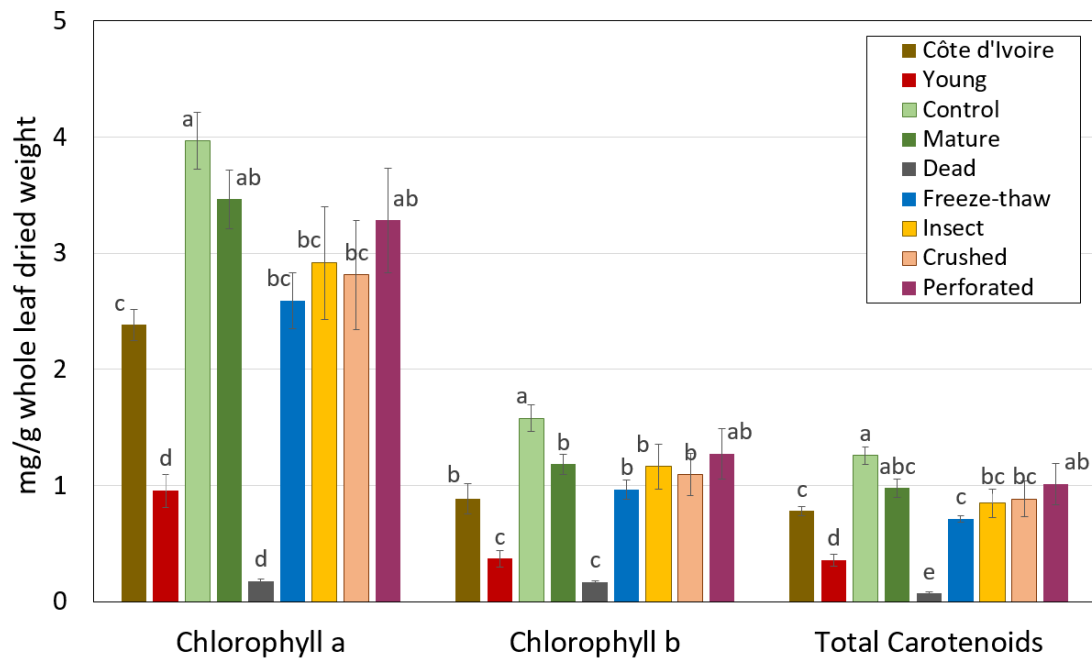
Figure 7.14: Chlorophyll and carotenoid concentrations in the leaf samples. A one way ANOVA was applied with a post-hoc Tukey test, the results of which are given using a>b>c>d>e. The error bars are the standard deviation from the mean of the three independent samples for each leaf type.
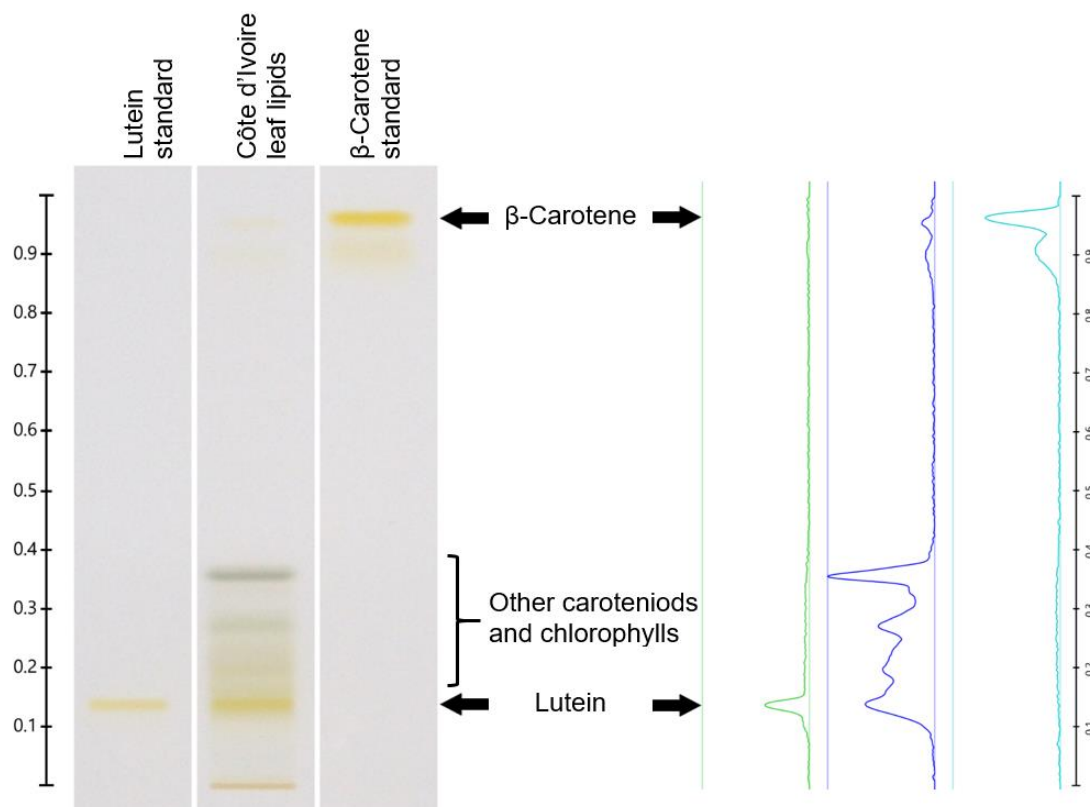
Figure 7.15: Lutein and β-carotene in Cote d'Ivoire leaves (28 μg in 10 μL dissolved sample applied to the plate). The plate is shown on the left, and the density profile on the right shows the presence of these two carotenoids more clearly within the sample. The other yellow bands may be other carotenoids, and the grey bands are likely to be chlorophyll as they glow red under UV light (Lichtenthaler and Buschmann, 2001).

7.3.3.6. Lipids from 'Dead' leaf

In section 7.3.3.2, a much higher than expected lipid amount was found in the dead leaves, and it was postulated that a weighing error might be the cause. The more detailed analysis of the lipids within this sample support this theory. Figure 7.11 shows that there was no MGDG or DGDG found in the dead leaf sample. Figure 7.12 shows a decreased amount of fatty acids in the dead leaf sample, and the fatty acids that remain have a shorter length or are more saturated, possibly being stored as triacylglycerols. Finally, Figure 7.14 shows decreased chlorophyll and carotenoid levels.

These 'Dead' leaves have undergone full natural senescence before analysis. This appears to be a highly regulated process since many of the by-products of chloroplast dismantling may be toxic to the plant (Domínguez and Cejudo, 2021). It starts with a trigger, which could be shade caused by another leaf (Buchanan-Wollaston, 2003), disease, drought stress or nitrogen deficiency (Buchanan-Wollaston, 1997) or is just developmentally regulated (Huber, 1987) and is reversible for a part of the senescence process (Buchanan-Wollaston, 2003). During natural senescence, the goal of the plant is to sequester the nitrogen, carbon and minerals from the leaf to other parts of the plant (Buchanan-Wollaston, 1997). These can then be used in new leaves or seeds. For the lipids in the chloroplast membrane, those of interest in this PhD, the thylakoids are first broken down in plastoglobules within the chloroplast to avoid toxicity (Domínguez and Cejudo, 2021), while the outer chloroplast membrane remains intact (Evans et al., 2010). This process converts a chloroplast into a gerontoplast, as was shown in Figure 1.26. Although the chloroplast deterioration that leads to a decrease in chlorophyll is an early manifestation of senescence, the chloroplast envelope remains intact until the late stages of leaf senescence (Thompson et al., 1998). Vesicles are formed during this dismantling, and the whole gerontoplast is engulfed by the vacuoles, where they are broken down for reabsorption by the plant (Domínguez and Cejudo, 2021). It appears that the galactolipids and chlorphyll are broken down quickly on initiation of leaf senescence, however phospholipids in the general lipid membrane and triacylglycerol in stores are broken down more slowly and may be the last lipids to be sequestered into the plant.

7.3.3.7. Acylated-galactolipids

Although acylated-galactolipids were not directly measured within the leaf lipid samples, it would appear from Figure 7.5 and Figure 7.6 that all of the samples may have some acylated-galactolipids present. There appear not to be just acyl-MGDG, but also acyl-MGMG and acyl-DGDG and acyl-DGMG. Reports in the literature are of

acyl-MGDG forming after the leaf has undergone abiotic stress (homogenisation, mechanical wounding or thawing after snap freezing) or biotic stress (avirulent bacteria or insect attack). One report specifically showed that no, or very minimal, acyl-MGDG was found in the leaves of A. thaliana, tomato and wheat before wounding, freezing or infecting with bacteria. However, this assessment was done directly after harvesting (Vu et al., 2014a). There seems to be an accumulation of these acylated galactolipids in the cocoa leaves after eight hours of storage post-harvest, but no other treatment, apart from storing in the dark, is required to be applied to the leaf.

7.3.4. Lipids present in cocoa leaves which may have a dietary benefit

Chloroplasts and carotenoids are of interest in food as they have many positive dietary effects. The presence of carotenoids in the diet has been shown to prevent eye disease and exert antioxidant, lipid-lowering, anti-inflammatory, anti-fibrotic, and insulin-sensitising properties (Johnson, 2002, Lee et al., 2019). Chlorophyll also has antioxidant and antimutagenic properties (Ferruzzi et al., 2002). Chlorophyll contains magnesium, low levels of which have been associated with Alzheimer's disease, insulin resistance and type-2 diabetes mellitus, hypertension, cardiovascular disease (e.g., stroke), migraines, and attention deficit hyperactivity disorder (ADHD) (Gröber et al., 2015).

α-linolenate (ALA) is an essential long-chain omega-3 fatty acid that must be consumed in the human diet as it cannot be metabolised in the body. It is the precursor to the other two main omega-3 fatty acids: eicosapentaenoic acid (EPA) and docosahexaenoic acid (DHA), which are metabolised in the liver, following a series of desaturations, elongations and a β-oxidation step (Metherel and Bazinet, 2019). ALA, EPA and DHA have been found to be beneficial to humans in many ways, such as modulation of satiety in overweight and obese volunteers (Parra et al., 2008),

prevention of sudden death (Albert et al., 2002), prevention of coronary heart disease (Calder, 2017), and treatment of rheumatoid arthritis, Alzheimer, and irritable bowel syndrome (Lorente-Cebrián et al., 2015). Significant improvements were found in children with developmental coordination disorder in reading, spelling, and behaviour when treated with omega-3 and omega-6 fatty acids (Richardson and Montgomery, 2005). However, as the leaf lipids themselves would be used in the chocolate at around only 0.2% (wt), it would be wise to consider the broader health context of chocolate itself.

The consumption of cocoa flavonoids has been shown to reduce cardiovascular mortality in numerous observational and research studies. Antioxidant effects of cocoa may influence insulin resistance and reduce the risk of diabetes. They may also positively affect the immune system, protect nerves from injury and inflammation, and have beneficial effects on satiety, cognitive function and mood (Katz et al., 2011). The European Food Safety Authority (EFSA) was presented with research studies by the chocolate manufacturer Barry Callebaut NV, whereby volunteers consumed 200 mg cocoa flavanols in the form of 2.5 g high-flavanol cocoa powder, 10 g high-flavanol dark chocolate, or as a food supplement capsule or tablet. In 2012, the EFSA approved the claim that "Cocoa flavanols help maintain the elasticity of blood vessels, which contribute to normal blood flow". Since this approval, scientific research has extended to a proposed link of cocoa flavanols with improvements in muscle growth, especially for the older population where sarcopenia and myopenia, both forms of muscle loss, is an issue (Tallon, 2015).

However, cocoa is predominantly consumed as energy-dense chocolate, which brings potentially detrimental health effects. The nutritional information of an Aero chocolate bar reveals that it contains 28.4% (wt) fat, 16.6% (wt) of which is saturated fat, and 57.6% (wt) sugar. A 36 g bar of this chocolate contains 194 kcal, 10.5 g fat and 6.1 g saturated fat, which represents 10% of the recommended adult daily calorie

intake (2000 kcal/day) and 31% of the recommended daily intake of saturated fat (20 g/day) (https://www.aerochocolate.co.uk/products/bars/aero-milk-chocolate-bar-36g). A survey of commercially available cocoa and chocolate in the United States showed that, while 10g of cocoa powder contained on average 227.34 mg of procyanidins (the group name for flavanols as monomers, dimers, oligomers and polymers), 40g of milk chocolate contained only 27.43 mg of procyanidins (Miller et al., 2009). A later study looked at the impact of cocoa flavanols on cardiovascular health and found that 900 mg of flavanols were required for a decrease in blood pressure and 100 mg of epicatechin (a particular flavanol) for an increase in flow-mediated vasodilation of blood vessels. They estimated that to achieve these doses with dark chocolate would require up to 500 g for the flavanols and up to 200 g for the epicatechin per day, which would be unrealistic and involve a high intake of calories and saturated fat. They also stated that milk chocolate is an inappropriate source of flavanols and recommended food supplements instead (Vlachojannis et al., 2016).

7.4. Conclusions

This chapter set out to create acyl-MGDG in leaves and evaluate if this was a possible alternative to PGPR as an emulsifier in chocolate. It appeared that all cocoa leaves acquired acylated galactolipids, whether or not they underwent mechanical wounding. This change may have merely resulted from senescence processes within the leaves in the eight hours from harvest to processing in the laboratory. This highlights the need to destroy the leaf enzymes directly upon harvesting if an accurate assessment of the leaves' healthy-state lipidomics is desired.

However, for the assessment of acyl-MGDG as a natural alternative to PGPR, this slow, natural accumulation of acyl-galactolipids has been a serendipitous occurrence.

The control leaf lipids, which had the most MGDG and DGDG of all the samples, had the highest amount of chlorophylls and also appeared to contain acyl-galactolipids, did show some promise as an alternative to PGPR, at half of PGPR's applied concentration, in the chocolate model. Therefore, the lipids from *Theobroma cacao* green leaves are proposed as a natural emulsifier to replace PGPR.

8. Overall conclusions and next steps

8.1. Overall conclusions

This PhD research aimed to further the understanding of the yield stress lowering properties of PGPR by considering molecular properties alongside physical material properties and exploiting new insights to locate an alternative yield stress lowering emulsifier to PGPR from natural sources. To this end, a methodology was devised to determine the impact of PGPR on the yield stress of a chocolate model comprising a 65% sugar-in-oil suspension. The yield stress lowering capability of five commercially available PGPRs chosen for this research was quantified and found to vary. Several methods were used to ascertain the differences in the molecular structure of the PGPR samples that led to these differences in functionality. It appears that the difference in functionality between the PGPR molecules was not the molecular weight range or the polyricinoleate chain lengths; it was the presence of hydroxyl groups on the end of these chains that appeared to reduce the efficacy of the PGPR sample and a longer polyglycerol chain may enhance it. PGPR molecules have a larger space between the acyl groups than most natural lipids that have a single glycerol backbone. As this aspect of PGPR has not yet been researched, a novel natural alternative was chosen to investigate if the spread-out acyl-groups were important for amphiphilic molecules' yield stress reducing functionality. Such a molecule was identified as acylated monogalactosyl diacylglycerol. It was not available in purified form for purchase, so it was obtained using two approaches and the lipids acquired from these methods were applied to the chocolate model. They were assessed using rheological measurements to obtain the yield stress value. The yield stress values were compared to the yield stress attained using PGPR to ascertain the novel lipid emulsifier's effectiveness.

Conclusions can be drawn addressing the specific hypotheses outlined in chapter 1:

1. *The observed differences between PGPRs in manufacturing can be determined as fact using rheological measurements and a chocolate model.*

    The rheological assessments of the PGPR samples in the chocolate model showed that a difference was measurable. Grindsted 90, recognised by formulators as the PGPR with the lowest efficacy out of the five PGPRs included in this PhD research in chocolate recipes, did indeed show the lowest yield stress reducing power. Palsgaard 4125 was better than Grindsted 90 but not as good as the remaining three PGPRs: Admul WOL 1408, Grindsted Super and Palsgaard 4150. These three PGPRs are marketed as 'high' performing PGPRs, and these are better at reducing the yield stress in the chocolate model. Therefore, this hypothesis has been proved correct.

2. *There are differences in the molecular characteristics in the PGPRs, which can be ascertained using analytical equipment.*

    Analysis of the molecular weight ranges of the five PGPRs showed that the samples are bearly distinguishable from each other. Only when the fatty acids at the end of the polyricinoleate chain, the 'capping' fatty acid, were analysed, was a difference revealed. Analysis using interfacial tension measurements also inferred that a longer polyglycerol chain might increase the ability of a PGPR molecule to lower yield stress.

3. *The differences in the functionality relate to molecular differences in the PGPRs.*

    Grindsted 90, the least effective PGPR, was found to have statistically more ricinoleic acid as the capping fatty acid than the other PGPRs. This observation

218

led to the theory that the hydroxyl group on the ricinoleate creates a hydrophilic end to the acyl chain that may be attracted to the sugar surface, causing the chain to fold back on itself. It is the long hydrophobic acyl chain extending into the continuous phase that has been shown to be so important to the functionality of the PGPR (Vernier, 1997).

4. *There are natural molecules that reflect these molecular characteristics.*

The finding in hypothesis 3 implies that a more efficient yield stress reducing emulsifier would not have a hydroxyl group at the end of the hydrophobic chain. In literature, the only record of ricinoleic acid found in a glycerolipid, apart from triacylglycerol (TAG), is as a phospholipid in the castor bean, which is a precursor to the TAG itself (Kim et al., 2011).

Therefore, to take a novel approach, it was decided to focus on the headgroup. A feature of PGPR is that the acyl groups are separated by a poly-glycerol molecule rather than the single glycerol found in most natural amphiphilic molecules. A molecule was uncovered in the literature with acyl groups separated by one or two galactose groups: acylated-monogalactosyl diacylglycerol (acyl-MGDG) or acylated-digalactosyl diacylglycerol (acyl-DGDG). To our knowledge, the surface-active properties of acyl-MGDG have not been investigated in regards to food use.

5. *These molecules can be extracted from leaves or other material, and they will have a yield stress reducing power akin to PGPR.*

Acylated galactolipids are not commercially available as purified lipids; therefore, two methods were chosen to obtain these: protein recombinant

technology to produce the enzyme to apply to an assay to create the molecule and stress-treating cocoa leaves to induce them to produce it themselves. The lipids from both methods were applied to the 65% (wt) sugar-in-oil chocolate model, and the yield stress obtained using the rheological protocol. The acyl-MGDG made using the protein recombinant technology showed little difference from the sample with no emulsifier applied. This could have been that the acyl-MGDG did not have effectiveness as an emulsifier, or it could be that the amounts applied was so small that any effect could not be shown. The lipids from the 'freeze-thaw' treated leaves and the unstressed 'control' leaves were applied to the chocolate model, and a yield stress reducing effect was observed. The application of the leaf lipids at 0.15 % (wt) of the chocolate model appeared to have a very similar effect to the application of 0.3 % (wt) Grindsted 90 PGPR. When the rheology data were analysed using ANOVA followed by a post-hoc Tukey test, it appeared that there was no significant difference between the Herschel Bulkley yield stress values from the addition of 0.15% control leaf lipids, 0.3% Grindsted 90 and 0.3% Palsgaard 4150 to the chocolate model. The lipids extracted from all the leaf types obtained from Côte d'Ivoire and the Eden Project, UK, were analysed, and it appeared that all contained an amount of acylated-galactolipids. This was unexpected as research until now has assumed that abiotic or biotic stress is required to stimulate the leaf to create acyl-MGDG as the enzyme responsible for its conversion is placed outside the chloroplast, in the cytosol. Merely the action of harvesting the leaves does cause lipolysis to occur. This effect is illustrated in the values of the galactolipids and the chlorophyll measurements in chapter 7. It, therefore, appears that the enzyme is activated and can access the galactolipids that are its substrate following mere storage of the leaves in the dark for several hours. This means that if acyl-MGDG is confirmed in future to have success as a yield stress reducing lipid, it will not be so cumbersome to create on an industrial scale.

To summarise the conclusions of this PhD research, the PGPR samples were investigated, and the only difference found following the experiments performed was that the presence of hydroxyl groups at the end of the polyricinoleate chains appear to reduce the PGPR efficacy. Acyl-MGDG was proposed as an alternative natural emulsifier because of the length of the hydrophilic group that allows more separation between the acyl groups. The effectiveness of cocoa leaf lipids as a yield stress reducing emulsifier was established; however, more research will be required to fully understand the most important molecules in those extracted.

8.2. Future work

The findings of this PhD research could be taken forward in different ways.

8.2.1. Verification of findings

There are areas in this research that need to be verified before firm conclusions can be made.

- The proposed models of PGPR interaction at the sugar surface could be developed further to consider potential dynamics, for example, bulk concentrations, diffusion, surface dynamics, and fatty acid stacking arrangements.

- The presence of acyl-MGDG was always inferred using HPTLC plates with a comparison to literature. It would be valuable to analyse the bands to make a positive identification. Methods include electrospray ionisation triple quadrupole mass spectrometry (Vu et al., 2014b) and high-performance liquid chromatography/mass spectrometry (Ibrahim et al., 2011, Nilsson et al., 2012).

- The amount of acyl-MGDG formed during the assay was low. Generating a new batch of enzyme followed by an assay containing 2 g of the enzyme and 1 g of each of the galactolipids may create enough acyl-MGDG to show an impact on the yield stress of the chocolate model or prove that this molecule is not a candidate for a natural replacement for PGPR.

- The concentration of leaf lipids included in the chocolate model varied between the different types. Repeating these experiments using the same amount of dried, powdered leaf to compare different lipid contents would clarify the impact of concentration over lipid content.

- Application into chocolate. The leaf lipids have good yield stress reducing abilities in the 65% (wt) sugar-in-oil suspension; however, no experiments have taken place using cocoa butter instead of sunflower oil or with the inclusion of cocoa and milk particles. Verification of the transfer of these properties into this different suspension is important before the leaf lipids can be declared a novel alternative to PGPR.

8.2.2. Consumer acceptance and environmental impacts of leaf lipids as a novel emulsifier

If leaf lipids in general, or acyl-MGDG in particular, is to be used as a yield stress modifier in food, then other factors need to be considered.

- Health benefits. The leaves have already been shown to include carotenoids, chlorophyll and α-linolenic acid, all of which have known health benefits:
  - Carotenoids have been shown to prevent eye disease and exert antioxidant, lipid-lowering, anti-inflammatory, anti-fibrotic, and insulin-sensitising properties (Johnson, 2002, Lee et al., 2019).
  - Chlorophyll has antioxidant and antimutagenic properties (Ferruzzi et al., 2002). It contains magnesium, low levels of which have been associated with Alzheimer's disease, insulin resistance and type-2 diabetes mellitus, hypertension, cardiovascular disease (e.g., stroke), migraines, and attention deficit hyperactivity disorder (ADHD) (Gröber et al., 2015).
  - α-linolenic acid (ALA) is an essential long-chain omega-3 fatty acid that is metabolised in the body to form two other essential omega-3 fatty acids: eicosapentaenoic acid (EPA), docosahexaenoic acid (DHA). Together, ALA, EPA and DHA have many beneficial health effects, including a cardioprotective effect and anti-inflammatory, anti-cancer

and anti-viral properties (Rajaram, 2014). It has been shown to help with rheumatoid arthritis, Alzheimer's, and irritable bowel syndrome (Lorente-Cebrián et al., 2015) and cause significant improvements in reading, spelling and behaviour when children with certain conditions are treated with omega-3 and omega-6 fatty acids (Richardson and Montgomery, 2005).

- o Most antinutrients are water-soluble; therefore, the probability of detecting them in the lipid fraction is minimal (Popova and Mihaylova, 2019); however, a thorough analysis should be performed.

- Chlorophylls are intensely green. The colour of dark chocolate may be enough to mask the chlorophyll pigments' effect, but the milk chocolate and white chocolate will show the colour as shown in Figure 8.1. Chlorophylls can be removed using solvents (Kim et al., 2020); however, this requires an additional processing step and the undesired use of solvents. PGPR is also used in margarine manufacture. If PGPR were to be swapped for leaf lipids, could consumers accept green chocolate or margarine?

- Volume required. In 2017, the five countries with the highest consumption of chocolate, Switzerland, Germany, Ireland, UK and Sweden, bought approximately 1351 million kg of chocolate (www.worldatlas.com and www.statista.com). If leaf lipids were to replace emulsifiers in these chocolate bars at 0.15% (wt), this would require 2.03 million kg of lipids, equating to 195 million leaves per year, where one leaf weighs 4 grams. Therefore, this may be an artisan product if cocoa leaf lipids are developed further for chocolate use. If a large enough supply can be found, utilisation of waste green matter may be an alternative, such as pea vine halm (Wattanakul et al., 2019).

- Method refinement. This method currently requires freeze-drying followed by grinding to create particles of less than 125 µm. The lipids are then extracted

using chloroform and methanol with water. This method would be restrictive and costly for large scale factory processes. Therefore, substituting a softer leaf, for instance, spinach, may make the process easier. The leaf can then merely be homogenised. The lipid extraction can occur immediately with the water that the leaf has released if an appropriate extraction solvent can be identified. Polar lipids, in general, extract well into chloroform and galactolipids into acetone (Christie and Han, 2010a); however, these solvents are both hazardous to the user. As an alternative to solvent extraction, supercritical carbon dioxide has been used to extract lipids from oils and leaves, but this had the most success with non-polar lipids. It has been found that adding ethanol may help to include the glycerolipids in this extraction (Sahena et al., 2009).

Figure 8.1: Leaf lipids in 65% (wt) sugar-in-oil chocolate model, demonstrating the effect of chlorophyll pigments.

8.2.3. Specific laboratory-based experiments

In this PhD thesis, some experiments were not possible to be performed due to time constraints. Several experiments could be performed to complement and strengthen the scientific findings in this work.

- PGPR reverse micelles. A zeta sizer or light scattering technique could be used to verify the presence and size of micelles of PGPR in chloroform and acetone (Ogino et al., 1988), as discussed in chapter 5. A visualisation of the micelles may be possible with cryo-scanning electron microscopy (cryo-SEM) (Pawlik et al., 2016).

- Acyl-MGDG presence in different leaves: From these experiments, it appears that acyl-MGDG is routinely formed, within hours, within the senescing leaf. Further experiments could be planned to observe if this molecule is found in different leaves and how long it takes for acyl-MGDG to be formed within the leaf following harvesting. The reason for the accumulation of acyl-MGDG in leaves is not yet conclusive. Several theories have been postulated. These include actively helping the plant to survive the stress imposed on it, for instance, by having a bactericidal effect; to serve as phytohormone reservoirs (where oxophytodienoic acid (OPDA) replaces a standard fatty acid); and to sequester free fatty acids released during acyl chain turnover, which, if allowed to accumulate in the leaf would cause damage (Song et al., 2021). Further research into this molecule would also add to this discussion.

References

2007a. Hydroxyl value. *In:* GOOCH, J. W. (ed.) *Encyclopedic Dictionary of Polymers.* New York, NY: Springer New York.

2007b. Iodine number. *In:* GOOCH, J. W. (ed.) *Encyclopedic Dictionary of Polymers.* New York, NY: Springer New York.

2007c. Saponification value. *In:* GOOCH, J. W. (ed.) *Encyclopedic Dictionary of Polymers.* New York, NY: Springer New York.

AČKAR, Đ., ŠKRABAL, S., ŠUBARIĆ, D., BABIĆ, J., MILIČEVIĆ, B. & JOZINOVIĆ, A. 2014. Rheological Properties of Milk Chocolates as Influenced by Milk Powder Type, Emulsifier, and Cocoa Butter Equivalent Additions. *International Journal of Food Properties,* 18**,** 1568-1574.

ADACHI, S. 1965. Thin-layer chromatography of carbohydrates in the presence of bisulfite. *Journal of Chromatography A,* 17**,** 295-299.

AEBI, M. 2009. Ch 16. Chocolate Panning. *In:* BECKETT, S. T. (ed.) *Industrial Chocolate Manufacture and Use: Fourth Edition.* Blackwell Publishing Ltd.

AESCHLIMANN, J.-M. & BECKETT, S. 2000. International inter-laboratory trials to determine the factors affecting the measurement of chocolate viscosity. *Journal of Texture Studies,* 31**,** 541-576.

AFOAKWA, E. O., PATERSON, A. & FOWLER, M. 2007. Factors influencing rheological and textural qualities in chocolate – a review. *Trends in Food Science & Technology,* 18**,** 290-298.

AFOAKWA, E. O., PATERSON, A. & FOWLER, M. 2008. Effects of particle size distribution and composition on rheological properties of dark chocolate. *European Food Research and Technology,* 226**,** 1259-1268.

AFOAKWA, E. O., PATERSON, A., FOWLER, M. & VIEIRA, J. 2009. Comparison of rheological models for determining dark chocolate viscosity. *International Journal of Food Science & Technology,* 44**,** 162-167.

ALBERT, C. M., CAMPOS, H., STAMPFER, M. J., RIDKER, P. M., MANSON, J. E., WILLETT, W. C. & MA, J. 2002. Blood levels of long-chain n–3 fatty acids and the risk of sudden death. *New England Journal of Medicine,* 346**,** 1113-1118.

ANDERSSON, M. X., HAMBERG, M., KOURTCHENKO, O., BRUNNSTROM, A., MCPHAIL, K. L., GERWICK, W. H., GOBEL, C., FEUSSNER, I. & ELLERSTROM, M. 2006. Oxylipin profiling of the hypersensitive response in Arabidopsis thaliana. Formation of a novel oxo-phytodienoic acid-containing galactolipid, arabidopside E. *J Biol Chem,* 281**,** 31528-37.

ARNOLD, G., SCHULDT, S., SCHNEIDER, Y., FRIEDRICHS, J., BABICK, F., WERNER, C. & ROHM, H. 2013. The impact of lecithin on rheology, sedimentation and particle interactions in oil-based dispersions. *Colloids and Surfaces A: Physicochemical and Engineering Aspects,* 418**,** 147-156.

ASTM 2017. Standard Test Methods for Hydroxyl Groups Using Acetic Anhydride Acetylation.

ATTAIE, H., BREITSCHUH, B., BRAUN, P. & WINDHAB, E. J. 2003. The functionality of milk powder and its relationship to chocolate mass processing, in particular the effect of milk powder manufacturing and composition on the physical properties of chocolate masses. *International journal of food science & technology,* 38**,** 325-335.

AZZI, A. 2018. Many tocopherols, one vitamin E. *Molecular aspects of medicine,* 61**,** 92-103.

BABIN, H., DICKINSON, E., CHISHOLM, H. & BECKETT, S. 2005. Interactions in dispersions of sugar particles in food oils: influence of emulsifier. *Food Hydrocolloids,* 19**,** 513-520.

BAHRAMI, N., YONEKURA, L., LINFORTH, R., CARVALHO DA SILVA, M., HILL, S., PENSON, S., CHOPE, G. & FISK, I. D. 2014. Comparison of ambient solvent

extraction methods for the analysis of fatty acids in non-starch lipids of flour and starch. *Journal of the Science of Food and Agriculture,* 94**,** 415-423.

BAHTZ, J., GUNES, D. Z., SYRBE, A., MOSCA, N., FISCHER, P. & WINDHAB, E. J. 2016. Quantification of Spontaneous W/O Emulsification and its Impact on the Swelling Kinetics of Multiple W/O/W Emulsions. *Langmuir,* 32**,** 5787-95.

BAILEY, B. A., STREM, M. D., BAE, H., DE MAYOLO, G. A. & GUILTINAN, M. J. 2005. Gene expression in leaves of Theobroma cacao in response to mechanical wounding, ethylene, and/or methyl jasmonate. *Plant Science,* 168**,** 1247-1258.

BAKER, B. S., BROWN, B. D. & ANANTHESWARAN, R. C. 2006. Measurement of yield stress in dark chocolate using controlled stress vane method. *Journal of texture studies,* 37**,** 655-667.

BALLANCE, P. & CROMBIE, W. M. 1958. Paper chromatography of saturated and unsaturated fatty acids. *Biochemical Journal,* 69**,** 632-640.

BAMFORD, H. F., GARDNER, K. J., HOWAT, G. R. & THOMSON, A. F. 1970. The use of polyglycerol polyricinoleate in chocolate. *Rev. Int. Choc.,* 25**,** 226-228.

BARBOSA, C., DIOGO, F. & ALVES, M. R. 2016. Fitting mathematical models to describe the rheological behaviour of chocolate pastes. 1738, 370016.

BARNES, G. T. & GENTLE, I. R. 2011. The gas-liquid interface: adsorption; films and foams; aerosols. *Interfacial Science: an introduction.* Oxford University Press.

BARNES, H. A. 1995. A review of the slip (wall depletion) of polymer solutions, emulsions and particle suspensions in viscometers: its cause, character, and cure. *Journal of Non-Newtonian Fluid Mechanics,* 56**,** 221-251.

BARNES, H. A. 1999a. The yield stress—a review or 'παντα ρει'—everything flows? *Journal of Non-Newtonian Fluid Mechanics,* 81**,** 133-178.

BARNES, H. A. 1999b. The Yield Stress - a review or παντα ρει - Everything flows? *Journal of Non-Newtonian Fluid Mechanics,* 81**,** 133-178.

BARNES, H. A. & NGUYEN, Q. D. 2001. Rotating vane rheometry—a review. *Journal of non-Newtonian fluid mechanics,* 98**,** 1-14.

BASTIDA-RODRÍGUEZ, J. 2013. The Food Additive Polyglycerol Polyricinoleate (E-476): Structure, Applications, and Production Methods. *ISRN Chemical Engineering,* 2013**,** 1-21.

BECKETT, S. T. 2019. *The Science of Chocolate*, The Royal Society of Chemistry.

BECKETT, S. T., PAGGIOS, K. & ROBERTS, I. 2017. Conching. *In:* BECKETT, S. T., FOWLER, M. S. & ZIEGLER, G. R. (eds.) *Beckett's Industrial Chocolate Manufacture and Use.* Fifth ed.: John Wiley & Sons Ltd.

BEN HALIMA, N., BEN SAAD, R., KHEMAKHEM, B., FENDRI, I. & ABDELKAFI, S. 2015. Oat (Avena sativa L.): Oil and Nutriment Compounds Valorization for Potential Use in Industrial Applications. *J Oleo Sci,* 64**,** 915-32.

BIDLACK, J. E. & JANSKY, S. 2018a. Ch 3. Cells. *Introductory Plant Biology.* 14 ed.: McGraw-Hill.

BIDLACK, J. E. & JANSKY, S. 2018b. Ch 7. Leaves. *Introductory Plant Biology.* 14th edition ed.

BIDLACK, J. E. & JANSKY, S. 2018c. Ch 10. Plant Metabolism. *Introductory Plant Biology.* 14 ed.

BIDLACK, J. E. & JANSKY, S. 2018d. Ch 11. Growth and Development. *Introductory Plant Biology.* McGraw-Hill.

BLANCO, E., HODGSON, D. J. M., HERMES, M., BESSELING, R., HUNTER, G. L., CHAIKIN, P. M., CATES, M. E., VAN DAMME, I. & POON, W. C. K. 2019. Conching chocolate is a prototypical transition from frictionally jammed solid to flowable suspension with maximal solid content. *Proc Natl Acad Sci U S A,* 116**,** 10303-10308.

BLIGH, E. G. & DYER, W. J. 1959. A rapid method of total lipid extraction and purification. *Canadian journal of biochemistry and physiology,* 37**,** 911-917.

BÓDALO, A., BASTIDA, J., MÁXIMO, M. F., MONTIEL, M. C., GÓMEZ, M. & ORTEGA, S. 2009. Screening and selection of lipases for the enzymatic production of polyglycerol polyricinoleate. *Biochemical Engineering Journal,* 46**,** 217-222.

BONARIUS, G. A., VIEIRA, J. B., VAN DER GOOT, A. J. & BODNÁR, I. 2014. Rheological behaviour of fibre-rich plant materials in fat-based food systems. *Food Hydrocolloids,* 40**,** 254-261.

BOUZAS, J. & BROWN, B. D. 1995. Interactions Affecting Microstructure, Texture, and Rheology of Chocolate Confectionary Products. *In:* GAONKAR, A. G. (ed.) *Ingredient Interactions: Effects on Food Quality.* Marcel Dekker Inc.

BRIGGS, J. L. & WANG, T. 2004. Influence of shearing and time on the rheological properties of milk chocolate during tempering. *Journal of the American Oil Chemists' Society,* 81**,** 117-121.

BROUGHTON, R., RUÍZ-LOPEZ, N., HASSALL, K. L., MARTÍNEZ-FORCE, E., GARCÉS, R., SALAS, J. J. & BEAUDOIN, F. 2018. New insights in the composition of wax and sterol esters in common and mutant sunflower oils revealed by ESI-MS/MS. *Food chemistry,* 269**,** 70-79.

BROWN, E. & JAEGER, H. M. 2014. Shear thickening in concentrated suspensions: phenomenology, mechanisms and relations to jamming. *Reports on Progress in Physics,* 77**,** 1-24.

BSI, B. S. I. 2018. Animal and vegetable fats and oils - Determination of iodine value. BSI Standards Limited.

BSI, B. S. I. 2020a. Animal and vegetable fats and oils – Determination of saponification value. BSI Standards Limited.

BSI, B. S. I. 2020b. Animal and vegetable fats and oils — Determination of acid value and acidity. BSI Standards Limited.

BUCHANAN-WOLLASTON, V. 1997. The molecular biology of leaf senescence. *Journal of experimental botany,* 48**,** 181-199.

BUCHANAN-WOLLASTON, V. 2003. POSTHARVEST PHYSIOLOGY| Senescence, Leaves. *In:* T., B. (ed.) *Encyclopedia of applied plant sciences.* Elsevier.

BUNEA, A., ANDJELKOVIC, M., SOCACIU, C., BOBIS, O., NEACSU, M., VERHE, R. & CAMP, J. V. 2008. Total and individual carotenoids and phenolic acids content in fresh, refrigerated and processed spinach (Spinacia oleracea L.). *Food Chem,* 108**,** 649-56.

BUTTE, W. 1983. Rapid method for the determination of fatty acid profiles from fats and oils using trimethylsulphonium hydroxide for transesterification. *Journal of Chromatography A,* 261**,** 142-145.

BUTTE, W., EILERS, J. & KIRSCH, M. 1982. Trialkylsulfonium-and trialkylselenoniumhydroxides for the pyrolytic alkylation of acidic compounds. *Analytical Letters,* 15**,** 841-850.

CALDER, P. 2017. New evidence that omega-3 fatty acids have a role in primary prevention of coronary heart disease. *Journal of Public Health and Emergency,* 1.

CARBONELL, S., HEY, M., MITCHELL, J., ROBERTS, C., HIPKISS, J. & VERCAUTEREN, J. 2004. Capillary flow and rheology measurements on chocolate crumb/sunflower oil mixtures. *Journal of food science,* 69**,** E465-E470.

CARPITA, N. C., RALPH, J. & MCCANN, M. C. 2015. The Cell Wall. *In:* BUCHANAN, B. B., GRUISSEM, W. & JONES, R. L. (eds.) *Biochemistry and Molecular Biology of Plants.* John Wiley & Sons.

CATON, F. & BARAVIAN, C. 2008. Plastic behavior of some yield stress fluids: from creep to long-time yield. *Rheologica Acta,* 47**,** 601-607.

CEC 2008. COMMISSION DIRECTIVE 2008/84/EC of 27 August 2008 laying down specific purity criteria on food additives other than colours and sweeteners. *Official Journal of the European Union,* L 253**,** 109-110.

CEC, C. O. T. E. C. 2001. Report from the Commission on Dietary Food Additive Intake in the European Union.

CHEN, Y., BIRESAW, G., CERMAK, S. C., ISBELL, T. A., NGO, H. L., CHEN, L. & DURHAM, A. L. 2020. Fatty Acid Estolides: A Review. *Journal of the American Oil Chemists' Society,* 97**,** 231-241.

CHRISTIANSEN, K. 2015. PGPR, Polyglycerolpolyricinoleate, E476. *In:* NORN, V. (ed.) *Emulsifiers in Food Technology.* John Wiley & Sons, Ltd.

CHRISTIE, W. W. 1993. Preparation of ester derivatives of fatty acids for chromatographic analysis. *Advances in lipid methodology,* 2**,** e111.

CHRISTIE, W. W. & HAN, X. 2010a. Ch 3. Lipid extraction, storage and sample handling. *Lipid Analysis.* Fourth ed. England: The Oily Press.

CHRISTIE, W. W. & HAN, X. 2010b. Ch 5. Chromatographic Analysis of phospholipids and glycosyldiacylglycerols. *In:* CHRISTIE, W. W. & HAN, X. (eds.) *Lipid Analysis.* The Oily Press.

CHRISTIE, W. W. & HAN, X. 2010c. Ch 8. Gas Chromatography Analysis of Fatty Acid Derivatives. *Lipid Analysis: Isolation, Separation, Identification and Lipidomic Analysis.* The Oily Press.

CLOITRE, M. & BONNECAZE, R. T. 2017. A review on wall slip in high solid dispersions. *Rheologica Acta,* 56**,** 283-305.

CRAPISTE, G. H., BREVEDAN, M. I. & CARELLI, A. A. 1999. Oxidation of sunflower oil during storage. *Journal of the American Oil Chemists' Society,* 76**,** 1437.

CREMONINI, M. A., LAGHI, L. & PLACUCCI, G. 2004. Investigation of commercial lecithin by ^{31}P NMR in a ternary CUBO solvent. *Journal of the Science of Food and Agriculture,* 84**,** 786-790.

DE GRAEF, V., DEPYPERE, F., MINNAERT, M. & DEWETTINCK, K. 2011. Chocolate yield stress as measured by oscillatory rheology. *Food Research International,* 44**,** 2660-2665.

DEDINAITE, A. & CAMPBELL, B. 2000. Interactions between mica surfaces across triglyceride solution containing phospholipid and polyglycerol polyricinoleate. *Langmuir,* 16**,** 2248-2253.

DINKGREVE, M., PAREDES, J., DENN, M. M. & BONN, D. 2016. On different ways of measuring "the" yield stress. *Journal of Non-Newtonian Fluid Mechanics,* 238**,** 233-241.

DIRECTIVE, E. P. A. C. 1995. EUROPEAN PARLIAMENT AND COUNCIL DIRECTIVE No 95/2/EC on food additives other than colours and sweeteners.

DO, T. A., HARGREAVES, J. M., WOLF, B., HORT, J. & MITCHELL, J. R. 2007. Impact of particle size distribution on rheological and textural properties of chocolate models with reduced fat content. *J Food Sci,* 72**,** E541-52.

DO, T. A. L., VIEIRA, J., HARGREAVES, J. M., MITCHELL, J. R. & WOLF, B. 2011. Structural characteristics of cocoa particles and their effect on the viscosity of reduced fat chocolate. *LWT - Food Science and Technology,* 44**,** 1207-1211.

DODDS, E. D., MCCOY, M. R., REA, L. D. & KENNISH, J. M. 2005. Gas chromatographic quantification of fatty acid methyl esters: flame ionization detection vs. electron impact mass spectrometry. *Lipids,* 40**,** 419-428.

DOMÍNGUEZ, F. & CEJUDO, F. J. 2021. Chloroplast dismantling in leaf senescence. *Journal of Experimental Botany*.

DÖRMANN, P. 2013. Galactolipids in Plant Membranes. *eLS.*

DOUCE, R. & JOYARD, J. 1980. Plant galactolipids. *Lipids: Structure and function.* Elsevier.

ECSPP 2019. WHO Expert Committee on Specifications for Pharmaceutical Preparations: 4.2 Determination of iodine value. *The International Pharmacopoeia.* Ninth Edition ed.

EL-HAMDY, A. & CHRISTIE, W. 1993. Preparation of methyl esters of fatty acids with trimethylsulphonium hydroxide—an appraisal. *Journal of Chromatography A,* 630**,** 438-441.

EVANS, I., RUS, A., BELANGER, E., KIMOTO, M. & BRUSSLAN, J. 2010. Dismantling of Arabidopsis thaliana mesophyll cell chloroplasts during natural leaf senescence. *Plant Biology,* 12**,** 1-12.

EVANS, R., JEE, M. H., SANDER, N. H., SMITH, I. H. & GIBSON, R. K. 1991. Surfactant. Google Patents.

FARMER, E. E. & MUELLER, M. J. 2013. ROS-mediated lipid peroxidation and RES-activated signaling. *Annual review of plant biology,* 64**,** 429-450.

FCC 2016. *Food Chemicals Codex*, United States Pharmacopeial Convention.

FENEUIL, B., ROUSSEL, N. & PITOIS, O. 2020. Yield stress of aerated cement paste. *Cement and Concrete Research,* 127**,** 105922.

FERNANDES, V. A., MÜLLER, A. J. & SANDOVAL, A. J. 2013. Thermal, structural and rheological characteristics of dark chocolate with different compositions. *Journal of Food Engineering,* 116**,** 97-108.

FERRUZZI, M., BÖHM, V., COURTNEY, P. & SCHWARTZ, S. 2002. Antioxidant and antimutagenic activity of dietary chlorophyll derivatives determined by radical scavenging and bacterial reverse mutagenesis assays. *Journal of food Science,* 67**,** 2589-2595.

FEWSTER, M. E., BURNS, B. J. & MEAD, J. 1969. Quantitative densitometric thin-layer chromatography of lipids using copper acetate reagent. *Journal of Chromatography A,* 43**,** 120-126.

FINCKE, H. 1965. Handbuch der Kakaoerzeugnisse. Springer-Verlag.

FOLCH, J., LEES, M. & STANLEY, G. S. 1957. A simple method for the isolation and purification of total lipides from animal tissues. *Journal of biological chemistry,* 226**,** 497-509.

FUCHS-GODEC, R. & PAVLOVIĆ, M. G. 2012. Synergistic effect between non-ionic surfactant and halide ions in the forms of inorganic or organic salts for the corrosion inhibition of stainless-steel X4Cr13 in sulphuric acid. *Corrosion Science,* 58**,** 192-201.

GARBOLINO, C. 2002. *The influence of surfactants and moisture on the colloidal and rheological properties of model chocolate dispersions.* The Pennsylvania State University.

GEDI, M. A., BRIARS, R., YUSELI, F., ZAINOL, N., DARWISH, R., SALTER, A. M. & GRAY, D. A. 2017. Component analysis of nutritionally rich chloroplasts: recovery from conventional and unconventional green plant species. *J Food Sci Technol,* 54**,** 2746-2757.

GITTINGS, S., TURNBULL, N., HENRY, B., ROBERTS, C. J. & GERSHKOVICH, P. 2015. Characterisation of human saliva as a platform for oral dissolution medium development. *Eur J Pharm Biopharm,* 91**,** 16-24.

GLICERINA, V., BALESTRA, F., DALLA ROSA, M. & ROMANI, S. 2016. Microstructural and rheological characteristics of dark, milk and white chocolate: A comparative study. *Journal of Food Engineering,* 169**,** 165-171.

GÓMEZ, J. L., BASTIDA, J., MÁXIMO, M. F., MONTIEL, M. C., MURCIA, M. D. & ORTEGA, S. 2011. Solvent-free polyglycerol polyricinoleate synthesis mediated by lipase from Rhizopus arrhizus. *Biochemical Engineering Journal,* 54**,** 111-116.

GOULD, J. M., FURSE, S. & WOLF, B. 2016. The Role of Endogenous Lipids in the Emulsifying Properties of Cocoa. *Frontiers in Chemistry,* 4**,** 11.

GRÖBER, U., SCHMIDT, J. & KISTERS, K. 2015. Magnesium in prevention and therapy. *Nutrients,* 7**,** 8199-8226.

HAAS, A. R. C. 1938. Water content of Avocado Fruit and Leaves. *California Avocado Association Yearbook,* 23**,** 97-102.

HARRIS, B. R. 1935. *Confection and method of producing same.*

HARRIS, T. 1968. Surface Active Lipids in Foods. Monograph No 32. *Society of Chemical Industry, England.*

HAYES, D., KLEIMAN, R., WEISLEDER, D., ADLOF, R., CUPERUS, F. & DERKSEN, J. 1995a. Occurrence of estolides in processed Dimorphotheca pluvialis seed oil. *Industrial Crops and Products,* 4**,** 295-301.

HAYES, D. G., KLEIMAN, R. & PHILLIPS, B. S. 1995b. The triglyceride composition, structure, and presence of estolides in the oils of Lesquerella and related species. *Journal of the American Oil Chemists' Society,* 72**,** 559-569.

HEGAZY, M. 2015. Novel cationic surfactant based on triazole as a corrosion inhibitor for carbon steel in phosphoric acid produced by dihydrate wet process. *Journal of Molecular Liquids,* 208**,** 227-236.

HEINZ, E. 1967a. Acylgalaktosyldiglycerid aus blatthomogenaten. *Biochimica et Biophysica Acta (BBA)-Lipids and Lipid Metabolism,* 144**,** 321-332.

HEINZ, E. 1967b. Über die enzymatische Bildung von Acylgalaktosyldiglycerid. *Biochimica et Biophysica Acta (BBA)-Lipids and Lipid Metabolism,* 144**,** 333-343.

HEINZ, E., RULLKOTTER, J. & BUDZIKIEWICZ, H. 1974. Acyl Digalactosyl Diglyceride from leaf homogenates. *Hoppe-Seyler's Z. Physiol. Chem.,* 355**,** 612-616.

HEINZ, V. & FRANKE, K. 2010. *E & E dokumentation AIF 15217 N: Investigations on effects of surface active components in concentrated lipophilic confectionary suspensions considering chocolate mass as example.* Deutsches Institut für Lebensmitteltechnik e.V. (DIL).

HELLGREN, L. I. & SANDELIUS, A. S. 2001. Age-dependent variation in membrane lipid synthesis in leaves of garden pea (Pisum sativum L.). *Journal of experimental botany,* 52**,** 2275-2282.

HIMELBLAU, E. & AMASINO, R. M. 2001. Nutrients mobilized from leaves of Arabidopsis thaliana during leaf senescence. *Journal of Plant Physiology,* 158**,** 1317-1323.

HUBER, D. 1987. Postharvest senescence: an introduction to the symposium. *HortScience (USA).*

IBRAHIM, A., SCHUTZ, A. L., GALANO, J. M., HERRFURTH, C., FEUSSNER, K., DURAND, T., BRODHUN, F. & FEUSSNER, I. 2011. The Alphabet of Galactolipids in Arabidopsis thaliana. *Front Plant Sci,* 2**,** 95.

IOCCC 2000. Viscosity of Cocoa and Chocolate Products - Analytical Method 46. International Office of Cocoa, Chocoalte and Sugar Confectionary.

ISBELL, T. A. 2011. Chemistry and physical properties of estolides. *Grasas y Aceites,* 62**,** 8-20.

ISBELL, T. A., EDGCOMB, M. R. & LOWERY, B. A. 2001. Physical properties of estolides and their ester derivatives. *Industrial Crops and Products,* 13**,** 11-20.

JAMES, N. M., HSU, C.-P., SPENCER, N. D., JAEGER, H. M. & ISA, L. 2019. Tuning interparticle hydrogen bonding in shear-jamming suspensions: Kinetic effects and consequences for tribology and rheology. *The journal of physical chemistry letters,* 10**,** 1663-1668.

JECFA 1992. Joint FAO/WHO Expert Committee on Food Additives: Compendium of Food Additive Specifications. Rome: Food and Agriculture Organization of the United Nations.

JOHANSSON, D. & BERGENSTÅHL, B. 1992a. The influence of food emulsifiers on fat and sugar dispersions in oils. I. Adsorption, sedimentation. *Journal of the American Oil Chemists Society,* 69**,** 705-717.

JOHANSSON, D. & BERGENSTÅHL, B. 1992b. The influence of food emulsifiers on fat and sugar dispersions in oils. II. Rheology, colloidal forces. *Journal of the American Oil Chemists' Society,* 69**,** 718-727.

JOHNSON, E. J. 2002. The role of carotenoids in human health. *Nutrition in clinical care,* 5**,** 56-65.

KAIMAINEN, M., AHVENAINEN, S., KAARISTE, M., JÄRVENPÄÄ, E., KAASALAINEN, M., SALOMÄKI, M., SALONEN, J. & HUOPALAHTI, R. 2012.

Polar lipid fraction from oat (Avena sativa): characterization and use as an o/w emulsifier. *European Food Research and Technology,* 235**,** 507-515.

KATZ, D. L., DOUGHTY, K. & ALI, A. 2011. Cocoa and chocolate in human health and disease. *Antioxidants & redox signaling,* 15**,** 2779-2811.

KEENTOK, M., MILTHORPE, J. & O'DONOVAN, E. 1985. On the shearing zone around rotating vanes in plastic liquids: theory and experiment. *Journal of non-Newtonian fluid mechanics,* 17**,** 23-35.

KIDMOSE, U., KNUTHSEN, P., EDELENBOS, M., JUSTESEN, U. & HEGELUND, E. 2001. Carotenoids and flavonoids in organically grown spinach (Spinacia oleracea L) genotypes after deep frozen storage. *Journal of the Science of Food and Agriculture,* 81**,** 918-923.

KIM, H. U., LEE, K.-R., GO, Y. S., JUNG, J. H., SUH, M.-C. & KIM, J. B. 2011. Endoplasmic reticulum-located PDAT1-2 from castor bean enhances hydroxy fatty acid accumulation in transgenic plants. *Plant and cell physiology,* 52**,** 983-993.

KIM, S. B., BISSON, J., FRIESEN, J. B., PAULI, G. F. & SIMMLER, C. 2020. Selective Chlorophyll Removal Method to "Degreen" Botanical Extracts. *Journal of Natural Products,* 83**,** 1846-1858.

KLEIMAN, R., SPENCER, G., EARLE, F., NIESCHLAG, H. & BARCLAY, A. 1972. Tetra-acid triglycerides containing a new hydroxy eicosadienoyl moiety in Lesquerella auriculata seed oil. *Lipids,* 7**,** 660-665.

KOOS, E. & WILLENBACHER, N. 2011. Capillary forces in suspension rheology. *Science,* 331**,** 897-900.

KRONBERG, B., HOLMBERG, K. & LINDMAN, B. 2014a. Ch 1. Types of surfactants, their synthesis, and applications. *Surface chemistry of surfactants and polymers.* John Wiley & Sons.

KRONBERG, B., HOLMBERG, K. & LINDMAN, B. 2014b. Ch 4. Surfactant Self-Assembly: General Aspects and Spherical Micelles. *Surface Chemistry of surfactants and polymers.* John Wiley and Sons.

KRONBERG, B., HOLMBERG, K. & LINDMAN, B. 2014c. Ch 12. Surface and Interfacial Tension. *Surface Chemistry of Surfactants and Polymers.* John Wiley and Sons.

KRÜGER, C. 2009. Ch 3. Sugar and Bulk Sweeteners. *In:* BECKETT, S. T. (ed.) *Industrial chocolate manufacture and use.* Blackwell Publishing Ltd.

LEE, Y., HU, S., PARK, Y.-K. & LEE, J.-Y. 2019. Health benefits of carotenoids: a role of carotenoids in the prevention of non-alcoholic fatty liver disease. *Preventive nutrition and food science,* 24**,** 103.

LEVETIN, E. & MCMAHON, K. 2016. Ch 4. Plant Physiology. *Plants and Society.* Seventh Edition ed. USA: McGraw-Hill Education.

LICHTENTHALER, H. K., AC, A., MAREK, M. V., KALINA, J. & URBAN, O. 2007. Differences in pigment composition, photosynthetic rates and chlorophyll fluorescence images of sun and shade leaves of four tree species. *Plant Physiol Biochem,* 45**,** 577-88.

LICHTENTHALER, H. K. & BUSCHMANN, C. 2001. Chlorophylls and carotenoids: Measurement and characterization by UV-VIS spectroscopy. *Current protocols in food analytical chemistry,* 1**,** F4. 3.1-F4. 3.8.

LIEDVOGEL, B. & KLEINIG, H. 1977. Lipid metabolism in chromoplast membranes from the daffodil: glycosylation and acylation. *Planta,* 133**,** 249-253.

LIN, J.-T., ARCINAS, A., HARDEN, L. R. & FAGERQUIST, C. K. 2006. Identification of (12-ricinoleoylricinoleoyl) diricinoleoylglycerol, an acylglycerol containing four acyl chains, in castor (Ricinus communis L.) oil by LC-ESI-MS. *Journal of agricultural and food chemistry,* 54**,** 3498-3504.

LIN, J. T. & CHEN, G. Q. 2013. Identification of tetraacylglycerols in lesquerella oil by electrospray ionization mass spectrometry of the lithium adducts. *Journal of the American Oil Chemists' Society,* 90**,** 1831-1836.

LINDECRANTZ, A., SVANBERG, L. & AHRNÉ, L. 2015. Effect of oat polar lipids on the quality of chocolate. SP Sveriges Tekniska Forskningsinstitut.

LIPP, M. & ANKLAM, E. 1998. Review of cocoa butter and alternative fats for use in chocolate—part A. Compositional data. *Food Chemistry,* 62**,** 73-97.

LIPTON, W. 1987. Senescence of leafy vegetables. *HortScience (USA),* 22**,** 854-859.

LLOYD, K. 2020. *Investigating Oat lecithin as a clean label ingredient in chocolate.* BSc (Hons) Food Science and technology, University of Lincoln.

LÖFGREN, L., STÅHLMAN, M., FORSBERG, G.-B., SAARINEN, S., NILSSON, R. & HANSSON, G. I. 2012. The BUME method: a novel automated chloroform-free 96-well total lipid extraction method for blood plasma. *Journal of lipid research,* 53**,** 1690-1700.

LORENTE-CEBRIÁN, S., COSTA, A. G., NAVAS-CARRETERO, S., ZABALA, M., LAIGLESIA, L. M., MARTÍNEZ, J. A. & MORENO-ALIAGA, M. J. 2015. An update on the role of omega-3 fatty acids on inflammatory and degenerative diseases. *Journal of physiology and biochemistry,* 71**,** 341-349.

MACALA, L., YU, R. & ANDO, S. 1983. Analysis of brain lipids by high performance thin-layer chromatography and densitometry. *Journal of lipid research,* 24**,** 1243-1250.

MANGOS, T. J. & BERGER, R. G. 1997. Determination of major chlorophyll degradation products. *Zeitschrift für Lebensmitteluntersuchung und-Forschung A,* 204**,** 345-350.

MARÉCHAL, E., BLOCK, M. A., DORNE, A. J., DOUCE, R. & JOYARD, J. 1997. Lipid synthesis and metabolism in the plastid envelope. *Physiologia Plantarum,* 100**,** 65-77.

MATAS, A. J., CUARTERO, J. & HEREDIA, A. 2004. Phase transitions in the biopolyester cutin isolated from tomato fruit cuticles. *Thermochimica Acta,* 409**,** 165-168.

MATSUZAKI, T., KOIWAI, A., KAWASHIMA, N. & MATSUYAMA, S. 2014. Formation of Acylmonogalactosyldiglyceride and Degradation of Polar Lipids in Leaf Homogenates of Tobacco. *Agricultural and Biological Chemistry,* 46**,** 723-729.

MCCAFFERTY, E. 2010. Ch 12. Corrosion Inhibitors. *Introduction to Corrosion Science.* Springer Science + Business Media.

MCCLEMENTS, D. J. 2015. *Food emulsions: principles, practices, and techniques*, CRC press.

MCLEAN, S., DAVIES, N. W., NICHOLS, D. S. & MCLEOD, B. J. 2015. Triacylglycerol estolides, a new class of mammalian lipids, in the paracloacal gland of the brushtail possum (Trichosurus vulpecula). *Lipids,* 50**,** 591-604.

MERCER, E. J. & HALAWEISH, F. 2010. Determination of Free Glycerol in Biodiesel via Solid-Phase Extraction and Spectrophotometric Analysis. *Journal of the American Oil Chemists' Society,* 88**,** 655-659.

METHEREL, A. H. & BAZINET, R. P. 2019. Updates to the n-3 polyunsaturated fatty acid biosynthesis pathway: DHA synthesis rates, tetracosahexaenoic acid and (minimal) retroconversion. *Progress in lipid research,* 76**,** 101008.

MEZGER, T. G. 2011a. Ch 2. Flow behaviour and viscosity. *The Rheology Handbook.*

MEZGER, T. G. 2011b. Ch 3. Rotational Tests. *In:* MEZGER, T. G. (ed.) *The Rheology Handbook.* Vincentz Network GmbH & Co.

MEZGER, T. G. 2011c. Ch 11. Instruments. *In:* MEZGER, T. G. (ed.) *The Rheology Handbook.* Third Edition ed.: Vincentz Network GmbN & Co.

MEZGER, T. G. 2014. The Rheology Handbook 4th edition ed. Germany: Vincentz Network, Hanover.

MEZGER, T. G. 2015. *Applied rheology*, Anton Paar.

MEZGER, T. G. 2017. *Applied Rheology,* Austria, Anton Paar GmbH.

MIDDENDORF, D., JUADJUR, A., BINDRICH, U. & MISCHNICK, P. 2015. AFM approach to study the function of PGPR's emulsifying properties in cocoa butter based suspensions. *Food Structure,* 4**,** 16-26.

MILLER, K. B., HURST, W. J., FLANNIGAN, N., OU, B., LEE, C., SMITH, N. & STUART, D. A. 2009. Survey of commercially available chocolate-and cocoa-containing products in the United States. 2. Comparison of flavan-3-ol content with nonfat cocoa solids, total polyphenols, and percent cacao. *Journal of agricultural and food chemistry,* 57**,** 9169-9180.

MINIFIE, B. W. 1980. Use of lecithin in chocolate and confectionary as an emulsifier and in powdered drinks as a wetting agent. *The Manufacturing Confectioner,* 60**,** 47-50.

MISRA, S., DATTA, A. K., CHOUDHURY, S. C. A. & GHOSH, A. 1987. Hydrocarbons and wax esters from seven species of mangrove leaves. *Phytochemistry,* 26**,** 3265-3268.

MOHAMAD, N. 2017. *Dark Chocolate: Understanding the Impact of Limonene on the Crystallization Properties and Application of Green Leaf Lipid Extract as a Flow Enhancer.* University of Nottingham.

MOHAMAD, N. J., GRAY, D. & WOLF, B. 2020. Spinach leaf and chloroplast lipid: A natural rheology modifier for chocolate? *Food Res Int,* 133**,** 109193.

MOLISCH, H. 1886. Zwei neue zuckerreactionen. *Monatshefte für Chemie und verwandte Teile anderer Wissenschaften,* 7**,** 198-209.

NILSSON, A. K., FAHLBERG, P., ELLERSTROM, M. & ANDERSSON, M. X. 2012. Oxo-phytodienoic acid (OPDA) is formed on fatty acids esterified to galactolipids after tissue disruption in Arabidopsis thaliana. *FEBS Lett,* 586**,** 2483-7.

NILSSON, A. K., JOHANSSON, O. N., FAHLBERG, P., KOMMURI, M., TOPEL, M., BODIN, L. J., SIKORA, P., MODARRES, M., EKENGREN, S., NGUYEN, C. T., FARMER, E. E., OLSSON, O., ELLERSTROM, M. & ANDERSSON, M. X. 2015. Acylated monogalactosyl diacylglycerol: prevalence in the plant kingdom and identification of an enzyme catalyzing galactolipid head group acylation in Arabidopsis thaliana. *Plant J,* 84**,** 1152-66.

NILSSON, A. K., JOHANSSON, O. N., FAHLBERG, P., STEINHART, F., GUSTAVSSON, M. B., ELLERSTROM, M. & ANDERSSON, M. X. 2014. Formation of oxidized phosphatidylinositol and 12-oxo-phytodienoic acid containing acylated phosphatidylglycerol during the hypersensitive response in Arabidopsis. *Phytochemistry,* 101**,** 65-75.

NYSTRÖM, L., SCHÄR, A. & LAMPI, A. M. 2012. Steryl glycosides and acylated steryl glycosides in plant foods reflect unique sterol patterns. *European journal of lipid science and technology,* 114**,** 656-669.

OGINO, K., KUBOTA, T., UCHIYAMA, H. & ABE, M. 1988. Micelle formation and micellar size by a light scattering technique. *Journal of Japan Oil Chemists' Society,* 37**,** 588-591.

OHLROGGE, J. B., BROWSE, J., JAWORSKI, J. G. & SOMERVILLE, C. 2015. Ch 8. Lipids. *In:* BUCHANAN, B. B., GRUISSEM, W. & JONES, R. L. (eds.) *Biochemistry and Molecular Biology of Plants.* Wiley.

OHTA, M., IWASAKI, M., KOUNO, K. & UEDA, Y. 1985. Mechanism of the Molisch reaction. *Chemical and pharmaceutical bulletin,* 33**,** 2862-2865.

ORFANAKIS, A., HATZAKIS, E., KANAKI, K., PERGANTIS, S. A., RIZOS, A. & DAIS, P. 2012. Characterization of Polyglycerol Polyricinoleate Formulations Using NMR Spectroscopy, Mass Spectrometry and Dynamic Light Scattering. *Journal of the American Oil Chemists' Society,* 90**,** 39-51.

ORTEGA-REQUENA, S., BÓDALO-SANTOYO, A., BASTIDA-RODRÍGUEZ, J., MÁXIMO-MARTÍN, M. F., MONTIEL-MORTE, M. C. & GÓMEZ-GÓMEZ, M. 2014. Optimized enzymatic synthesis of the food additive polyglycerol polyricinoleate (PGPR) using Novozym® 435 in a solvent free system. *Biochemical Engineering Journal,* 84**,** 91-97.

ORTEGA-REQUENA, S., SERRANO-ARNALDOS, M., MONTIEL, M., MÁXIMO, F., BASTIDA, J. & MURCIA, M. 2019. Biocatalytic Synthesis of Polymeric Esters

Used as Emulsifiers. *Chemical and Biochemical Engineering Quarterly,* 33**,** 79-86.

ORTEGA-REQUENA, S., GÓMEZ, J. L., BASTIDA, J., MÁXIMO, F., MONTIEL, M. C. & MURCIA, M. D. 2014. Study of different reaction schemes for the enzymatic synthesis of polyglycerol polyricinoleate. *Journal of the Science of Food and Agriculture,* 94**,** 2308-2316.

OSBORN, S. 2015. Labelling relating to natural ingredients and additives. *Advances in Food and Beverage Labelling.*

OVARLEZ, G., MAHAUT, F., BERTRAND, F. & CHATEAU, X. 2011. Flows and heterogeneities with a vane tool: Magnetic resonance imaging measurements. *Journal of Rheology,* 55**,** 197-223.

PARRA, D., RAMEL, A., BANDARRA, N., KIELY, M., MARTÍNEZ, J. A. & THORSDOTTIR, I. 2008. A diet rich in long chain omega-3 fatty acids modulates satiety in overweight and obese volunteers during weight loss. *Appetite,* 51**,** 676-680.

PAWLIK, A., KURUKJI, D., NORTON, I. & SPYROPOULOS, F. 2016. Food-grade Pickering emulsions stabilised with solid lipid particles. *Food & function,* 7**,** 2712-2721.

PIERRE, A., PERROT, A., HISTACE, A., GHARSALLI, S. & KADRI, E. 2017. A study on the limitations of a vane rheometer for mineral suspensions using image processing. *Rheologica Acta,* 56**,** 351-367.

POPOVA, A. & MIHAYLOVA, D. 2019. Antinutrients in plant-based foods: A review. *The Open Biotechnology Journal,* 13.

PRENTICE, J. H. 1984. *Measurement in the Rheology of Foodstuffs*, Elsevier Applied Science Publishers.

PRINZ, J. F. & LUCAS, P. W. 1997. An optimization model for mastication and swallowing in mammals. *Proceedings of the Royal Society of London. Series B: Biological Sciences,* 264**,** 1715-1721.

PROTHON, F. 2017. SweOat Oil for food applications. Swedish Oat Fibre.

PURITE 2008. *Select Fusion Operator's Manual.*

RAJARAM, S. 2014. Health benefits of plant-derived α-linolenic acid. *The American journal of clinical nutrition,* 100**,** 443S-448S.

RECTOR, D. 2000. Chocolate-controlling the flow. *Manuf. Confect,* 80**,** 63-70.

RICHARDS, J. A., GUY, B. M., BLANCO, E., HERMES, M., POY, G. & POON, W. C. K. 2020. The role of friction in the yielding of adhesive non-Brownian suspensions. *Journal of Rheology,* 64**,** 405-412.

RICHARDSON, A. J. & MONTGOMERY, P. 2005. The Oxford-Durham study: a randomized, controlled trial of dietary supplementation with fatty acids in children with developmental coordination disorder. *Pediatrics,* 115**,** 1360-1366.

ROUSSET, P. & BERTOLI, C. 1998. Characterisation of PGPR as a rheology modifier for use in chocolate. Nestle.

ROUSSET, P., SELLAPPAN, P. & DAOUD, P. 2002. Effect of emulsifiers on surface properties of sucrose by inverse gas chromatography. *Journal of Chromatography A,* 969**,** 97-101.

RUNYON, E. H. 1936. Ratio of water content to dry weight of leaves of the Creosote bush. *Botanical Gazette,* 97**,** 518-553.

SAHAKA, M., AMARA, S., LECOMTE, J., RODIER, J.-D., LAFONT, D., VILLENEUVE, P., GONTERO, B. & CARRIÈRE, F. 2021. Quantitative monitoring of galactolipid hydrolysis by pancreatic lipase-related protein 2 using thin layer chromatography and thymol-sulfuric acid derivatization. *Journal of Chromatography B,* 1173**,** 122674.

SAHASRABUDHE, M. 1979. Lipid composition of oats (Avena sativa L.). *Journal of the American oil chemists' society,* 56**,** 80-84.

SAHENA, F., ZAIDUL, I., JINAP, S., KARIM, A., ABBAS, K., NORULAINI, N. & OMAR, A. 2009. Application of supercritical CO2 in lipid extraction–A review. *Journal of Food Engineering,* 95**,** 240-253.

SCHANTZ, B. & ROHM, H. 2005. Influence of lecithin–PGPR blends on the rheological properties of chocolate. *LWT - Food Science and Technology,* 38**,** 41-45.

SERVAIS, C., RANC, H. & ROBERTS, I. 2003. Determination of chocolate viscosity. *Journal of Texture Studies,* 34**,** 467-497.

SETH, J. R., CLOITRE, M. & BONNECAZE, R. T. 2008. Influence of short-range forces on wall-slip in microgel pastes. *Journal of Rheology,* 52**,** 1241-1268.

SHAMU, T. J. & HÅKANSSON, U. 2019. Rheology of cement grouts: On the critical shear rate and no-slip regime in the Couette geometry. *Cement and Concrete Research,* 123.

SINGH, R., DE, S. & BELKHEIR, A. 2013. Avena sativa (Oat), a potential neutraceutical and therapeutic agent: an overview. *Crit Rev Food Sci Nutr,* 53**,** 126-44.

SMEDLEY, S. R., SCHROEDER, F. C., WEIBEL, D. B., MEINWALD, J., LAFLEUR, K. A., RENWICK, J. A., RUTOWSKI, R. & EISNER, T. 2002. Mayolenes: Labile defensive lipids from the glandular hairs of a caterpillar (Pieris rapae). *Proceedings of the National Academy of Sciences,* 99**,** 6822-6827.

SMITH, M. A. & ZHANG, H. 2016. Apocynaceae seed lipids: characterization and occurrence of isoricinoleic acid and triacylglycerol estolides. *Journal of the American Oil Chemists' Society,* 93**,** 105-114.

SOKMEN, A. & GUNES, G. 2006. Influence of some bulk sweeteners on rheological properties of chocolate. *LWT-food Science and Technology,* 39**,** 1053-1058.

SONG, Y., ZOONG LWE, Z. S., WICKRAMASINGHE, P. A. D. B. V. & WELTI, R. 2021. Head-Group Acylation of Chloroplast Membrane Lipids. *Molecules,* 26**,** 1273.

STAEHELIN, L. A. 2015a. Ch 1. Membrane Strurcture and Membranous Organelles. *In:* BUCHANAN, B. B., GRUISSEM, W. & JONES, R. L. (eds.) *Biochemistry and molecular biology of plants.* Second ed.: John Wiley & Sons.

STAEHELIN, L. A. 2015b. Membrane Structure and Membranous Organelles. *In:* BUCHANAN, B. B., GRUISSEM, W. & JONES, R. L. (eds.) *Biochemistry and molecular biology of plants.* USA: John Wiley & sons.

STAUFFER, C. E. 2005. Emulsifiers for the food industry. *In:* SHAHIDI, F. (ed.) *Bailey's industrial oil and fat products.* 6 ed.: John Wiley & Sons, Inc.

STEINER, E. H. 1963. Some Aspects of Chocolate and Confectionary Research. *The Manufacturing Confectioner,* May**,** 54-58.

STEINER, E. H. 1972. Melted Chocolate: Measuring its viscosity. *The Manufacturing Confectioner,* September**,** 24-28.

STRIEGEL, A. M., YAU, W. W., KIRKLAND, J. J. & BLY, D. D. 2009. Ch 8. Calibration. *Modern Size-Exclusion Liquid Chromatography: Practice of Gel Permeation and Gel Filtration Chromatography.* 2 ed.: John Wiley & Sons, Inc.

TALLON, M. J. 2015. Ch 4. Authorised EU health claim for cocoa flavanols. *In:* SADLER, M. J. (ed.) *Foods, Nutrients and Food Ingredients with Authorised EU Health Claims, Volume 2.* Elsevier.

TAYLOR, J. E., VAN DAMME, I., JOHNS, M. L., ROUTH, A. F. & WILSON, D. I. 2009. Shear rheology of molten crumb chocolate. *J Food Sci,* 74**,** E55-61.

THOMPSON, J. E., FROESE, C. D., MADEY, E., SMITH, M. D. & HONG, Y. 1998. Lipid metabolism during plant senescence. *Progress in lipid research,* 37**,** 119-141.

TRONCOSO-PONCE, M. A., CAO, X., YANG, Z. & OHLROGGE, J. B. 2013. Lipid turnover during senescence. *Plant Sci,* 205-206**,** 13-9.

VAN DER VAART, K., DEPYPERE, F., GRAEF, V. D., SCHALL, P., FALL, A., BONN, D. & DEWETTINCK, K. 2013. Dark chocolate's compositional effects revealed

by oscillatory rheology. *European Food Research and Technology,* 236**,** 931-942.

VERNIER, F. C. 1997. *Influence of emulsifiers on the rheology of chocolate and suspensions of cocoa or sugar particles in oil.* PhD, The University of Reading.

VLACHOJANNIS, J., ERNE, P., ZIMMERMANN, B. & CHRUBASIK-HAUSMANN, S. 2016. The impact of cocoa flavanols on cardiovascular health. *Phytotherapy Research,* 30**,** 1641-1657.

VOON, P. T., NG, T. K. W., LEE, V. K. M. & NESARETNAM, K. 2011. Diets high in palmitic acid (16: 0), lauric and myristic acids (12: 0+ 14: 0), or oleic acid (18: 1) do not alter postprandial or fasting plasma homocysteine and inflammatory markers in healthy Malaysian adults. *The American journal of clinical nutrition,* 94**,** 1451-1457.

VOSMANN, K., SCHULTE, E., KLEIN, E. & WEBER, N. 1998. Formation of N-and O-methyl derivatives of lipids containing amino, amide or hydroxy groups by the pyrolytic reaction with trimethylsulfonium hydroxide. *Lipid/Fett,* 100**,** 334-342.

VU, H. S., ROTH, M. R., TAMURA, P., SAMARAKOON, T., SHIVA, S., HONEY, S., LOWE, K., SCHMELZ, E. A., WILLIAMS, T. D. & WELTI, R. 2014a. Head-group acylation of monogalactosyldiacylglycerol is a common stress response, and the acyl-galactose acyl composition varies with the plant species and applied stress. *Physiol Plant,* 150**,** 517-28.

VU, H. S., SHIVA, S., ROTH, M. R., TAMURA, P., ZHENG, L., LI, M., SAROWAR, S., HONEY, S., MCELLHINEY, D., HINKES, P., SEIB, L., WILLIAMS, T. D., GADBURY, G., WANG, X., SHAH, J. & WELTI, R. 2014b. Lipid changes after leaf wounding in Arabidopsis thaliana: expanded lipidomic data form the basis for lipid co-occurrence analysis. *Plant J,* 80**,** 728-43.

WALKER, J. H. 2009. Ch 11. Bulk Chocolate Handling. *In:* BECKETT, S. T. (ed.) *Industrial Chocolate Manufacture and Use: Fourth Edition.* 4 ed.: Blackwell Publishing Ltd.

WALLS, H. J., CAINES, S. B., SANCHEZ, A. M. & KHAN, S. A. 2003. Yield stress and wall slip phenomena in colloidal silica gels. *Journal of Rheology,* 47**,** 847-868.

WATTANAKUL, J. 2020. *Nutrient value and stability of chloroplast-rich fraction (CRF) material from pea vine haulm, and the role of galactolipolytic enzymes during digestion.* Doctor of Philosophy, University of Nottingham.

WATTANAKUL, J., SAHAKA, M., AMARA, S., MANSOR, S., GONTERO, B., CARRIERE, F. & GRAY, D. 2019. In vitro digestion of galactolipids from chloroplast-rich fraction (CRF) of postharvest, pea vine field residue (haulm) and spinach leaves. *Food Funct,* 10**,** 7806-7817.

WEST, R. & ROUSSEAU, D. 2018. The role of nonfat ingredients on confectionery fat crystallization. *Crit Rev Food Sci Nutr,* 58**,** 1917-1936.

WHATLEY, J. & WHATLEY, F. 1987. When is a chromoplast? *New phytologist,* 106**,** 667-678.

WILSON, R., VAN SCHIE, B. & HOWES, D. 1998. Overview of the preparation, use and biological studies on polyglycerol polyricinoleate (PGPR). *Food and Chemical Toxicology,* 36**,** 711-718.

WINDHAB, E. J. 2000. Fluid immobilization–a structure-related key mechanism for the viscous flow behavior of concentrated suspension systems. *Applied Rheology,* 10**,** 134-144.

WOLF, B. 2017. Chocolate Flow Properties. *In:* BECKETT, S. T., FOWLER, M. & ZIEGLER, G. R. (eds.) *Beckett's industrial chocolate manufacture and use.* Fifth ed.: John Wiley & Sons Ltd.

WOLFF, R. L., CHRISTIE, W. W., PEDRONO, F., MARPEAU, A. M., TSEVEGSUREN, N., AITZETMULLER, K. & GUNSTONE, F. D. 1999. Delta5-olefinic acids in the seed lipids from four Ephedra species and their distribution

between the alpha and beta positions of triacylglycerols. Characteristics common to coniferophytes and cycadophytes. *Lipids,* 34**,** 855-64.

YAMAUCHI, K., TANABE, T. & KINOSHITA, M. 1979. Trimethylsulfonium hydroxide: a new methylating agent. *The Journal of Organic Chemistry,* 44**,** 638-639.

YAMAUCHI, N. & WATADA, A. E. 1991. Regulated chlorophyll degradation in spinach leaves during storage. *Journal of the American Society for Horticultural Science,* 116**,** 58-62.

YANG, Z. & OHLROGGE, J. B. 2009. Turnover of fatty acids during natural senescence of Arabidopsis, Brachypodium, and switchgrass and in Arabidopsis β-oxidation mutants. *Plant Physiology,* 150**,** 1981-1989.

ZERKOWSKI, J. A. 2008. Estolides: From structure and function to structured and functionalized. *Lipid Technology,* 20**,** 253-256.

ZIEGLER, G. R., GARBOLINO, C. & COUPLAND, J. N. 2003. The Influence of Surfactants and Moisture on the colloidal and rheological properties of model chocolate dispersions. *3rd International Symposium on Food Rheology and Structure.* Zurich.

ZIEGLER, G. R. & HOGG, R. 2009. Ch 7. Particle Size Reduction. *In:* BECKETT, S. T. (ed.) *Industrial chocolate manufacture and use.* Blackwell Publishing Ltd.

ZIEGLER, G. R. & HOGG, R. 2017. Particle Size Reduction. *In:* BECKETT, S. T., FOWLER, M. & ZIEGLER, G. R. (eds.) *Beckett's Industrial Chocolate Manufacture and Use.* John Wiley & Sons Ltd.

Appendices

Appendix 1

All geometries were checked using Silicone Oil (viscosity 10,000 cSt at 25 °C)
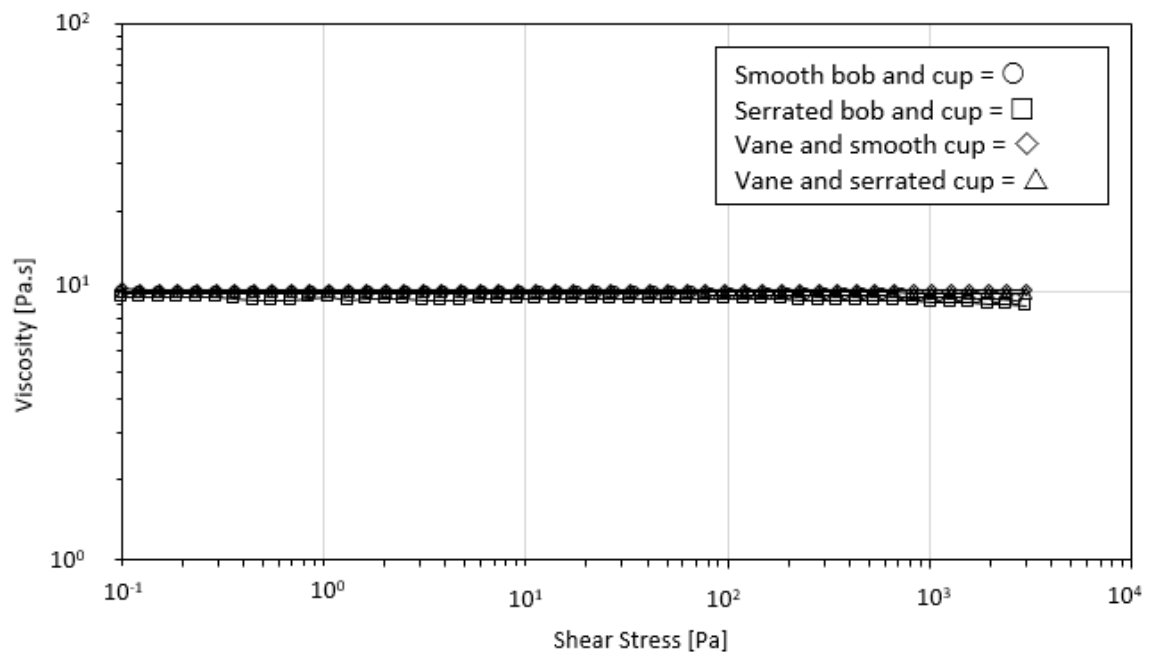
Appendix 2

Equilibrium interfacial tension values (mN/m) for the five PGPRs (see section 4.3.2).

Treated sunflower oil, without added emulsifier, had an interfacial tension of 24.0 mN/m

Conc [%]	Equilibrium interfacial tension values [mN/m]									
	Admul WOL 1408		Grindsted 90		Grindsted Super		Palsgaard 4125		Palsgaard 4150	
	B1	B2	B1	B2	B1	B2	B1	B2	B1	B2
0.02	21.1	21.1	21.5	21.5	20.6	20.8	20.6	20.8	19.6	19.3
0.04	18.4	18	18.8	19.1	16.9	17	18.1	18.4	15.3	15.4
0.08	12	11.8	14.4	14.5	11.3	11.1	12	11.9	9.4	9.4
0.16	5.5	5.7	9.2	8.9	4.5	4.8	6.1	6.3	3.7	4.1
0.31	2.2	2.3	3.5	3.7	2.8	2.8	2.9	3	2.5	2.3
0.63	2.1	2.1	3	2.9	2.7	2.7	2.4	2.5	2.3	2.3
1.25	2.2	2.2	2.7	2.7	2.7	2.7	2.4	2.4	2.3	2.3
2.5	2.2	2.3	2.5	2.6	2.7	2.7	2.4	2.4	2.3	2.3
5	2.2	2.2	2.5	2.5	2.7	2.7	2.4	2.4	2.3	2.3

Appendix 3

Full gene sequence of the DNA within the T7 promoter and terminator

The black portion is the At2g42690 gene, which codes for the AGAP-1 protein:

NNNNNNNNNNNNNNNNNNNTCTANNNNNANNTTTGTTTAACTTTAAGAAGGAGATA
TACATATGTCTGGTTCTCATCATCATCATCATCATAGCAGCGGTATGTCCCCTAT
ACTAGGTTATTGGAAAATTAAGGGCCTTGTGCAACCCACTCGACTTCTTTTGGA
ATATCTTGAAGAAAAATATGAAGAGCATTTGTATGAGCGCGATGAAGGTGATAA
ATGGCGAAACAAAAGTTTGAATTGGGTTTGGAGTTTCCCAATCTTCCTTATTAT
ATTGATGGTGATGTTAAATTAACACAGTCTATGGCCATCATACGTTATATAGCTG
ACAAGCACAACATGTTGGGTGGTTGTCCAAAAGAGCGTGCAGAGATTTCAATG
CTTGAAGGAGCGGTTTTGGATATTAGATACGGTGTTTCGAGAATTGCATATAGT
AAAGACTTTGAAACTCTCAAAGTTGATTTTCTTAGCAAGCTACCTGAAATGCTGA
AAATGTTCGAAGATCGTTTATGTCATAAAACATATTTAAATGGTGATCATGTAAC
CCATCCTGACTTCATGTTGTATGACGCTCTTGATGTTGTTTTATACATGGACCCA
ATGTGCCTGGATGCGTTCCCAAAATTAGTTTGTTTTAAAAAACGTATTGAAGCTA
TCCCACAAATTGATAAGTACTTGAAATCCAGCAAGTATATAGCATGGCCTTTGC
AGGGCTGGCAAGCCACGTTTGGTGGTGGCGACCATCCTCCAAAATCGGATCT
GGGCCACACAGGCCATAGATCTGGTACCGACGACGACGACAAGGCCATGGCT
GATATCGGATCCCTAATGGCTACAACAACCACATCATGGGAAGAACTCTTAGG
CTCAAAGAATTGGGACACTATCTTAGACCCATTAGACCAATCACTTAGGGAACT
CATCTTACGTTGTGGCGACTTTTGTCAAGCCACCTACGATGCCTTCGTCAACGA
CCAAAACTCCAAGTACTGTGGAGCCAGCCGCTACGGCAAATCTTCTTTCTTCGA
CAAGGTCATGCTCGAAAACGCTTCCGACTACGAGGTTGTAAACTTCCTCTACG
CCACAGCTCGTGTTTCTCTCCCCGAAGGTTTGCTTCTCCAATCACAATCAAGAG
ATTCTTGGGACCGTGAGTCTAACTGGTTTGGCTACATTGCTGTCACGTCTGATG
AACGGTCTAAGGCTTTAGGACGCCGTGAGATCTATATAGCTTTGAGAGGAACG
AGCAGGAACTATGAGTGGGTCAATGTTTTGGGTGCTAGGCCAACTTCAGCTGA
CCCCTTGCTGCACGGACCCGAGCAGGATGGTTCTGGTGGTGTAGTTGAAGGT
ACGACTTTTGATAGTGACAGTGAAGATGAAGAAGGGTGTAAGGTGATGCTCGG
GTGGCTCACAATCTATACTTCTAATCACCCCGAATCGAAATTCACTAAGCTGAG
TCTACGGTCACAGTTGTTAGCCAAGATCAAGGAGCTTCTGTTGAAGTATAAGGA
CGAGAAACCGAGCATTGTGTTGACTGGACATAGCTTGGGAGCTACAGAGGCTG
TTCTGGCCGCCTATGATATAGCTGAGAACGGTTCCAGTGATGATGTTCCGGTC
ACTGCTATAGTCTTTGGTTGTCCACAGGTAGGAAACAAGGAGTTCAGAGACGA
AGTAATGAGTCACAAGAACTTAAAGATCCTCCATGTAAGGAACACGATTGATCT
CTTAACTCGATACCCAGGGGGGACTTTTAGGGTATGTGGACATAGGAATAAACTT
TGTGATCGATACAAAGAAGTCACCGTTCCTAAGCGATTCAAGGAATCCAGGGG
ATTGGCATAATCTTCAGGCGATGTTACATGTTGTAGCTGGATGGAATGGGAAGA
AAGGAGAGTTTAAACTGATGGTTAAGAGAAGTATTGCATTAGTGAACAAGTCAT
GCGAGTTCTTGAAAGCTGAGTGTTTGGTGCCAGGATCTTGGTGGGTAGAGAAG
AACAAAGGACTGATCAAGAACGAAGATGGTGAATGGGTTCTTGCTCCCGTTGA
AGAAGAACCTGTACCTGAATTCAAGCNNGCGGCCGCACTCGAGCACCACCAC
CACCACCACTGAGATCCGGCTGCTAAC

242

The amino acid sequence of the AGAP-1 protein:

```
MATTTTSWEE  LLGSKNWDTI  LDPLDQSLRE  LILRCGDFCQ  ATYDAFVNDQ
NSKYCGASRY  GKSSFFDKVM  LENASDYEVV  NFLYATARVS  LPEGLLLQSQS
RDSWDRESN   WFGYIAVTSD  ERSKALGRRE  IYIALRGTSR  NYEWVNVLGA
RPTSADPLLH  GPEQDGSGGV  VEGTTFDSDS  EDEEGCKVML  GWLTIYTSNH
PESKFTKLSL  RSQLLAKIKE  LLLKYKDEKP  SIVLTGHSLG  ATEAVLAAYD
IAENGSSDDV  PVTAIVFGCP  QVGNKEFRDE  VMSHKNLKIL  HVRNTIDLLT
RYPGGLLGYV  DIGINFVIDT  KKSPFLSDSR  NPGDWHNLQA  MLHVVAGWNG
KKGEFKLMVK  RSIALVNKSC  EFLKAECLVP  GSWWVEKNKG  LIKNEDGEWV
LAPVEEEPVP  EF
```

The plasmid (pGS-21a) map can be found here:

https://www.genscript.com/gsfiles/vector-map/bacteria/pGS-21a.pdf?893241494